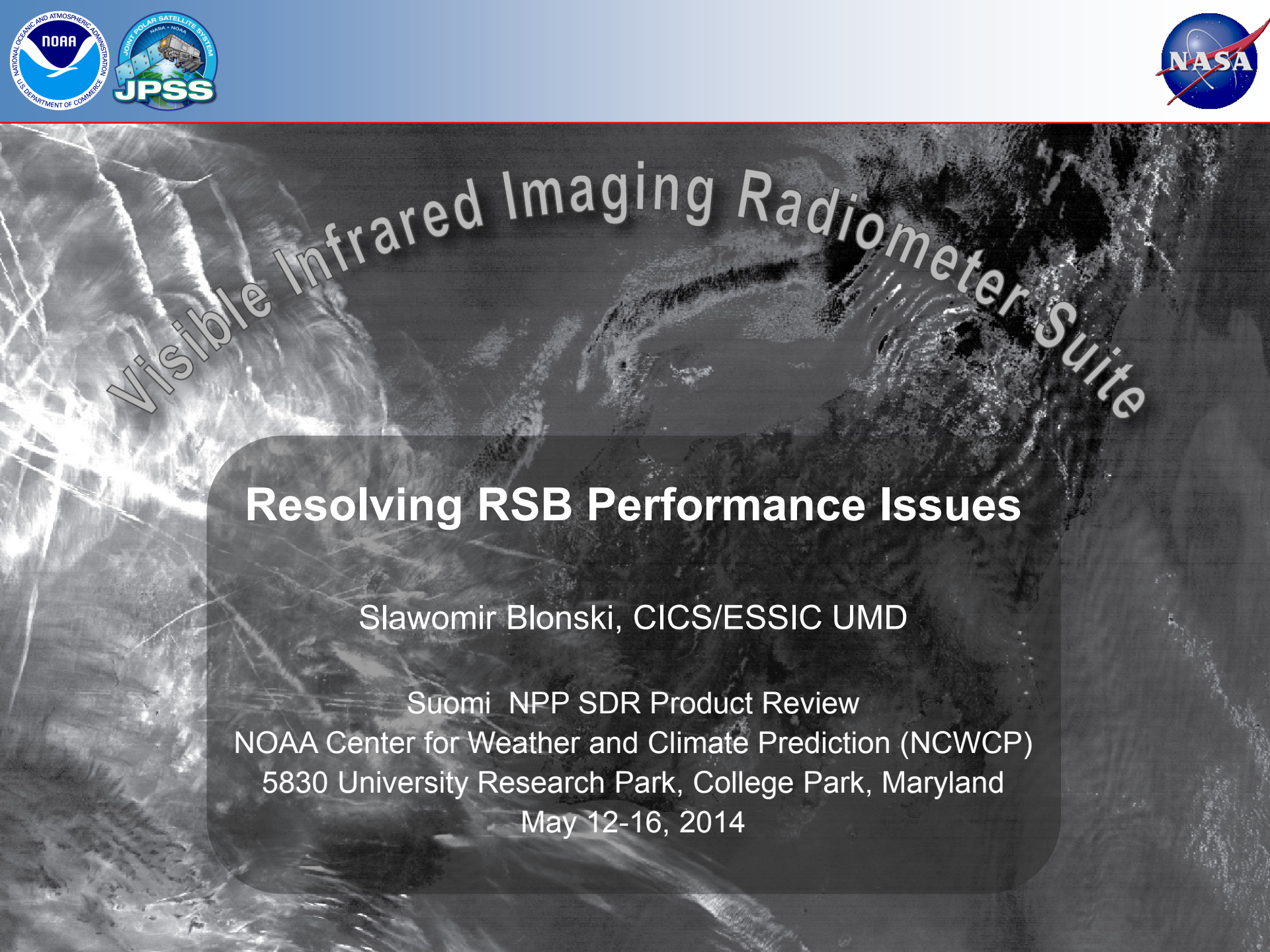

Resolving RSB Performance Issues

Slawomir Blonski, CICS/ESSIC UMD

Suomi NPP SDR Product Review
NOAA Center for Weather and Climate Prediction (NCWCP)
5830 University Research Park, College Park, Maryland
May 12-16, 2014

VIIRS RSB Radiometric Calibration

Calibration equation for earth view data:

$$L = \langle F \rangle \cdot (c_0 + c_1 \Delta n + c_2 \Delta n^2) \,/\, RVS \qquad \Delta n = n_{EV} - \langle n_{SV} \rangle$$

F factor derived from solar diffuser measurements:

$$F = \frac{E_{sun}(d) \cdot \cos AOI \cdot \tau_{SDS} \cdot BRDF_{SD}}{c_0 + c_1 \Delta n_0 + c_2 {\Delta n_0}^2} \qquad \Delta n_0 = n_{SD} - \langle n_{SV} \rangle$$

$$E_{sun}(d) = \frac{\int RSR(\lambda) \cdot \frac{\Phi_{sun}(\lambda)}{4\pi d^2} d\lambda}{\int RSR(\lambda) d\lambda}$$

- Solar calibration (F) conducted once per orbit
- Solar diffuser stability ($BRDF$) measured once per day: the H factor
- Calibration coefficients $\langle F \rangle$ updated once per week
- Lunar calibration conducted once per month (except summer) as a consistency check

VIIRS RSB Calibration Updates

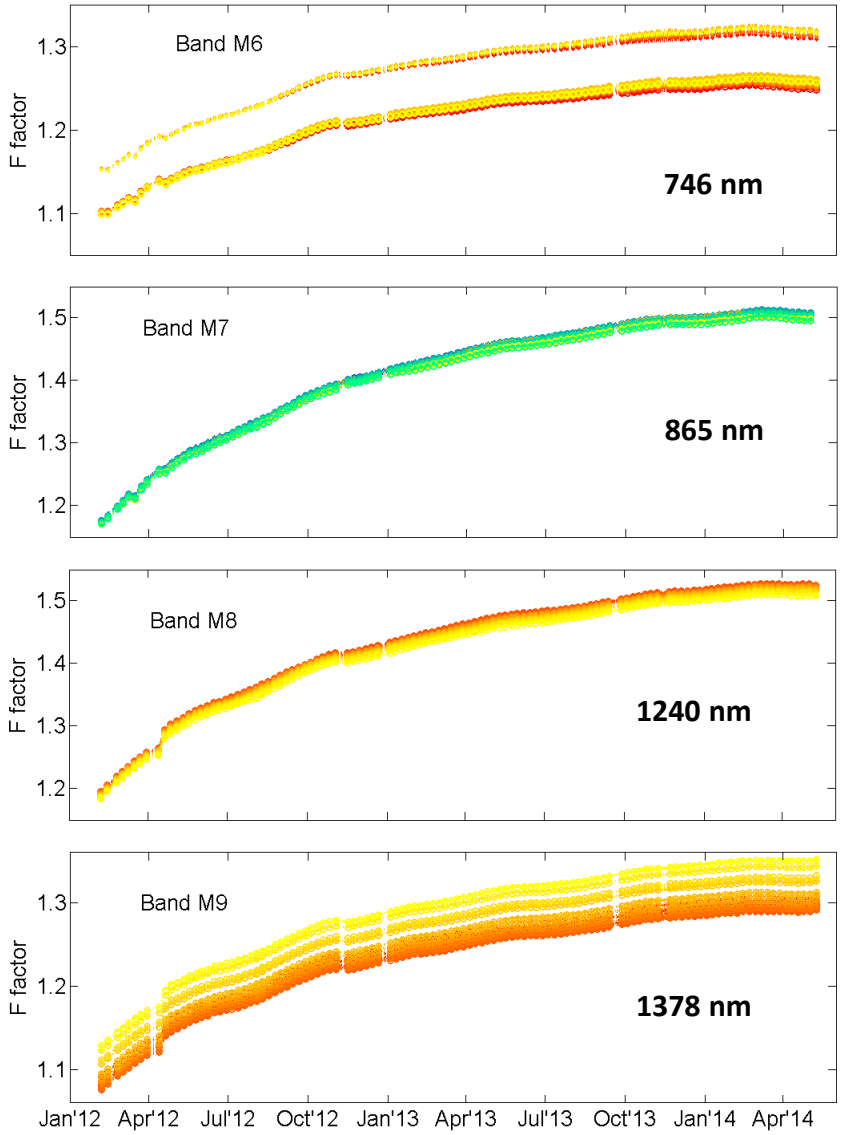

- VIIRS telescope mirrors degradation forced weekly updates of the operational F factors for the reflective solar bands
- The largest changes occurred for the near-infrared (NIR) band M7 and the short-wave-infrared (SWIR) band M8
- The NIR band M6 and the SWIR band M9 were less affected by the degradation
- Even smaller changes due to the telescope degradation occurred for bands M5, M10, and M11
- The F factors trends changed since February 2014 (discussed later)

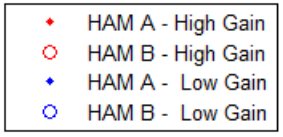

Red → *Yellow*

Blue → *Green*

Calibration Parameters Changes

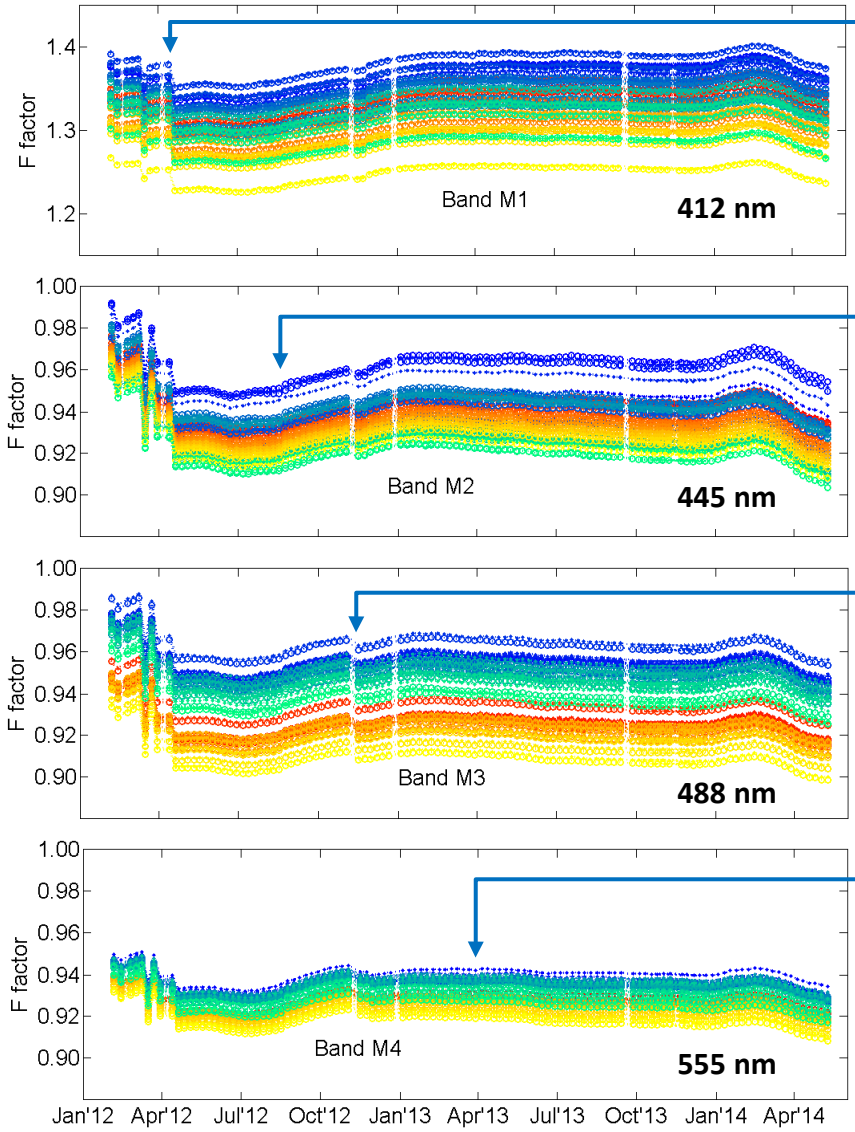

Apr'12 – Initial updates of IDPS code and processing parameters completed:
increased short-term stability of the calibration

Aug'12 – F factor prediction between updates implemented:
increased calibration accuracy

Nov'12 – Solar diffuser processing parameters updated:
increased long-term stability of the calibration

Apr'13 – Spectral response functions updated:
very small effect

- Unexpected transient F factor increase (up to 1%) in early 2014

Automated Radiometric Calibration

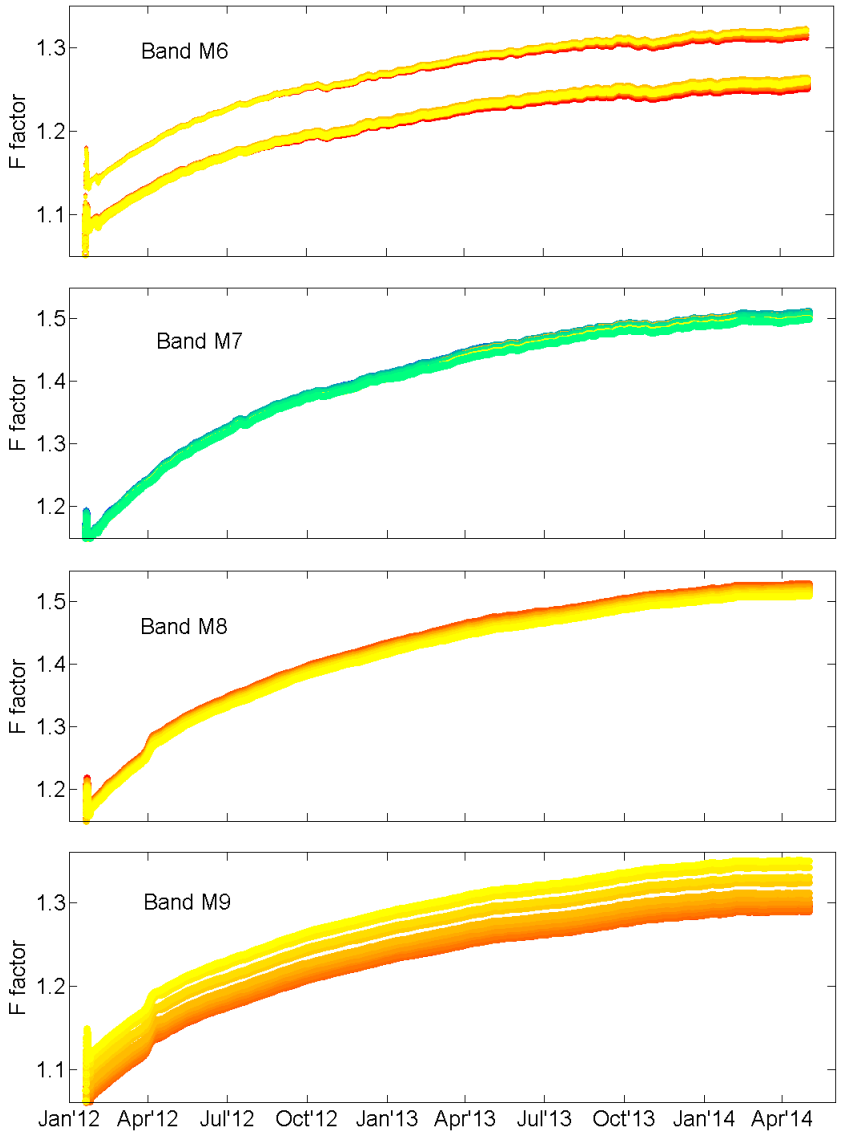

- An automated calibration procedure has been implemented in the IDPS software to update the F factor predictions after every orbit, instead of every week

  Rausch, K., Houchin, S., Cardema, J., Moy, G., Haas, E., De Luccia, F.J., *J. Geophys. Res. Atmos.*, **118** (2013) 13,434-13,442

- The F factors calculated by the automated procedure have not been used yet in the operational production of the VIIRS SDR
- We have used the upgraded software to reprocess the solar calibration data from the first two years of the Suomi NPP mission
- For the bands affected by the telescope degradation, the F factor changes predicted by the automated procedure agree well with the operational F factors

Improved Calibration Stability

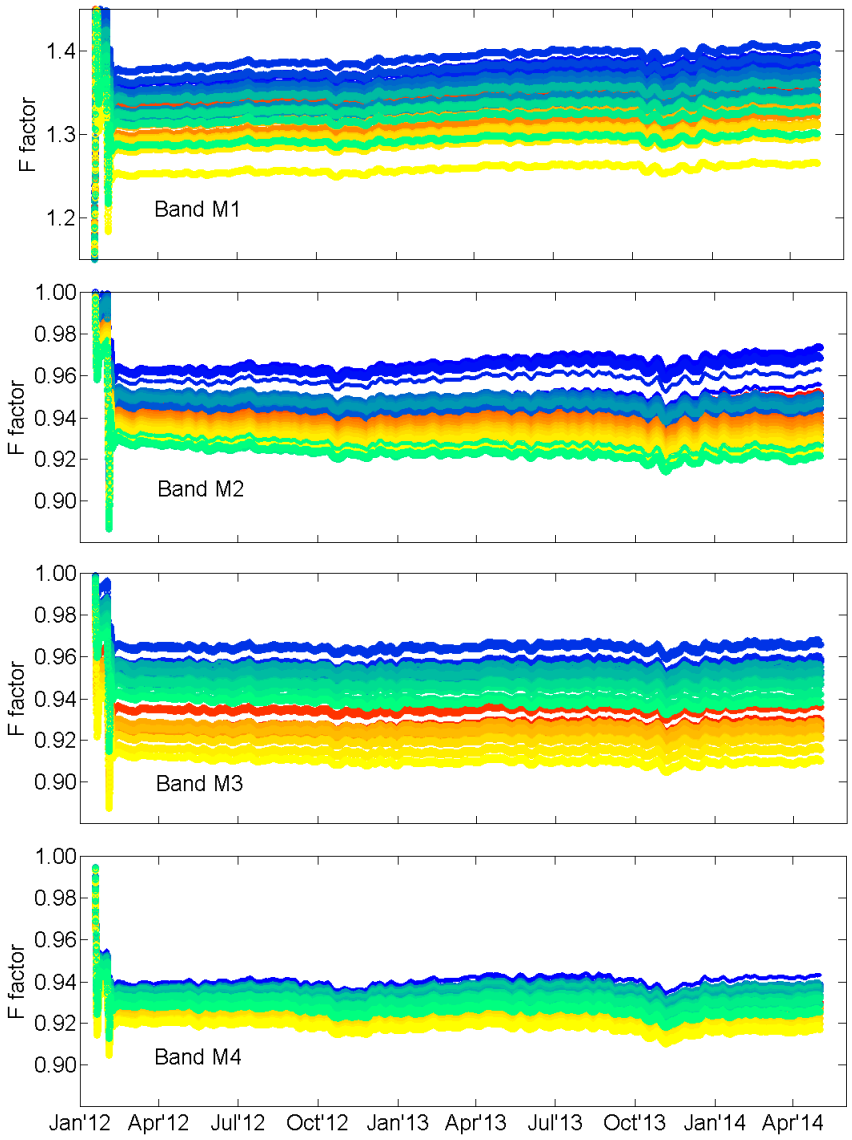

- For the bands not significantly affected by the telescope degradation, the automated calibration procedure improves long-term stability of the predicted F factors
- Even with the current set of the processing parameters (look-up tables), the predicted long-term changes of the F factors are either slow or non-existent
- Periods from October to December of each year are exceptions due to the limited number of valid solar diffuser reflectance measurements
- Although further improvements are still needed, the automated calibration procedure, when applied, would already improve the SDR products

Calibration Trend Change

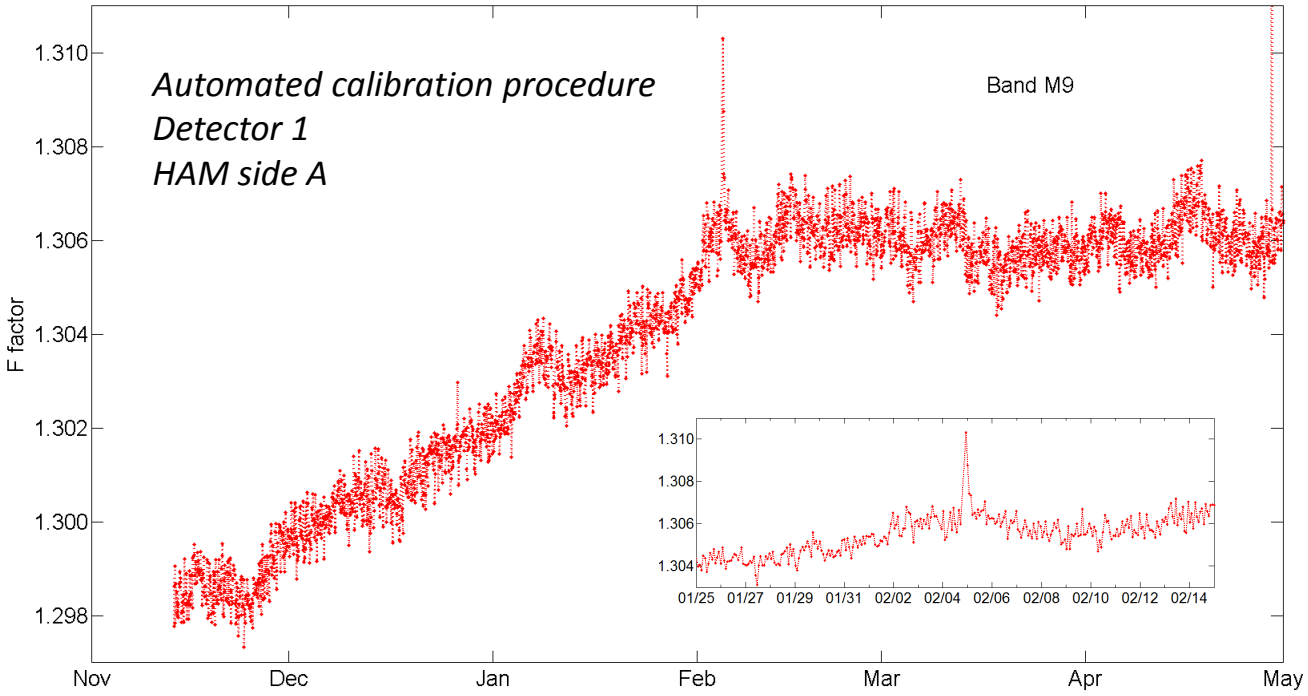

- On February 4, 2014, VIIRS single-board computer lockup anomaly occurred and lasted longer than one orbit
- Following recovery from the anomaly (marked by the spike in the M9 F factors: see the insert graph), the F factor trends have changed

- Despite fluctuations in the calculated F factor values, it is clear that the F factors for the SWIR bands are no longer increasing due to the telescope throughput degradation (note that solar diffuser reflectance is assumed constant for the SWIR bands)
- The telescope degradation may have stopped if during the February 4 anomaly the telescope mirrors temperature increased enough to “bake out” water ice that after the UV photolysis was providing protons for the tungsten oxide color center formation

Solar Diffuser Degradation Trend

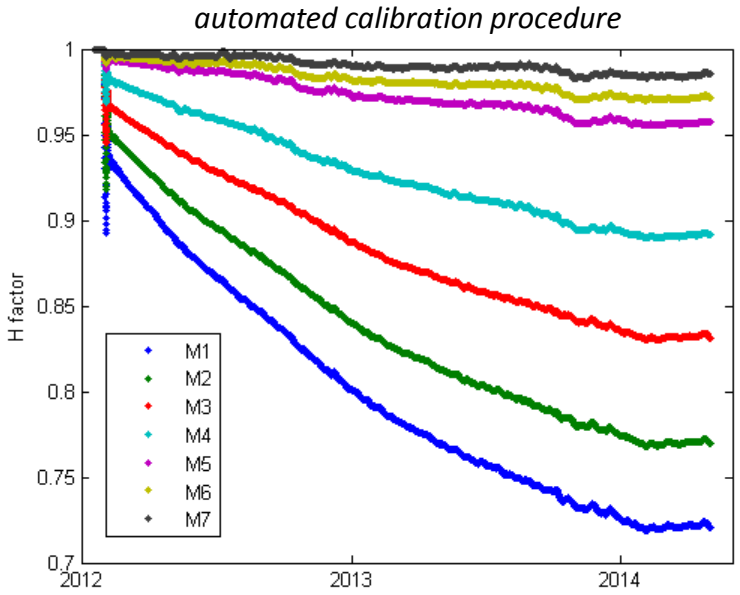

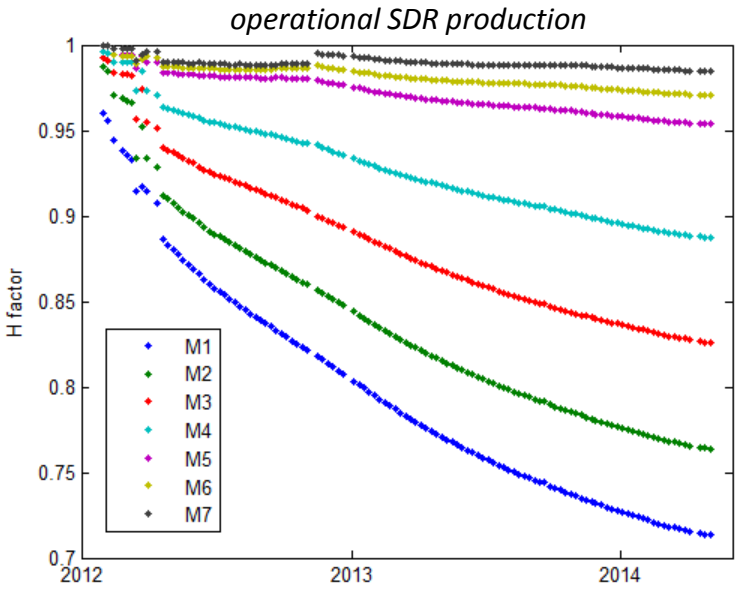

- When the solar diffuser monitoring data are analyzed with the automated calibration procedure, the reflectance degradation trend changes in February 2014: the decrease has diminished
- If during the February 4 anomaly the solar diffuser temperature increased above ~360 K, the hydrocarbons that cause the degradation may have been baked out (in vacuum)

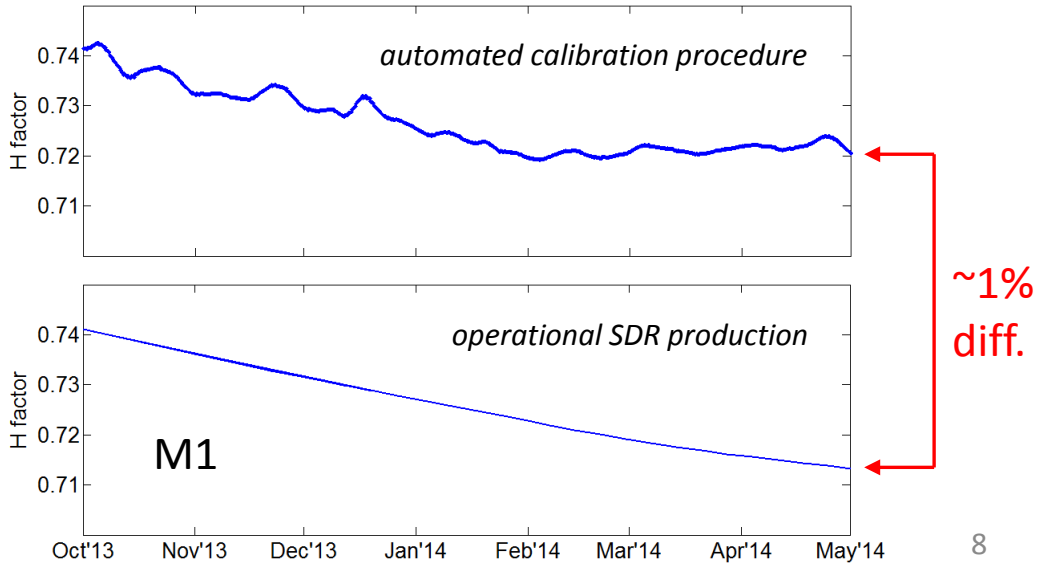

Effects on Radiometric Calibration

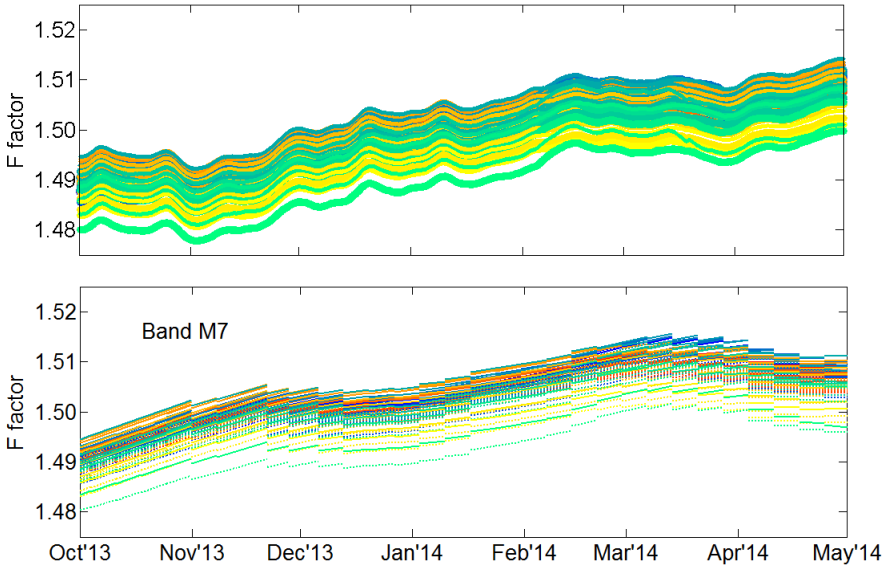

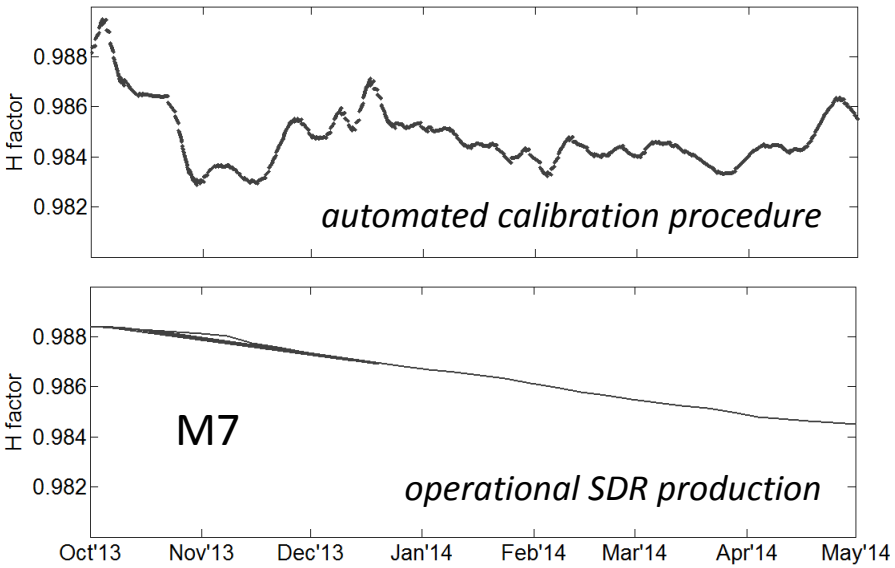

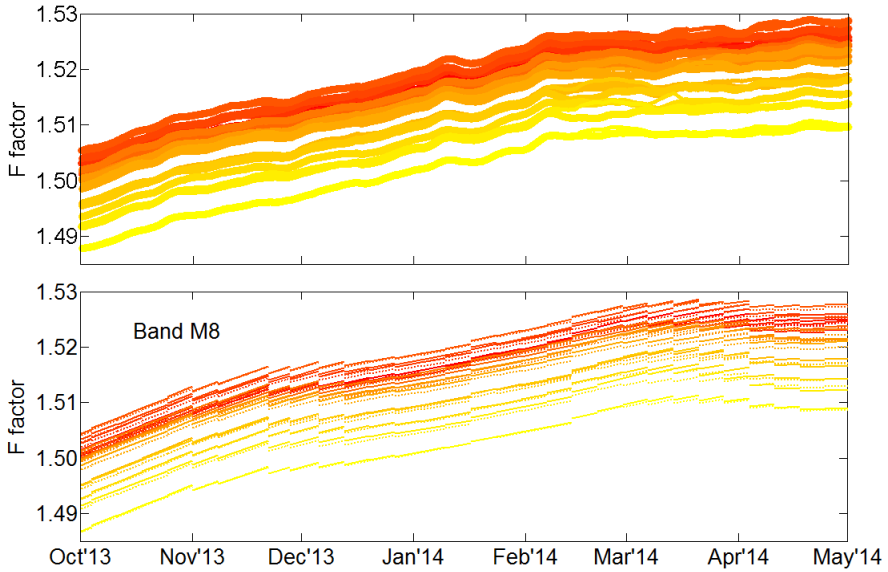

- For the bands not corrected by the H factors (SWIR), the automated procedure calibration responded more timely to the calibration trend changes
- Additionally, for the bands corrected by the H factors, the automated procedure responded better to the changes in the solar diffuser degradation

Summary

- Radiometric calibration applied to the VIIRS RSB measurements for the SDR production has been improved several times since the launch of the Suomi NPP satellite: updates of the processing parameters improved stability of the radiometric calibration between 2012 and 2013
- A new, automated procedure derives the coefficients once per orbit from the onboard solar diffuser measurements: calibration coefficients derived by the automated procedure appear even more stable throughout duration of the mission
- Implementation of the automated calibration procedure in the operational SDR production is currently planned for June 2014, but it should proceed as soon as effects of the VIIRS-SDR-DELTA-C-LUT update on May 1, 2014 stabilize
- The automated calibration procedure also appears to provide a better response to the calibration trend changes occurring since February 2014

Reducing Onboard Calibration Uncertainties for S-NPP VIIRS RSB

Jack Xiong[1], Jon Fulbright[2], Ning Lei[2], Zhipeng Wang[2]

Jeff McIntire[2], Boryana Efremova[2], and Vincent Chiang[2]

1. NASA GSFC; 2. Sigma Space Corp.

Acknowledgements:

VIIRS Characterization Support Team (VCST), NASA GSFC

S-NPP/JPSS VIIRS SDR Team

MODIS Characterization Support Team (MCST), NASA GSFC

Outline

- **Background**
- **RSB On-orbit Calibration**
- **Calibration Improvements and Discussions**
  - New SD and SDSM screen transmission (or VF)
  - Correction for the solar vector error
  - Impact assessment due to modulated RSR and mitigation strategy
  - Lunar calibration improvement (working with USGS and CNES)
  - SWIR Calibration (MODIS lessons)
- **Future Work and Summary**

Background

Visible Infrared Imaging Radiometer Suite (VIIRS)

- **Key instrument on S-NPP and future JPSS satellites**
  - S-NPP launched on October 28, 2011
  - JPSS-1 launch in 2017
    - Sensor ambient phase 1&2 completed
    - Sensor TVAC testing in July, 2014
- **Strong MODIS heritage**
  - Spectral band selection
  - On-board calibrators
  - Operation and calibration
    - Strategies for planning/scheduling
    - Data analysis methodologies / tools

S-NPP VIIRS provides linkage btw EOS (MODIS) and future JPSS (VIIRS) and extends long-term data records for studies for the Earth's land, oceans, and atmosphere

VIIRS On-board Calibrators (MODIS Heritage)

Solar Diffuser

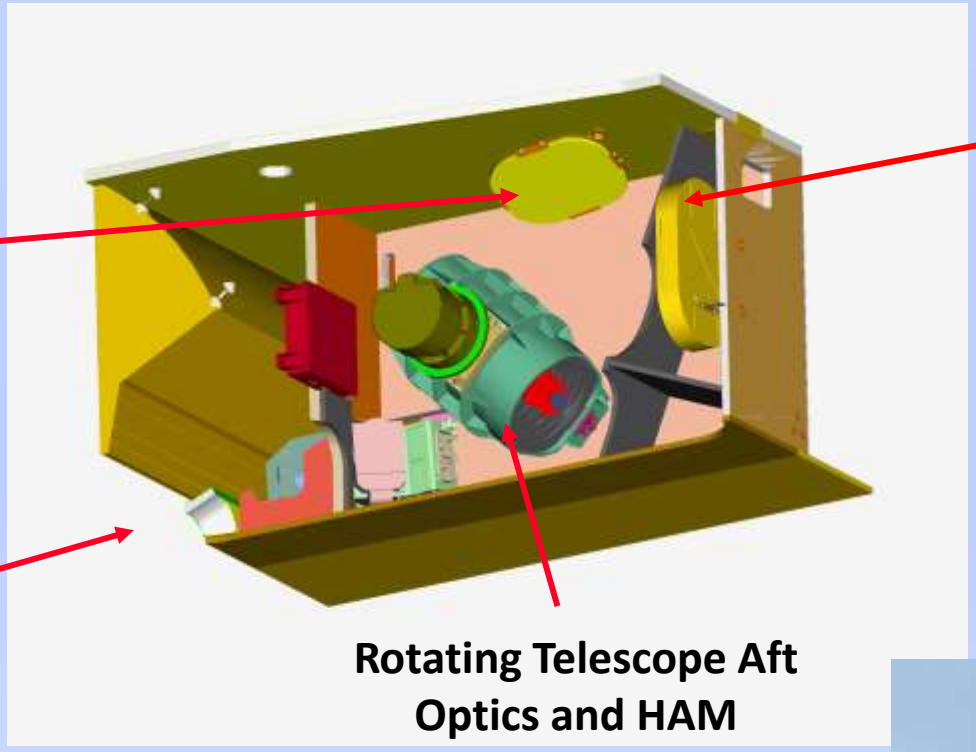

Rotating Telescope Aft Optics and HAM

Blackbody

Extended SV Port (Lunar Observations)

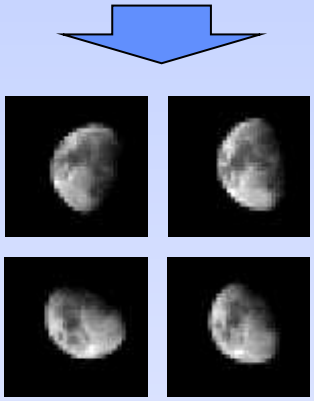

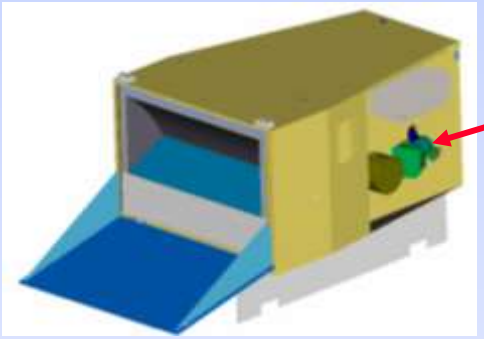

Solar Diffuser Stability Monitor

VIIRS RSB On-orbit Calibration

On-orbit Calibration Methodologies:

- **Solar Calibration (RSB)**
  - Quadratic calibration algorithm
  - Linear calibration coefficients derived/updated from SD observations
  - SD degradation tracked by SDSM
- **Lunar Calibration (RSB)**
  - Regularly scheduled at the “same” phase angles
  - Observed through instrument SV port with a data sector rotation
  - Implemented via S/C roll maneuvers (some constraints)
  - Referenced to the ROLO model (USGS)

Calibration Improvements and Discussions

- New SD and SDSM screen transmission (or VF)
- Correction for the solar vector error
- Impact assessment due to modulated RSR and mitigation strategy
- Lunar calibration improvement (working with USGS and CNES)
- SWIR Calibration (MODIS lessons)

New SD and SDSM Transmission Screens

Yaw maneuver solar angles (SDSM screen coord.)

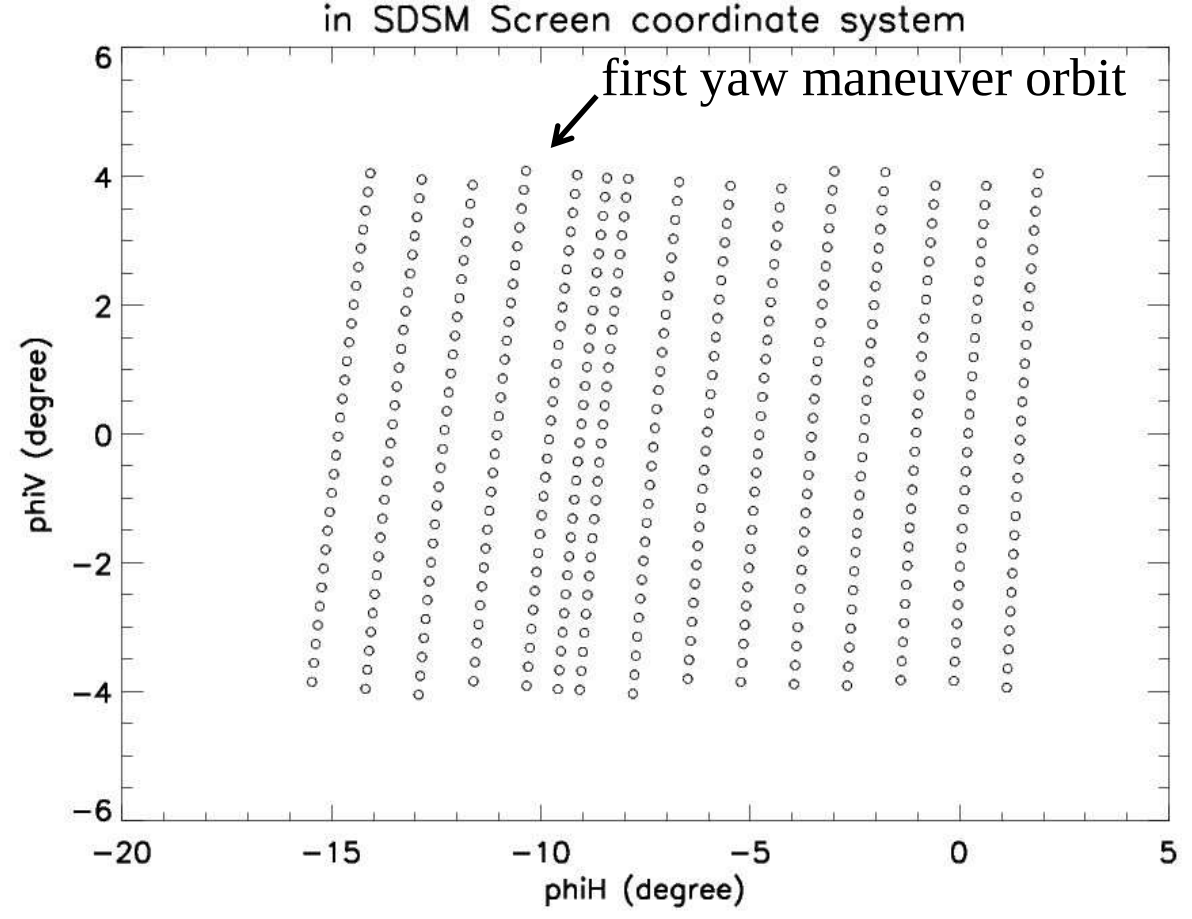

(when the SDSM sees the sun)

Large step size in phiH

Unable to resolve the screen transmittance in detail, resulting in large undulation in the H-factor

Regular on-orbit data

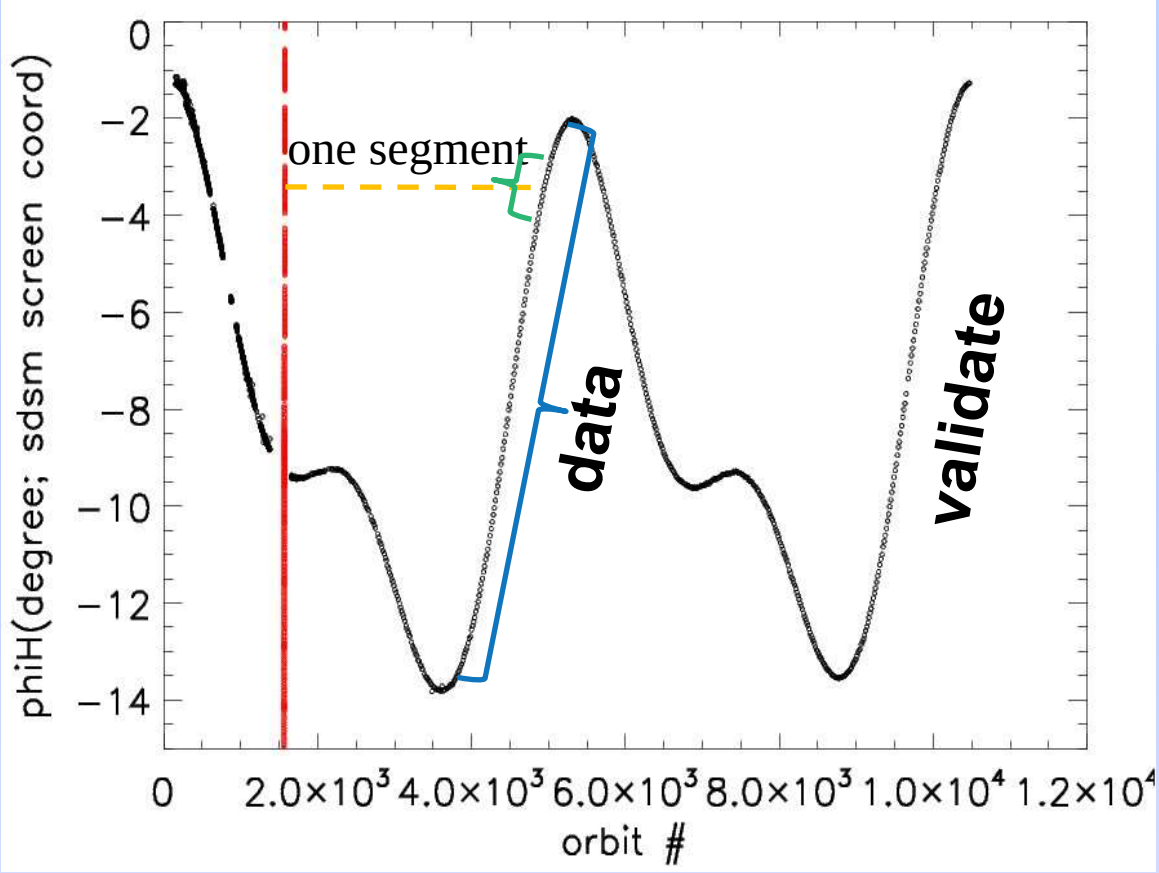

Very fine step size in phiH -> resolve the transmittance in detail

Procedure

(1) Divide the regular on-orbit data (~3-month) into segments with each covers **one yaw maneuver orbit in solar angles**

(2) Compute transmittance for each segment and interpolate the transmittance at the yaw maneuver solar angles

(3) Tau(yaw) and Tau(non-yaw) differ by a scale factor due to drifts in solar power and the SDSM detector gain, find the scale factor through a least-square fit**; multiply Tau(non-yaw) by the scale factor.**

(4) Combine tau (non-yaw) with linear adjustments.

Results

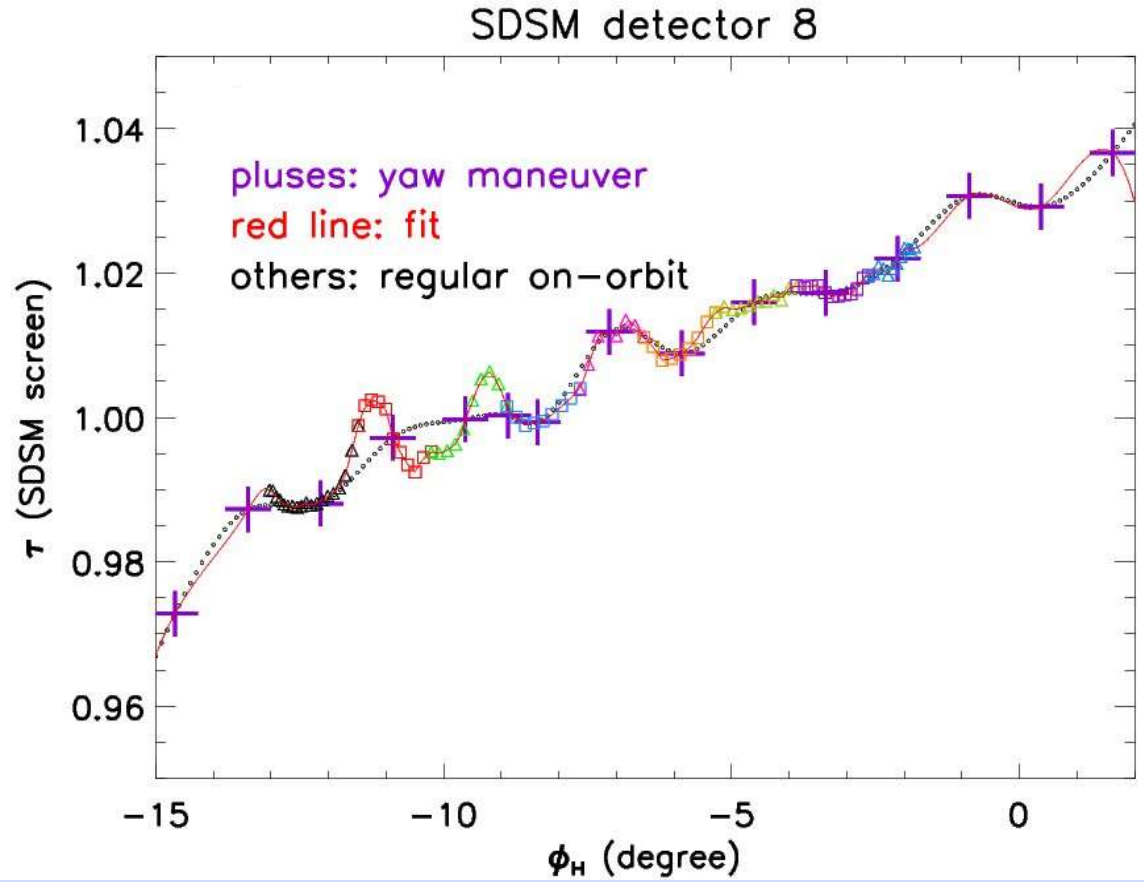

At phiV=0

Very fine details of transmittance revealed

Transmittance indicated by the red line is used to compute the H-factor

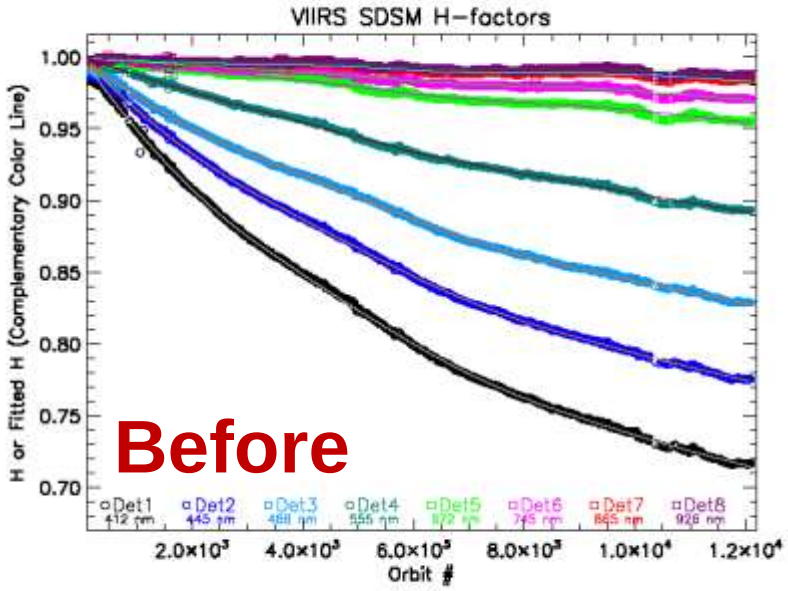
VIIRS SDSM H-factors
H or Fitted H (Complementary Color Line)
1.00
0.95
0.90
0.85
0.80
0.75
0.70
Before
Det1 412 nm
Det2 445 nm
Det3 488 nm
Det4 555 nm
Det5 672 nm
Det6 745 nm
Det7 865 nm
Det8 926 nm
2.0×10³
4.0×10³
6.0×10³
8.0×10³
1.0×10⁴
1.2×10⁴
Orbit #

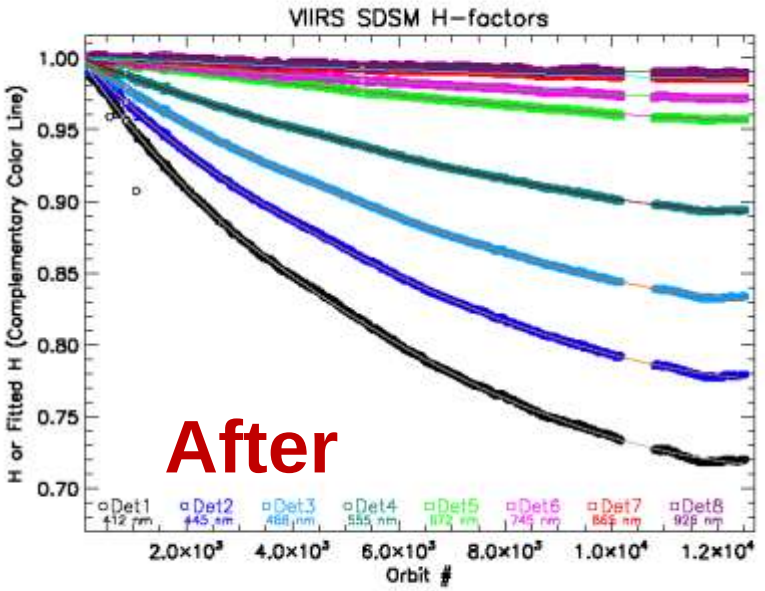
VIIRS SDSM H-factors
H or Fitted H (Complementary Color Line)
1.00
0.95
0.90
0.85
0.80
0.75
0.70
After
Det1 412 nm
Det2 445 nm
Det3 488 nm
Det4 555 nm
Det5 672 nm
Det6 745 nm
Det7 865 nm
Det8 926 nm
2.0×10³
4.0×10³
6.0×10³
8.0×10³
1.0×10⁴
1.2×10⁴
Orbit #

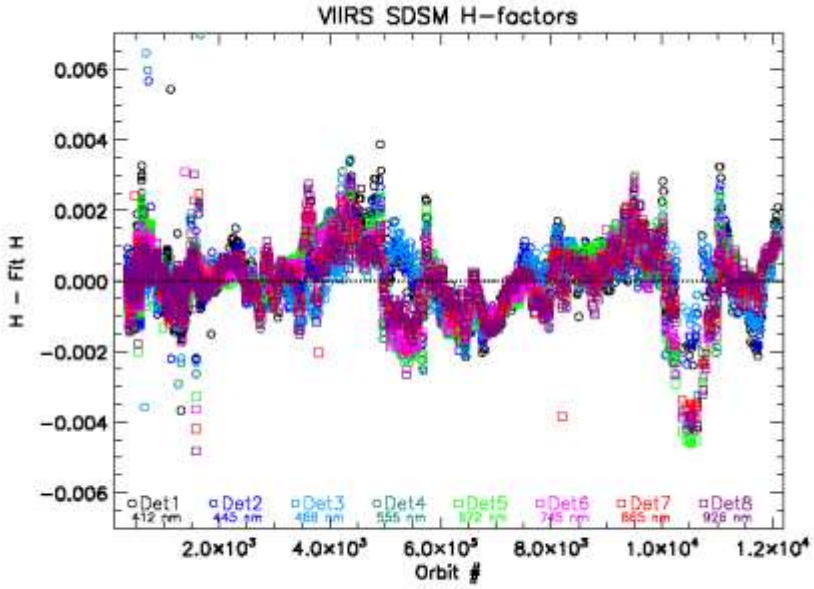
VIIRS SDSM H-factors
H - Fit H
0.006
0.004
0.002
0.000
−0.002
−0.004
−0.006
Det1 412 nm
Det2 445 nm
Det3 488 nm
Det4 555 nm
Det5 672 nm
Det6 745 nm
Det7 865 nm
Det8 926 nm
2.0×10³
4.0×10³
6.0×10³
8.0×10³
1.0×10⁴
1.2×10⁴
Orbit #

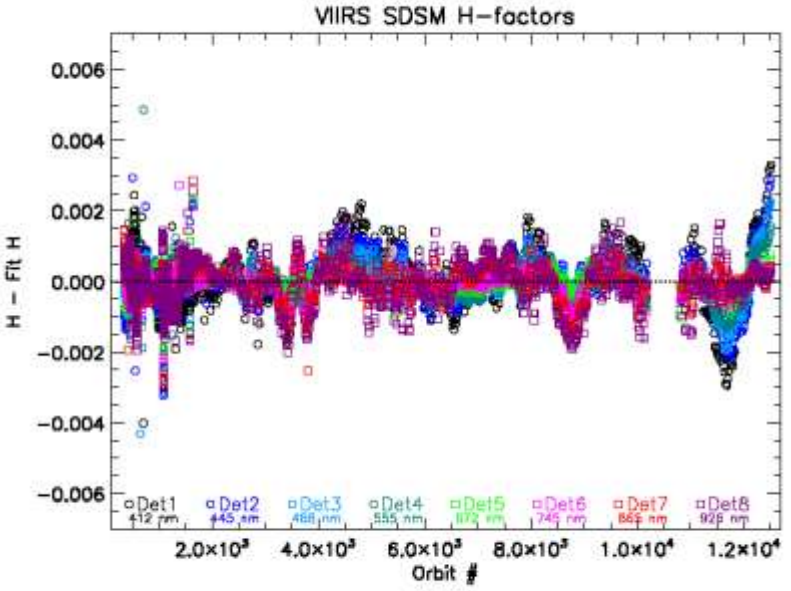
VIIRS SDSM H-factors
H - Fit H
0.006
0.004
0.002
0.000
−0.002
−0.004
−0.006
Det1 412 nm
Det2 445 nm
Det3 488 nm
Det4 555 nm
Det5 672 nm
Det6 745 nm
Det7 865 nm
Det8 926 nm
2.0×10³
4.0×10³
6.0×10³
8.0×10³
1.0×10⁴
1.2×10⁴
Orbit #

Correction for the Solar Vector Error

Solar Vector Correction

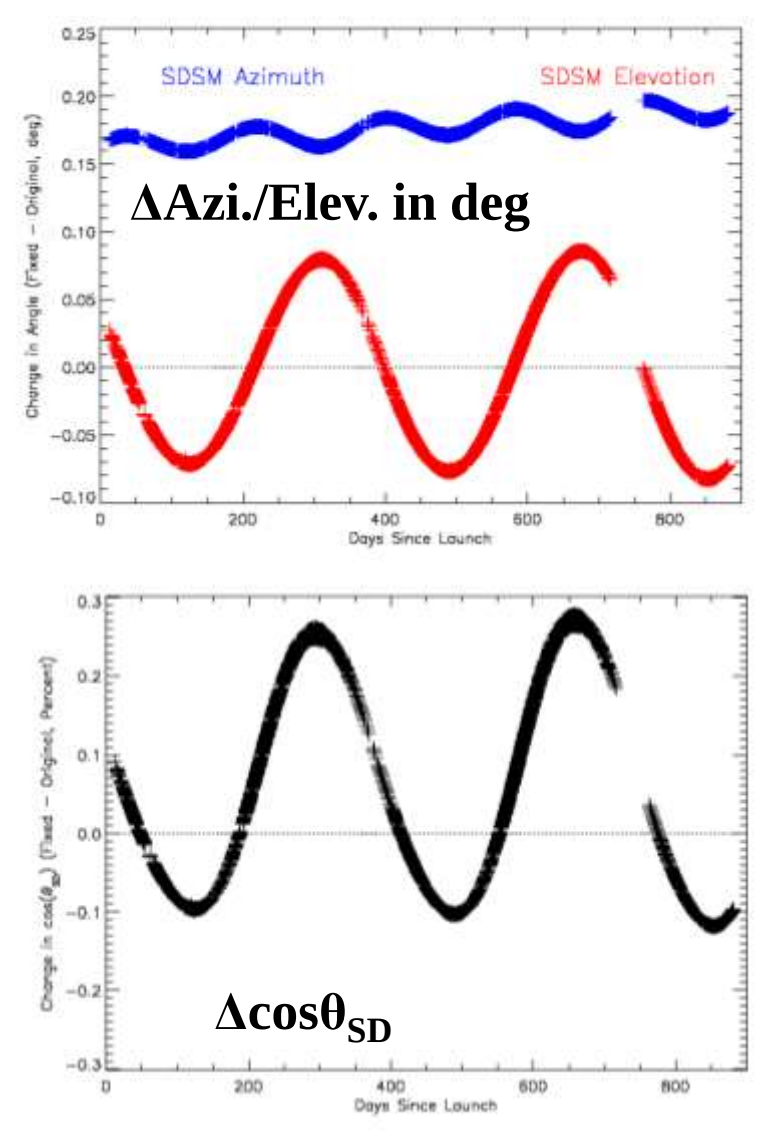

- A problem in the application of the Common GEO library leads to a slight, but important (~0.2 deg.) error in the solar angles used in the RSB radiometric calibration.
- The problem has been identified (mismatch of ECI frames when computing the transformation to spacecraft coordinates), the CRR has been submitted, and the effects on the radiometric calibration has been evaluated.

Solar Vector Correction

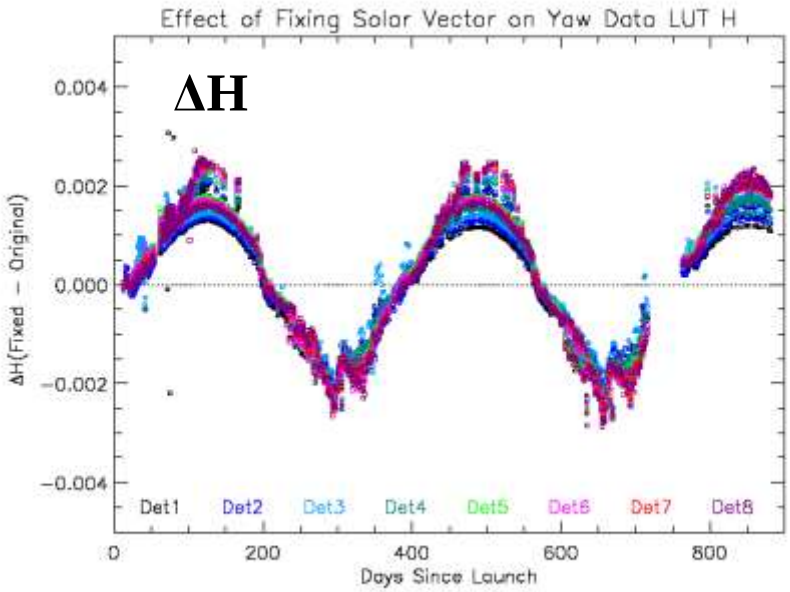

- After the corrected solar vector is used to re-evaluate the entire algorithm (including developing a new screen based on the new solar vectors).

- The change in the H-factors are mainly due to the change of the $1/\cos \theta_{SD}$ term in the calculation.

Solar Vector Correction

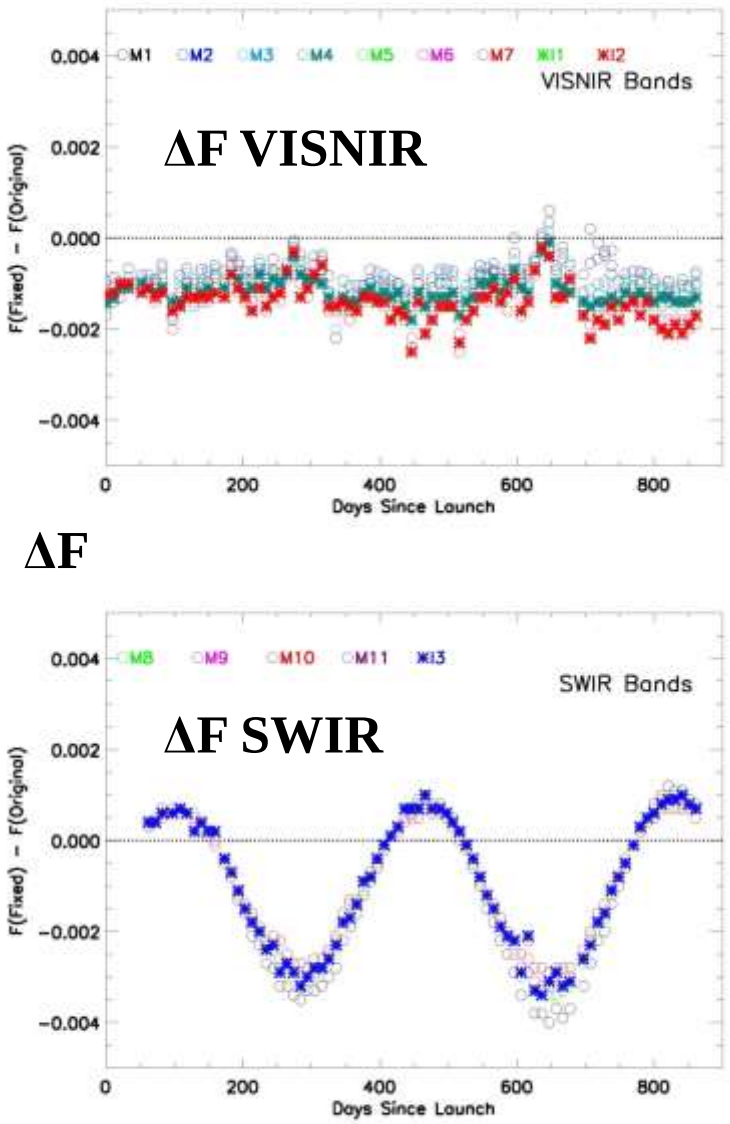

- Same end-to-end reanalysis applied for the F-factors, too.
- The VISNIR F-factors have a cos θ_{SD} term which cancels the effect from the H-factors.
- For the SWIR bands, H = 1 by definition, so the cos θ_{SD} term is not cancelled out. This seasonal oscillation of ~0.5% can is in the uncorrected F-factors, but is small compared to the overall change in F.

RSR Modulation Impact Assessment

Modulated RSR

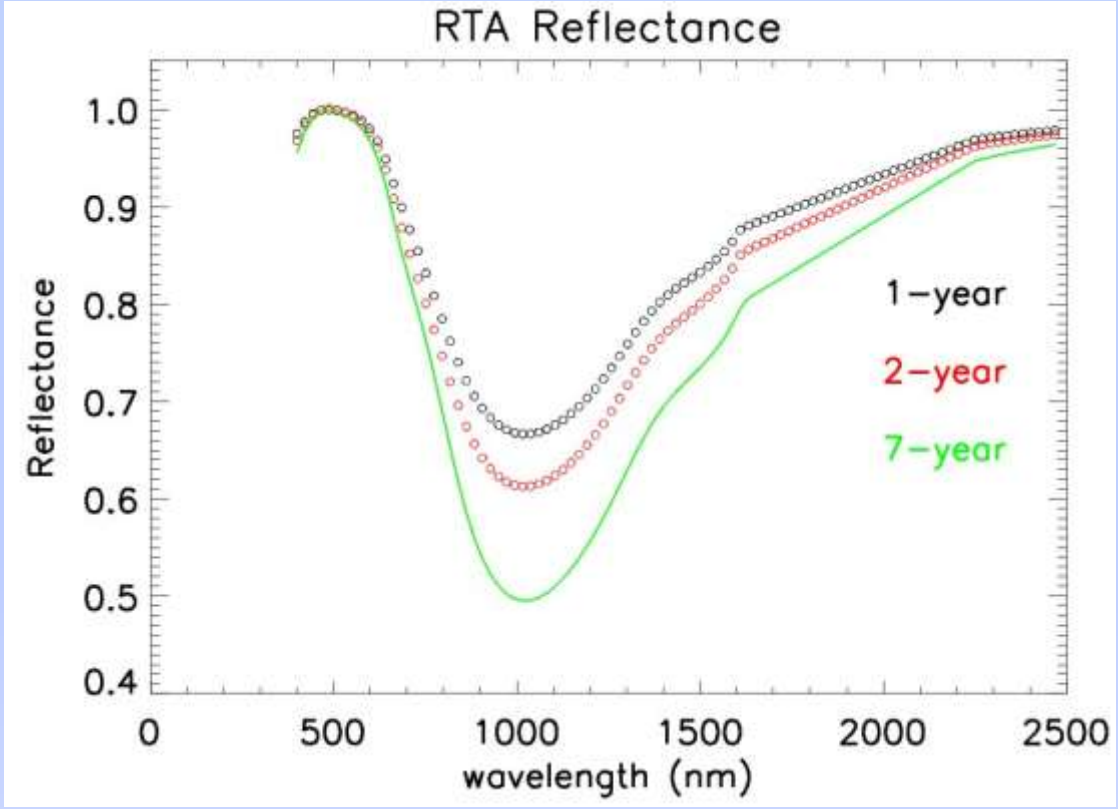

strong wavelength dependent

affect detector relative spectral response

$$RSR_{\text{modulated}}(\lambda,t)=\frac{RSR_{\text{original}}(\lambda)D(\lambda,t)}{\max\left(RSR_{\text{original}}(\lambda)D(\lambda,t)\right)}$$

Additional data from VIIRS improves the prediction of end-of-life performance; convergence in prediction indicates greater accuracy.

Impact of λ-dependent Changes in Detector Response

Mirror Degradation Impact on Sensor Relative Spectral Response

λ dependent optics degradation

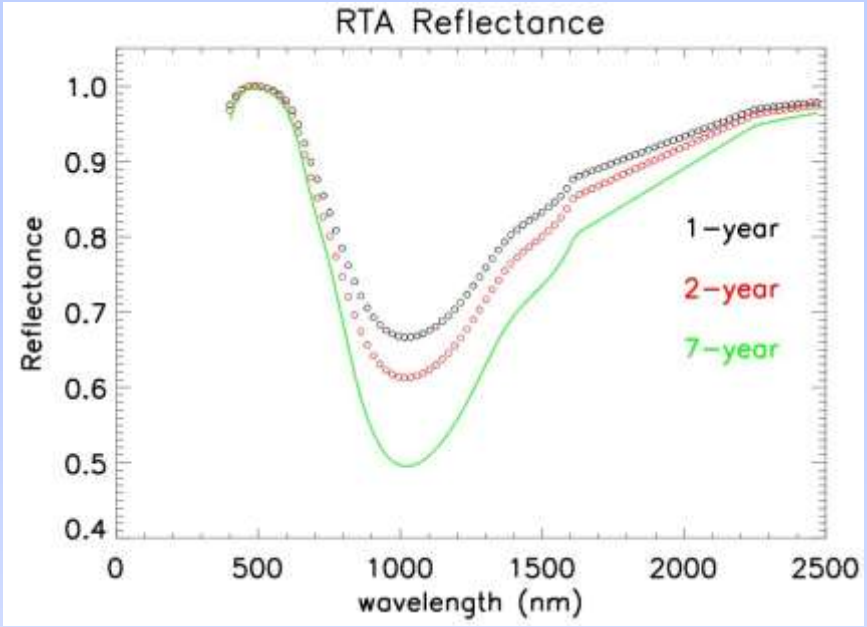

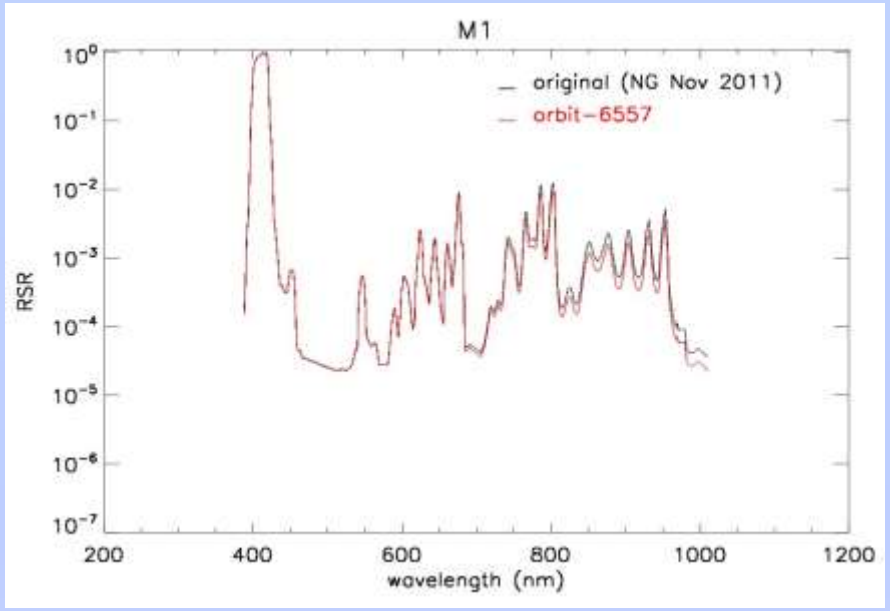

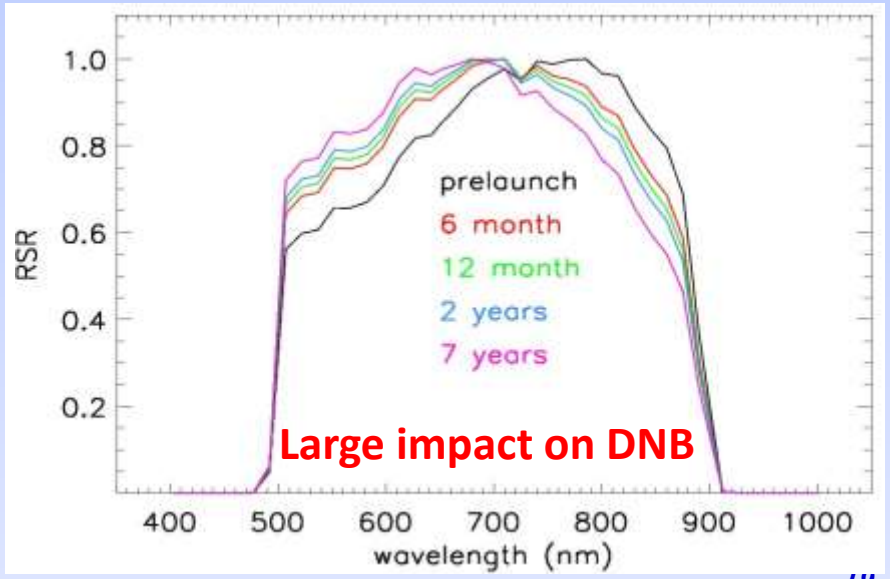

Modulate RSR has been applied to VIIRS calibration and data production

Lunar Calibration (Trending) Improvements

Lunar Trending Improvements

- Lunar observations are not part of the primary calibration of the VIIRS RSB, but they are an important way to verify and improve the RSB calibration.
- There have been 22 scheduled lunar observations that have provided radiometric data (4 Jan 2012 to 10 May 2014).
- Over 70 “unscheduled” serendipitous lunar observations can be analyzed for additional data points.

$$F_{Moon} = \frac{I_{ROLO}}{I_{Pre\_Launch}} = \frac{I_{ROLO}}{\sum\left(c_0 + c_1 dn + c_2 dn^2\right)}$$

where:

- Summation is over all scans, samples, and detectors,
- c_i coefficients are the temperature-corrected pre-launch values,
- I_{ROLO} is the event-specific ROLO model radiance (T. Stone).

Lunar Trending Improvements

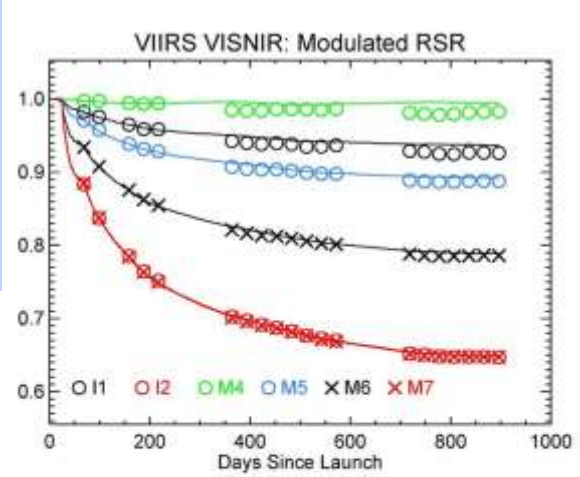

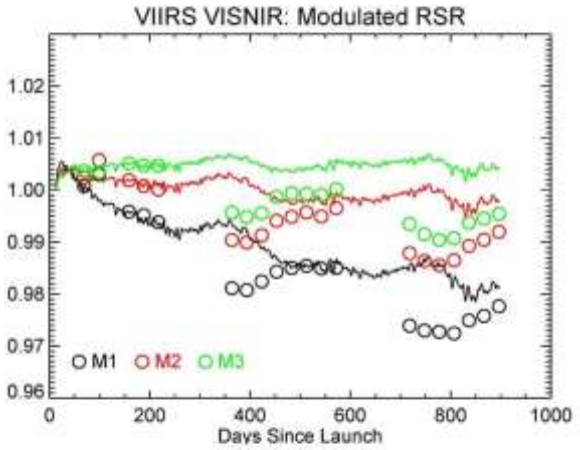

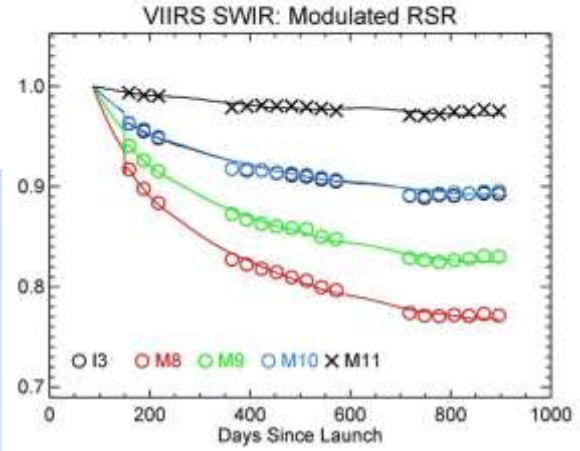

1/F-factor (Norm. to 2011-11-08)

The present comparison shows good general agreement between the SD gain (=1/F; lines) and the lunar gain (symbols).

Seasonal variations are apparent, especially in the blue VISNIR bands (M1, M2 and M3). This is NOT corrected by the solar vector fix, but there appear to be (equal? opposite?) seasonal effects in both gains.

Tom Stone (USGS) and CNES are working together to improve the ROLO model, but it is our job to continually improve the VIIRS calibration using the best science available.

Lunar Trending Improvements

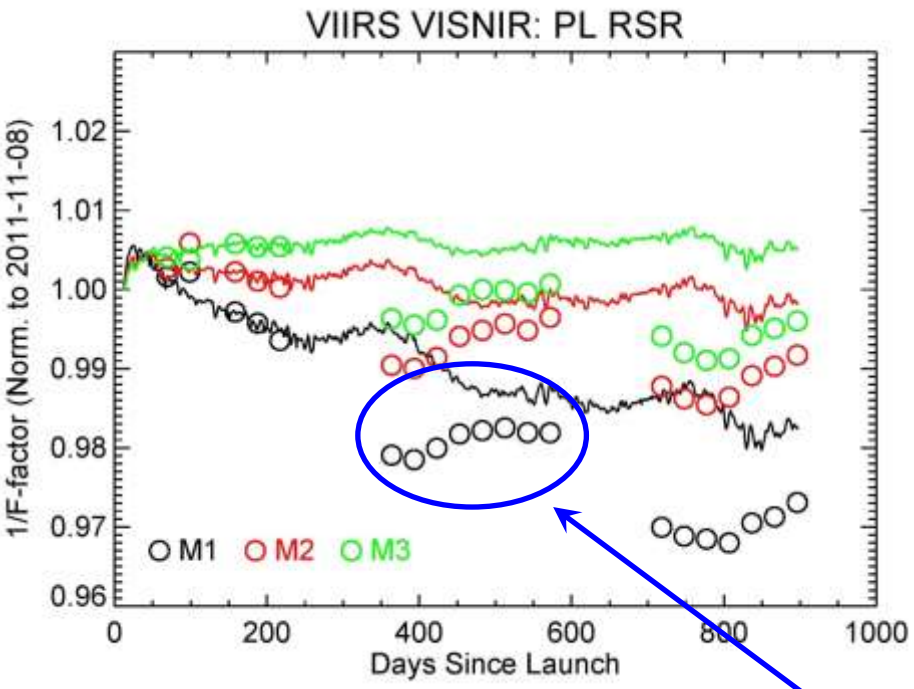

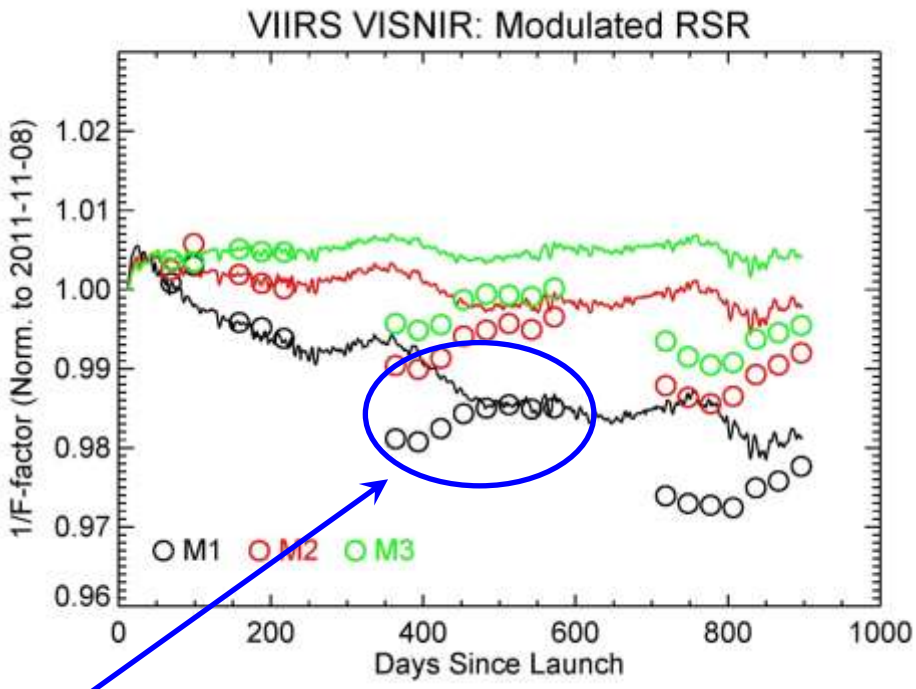

Incorporating modulated RSRs into both the SD and lunar calibration (in the ROLO models) improved the agreement. This supports the use of modulated RSRs in the calibration.

Lunar Trending Improvements

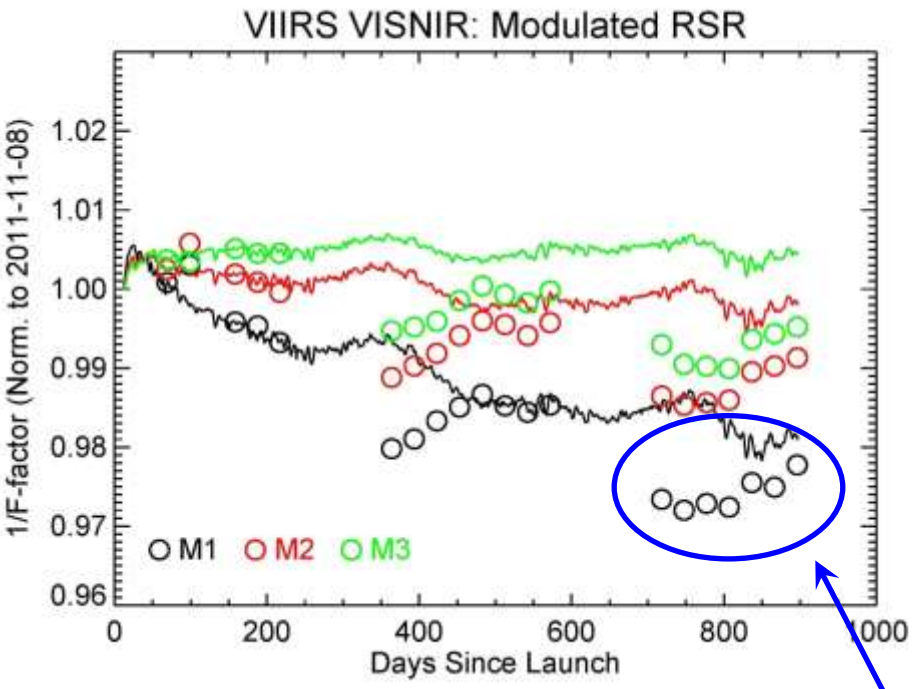

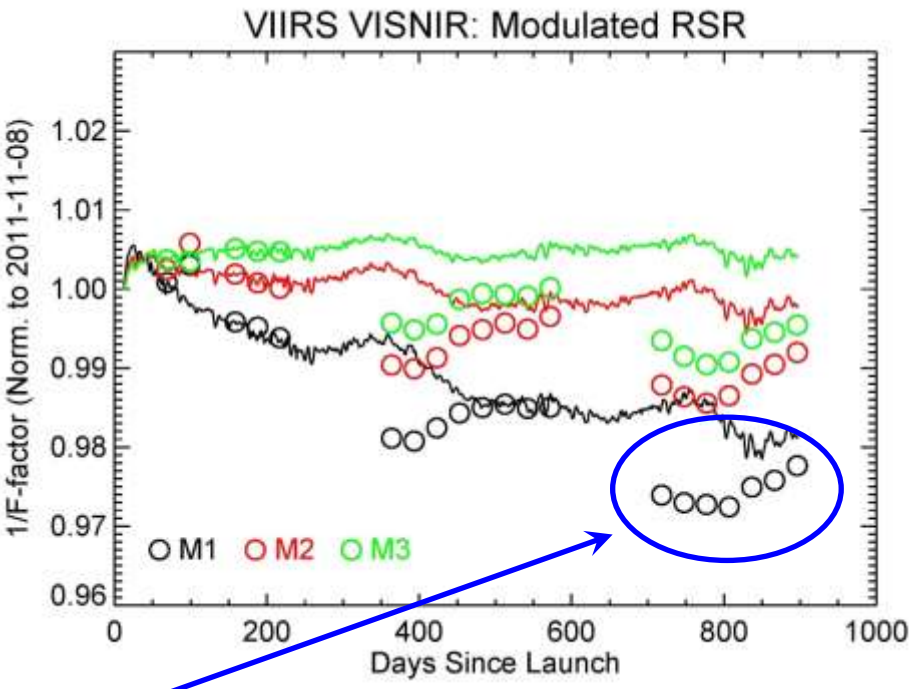

Improvements in the processing of the lunar data (in this case incorporating more scans into the analysis) has improved the internal uncertainties.

SWIR:
Effects due SD Degradation

SWIR-band SD Degradation

- **Current calibration assumes SD degradation beyond ~926 nm is extremely small and can be ignored (e.g., H = 1).**
  - The measured H-factor at 926 nm is measured to be 0.991, so SD degradation at SWIR wavelength is slowly occurring.
- **MODIS RSB calibration performed using a SD with its degradation monitored using the SDSM (wavelength coverage:412-936 nm)**
  - Terra SDSM D9 (936 nm) change over ~14 years on-orbit is measured to be ~2.3%. Aqua SDSM D9 change over ~12 years is 0.6%.
  - MCST has implemented a correction for Band 5 (1.24 µm) using pseudo-invariant desert targets and find a 1.5% degradation in Band 5 for Terra and a <0.3% degradation for Aqua.
  - Data from Deep Convective Cloud (DCC; data courtesy David Doelling/Raj Bhatt, NASA Langley) backs up the desert site results.
- **If the same trend holds for VIIRS, the H-factor for the M8 band should be around 0.4% or less, but the ground-site trending is not sensitive enough, *yet*. VCST will closely monitor and accurately quantify the correction for M8**

SWIR-band SD Degradation

MODIS Terra and Aqua

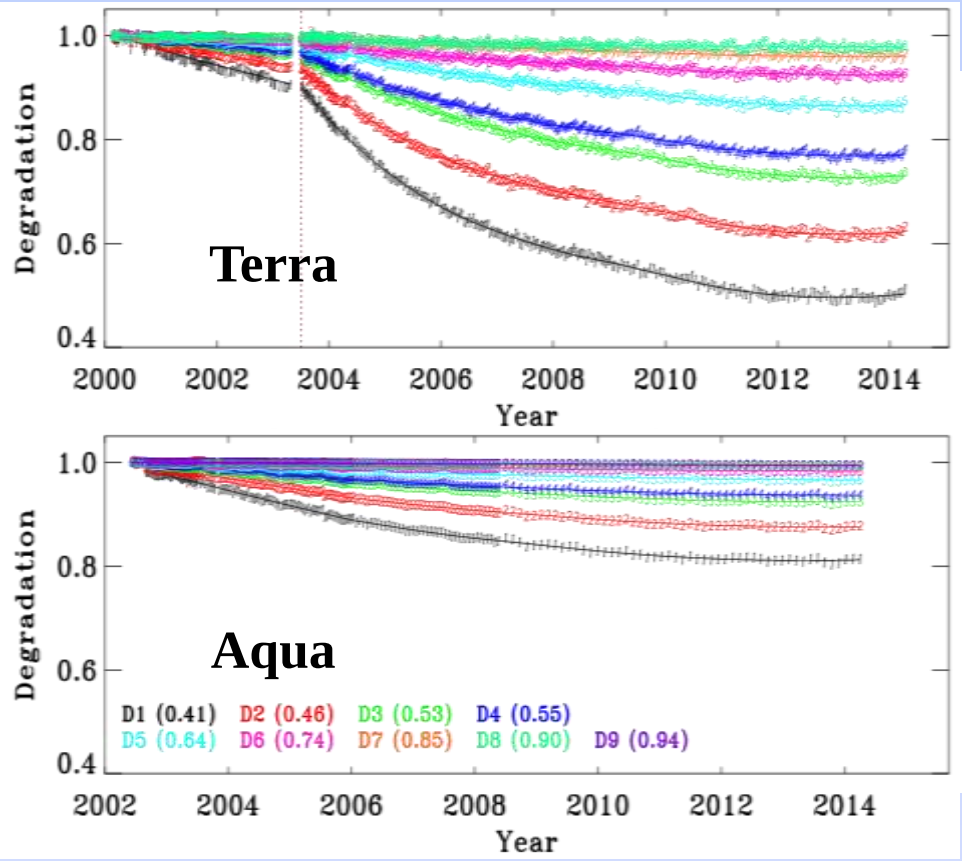

S-NPP VIIRS

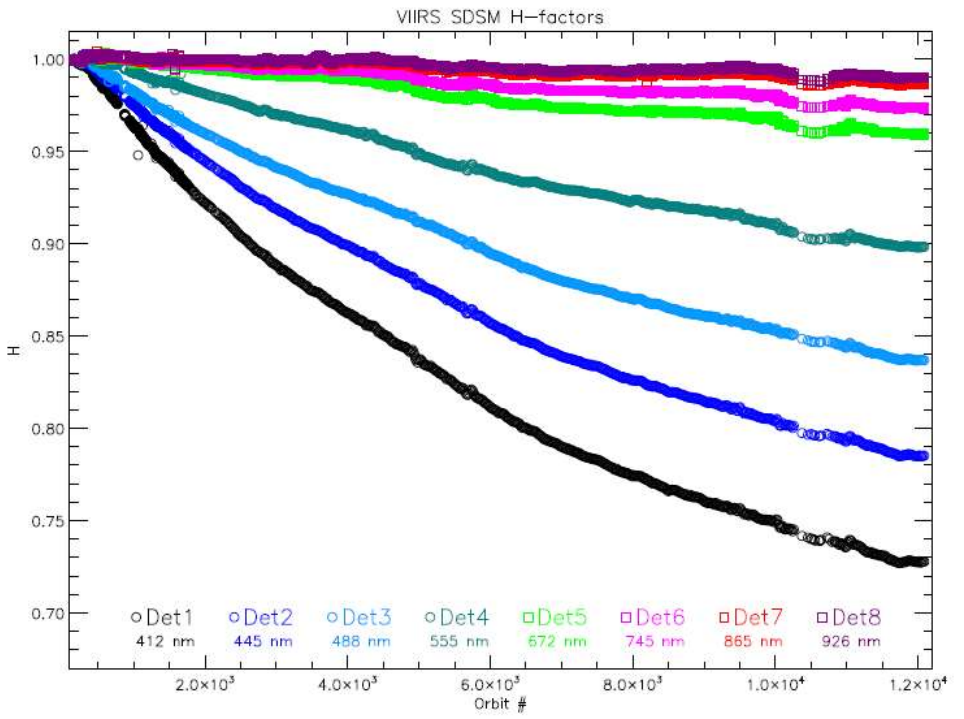

D9 Degradation (936 nm):
Terra 2.3%
Aqua 0.6%

D8 Degradation (926 nm):
S-NPP 0.9%

EV-based Evaluation of Terra Band 5 Response

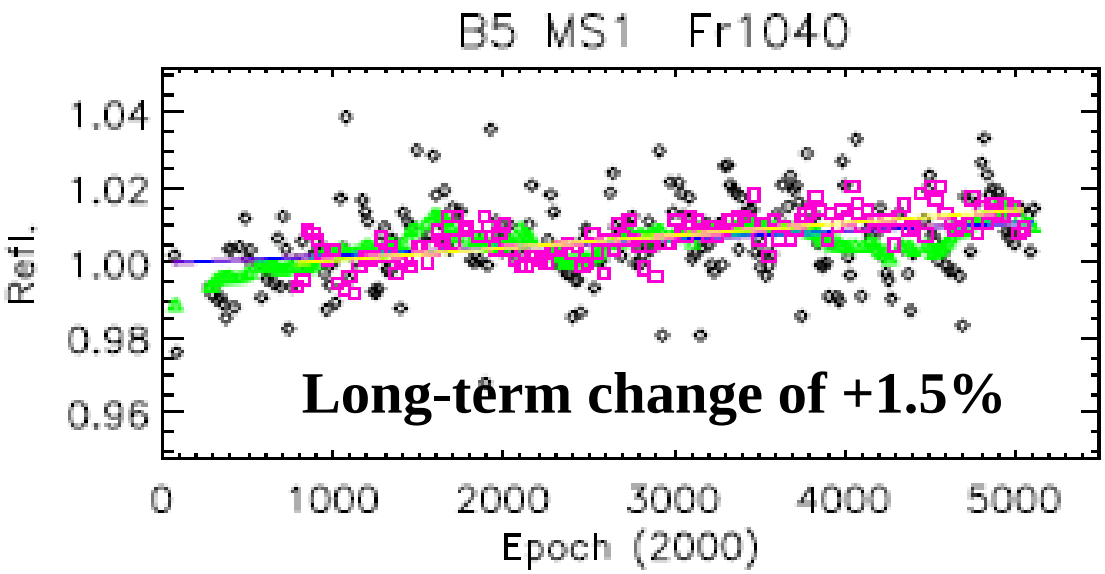

TOA EV reflectance from Libya 4 (BRDF correction applied)

Moving window yearly average of the TOA reflectance trends

DCC trends

Measurements normalized to the first points of the fitted curves

Correction for the upper drift in Terra B5 to be applied in C6

Future Work and Summary

- **Finalize and Implement Solar Vector Correction in RSB Calibration**
  - Further improvements of SD VF for F-factor computation
  - Use in reprocessing mission data
- **Understand and Resolve SD and Lunar Calibration Difference**
- **Monitor and Improve SWIR Calibration (as needed)**
- **Track and Study Potential Changes in RSB RVS (not covered here)**
- **Overall VIIRS RSB Calibration Meet the Design Requirements**
  - Constant improvements
  - Dedicated calibration and monitoring effort
  - Collaboration and independent assessments
  - Interaction with science community and other sensor calibration team, such as MCST

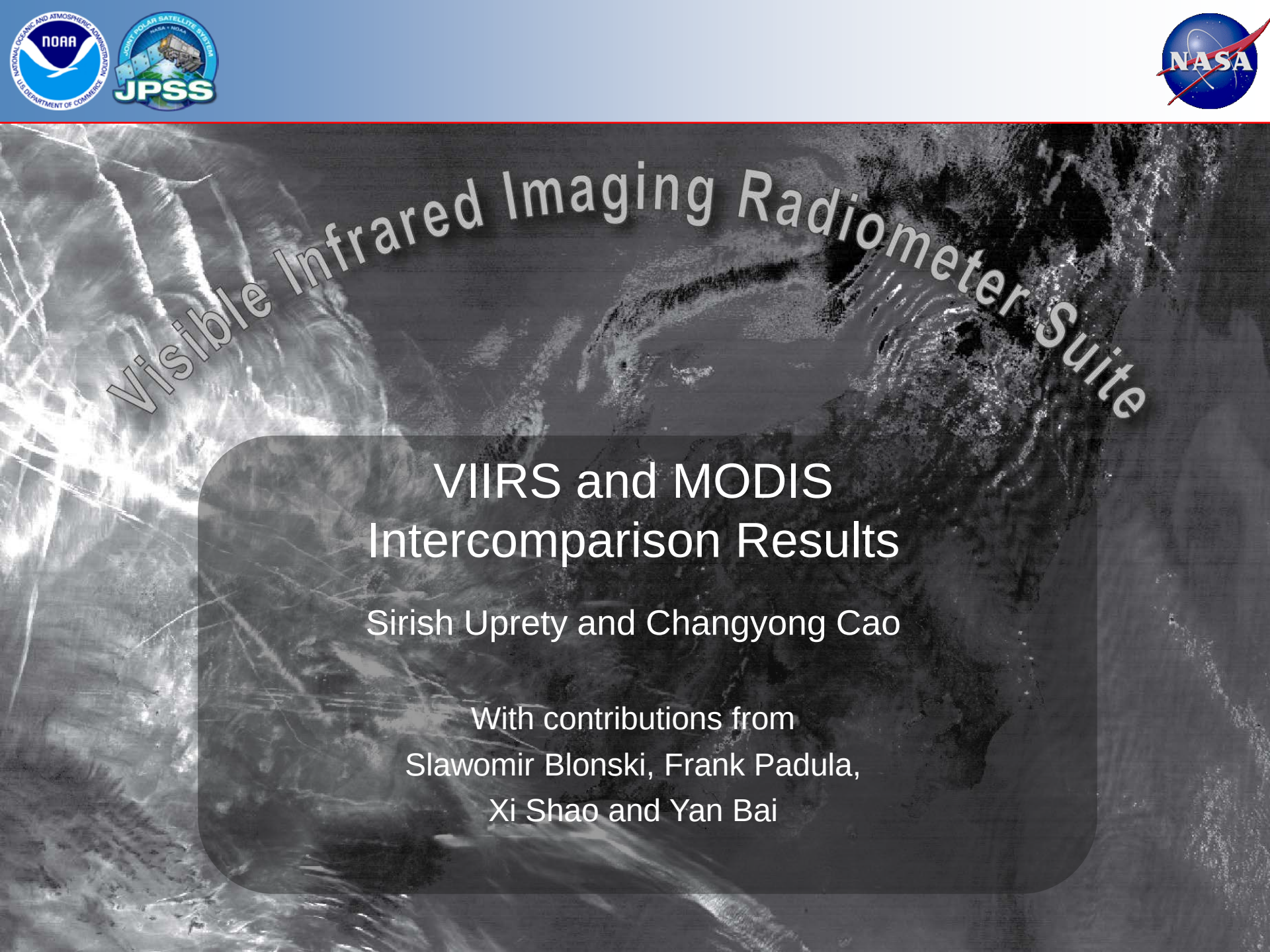

VIIRS and MODIS Intercomparison Results

Sirish Uprety and Changyong Cao

With contributions from
Slawomir Blonski, Frank Padula,
Xi Shao and Yan Bai

Outline

- Background
- S-NPP VIIRS and AQUA MODIS bands
  - Matching bands
  - Spectral bias over ocean and desert
- On-orbit intercomparison results
  - Radiometric bias over ocean and desert using SNO-x
  - Off-nadir comparison
- Summary

Objective

- To valuate the radiometric stability and accuracy of VIIRS RSB.

Background

- Degradation of satellite instruments over time is a common phenomena.
- Stability/characterization of sensors are critical to provide radiometrically accurate and consistent data products.
- VIIRS and MODIS sensors are compared at overlapping regions of extended SNO orbits over ocean and North African deserts to assess radiometric bias.
- The major uncertainties can be due to,
  - cloud movement, residual cloud contamination and cloud shadow
  - sun glint over ocean surface
  - BRDF and atmospheric absorption variability
  - spectral differences
  - co-location errors
  - very low signal strength for some channels over ocean (M5, M6 and M7: Radiance < ~20 w/m2-sr-μm)

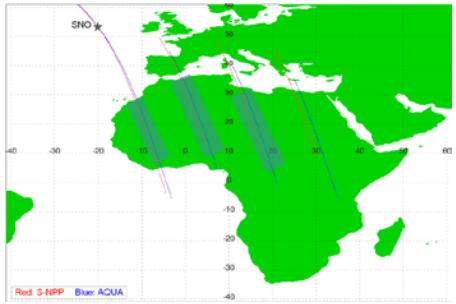

VIIRS and MODIS Matching Bands and Spectral Bias

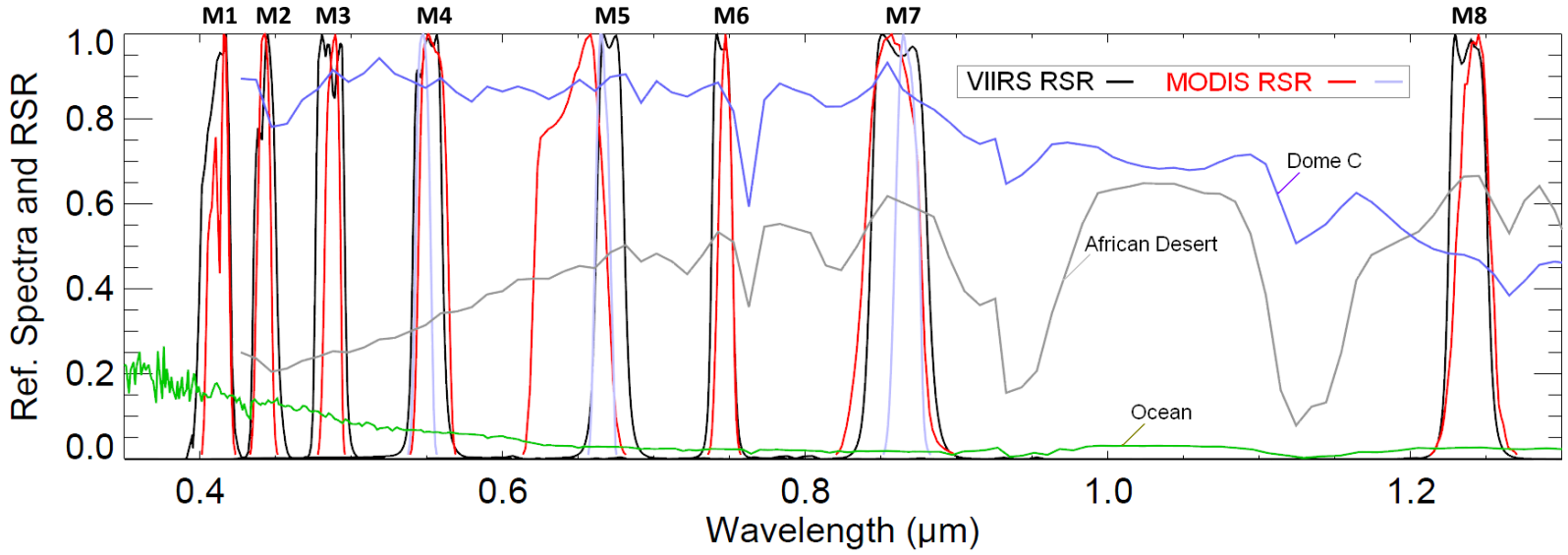

VIIRS	Desert Bias (V-M)×100%/M		Ocean Bias (V-M)×100%/M	
	Hyperion	MODTRAN	AVIRIS	*MODTRAN*
M-1	-	-0.26%	-1.10%	-1.40%
M-2	-0.94% ± 0.03%	0.01%	0.52%	0.70%
M-3	-0.47% ± 0.07 %	0.00%	-0.45%	0.36%
M-4	-1.63% ± 0.17%	-1.04%	0.79%	-1.17%
M-5	7.8% ± 0.06%	9.72%	0.92%	0.45%
M-6	-		1.41%	0.40%
M-7	1.56% ± 0.16%	1.22%	2.76%	0.87%
M-8	0.18% ± 0.18%	-0.39%	-	-

VIIRS		MODIS		Compared at
Band	Wavelength (μm)	Band	Wavelength (μm)	
M1	0.402 - 0.422	8	0.405 - 0.420	Desert and Ocean
M2	0.436 - 0.454	9	0.438 - 0.448	Desert and Ocean
M3	0.478 - 0.498	10	0.483 - 0.493	Desert and Ocean
M4	0.545 - 0.565	4	0.545 - 0.565	Desert
		12	0.546 - 0.556	Ocean
M5	0.662 - 0.682	1	0.620 - 0.670	Desert
		13	0.662 - 0.672	Ocean
M6	0.739 - 0.754	15	0.743 - 0.753	Ocean
M7	0.846 - 0.885	2	0.841 - 0.876	Desert
		16	0.862 - 0.877	Ocean
M8	1.230 - 1.250	5	1.230 - 1.250	Desert and Dome C

VIIRS Bias Over Desert using SNO-x

Observed Bias

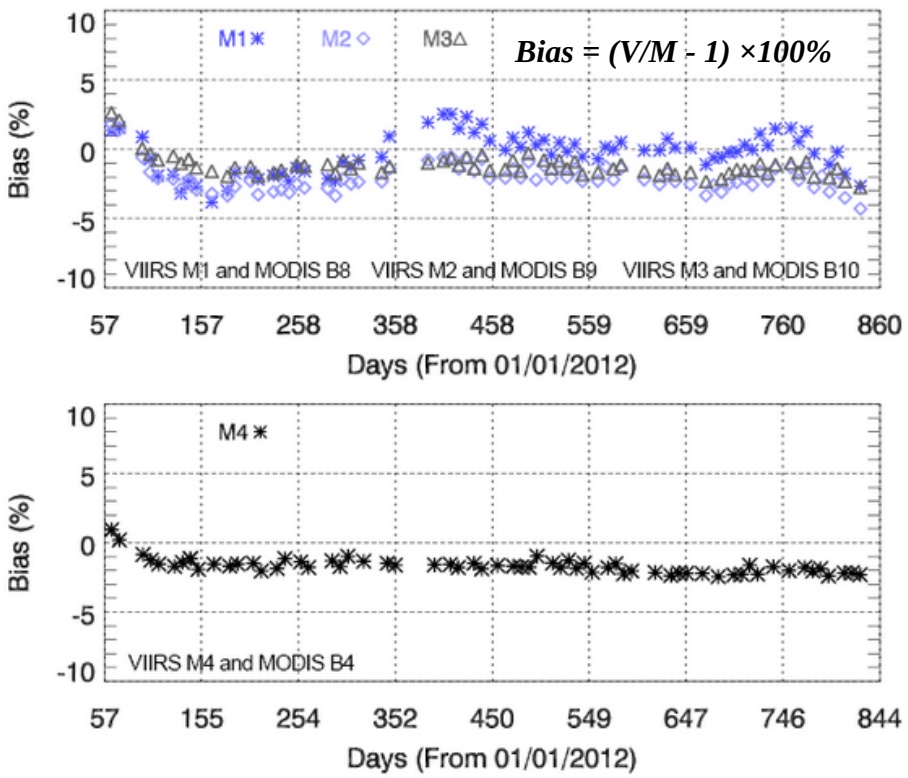

After accounting spectral differences

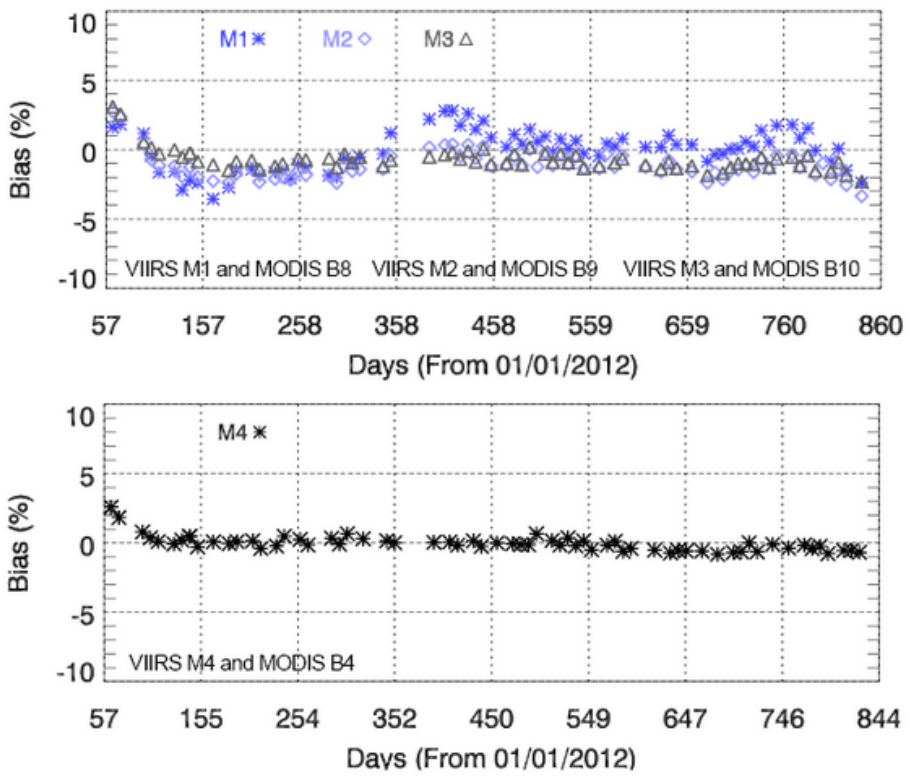

- Large negative bias during early 2012 is due to the update of SDSM transmission screen data.
- M1 to M3 bias is getting larger in recent months (from early 2014).
  - ➢ Possibly due to the recent change in F-factor trend seen after February 2014.
- M1 shows positive bump in bias during early 2013 which repeats in early 2014 as well!
- M4 is the most stable band with a small decreasing trend in bias of ~1% after May 2013.

VIIRS Bias over Desert (M5 to M8)

Observed Bias

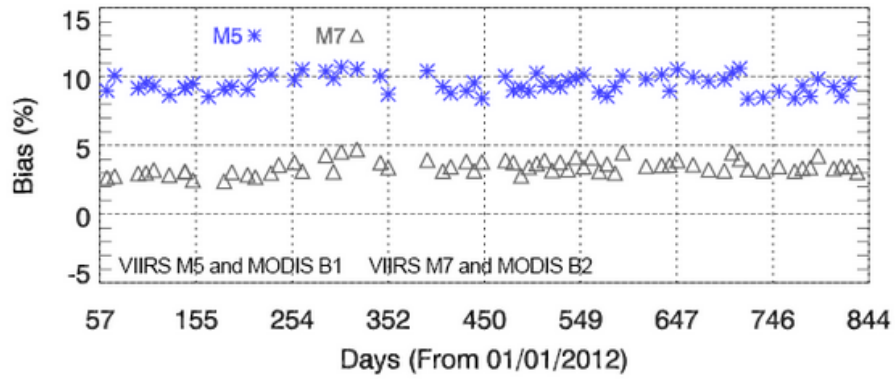

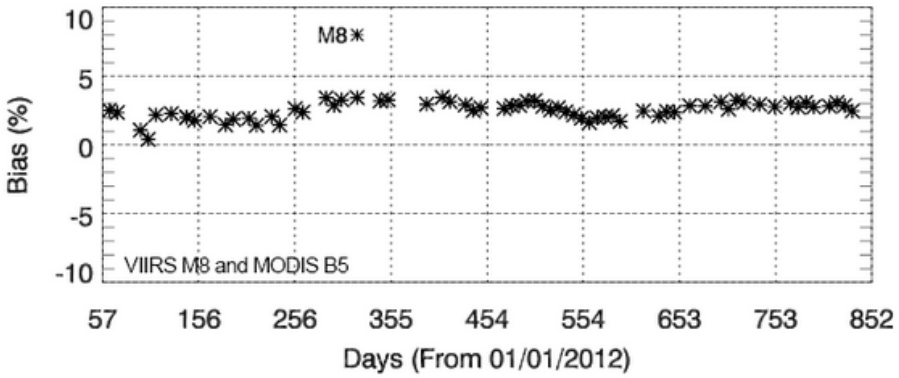

After accounting spectral differences

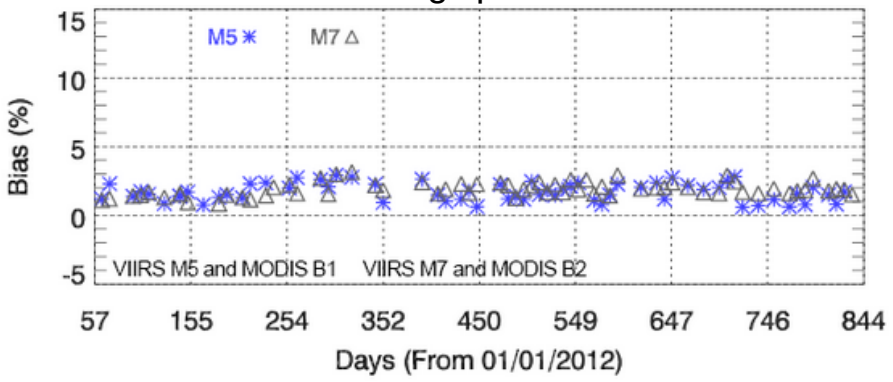

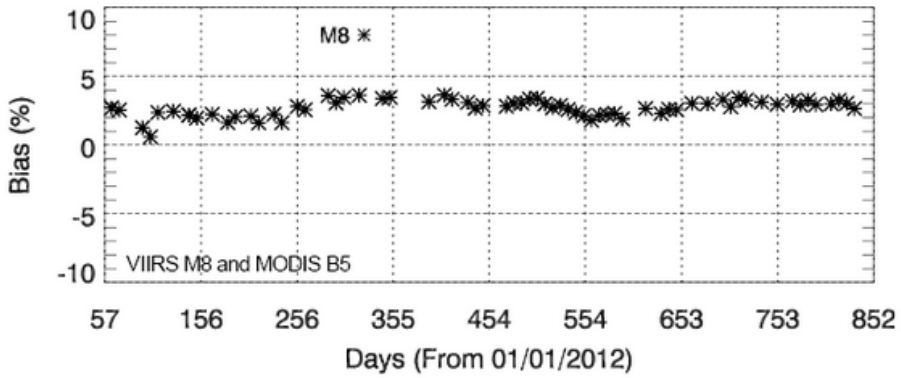

- Large bias exists for M5 (0.65 μm) mainly due to spectral differences of MODIS and VIIRS.
- After accounting spectral differences, bias is significantly decreased to around 2% for both M5 and M7.
- M8 bias is nearly 3%. Note that the bias was smaller during few months after launch.

Observed Radiometric Bias over Ocean

- Bias trends over desert and ocean are consistent during early 2012 showing large dip.
- M1 and M2 shows larger bias during early 2013 similar to what was seen over the desert.
- After early 2013, M1 is slightly increasing whereas M2 and M3 in general flat bias trend.
- The time difference of about 10 to 15 minutes makes bias estimation process more complicated due to movement of clouds by adding uncertainty.

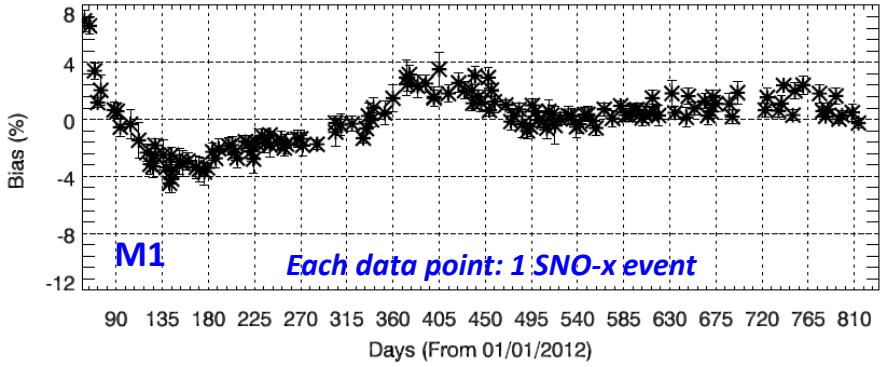

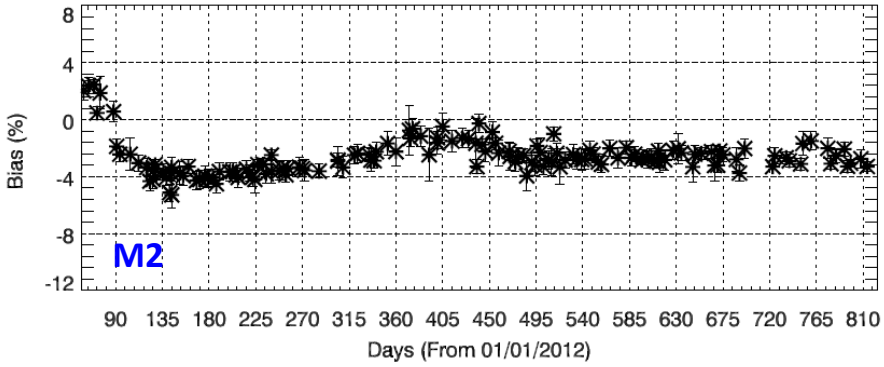

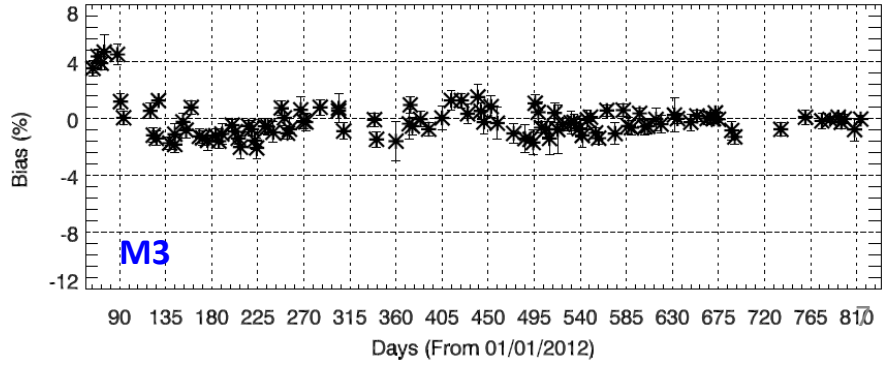

Observed Radiometric Bias over Ocean

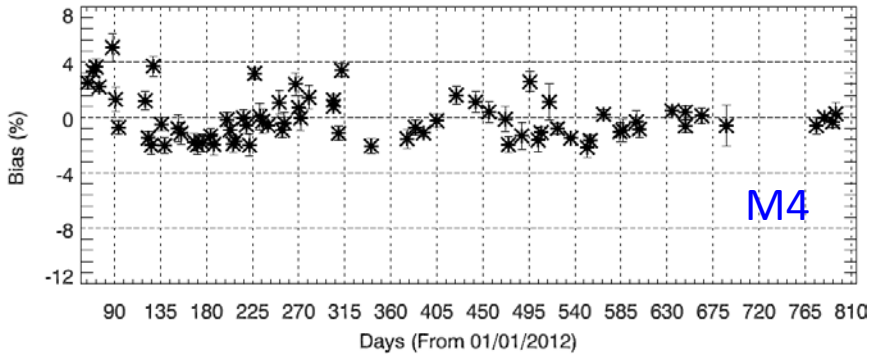

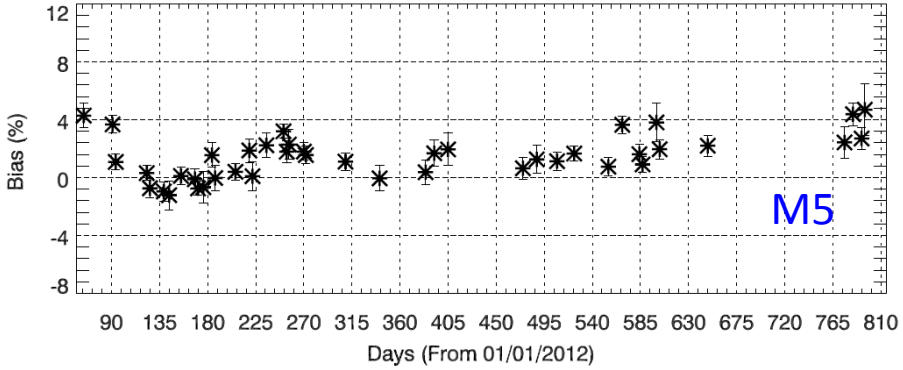

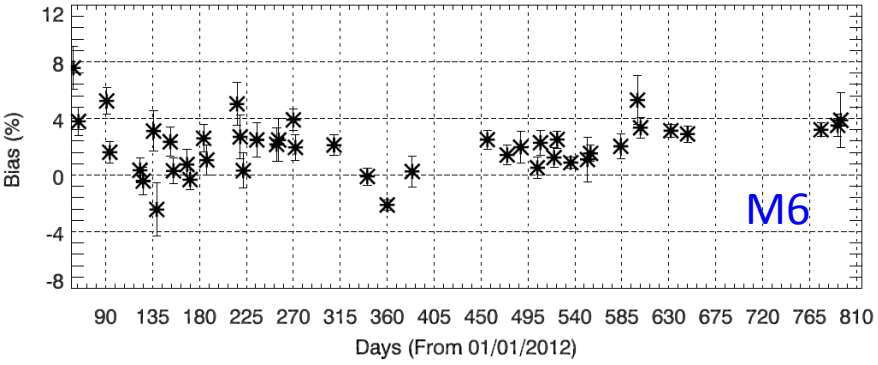

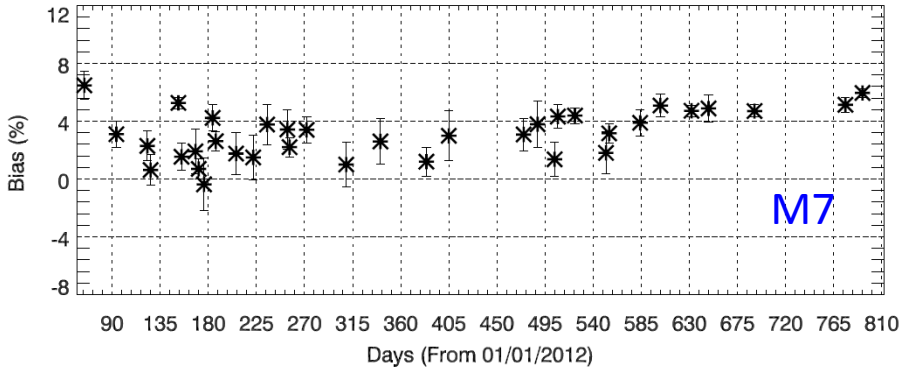

- Number of valid ROIs are much smaller for M4 through M7 as compared to M1 through M3.
- Very small signal strength (< 5% reflectance) for bands M5 through M7 makes the bias trends noisier.
- Most strict cloud mask used along with spatial uniformity of 0.9% to filter out invalid bias data.
- M6 and M7 bias are larger after July 2013. However, there are few data points to conclude this trend.
- Very few bias data points exists during winter months.

Bias Time Series Summary

- VIIRS VNIR bands (M1-M7) indicate the observed radiometric bias **at nadir** to be within 2% ± 1% relative to MODIS for most or the bands.
- Bands M1 to M3 suggests increasing bias since early 2014.
- Some bands (M5, M6 and M7) show much larger variability and few bias data points mainly due to their small signal strength over ocean. This increases the uncertainty in bias estimation to greater than 1%.
- M7 bias over ocean indicates an increase after mid 2013 to nearly 4% but there are few points to verify and this needs further investigation.
- SNO-x technique will be used to regularly monitor VIIRS radiometric performance.

Ref:
Uprety, Sirish, Changyong Cao, Xiaoxiong Xiong, Slawomir Blonski, Aisheng Wu, Xi Shao, 2013: Radiometric Intercomparison between Suomi-NPP VIIRS and Aqua MODIS Reflective Solar Bands Using Simultaneous Nadir Overpass in the Low Latitudes. J. Atmos. Oceanic Technol., 30, 2720–2736.

VIIRS Off-nadir Bias Analysis over Ocean

- Bias estimation is extended from nadir (shown in previous slides) to scan edges over ocean.
- Implemented for SNO-x events over ocean (2013 and 2014)
- At nadir, both VIIRS and MODIS observe same ocean target with almost identical viewing geometry.
- At larger scan angles, the viewing geometry changes due to different altitude of S-NPP and AQUA satellites. This mainly changes the sensor zenith angles for the two instruments.
- The altitude differences causes 0° to 5° differences in sensor zenith for MODIS and VIIRS.
- The time differences of 10 to 15 minutes causes 1° to 2° change in solar zenith angles of the two instruments. However, the impact is very small due to the comparison in reflectance unit.

VIIRS Observed Bias

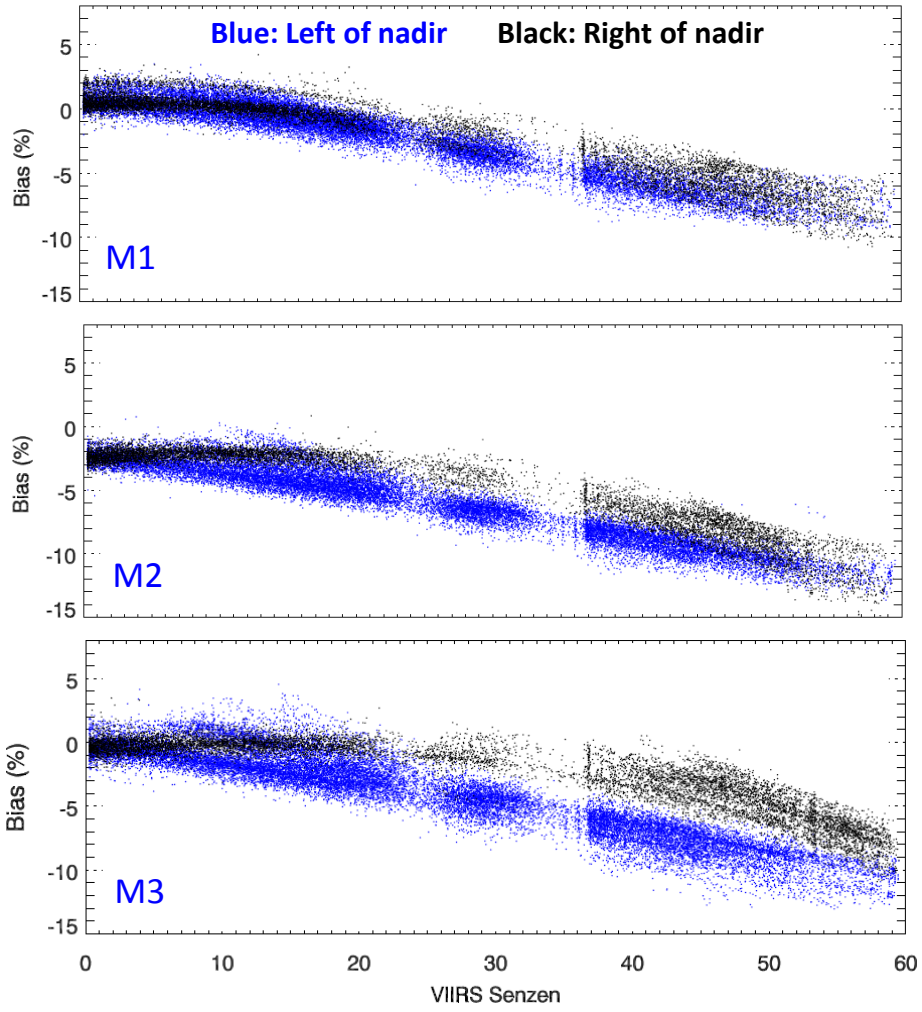

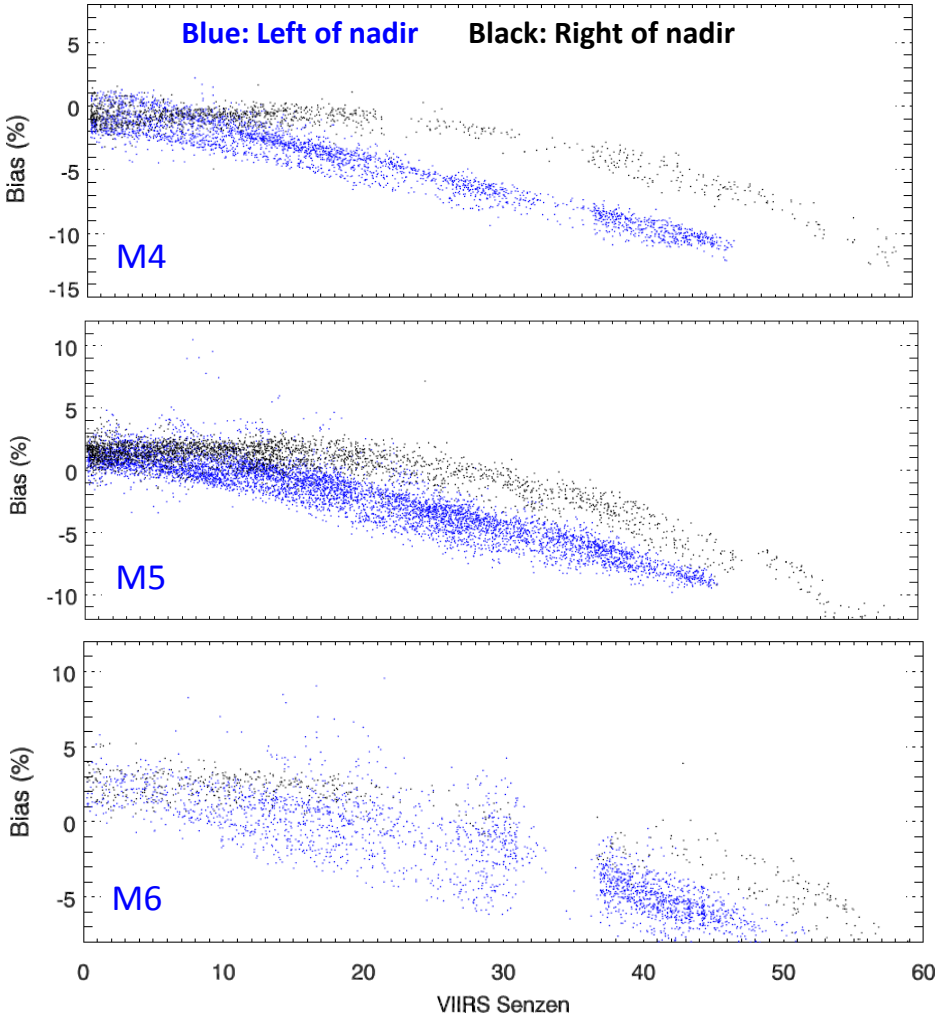

- Bias increases from within 2% to more than 10% as a function of view zenith angle for most of the bands.

Sensor Zenith Difference

- Altitude difference between VIIRS and MODIS results in sensor zenith difference for collocated ROIs.
- Senzen difference: 0° at nadir to ~5° at large sensor zenith.
- The impact could be corrected to some extent by using radiative transfer models such as MODTRAN, 6S.

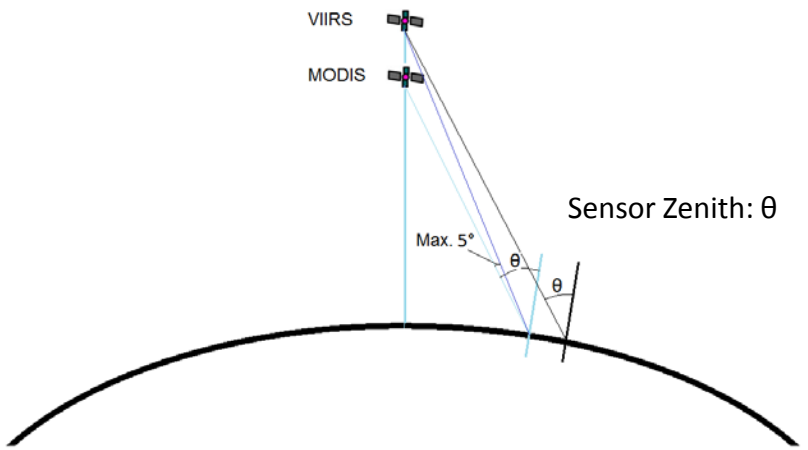

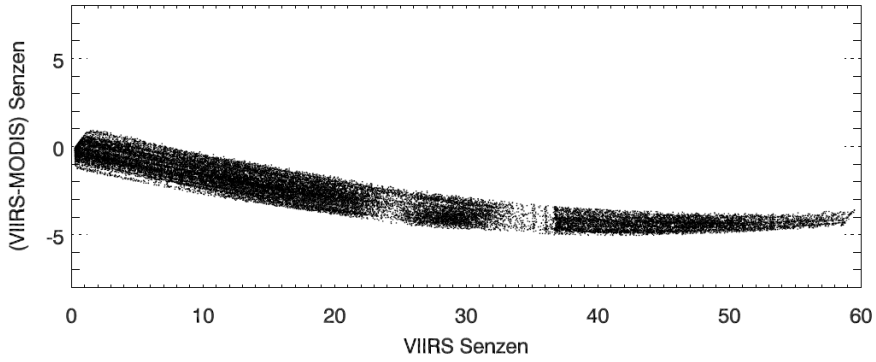

6S simulations of VIIRS TOA Radiance

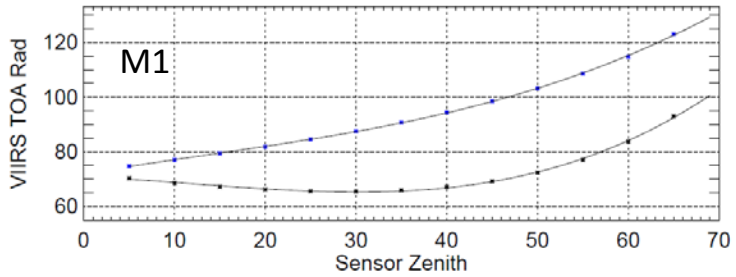

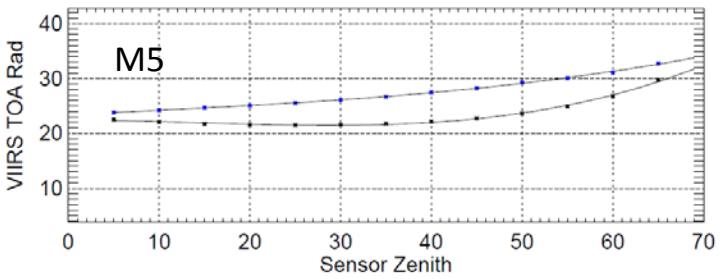

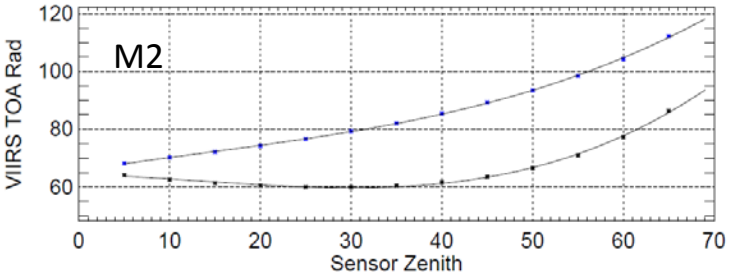

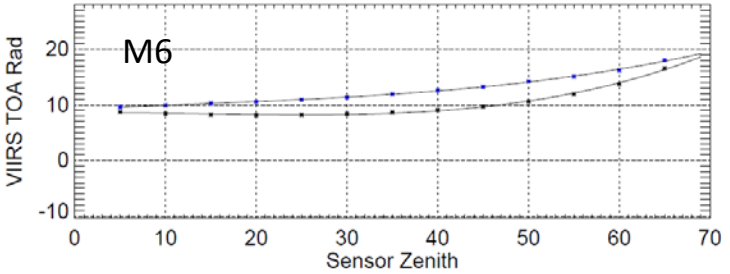

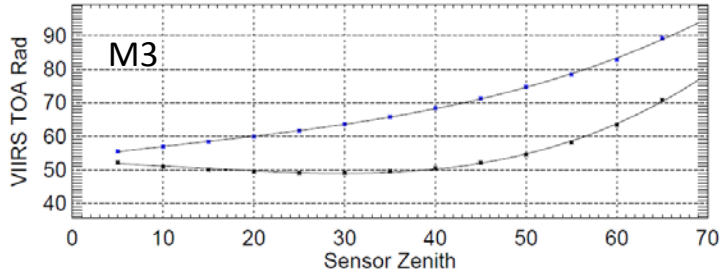

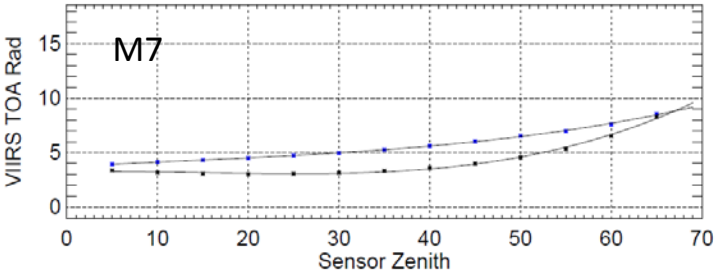

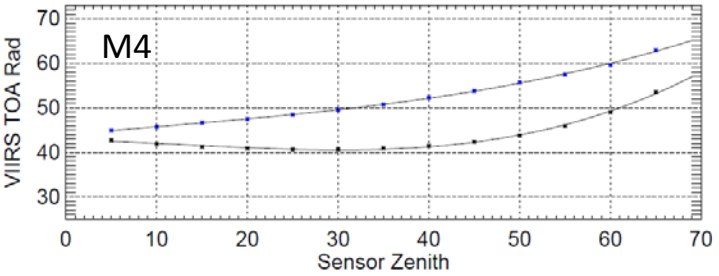

Note:

Blue dots: Negative sensor azimuth

Black dots: Positive sensor azimuth

M1 Off-nadir Bias Analysis

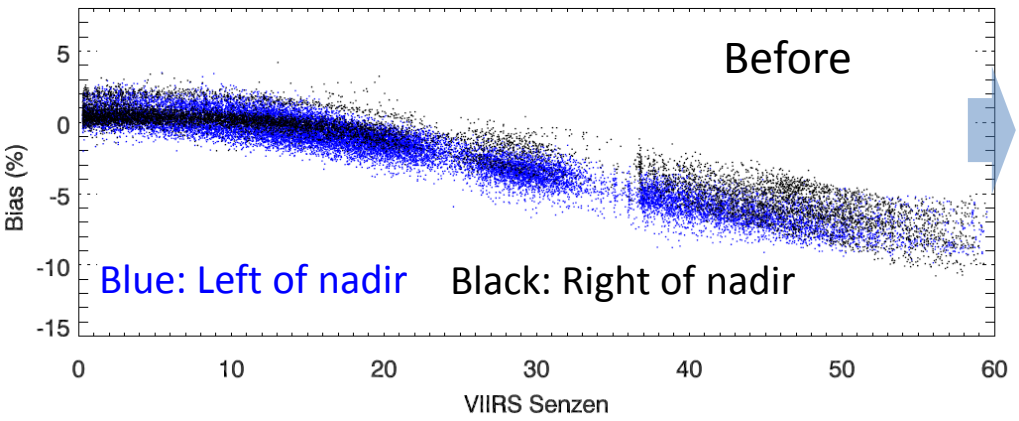

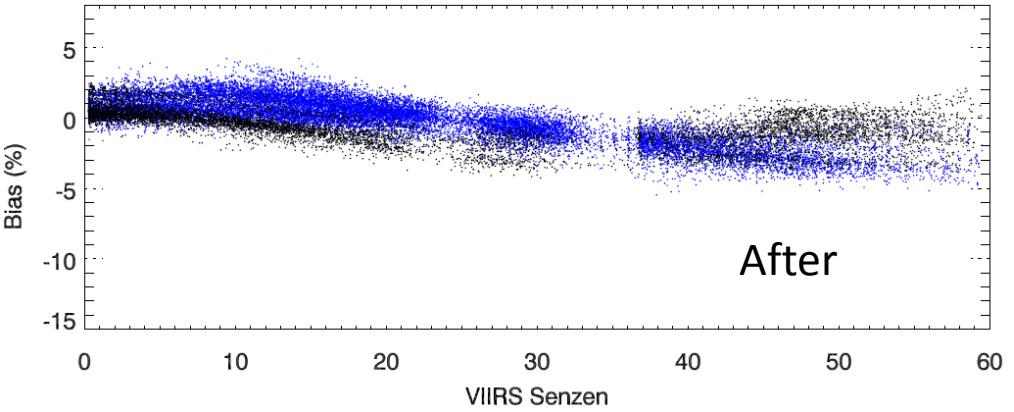

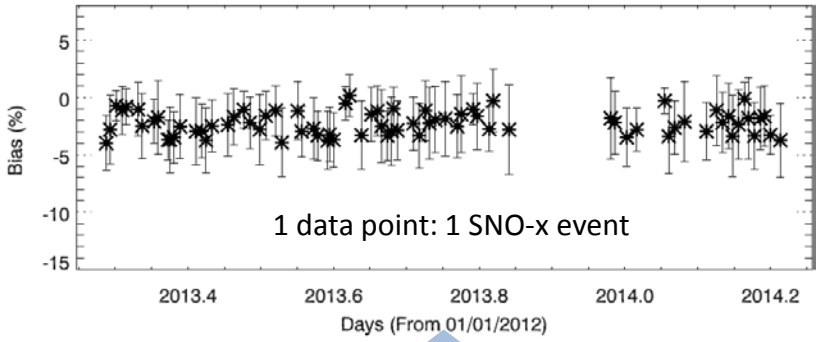

Large 1-sigma bar: Bias varying from nearly 2% to -10% (nadir to the edges)

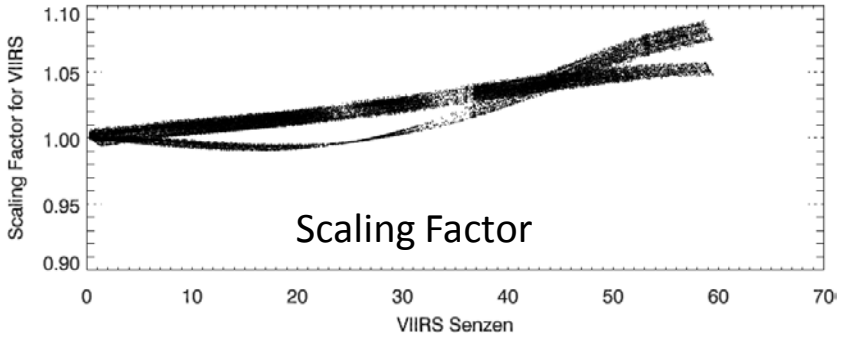

Figure. M1 bias before and after correcting for senzor zenith differences using 6S simulation

- Bias is much improved after correction for M1.
- The two bias trends are still distinguishable.

After Correcting for Sensor Zenith

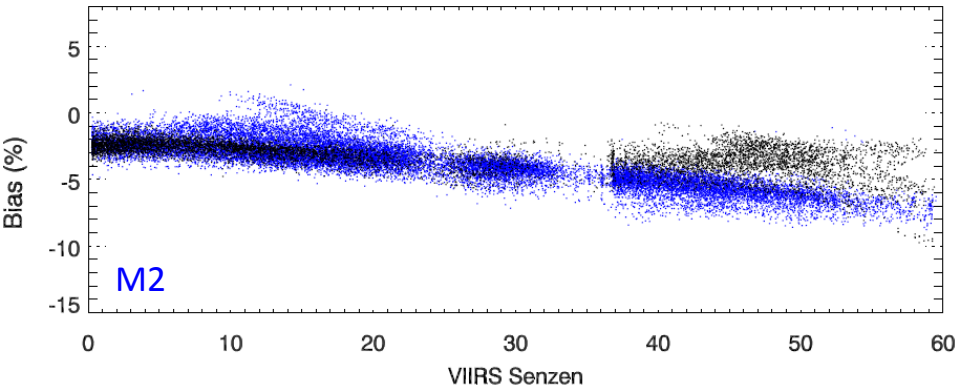

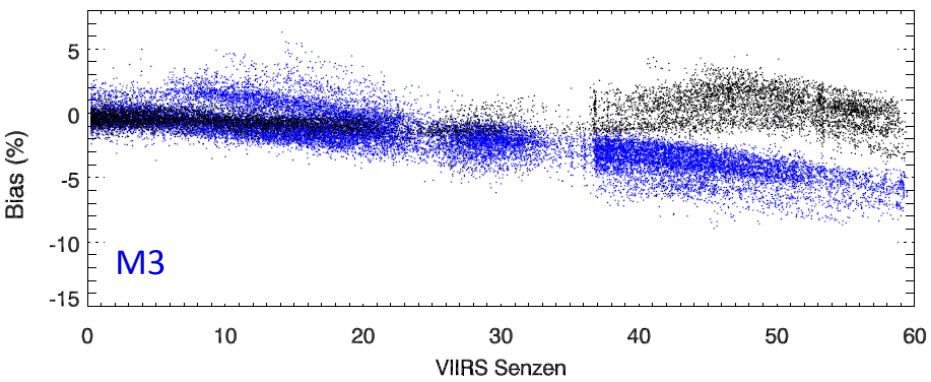

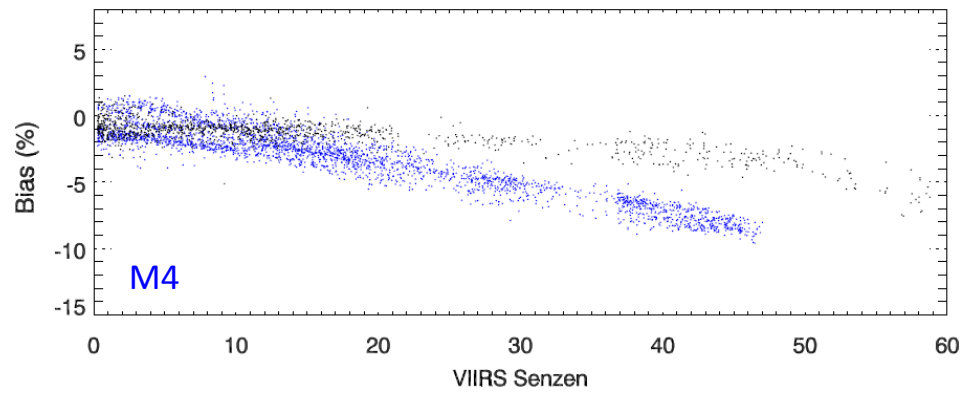

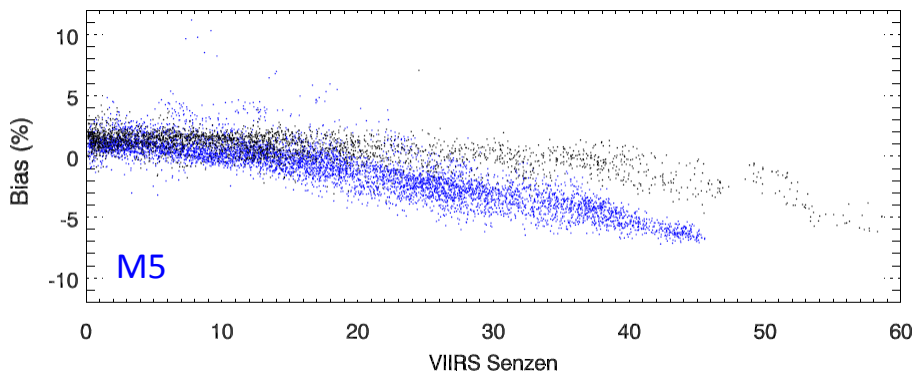

- Sensor zenith correction improves to some extent.
- Large bias (>5%) still exists @ higher scan angles.
- The two bias trends are still distinct.

Off-nadir Bias Summary

- Observed radiometric bias suggest increasing trend with increasing scan angle.
- Two bias trends exist, one for each side of the sensor nadir track (+ve and –ve sensor azimuth).
- After correcting sensor zenith differences, the bias trend is improved, however, there is still large bias (more than 5%) for most of the bands.
- What are the possible causes?
  - Model: 6S model simulation might not represent the exact observation scenario including the atmospheric variability.
  - Polarization impact at large scan angles for MODIS and VIIRS?
  - How well is RVS characterized for MODIS and VIIRS? Is the uncertainty similar on both cross-track sides?
  - calibration uncertainties of MODIS and VIIRS @ large scan angles?
  - BRDF impact?

Questions?

Backup

SNO-x Inter-comparison Methodology

1. Identify low latitude SNO events
2. collect VIIRS SDR (~750m) and MODIS L1b (1km) data for SNO-x orbits

Note: MODIS collection 6 data is used

Map VIIRS into MODIS lat/lon grid

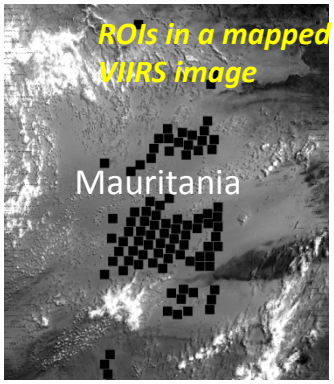

ROI selection
- spatial uniformity < 2% (Desert), < 1% (Ocean)
- sensor zenith: <10° (Desert), <6° (Ocean)
- strict cloud mask criteria for ocean
- ROI size: VIIRS and MODIS: 25km × 25km

- Extract TOA reflectance mean for each ROI and compute ***Bias=(VIIRS – MODIS)*100%/MODIS***
- Compute bias mean by using all ROIs for each SNO event
- Construct and analyze the bias time series

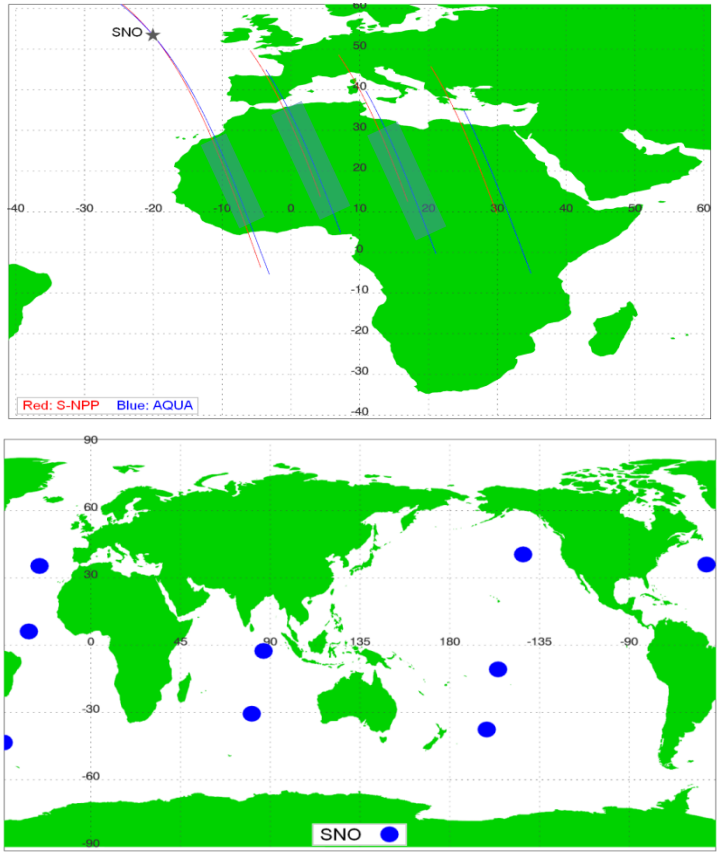

Figure: Orbits showing Low latitude SNO events i) Extended SNOs to desert ii) SNOs over ocean

- SNO time difference of more than 8 minutes causes the movement of clouds and its shadows.
- Latitude limits: ±40°

Trending of Suomi-NPP VIIRS Radiometric Stability with Lunar Band Ratio

Xi Shao[1], Taeyoung (Jason) Choi[2], Changyong Cao[3], Slawomir Blonski[1], and Fuzhong Weng[3]

1. UMD, 2. ERT, 3. NOAA/NESDIS/STAR

Suomi NPP SDR Product Review
NOAA Center for Weather and Climate Prediction (NCWCP)
5830 University Research Park, College Park, Maryland
May 12-16, 2014

Outline

- Scheduled lunar observation by VIIRS
- Deriving Lunar Band Ratio (LBR) from observation
- Overall stability trending of VIIRS with LBR
- Comparison of LBR with F factor trending and discussion
- Summary

List of scheduled lunar Observations by VIIRS

Date	Target time	Roll angle	Date	Target time	Roll angle
4/2/2012	23:05:11	-3.989	10/14/2013	21:39:19	-1.305
5/2/2012	10:20:06	-3.228	11/13/2013	6:57:41	-7.981
10/25/2012	6:58:15	-4.048	12/12/2013	19:35:46	-9.438
11/23/2012	21:18:20	-9.429	1/11/2014	9:59:45	-6.727
12/23/2012	15:00:50	-7.767	2/10/2014	5:34:12	-3.714
2/21/2013	9:31:25	-1.712	3/12/2014	1:11:43	-3.945
3/23/2013	3:29:00	-3.32	4/10/2014	20:53:15	-4.977
4/21/2013	19:47:54	-3.882			

- Raw Data Record (RDR) for lunar observations are collected
- All of events collected at nearly the same lunar phases (-51.3 to -50.3 degree).
- In total, 15 events are analyzed

Lunar images in the reflective solar bands of VIIRS on March 12th, 2014

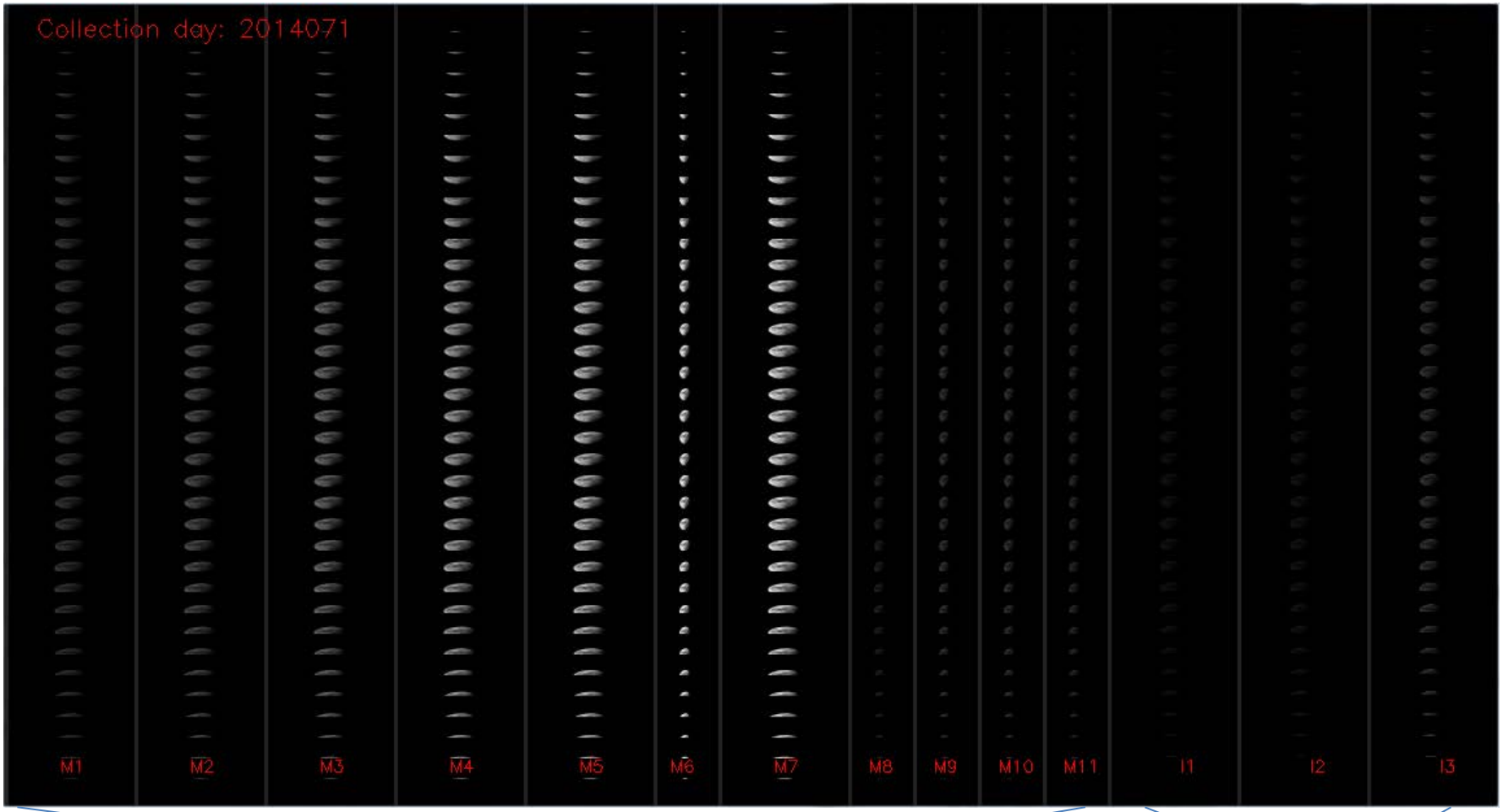

Moon in Earth View for M6

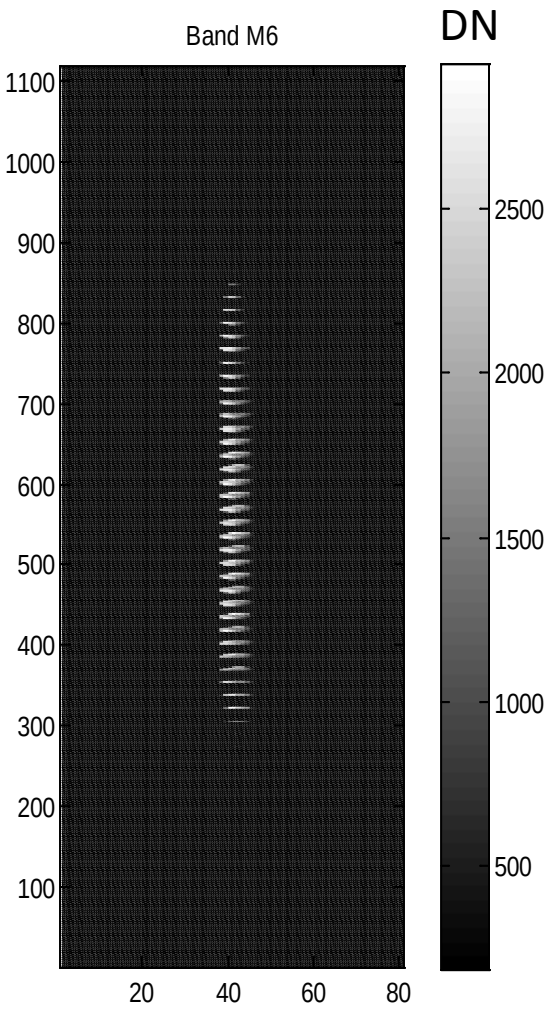

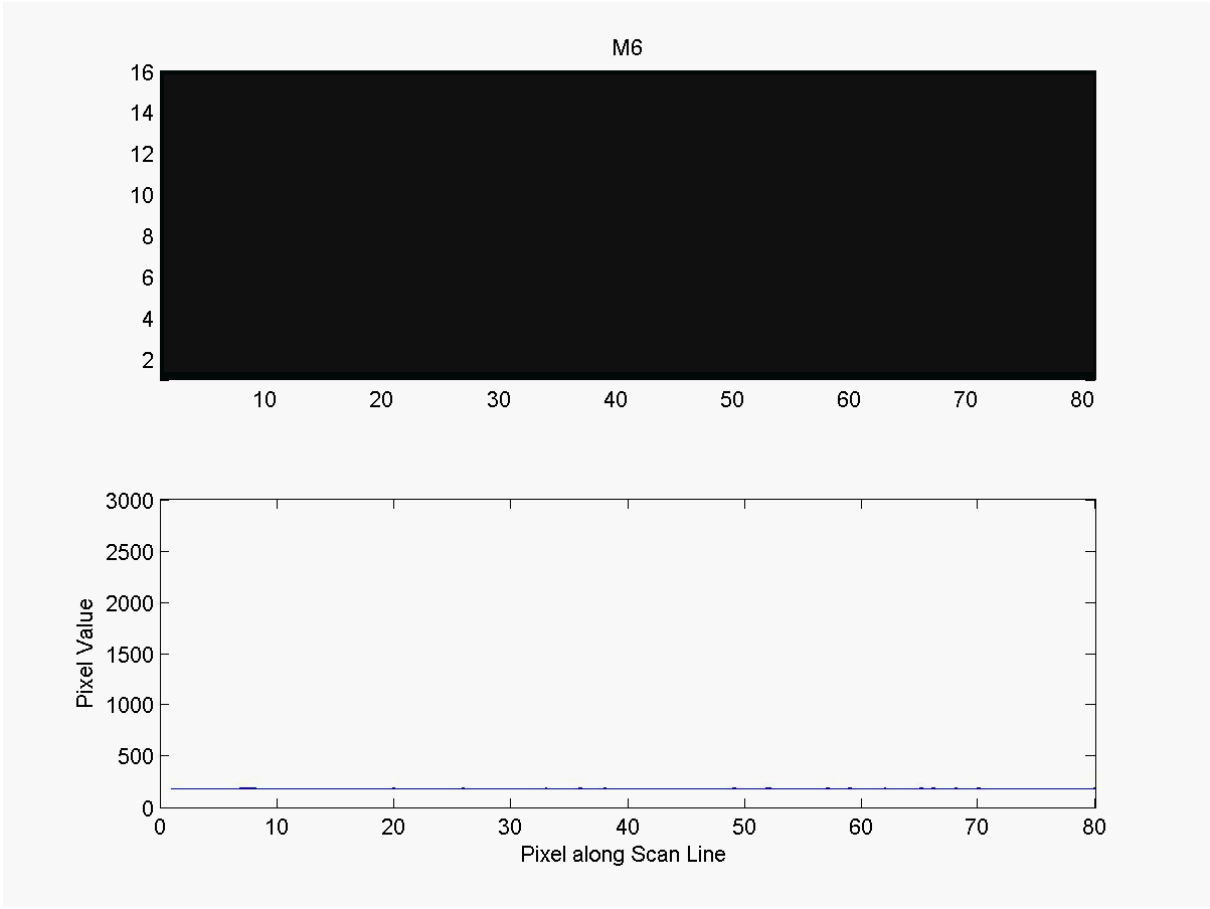

Data Processing: Total Lunar DN

One Scan for M6 Band

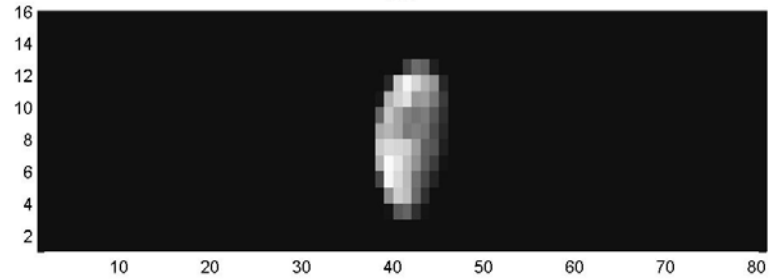

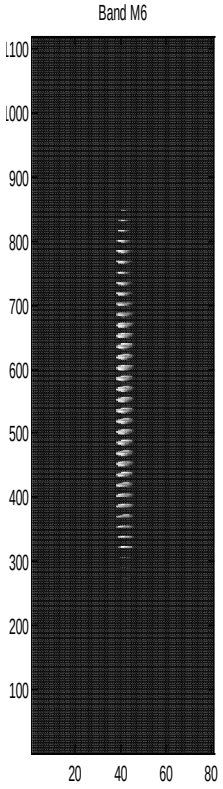

Total Pixel Value in the Moon Vs. Scan (with background removed for each detector)

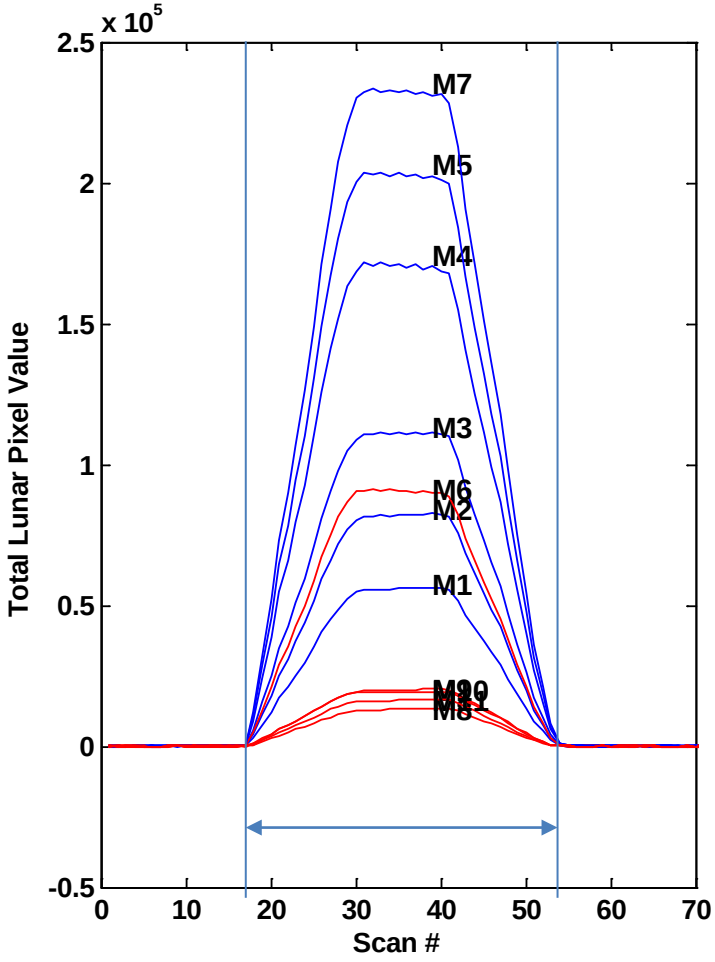

$$Total\ Lunar\ DN(M\ or\ I) = \sum_{Scans\ with\ Moon} \sum_{Pixels\ within\ Scan} DN_{pixel} - DN_{backgrou}$$

$$LBR(M\ or\ I) = \frac{Total\ Lunar\ DN\ (M\ or\ I)}{Total\ Lunar\ DN\ (M4)}$$

Pros and Cons of LBR Analysis

- Pros
  - Simple calculation and does not rely on lunar irradiance model and not subject to uncertainties embedded in the model
  - Dependences on Sun-Earth and Moon-Earth distances naturally cancel out
  - Especially useful for scheduled lunar observations of VIIRS taken at nearly the same lunar phase and effects of lunar phase cancel out
  - Pure DN ratios and not subject to uncertainty of onboard calibration
- Cons
  - Need to select a stable band as the reference band
  - Can only reveal relative stability of VIIRS

LBR for VIIRS M1-7, I1-2 Bands

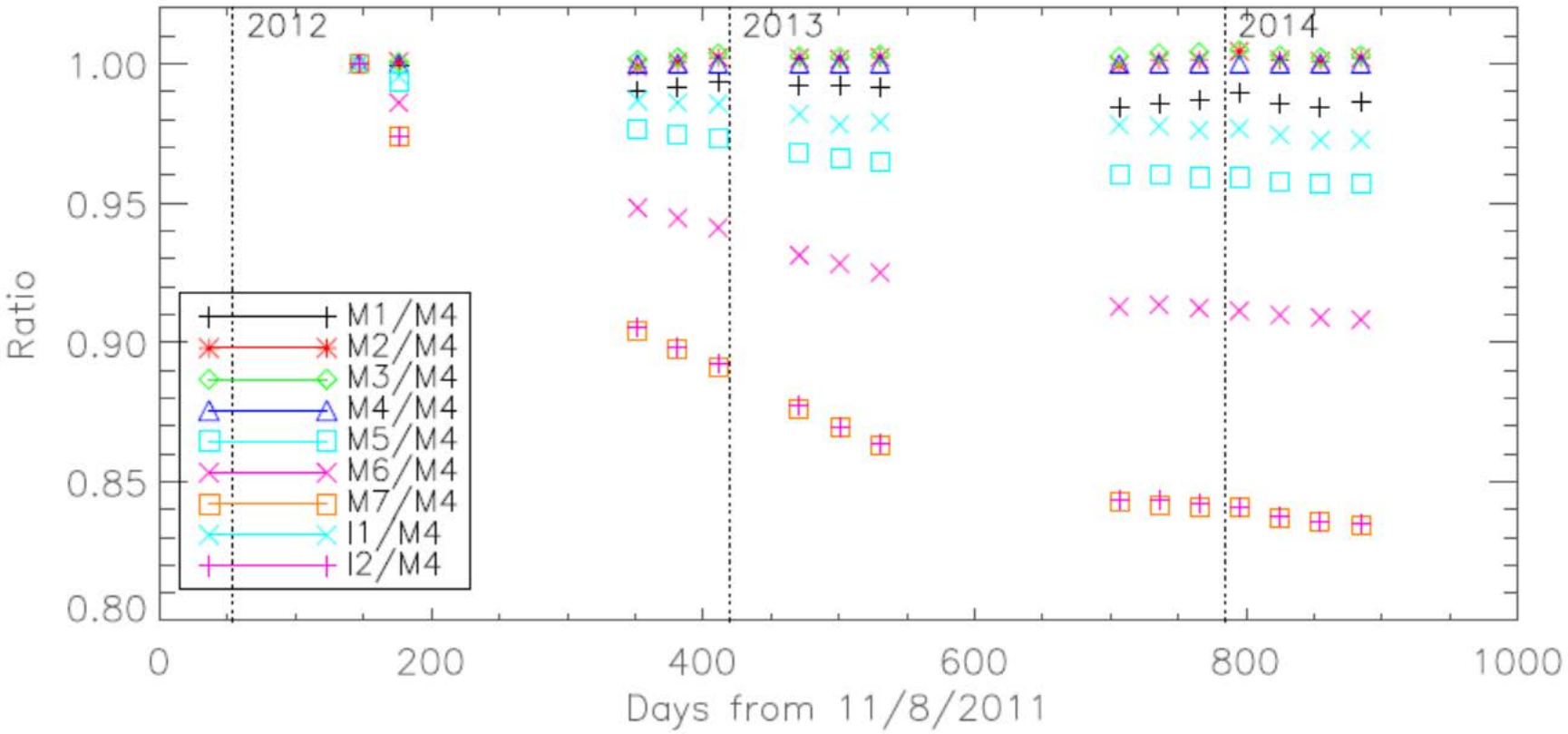

LBR for VIIRS M8-11, I3 Bands

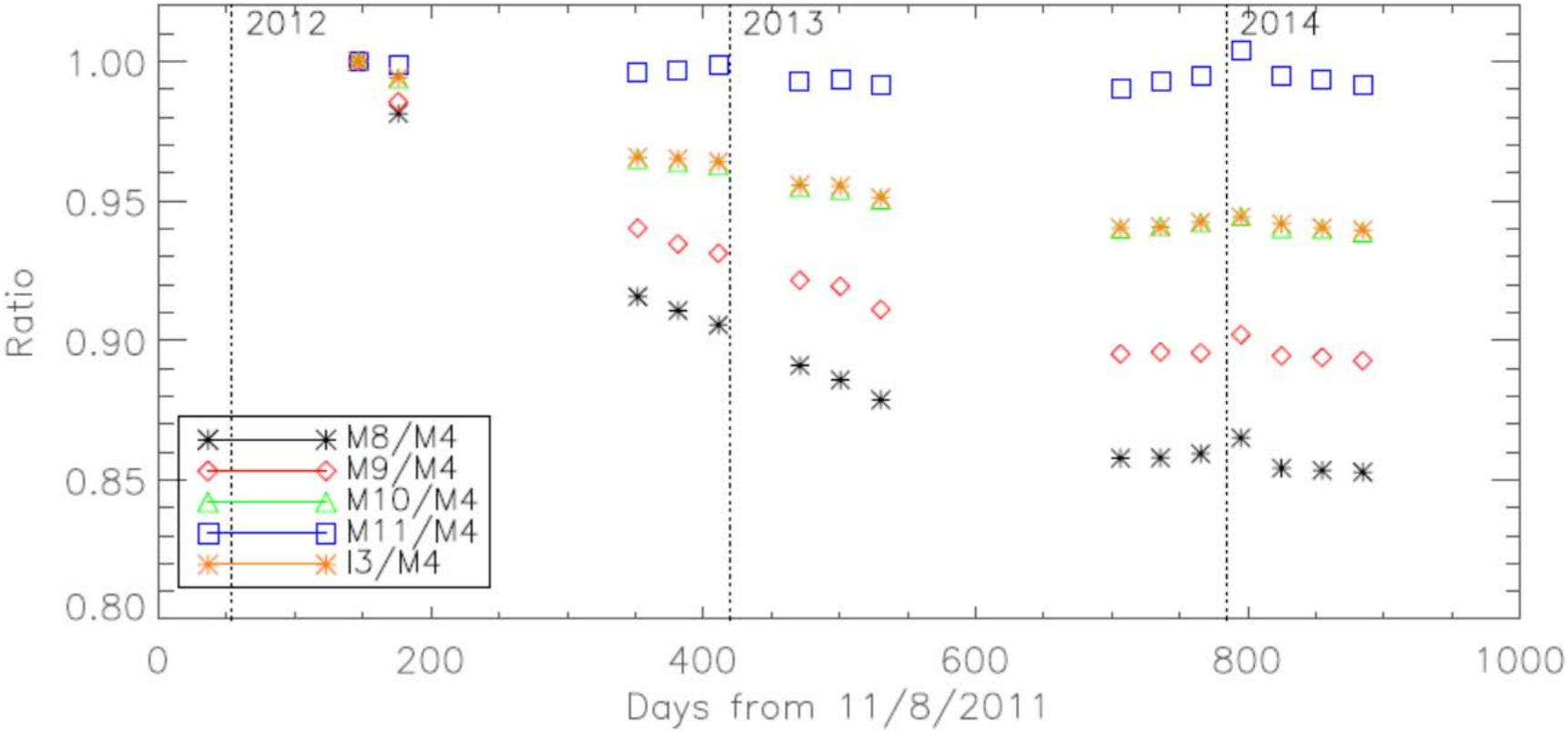

F factors derived from onboard Calibration with Solar Diffuser

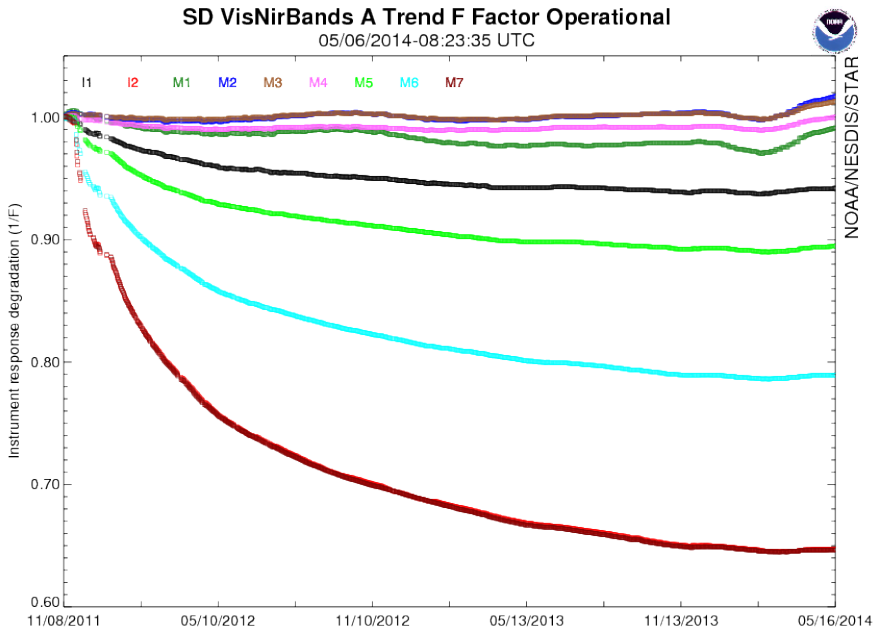

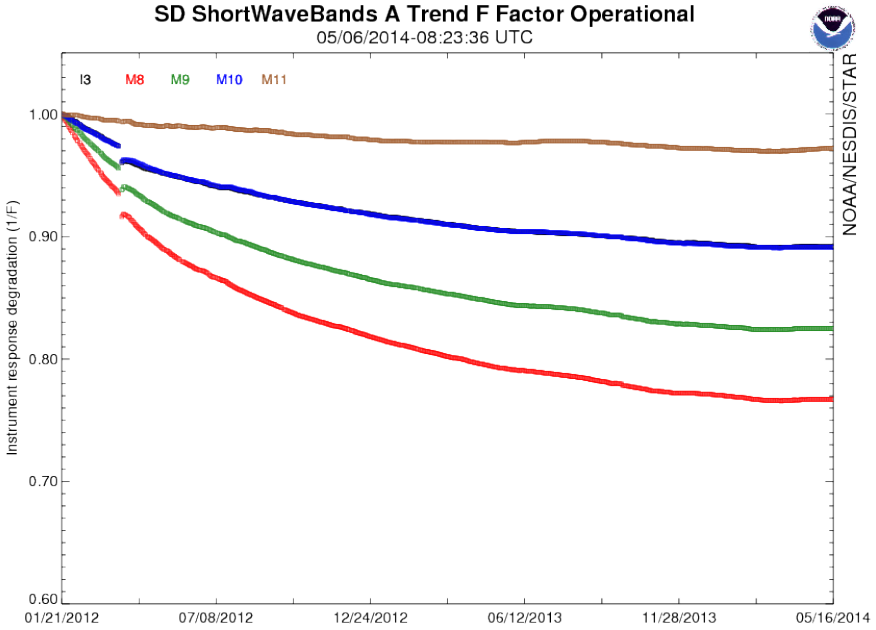

- The band M4 provides stable F factors over the VIIRS lifetime
- The operational F factors are normalized by band M4 and compared to the LBR for VIIRS stability assessment.

Comparison of LBR with SD F factors for M1-3 Bands

- VisNIR bands M1~M4 (400 to 600 nm)
  - All the LBRs are normalized by its first point and placed on the F factor ratios.
  - The LBRs are following the annual oscillation pattern but not as strong as F factor ratios.
  - Percent variation range of LBR in band M1 is 1.6%, M2 is 0.6%, and M3 is 0.5%.

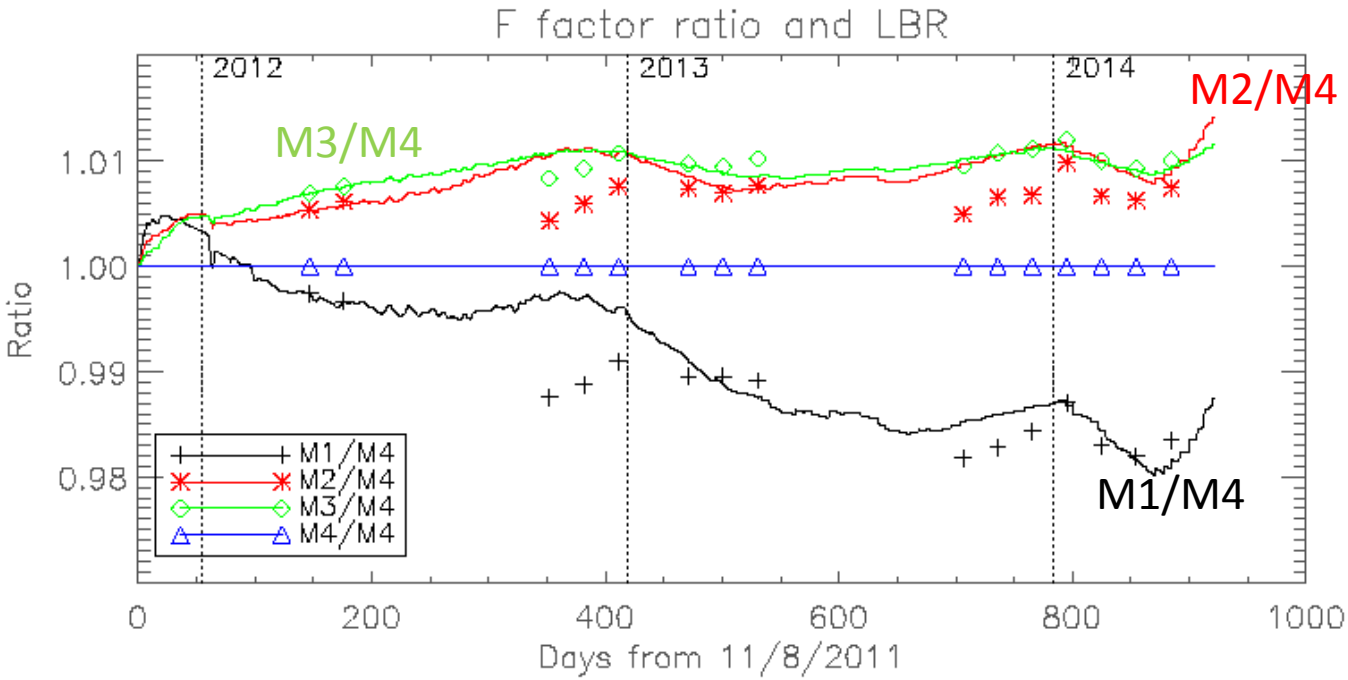

Comparison of LBR with SD F factors for M5-7 and I1-2 Bands

- VisNIR bands M5, M6, M7, I1 and I2 (600 to 900nm)
  - LBRs are following general F factor ratio trends.
  - Differences between LBRs and F factor ratios are growing.
    - With time and center wavelength
  - I2 and M7 ratios are almost identical.

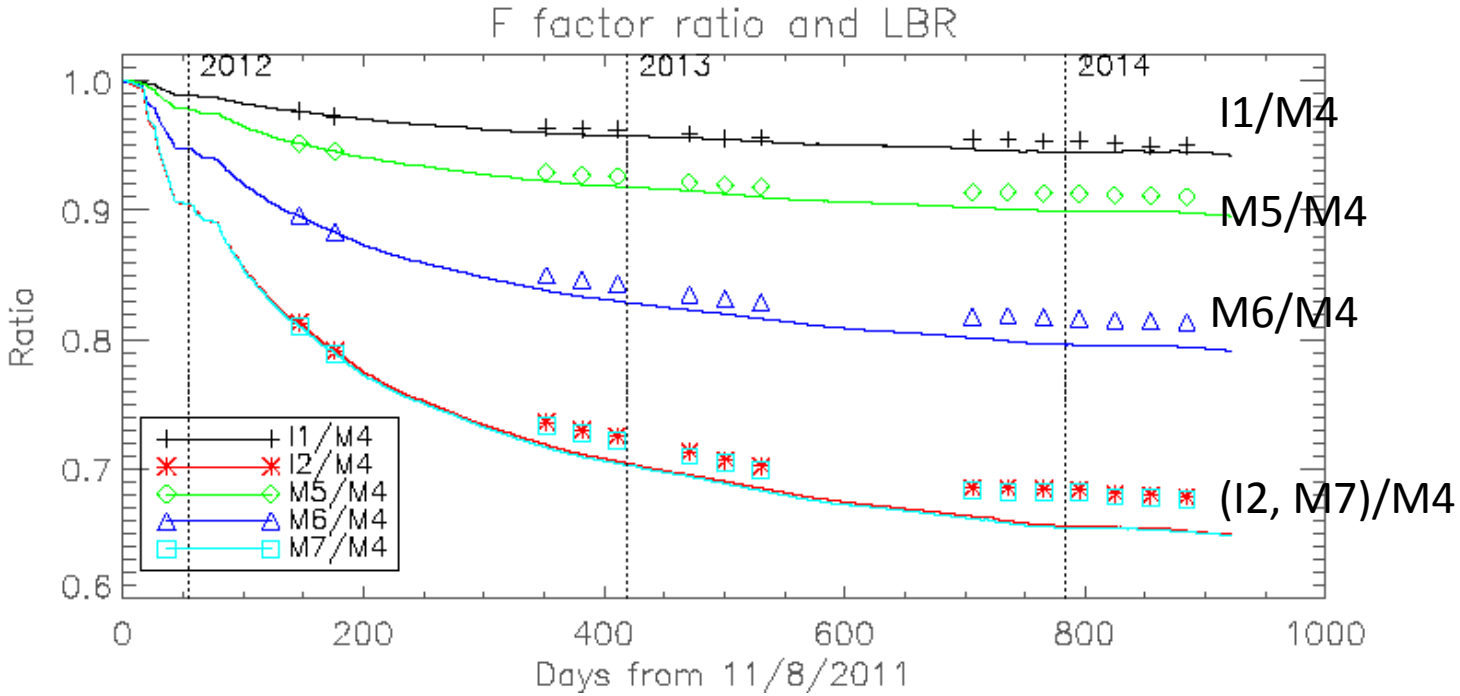

Comparison of LBR with SD F factors for M8-11 and I3 Bands

- S/WMIR bands M8~M11 and I3 (1.2 to 2.5 µm)
  - There is no SD degradation (H factor) applied in these bands.
  - There are differences between F factor ratios and LBR.
  - Trend of M10 and I3 are almost identical

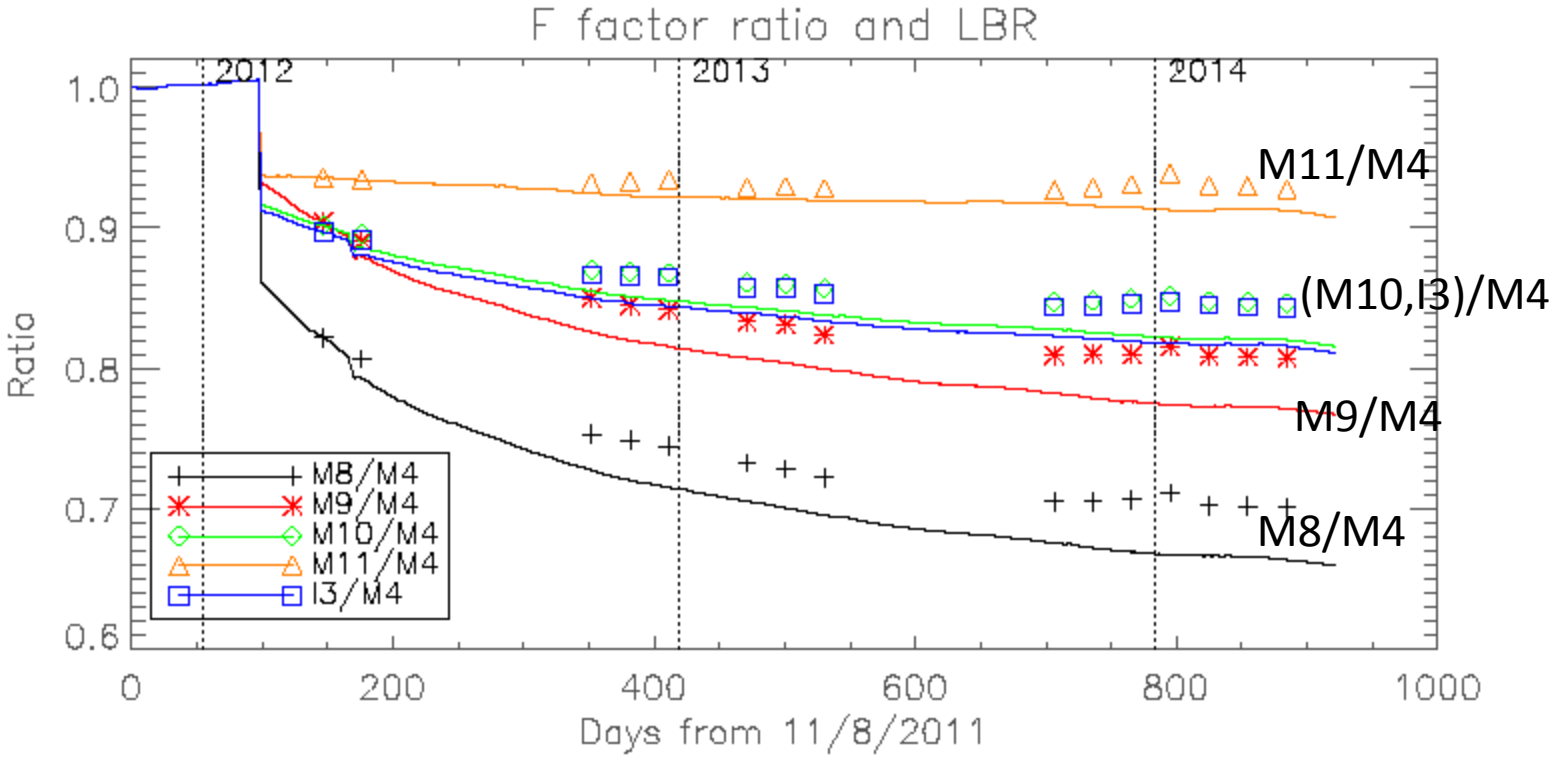

LBR for I2/M7 and I3/M10

- I2/M7 and I3/M10 ratios consistency check.
  - The LBR and F factor ratios are consistent approximately within 0.2%.

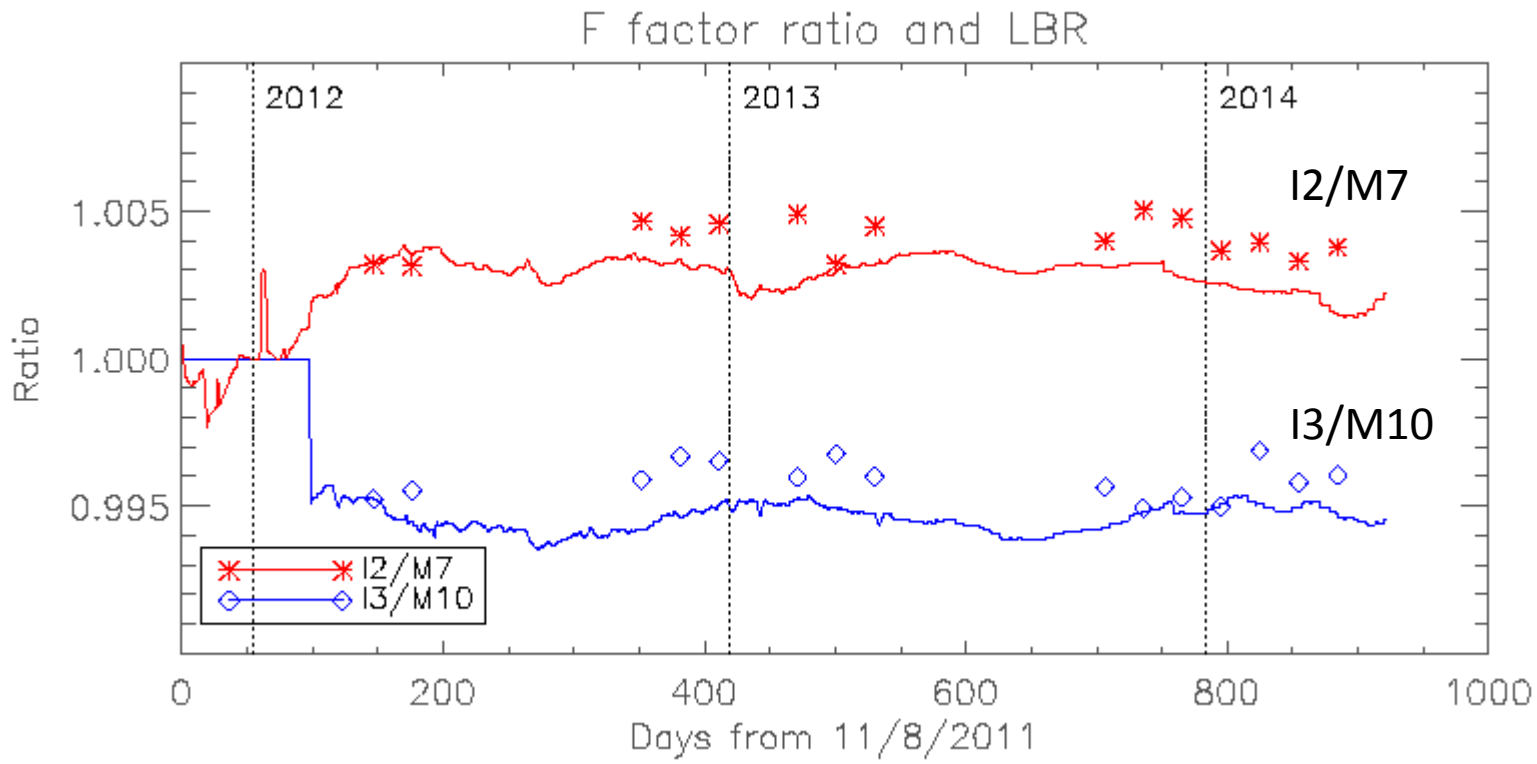

Overall Performance of LBR vs. SD F Factors

- LBR / F factor ratio
  - The differences increase over time.
  - Strong wavelength-dependence

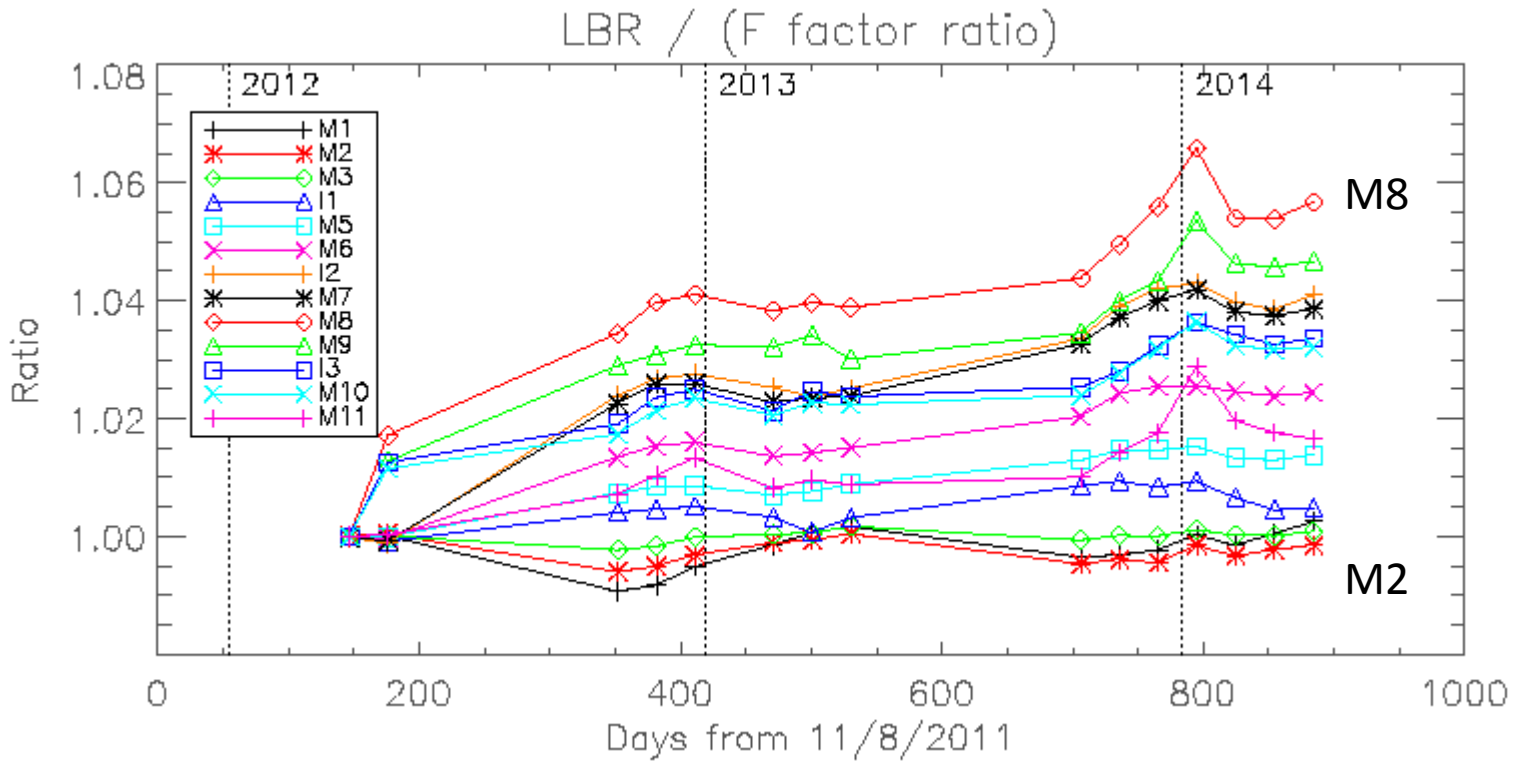

LBR vs. SD F Factor Ratios

- Wavelength dependence of LBR / F factor ratio
  - Using the 3/12/2014 data collection.
  - Most consistent for M1-M4 bands.
  - Ratios increases in the M5 ~ M8 bands.
  - Ratios decreases in the short wave IR (M8-M11) bands.
  - Further analysis are needed to explain the dependence.

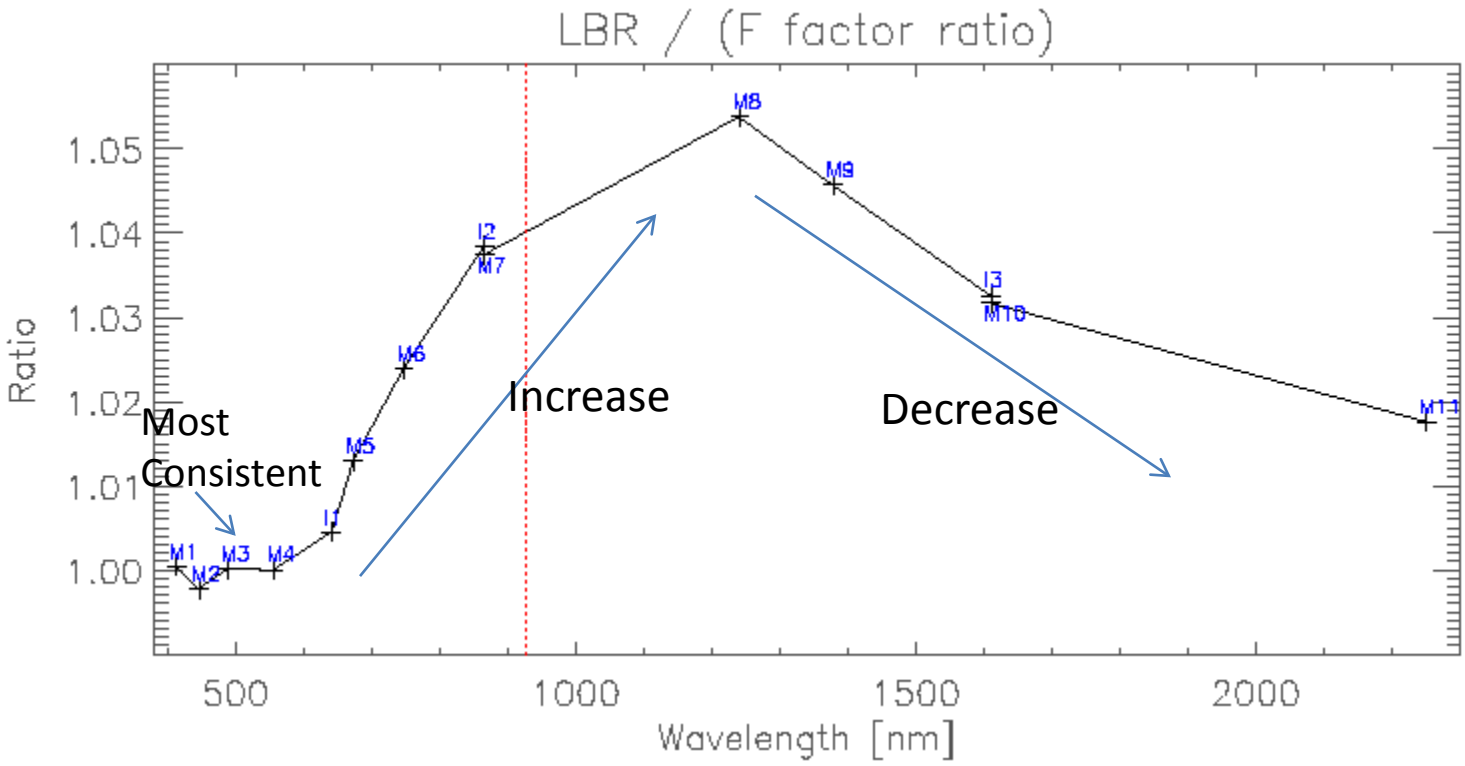

Summary

- Demonstrated that LBR can be used to perform long-term stability monitoring of VIIRS solar bands
- Comparison with SD F factors reveals the relative degradation of instruments.
  - Stability of M1-M3 bands, VISNIR (M5-7, I1-2) bands and S/WMIR (M8-11, I3) bands
  - Consistency of I2/M7 and I3/M10 bands
- Reveals the wavelength dependence of LBR vs. SD F Factor Ratios
- Future work
  - Continue to monitor VIIRS stability with LBR
  - Investigate wavelength dependence of LBR vs. SD F Factor Ratios

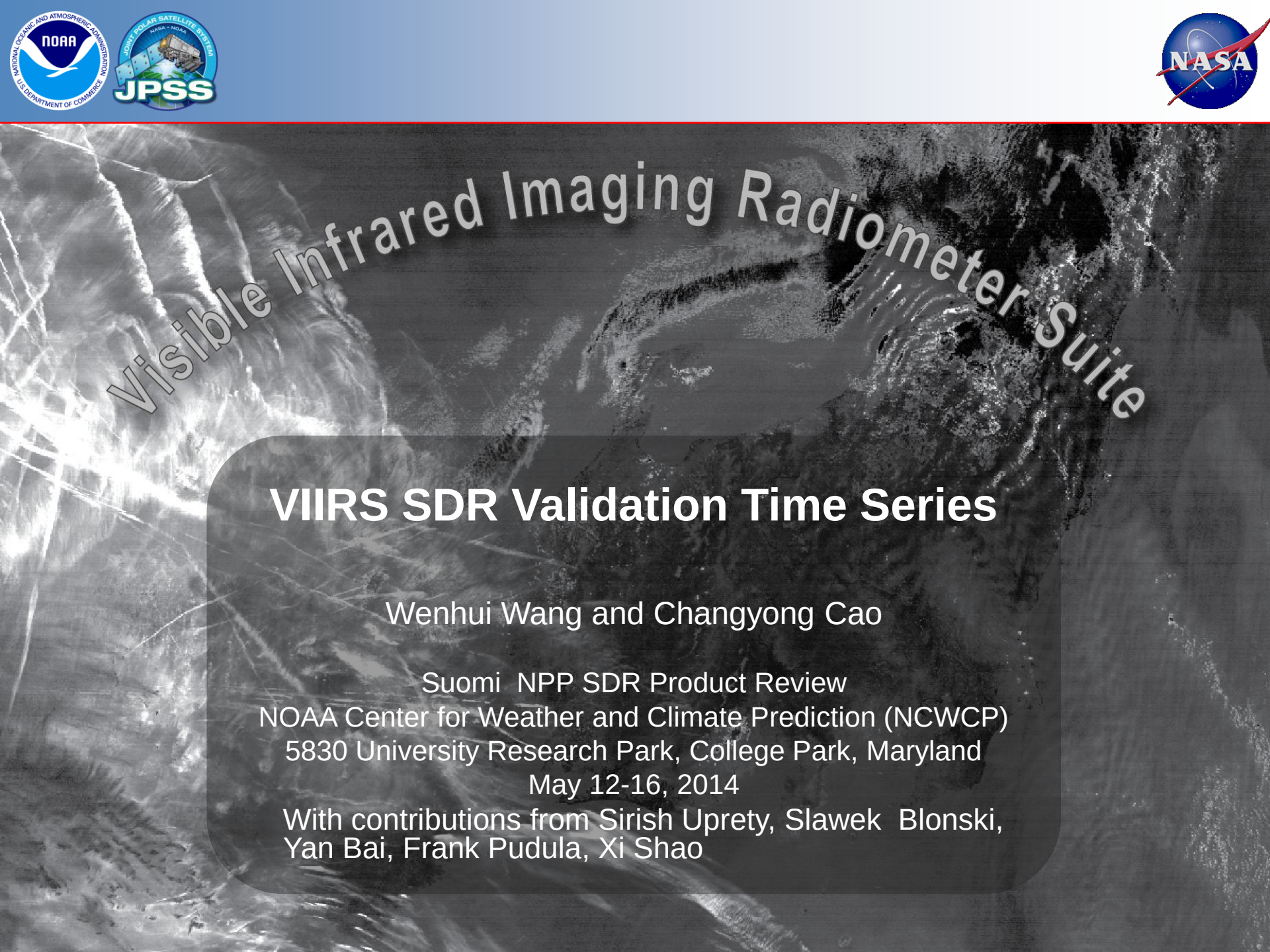

VIIRS SDR Validation Time Series

Wenhui Wang and Changyong Cao

Suomi NPP SDR Product Review
NOAA Center for Weather and Climate Prediction (NCWCP)
5830 University Research Park, College Park, Maryland
May 12-16, 2014

With contributions from Sirish Uprety, Slawek Blonski, Yan Bai, Frank Pudula, Xi Shao

Outline

- Background
- Validation sites time series
- Deep Convective Clouds (DCC) time series
- Inter-channel consistency analysis using validation time series
- Summary & future work

Background

- Visible Infrared Imaging Radiometer Suite (VIIRS): 22 spectral bands
  - 14 Solar Reflective Bands (RSB)
  - 7 Thermal Emissive Bands (TEB)
  - 1 Day-Nigh Band (DNB)

- On-board calibration is complex

- It is important to use independent validation time series to evaluate post-launch calibration stability
  - Require large volume of data
  - Very time consuming

Objective: develop long-term validation time series for VIIRS calibration stability monitoring

- Validation sites time series over well-establish sites
- Deep Convective Clouds (DCC) Time Series
- Maximize automation

Validation Sites Time Series

Validation Sites Time Series

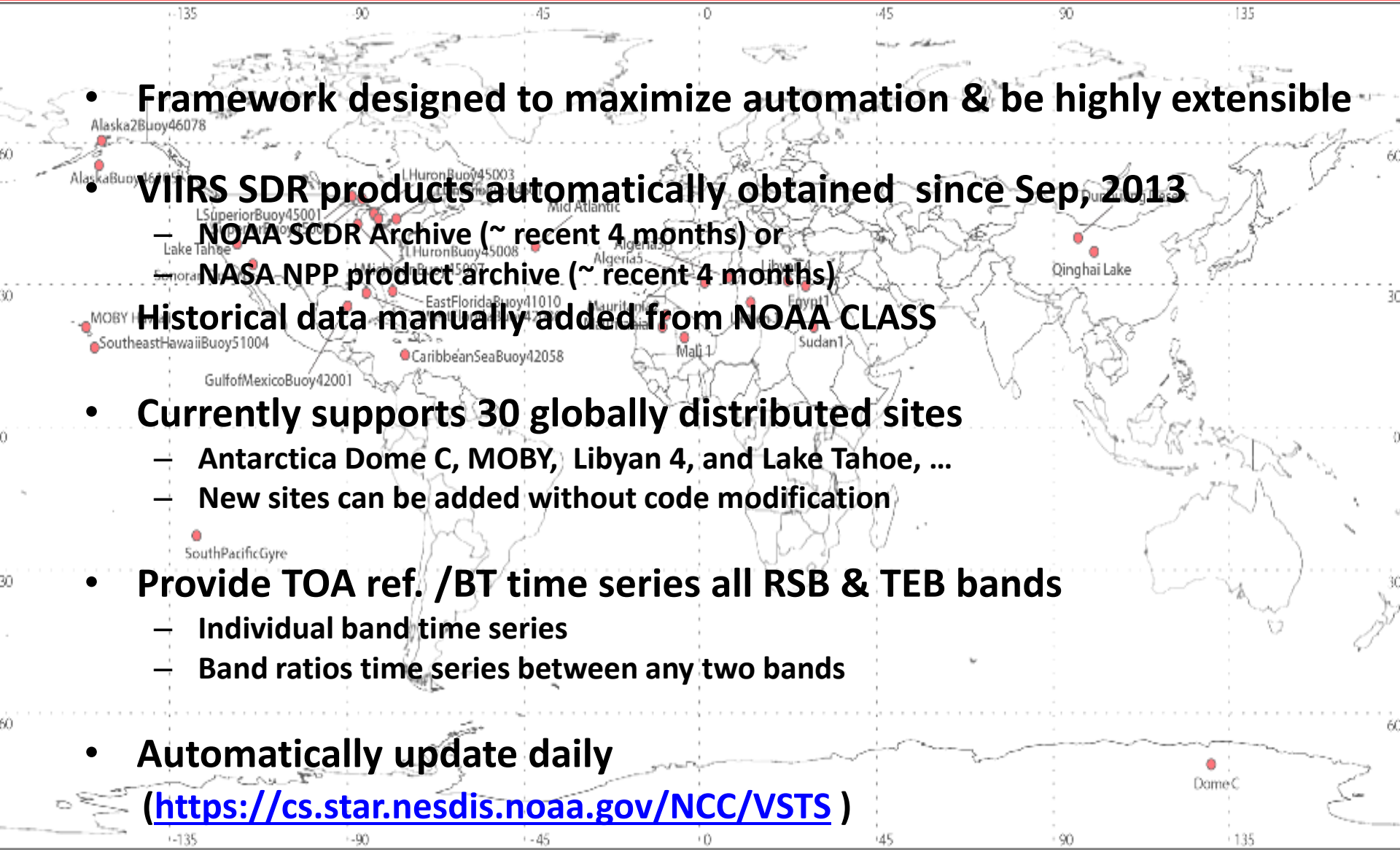

- **Framework designed to maximize automation & be highly extensible**
- **VIIRS SDR products automatically obtained since Sep, 2013**
  - **NOAA SCDR Archive (~ recent 4 months) or**
  - **NASA NPP product archive (~ recent 4 months)**
- **Historical data manually added from NOAA CLASS**
- **Currently supports 30 globally distributed sites**
  - **Antarctica Dome C, MOBY, Libyan 4, and Lake Tahoe, …**
  - **New sites can be added without code modification**
- **Provide TOA ref. /BT time series all RSB & TEB bands**
  - **Individual band time series**
  - **Band ratios time series between any two bands**
- **Automatically update daily**

(https://cs.star.nesdis.noaa.gov/NCC/VSTS)

VIIRS Validation Sites Time Series Methodology

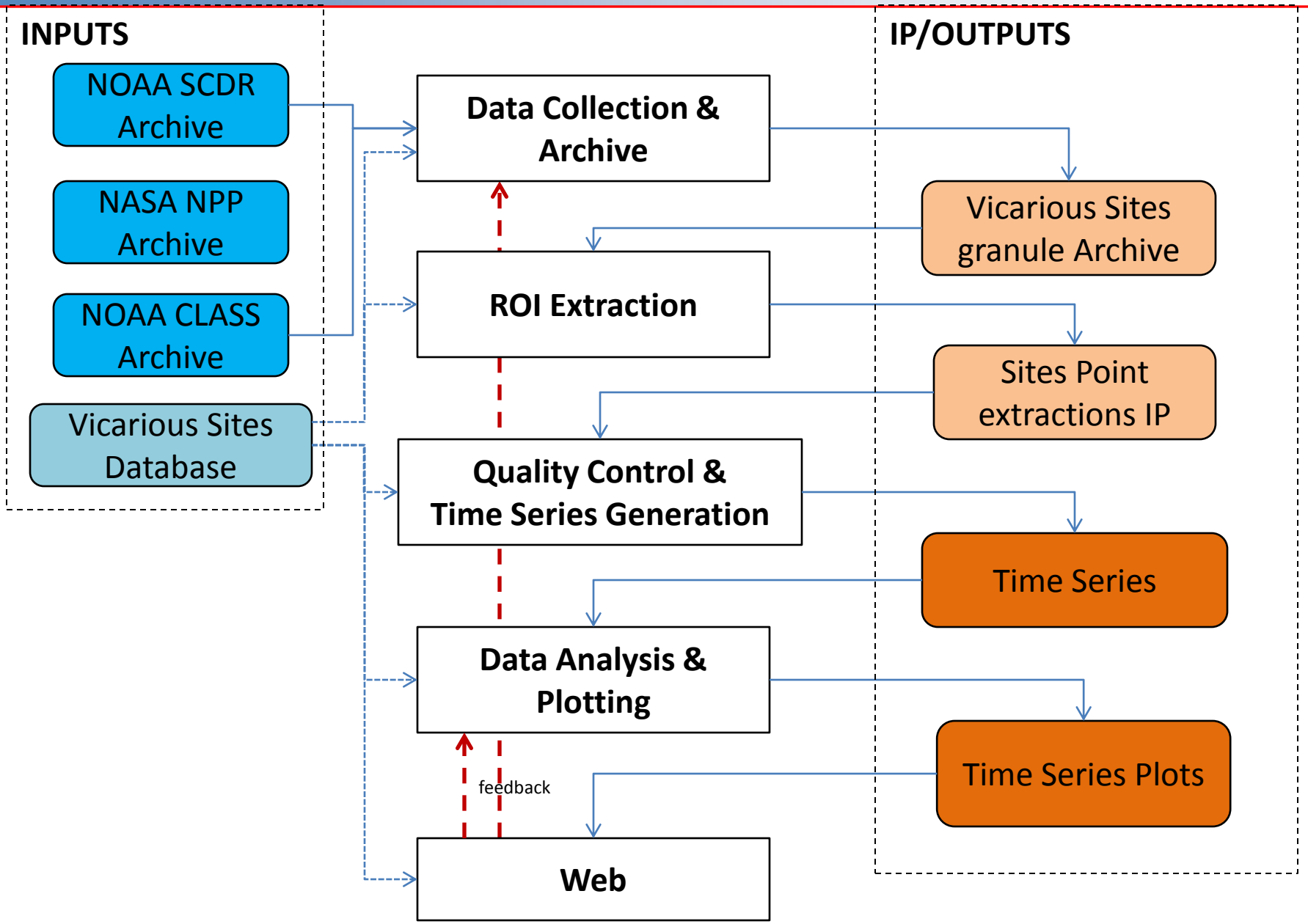

Examples (2013/09 – present)

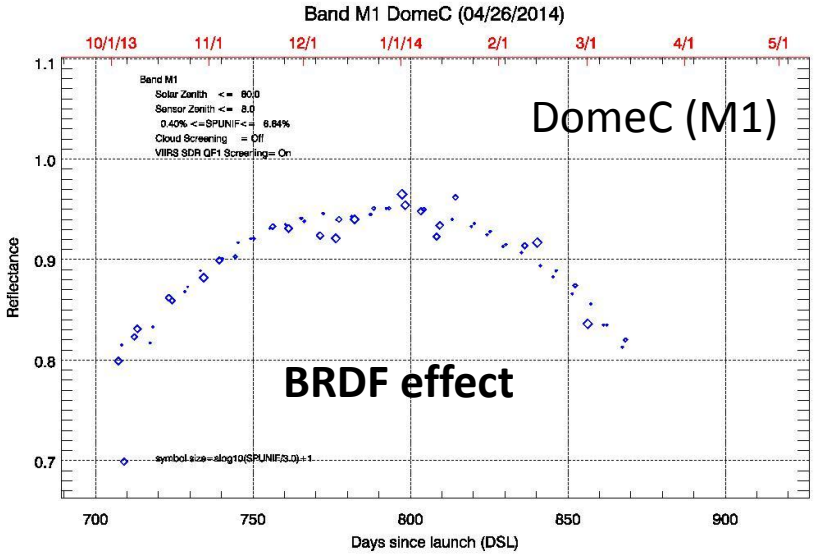

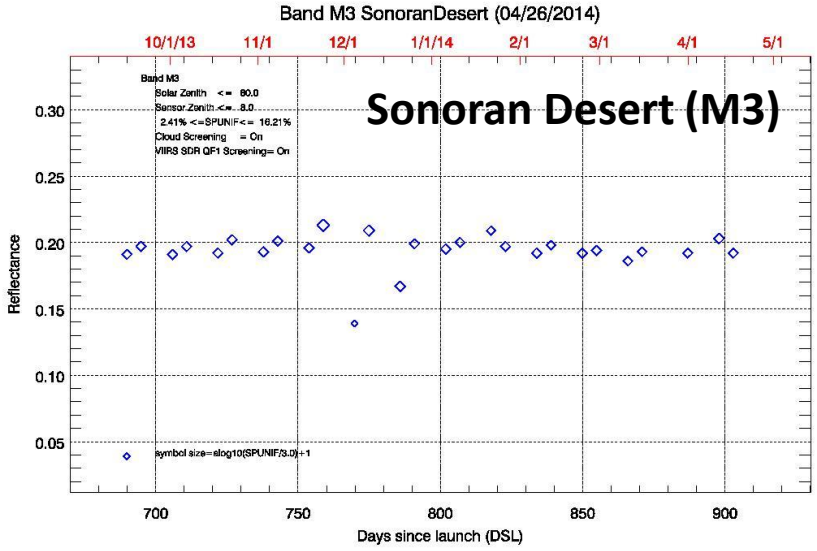

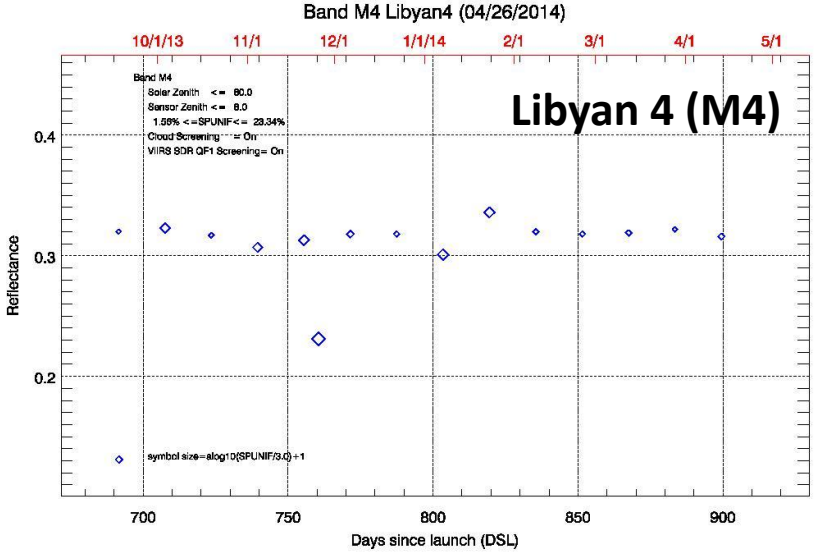

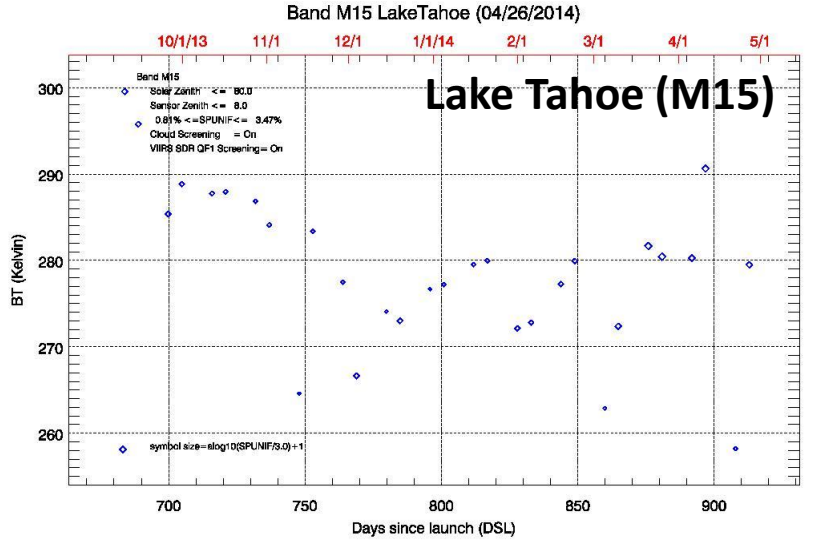

https://cs.star.nesdis.noaa.gov/NCC/VSTS

MOBY Hawaii (2012/02 – present)

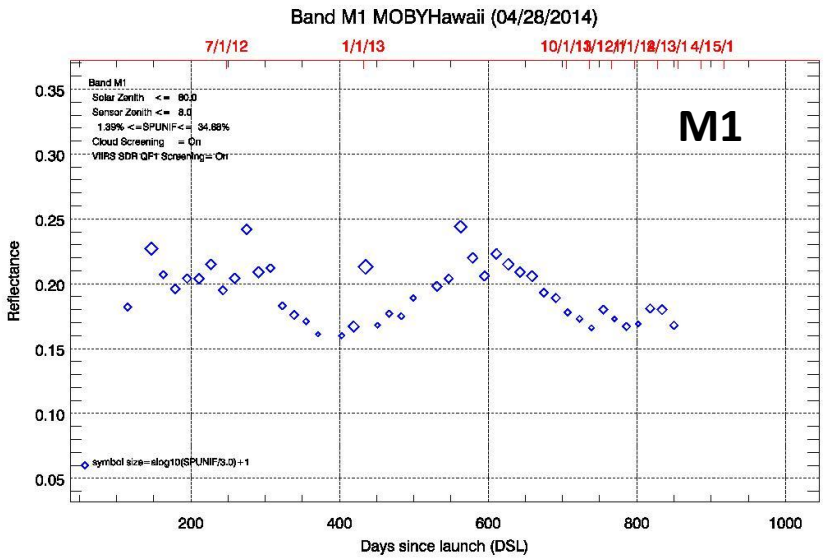

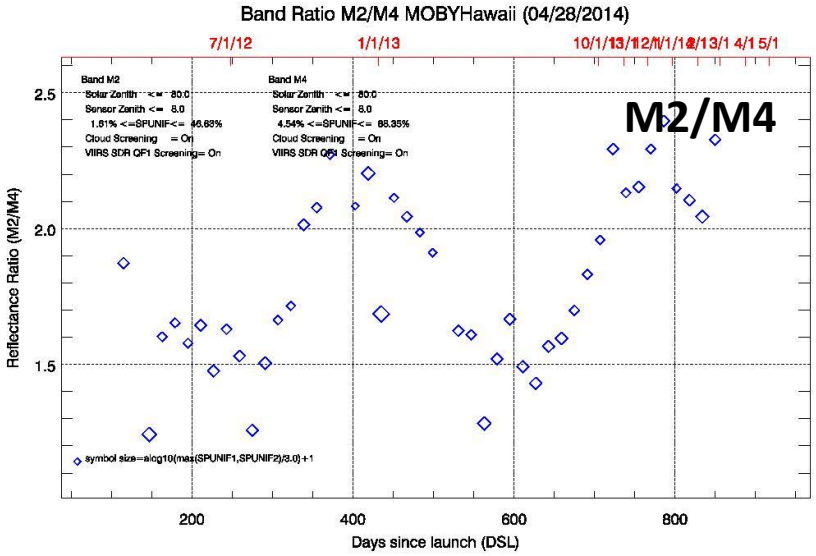

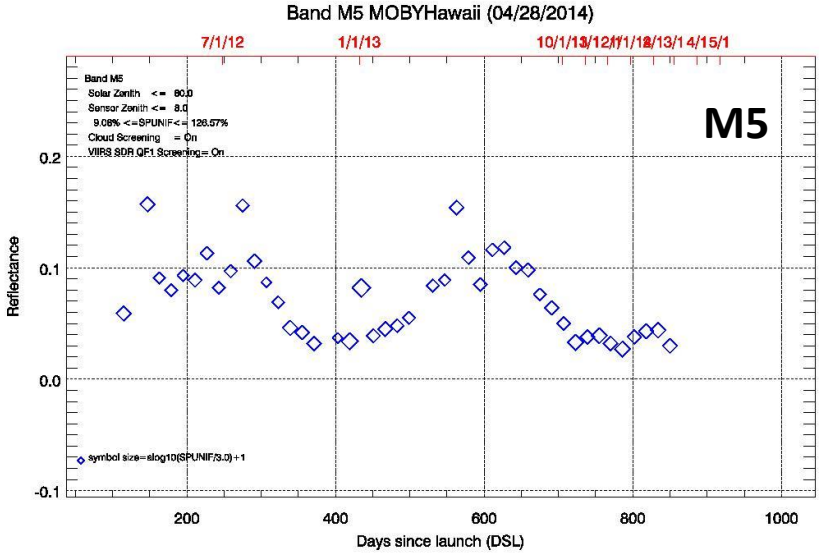

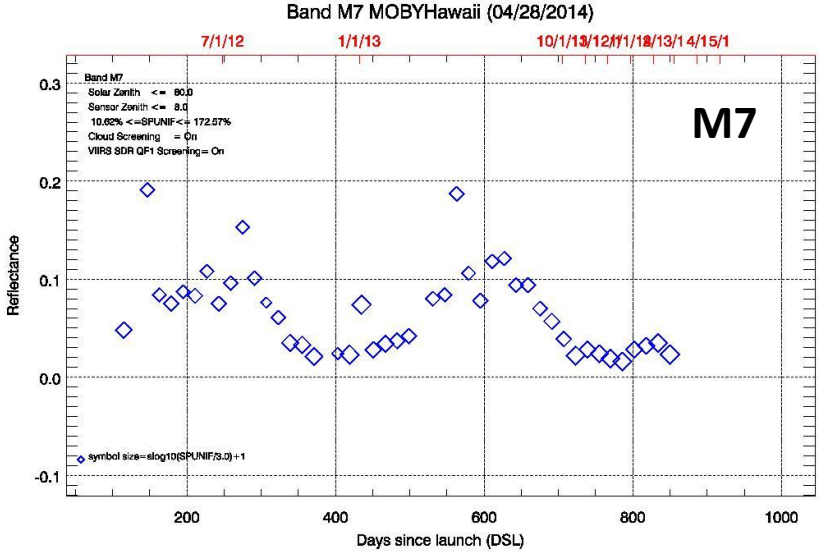

Variation not due to calibration, but seasonal cycle https://cs.star.nesdis.noaa.gov/NCC/VSTS

Deep Convective Clouds (DCCs) Time Series

VIIR DCC Time Series

- **Deep Convective Clouds (DCCs)**
  - extremely cold clouds mostly occur over the ITCZ
  - Start from PBL and ascend to the TTL
  - Bright calibration targets with nearly Lambertian reflectance

- **The DCC Technique**
  - Widely used for RSB vicarious calibration
    Hu et al. 2004; Doelling et al. 2013, 2004; Aumann 2007; Minnis et al. 2008 ; Sohn et al. 2009; Fougnie and Bach 2009; Chen et al. 2013
  - Statistical -based
  - Advantages
    - **Above DCCs, minimal atmospheric effects**
    - **Identified using a single LWIR band centered at ~11 µm (TB11)**
    - **Abundance of data**

DCC Identification for VIIRS

VIIRS DCC Identification Criteria

(Adapted from Doelling et al. 2013; Minnis et al. 2008)

1. TB11 (M15/I5) <= 205 K
2. σ (TB11) of the subject pixel and its eight adjacent pixels <= 1K
3. σ (ref) of the subject pixel and its eight adjacent pixels <= 3%
4. Solar zenith angle (SZA) <= 40°
5. View zenith angle (VZA) <= 35°

   - to avoid the bow-tie effect in VIIRS SDR product

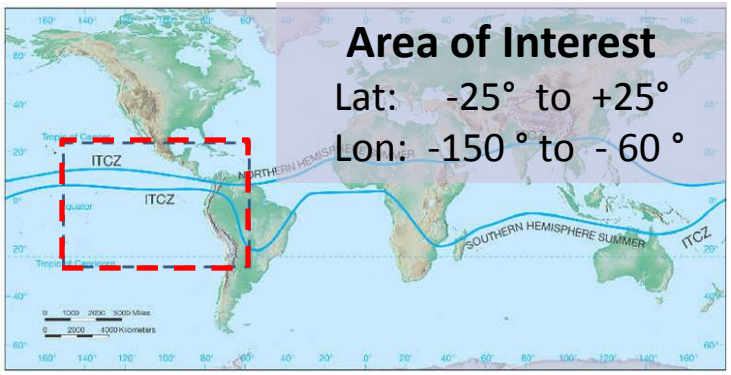

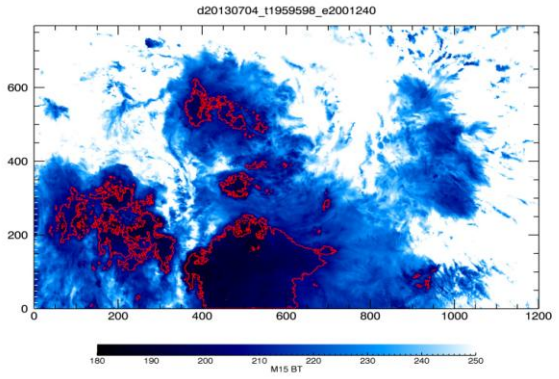

Monthly Probability Distribution Functions(PDFs)

Anisotropic effects corrected using **Hu et al. (2004)** Angular Distribution Model

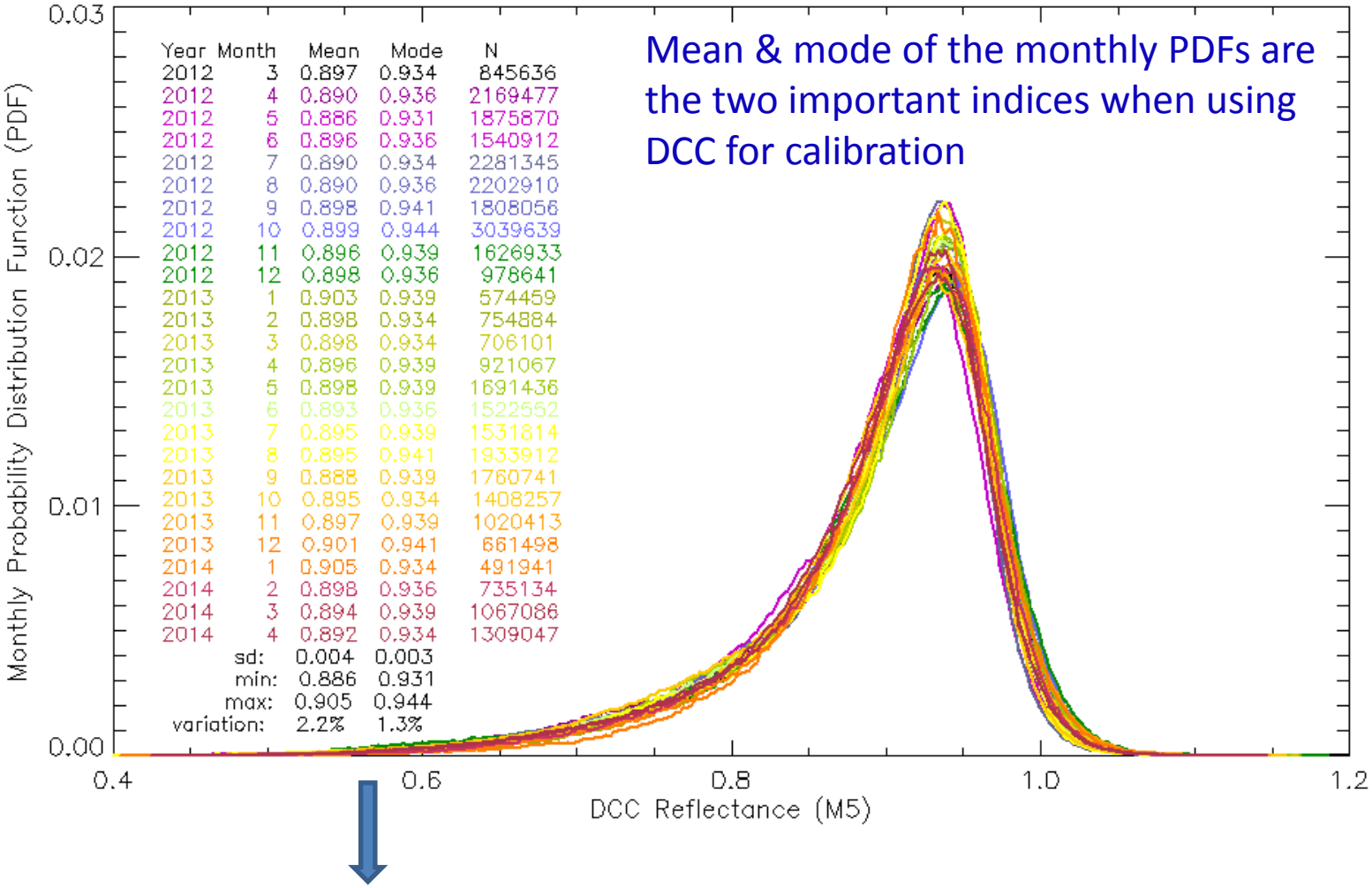

Year	Month	Mean	Mode	N
2012	3	0.897	0.934	845636
2012	4	0.890	0.936	2169477
2012	5	0.886	0.931	1875870
2012	6	0.896	0.936	1540912
2012	7	0.890	0.934	2281345
2012	8	0.890	0.936	2202910
2012	9	0.898	0.941	1808056
2012	10	0.899	0.944	3039639
2012	11	0.896	0.939	1626933
2012	12	0.898	0.936	978641
2013	1	0.903	0.939	574459
2013	2	0.898	0.934	754884
2013	3	0.898	0.934	706101
2013	4	0.896	0.939	921067
2013	5	0.898	0.939	1691436
2013	6	0.893	0.936	1522552
2013	7	0.895	0.939	1531814
2013	8	0.895	0.941	1933912
2013	9	0.888	0.939	1760741
2013	10	0.895	0.934	1408257
2013	11	0.897	0.939	1020413
2013	12	0.901	0.941	661498
2014	1	0.905	0.934	491941
2014	2	0.898	0.936	735134
2014	3	0.894	0.939	1067086
2014	4	0.892	0.934	1309047
	sd:	0.004	0.003	
	min:	0.886	0.931	
	max:	0.905	0.944	
	variation:	2.2%	1.3%	

The mode of monthly PDFs is more stable than the mean (1.3% vs. 2.2%)

DCC Radiometric Sensitivity (M5, M7, I2, June-Sep 2013)

Sensitivity to calibration bias

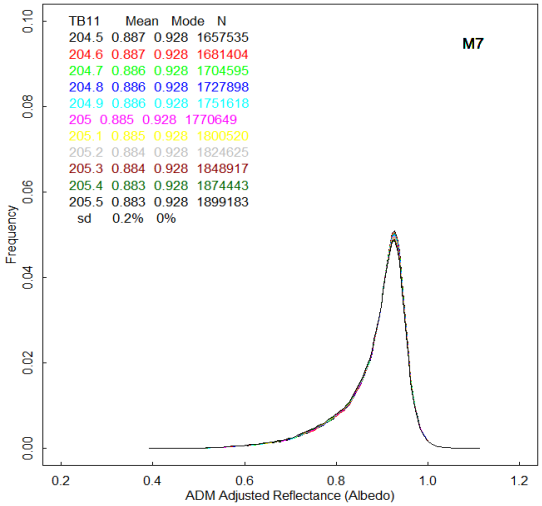

- **Mean & mode insensitive to TB11 calibration bias on the order of 0.5 K**
  - Mode is more stable
- **Mean of monthly PDFs is a function of**
  - TB11, spatial resolution, & cluster size
- **Mode is more stable than mean**, in terms of TB11 threshold, spatial resolution, cluster size, calibration bias

  Also more uniform regionally & temporally (Doelling 2013)

Wang, W. and C. Cao (2014). DCC radiometric sensitivity to spatial resolution, cluster size, and LWIR calibration bias based on VIIRS observations. Submitted to JTECH, under revision.

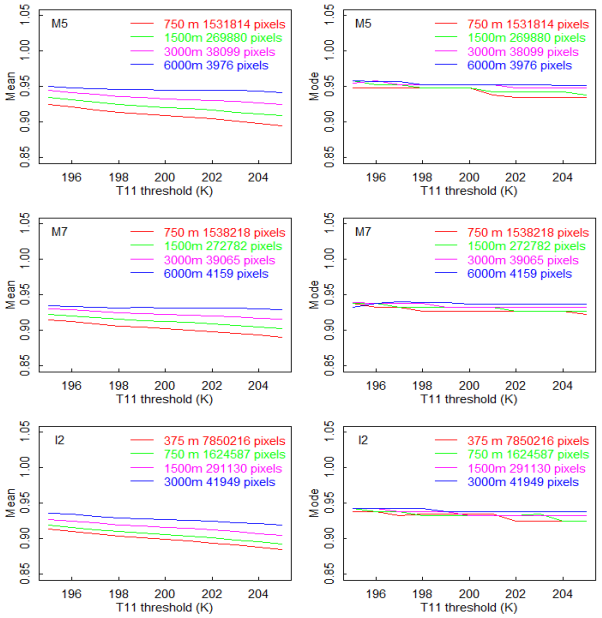

Sensitivity to spatial reso. & TB11 threshold

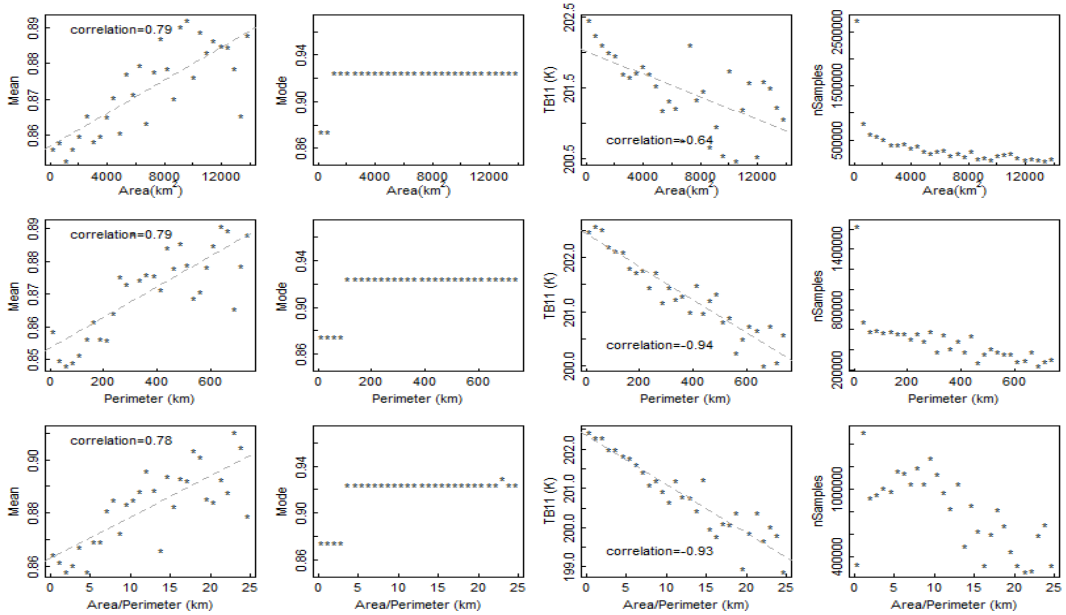

Sensitivity to cluster size & TB11

VIIRS DCC Mode Time Series
(M1-M5, M7)

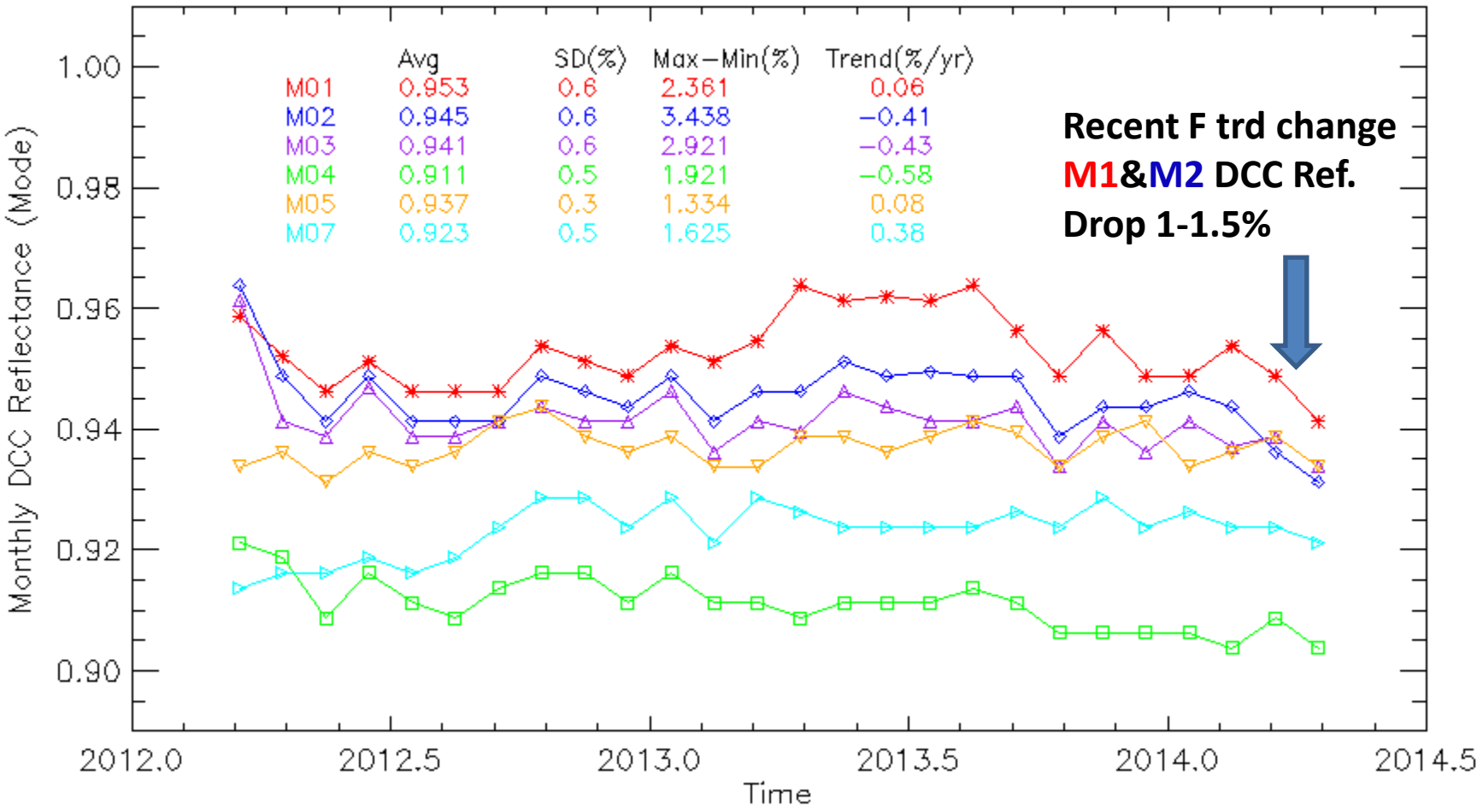

- No obvious seasonal cycle
- σ <=0.6% for all bands
- Max - Min <3.5 % for all bands
- M4, M5 & M7 are more stable

Calibration Changes Detection Using DCC mode time series

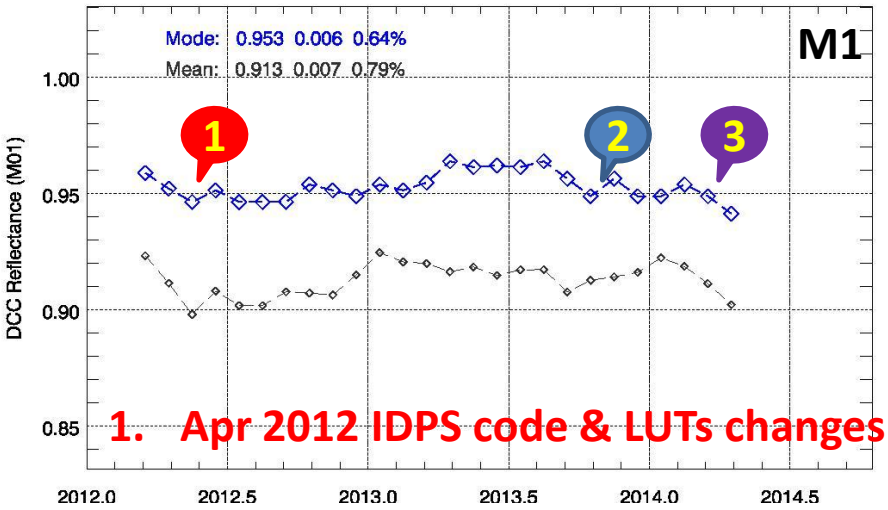

1. Apr 2012 IDPS code & LUTs changes

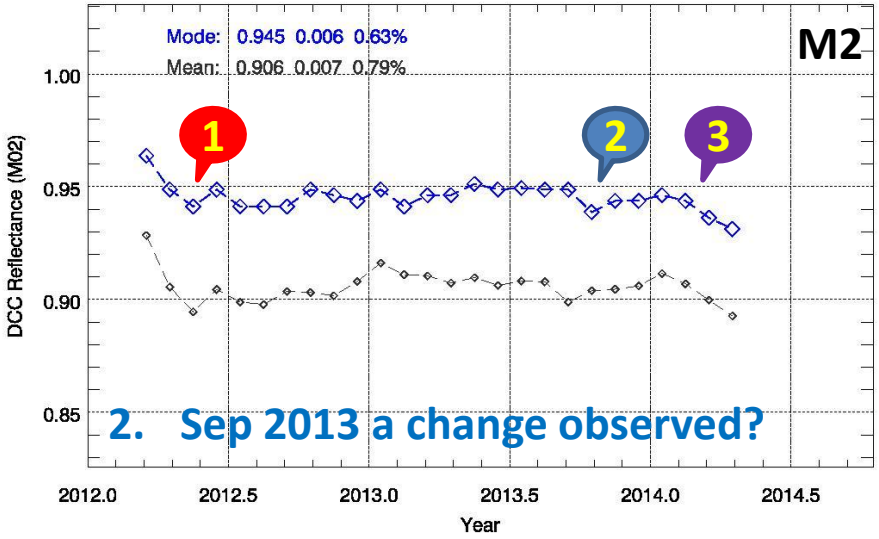

2. Sep 2013 a change observed?

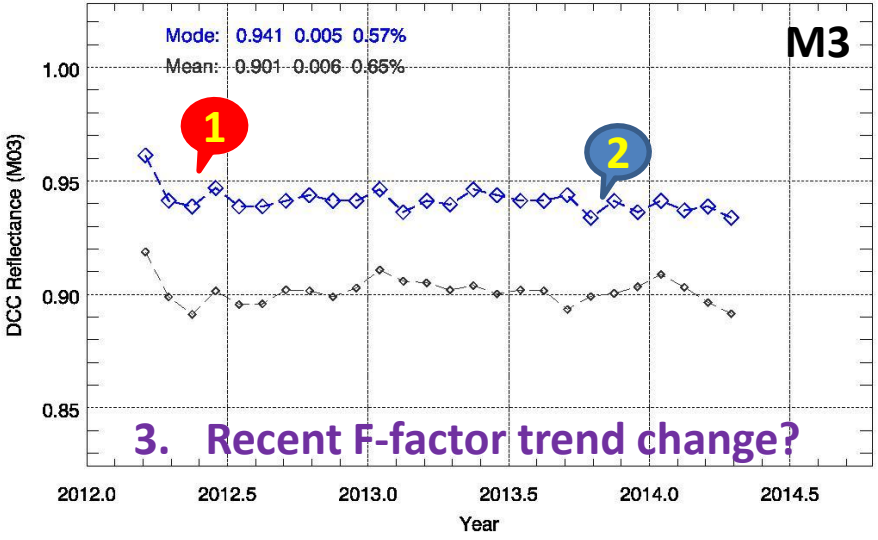

3. Recent F-factor trend change?

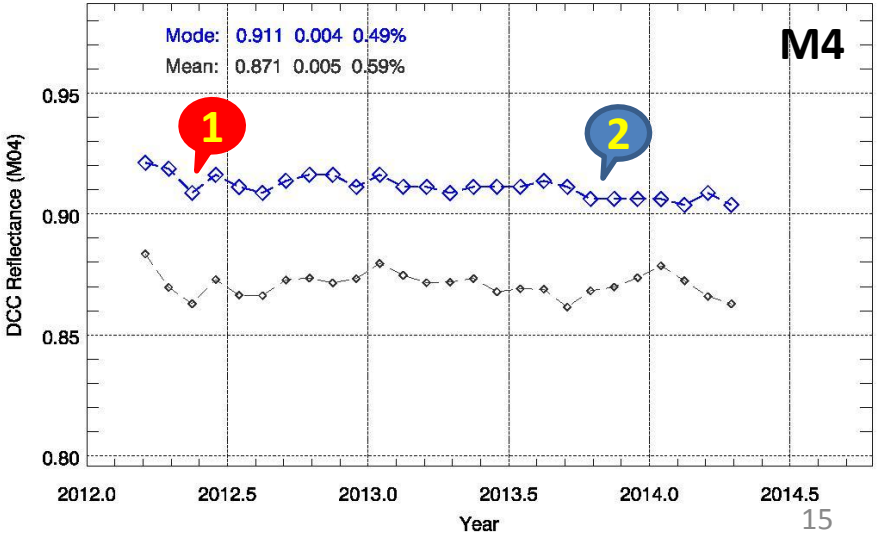

Calibration Change Detection Using DCC band ratio time series

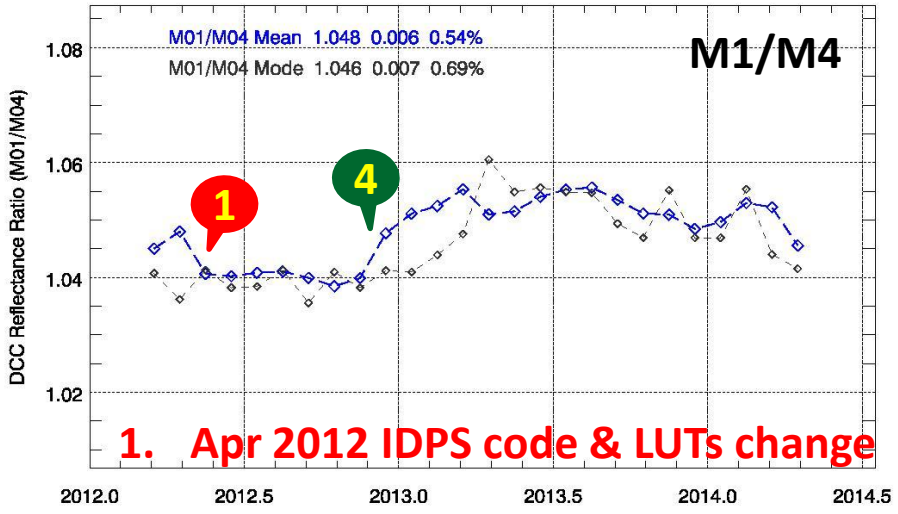

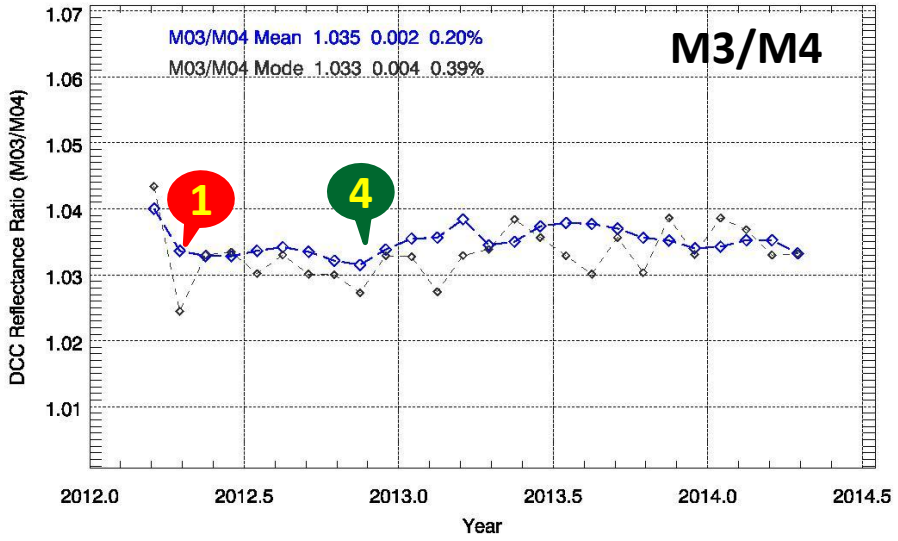

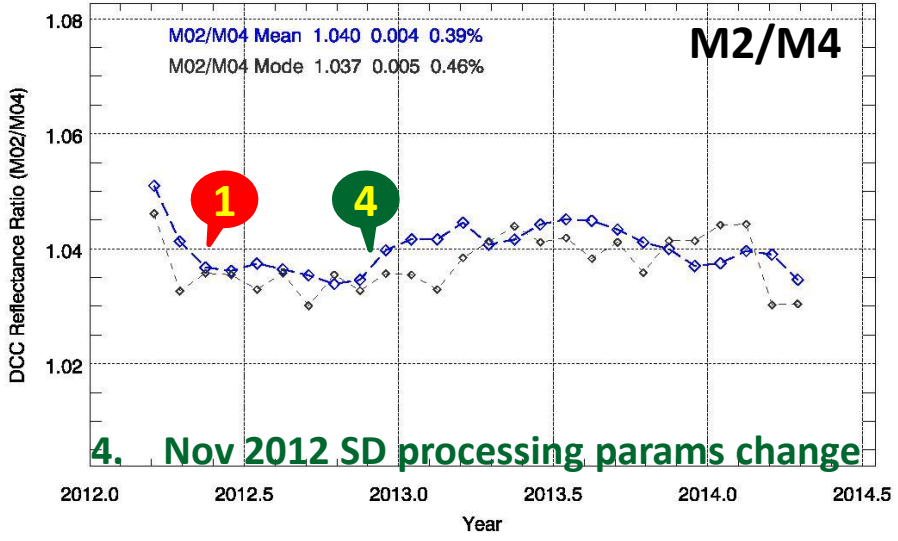

Using M4 as reference

DCC mean ratio is stable than mode ratio, effects due to various factors sig. reduced by ratio

2012 & 2013 show different ratio patterns
→ coincident with OC group complains

VIIRS DCC Mode Time Series vs. VIIRS-MODIS(Aqua-collection6) SNO Time Series

DCC vs SNO (polar)

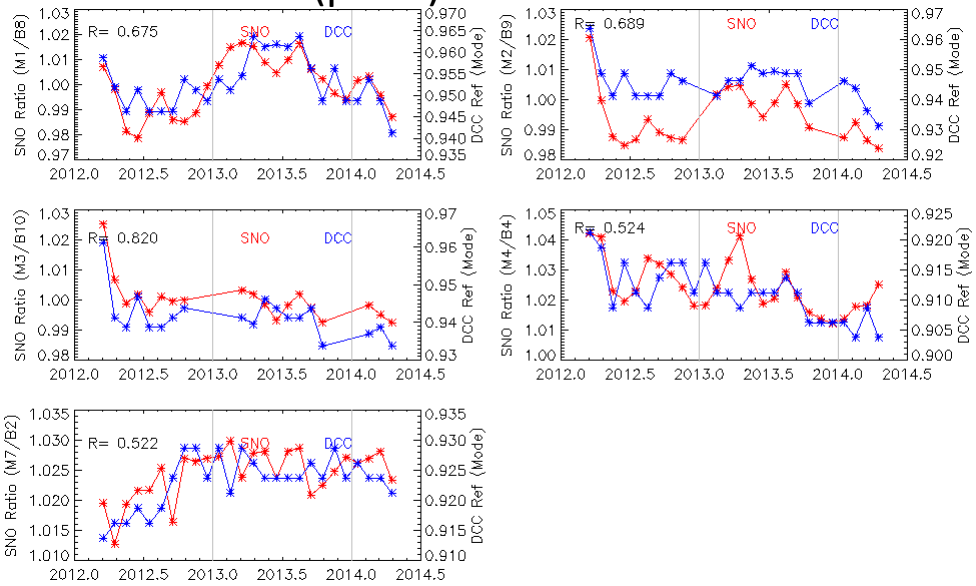

DCC vs SNO-x (desert)

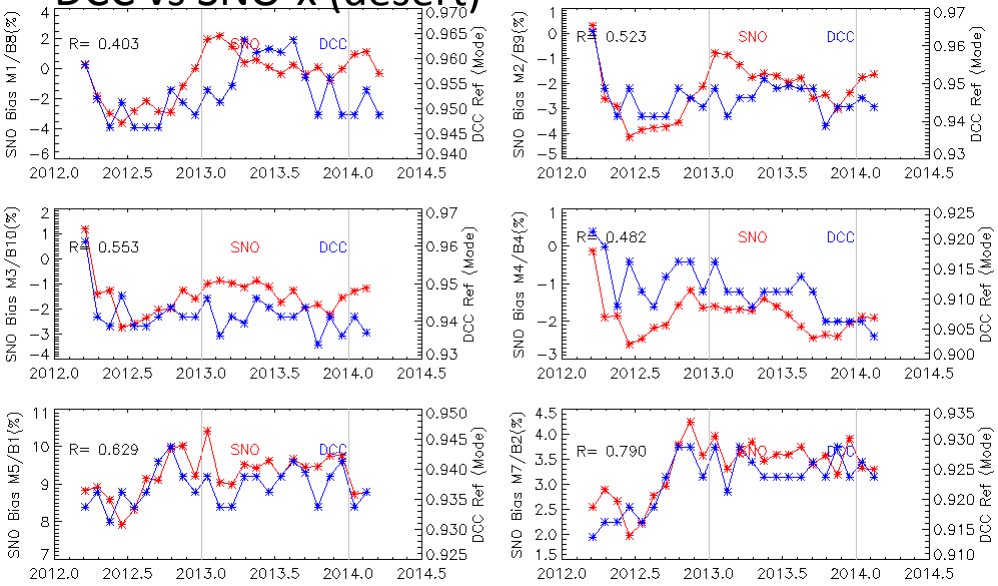

- **DCC time series correlated with SNO & SNO-x time series**
- DCC time series are more stable
  - Scales in the two y-axes are different
- All time series: M5 & M7 more stable than M1-M4
- DCC time series are valuable for monitoring VIIRS calibration stabilities

SNO time series courtesy of Slawek Blonskii
SNO-x time series courtesy of Sirish Uprety

Inter-channel consistency analysis using validation time series

1. M7 vs. I2 comparison
2. M10 vs. I3 comparison

M7 vs. I2 Comparison

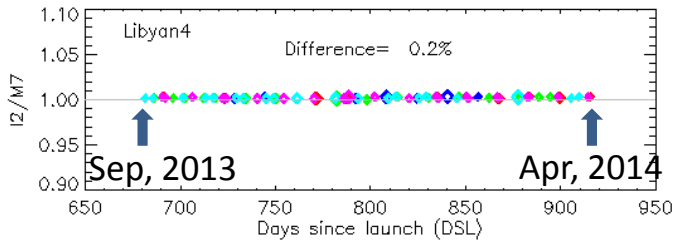

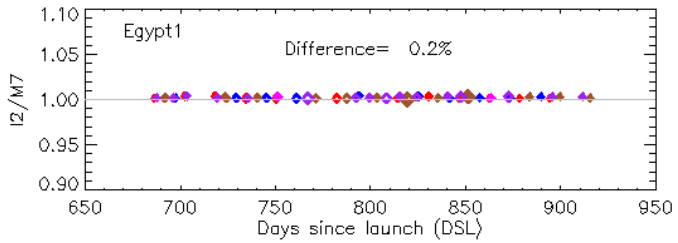

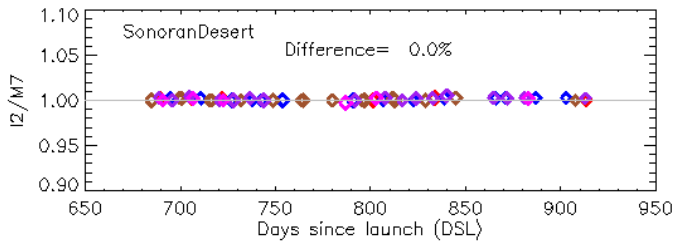

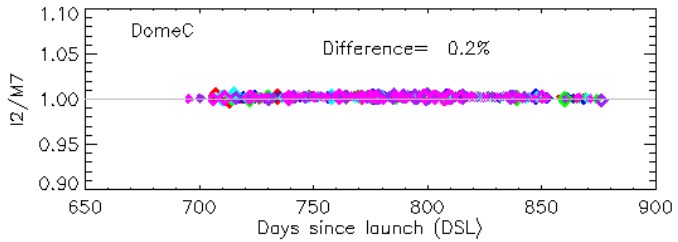

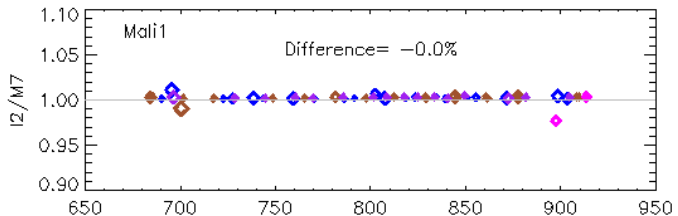

M7 is generally consistent with I2

0-0.2% **(validation sites time series)**

0.2% **(DCC time series)**

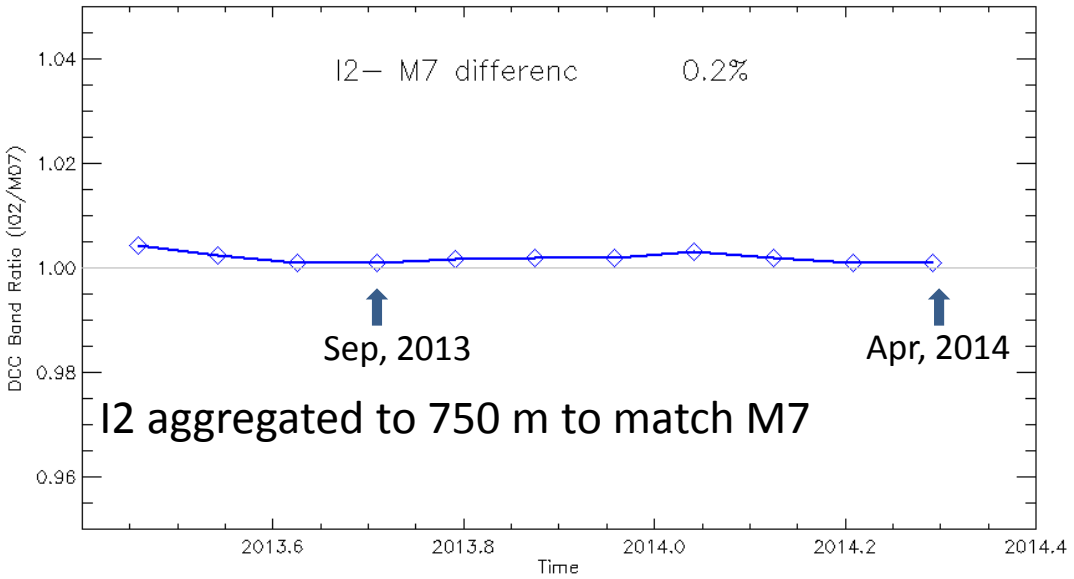

I2 aggregated to 750 m to match M7

BRDF & atmo. effects cancel out by band ratio

M10 vs. I3 Comparison

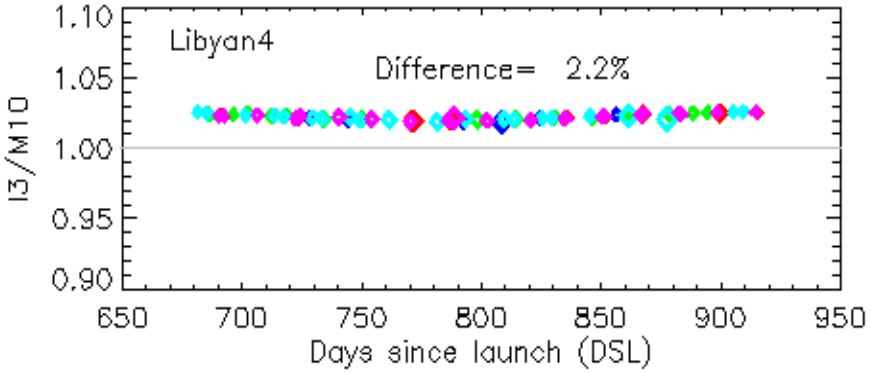

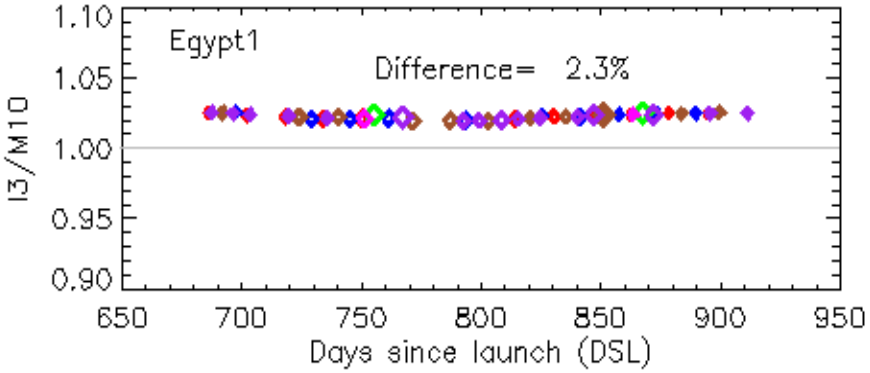

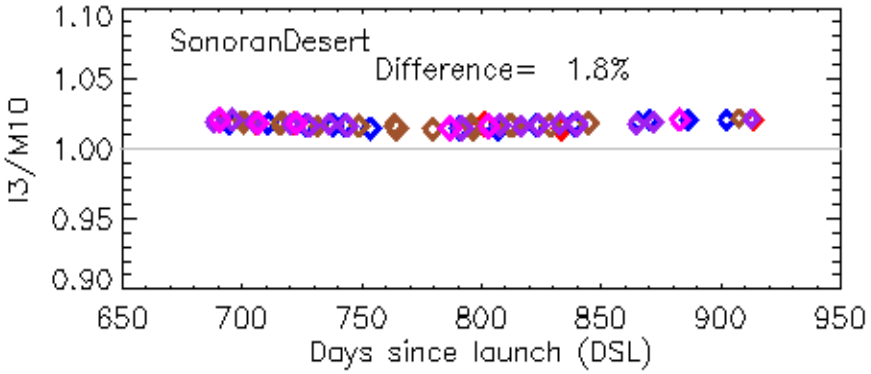

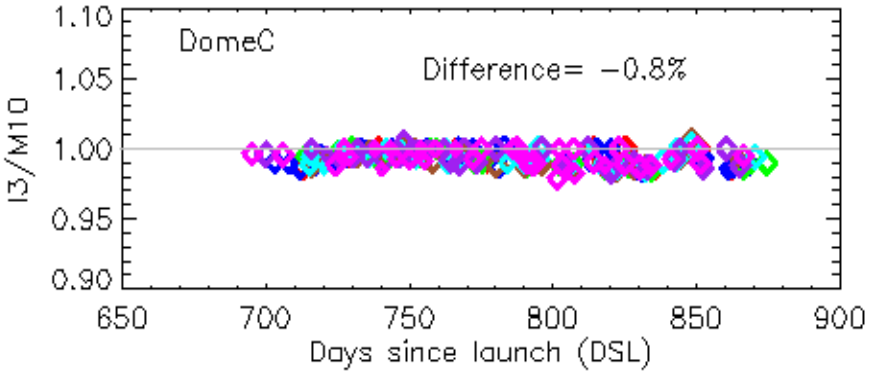

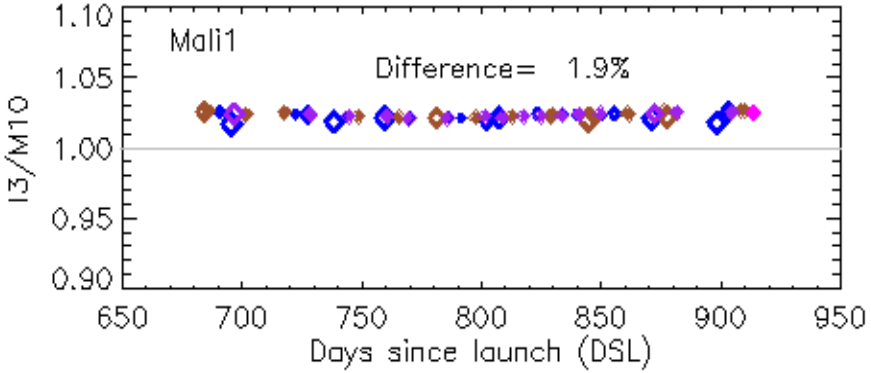

Large M10/I3 difference:

-0.8 – 2.3%

scene dependent

Summary & Future Work

- STAR VIIRS SDR support team developed validation time series for VIIRS calibration stability monitoring
  - Validation sites time series
    - Automatic data collection since Sep, 2013
    - 30 globally distributed sites
    - RSB & TEB bands time series & band ratio time series update daily
  - DCC time series
    - Completed M1-M5, M7 (2012/03 – present) , update monthly
    - Capable of capture calibration changes

- Next Step
  - Improve quality control for validation time series, esp. for sites over oceans & lakes
  - Support DNB
  - Incorporating historical data for all sites (CLASS)
  - In-depth data analysis (BRDF, atmosphere correction, …)

  - Develop DCC time series for DNB (day/night), M8-M11, I1-I3

- The methodologies can be adapted easily to support future JPSS missions and other instruments such as GOES-R/ABI.

Backups

DCC Time Series (Mean)

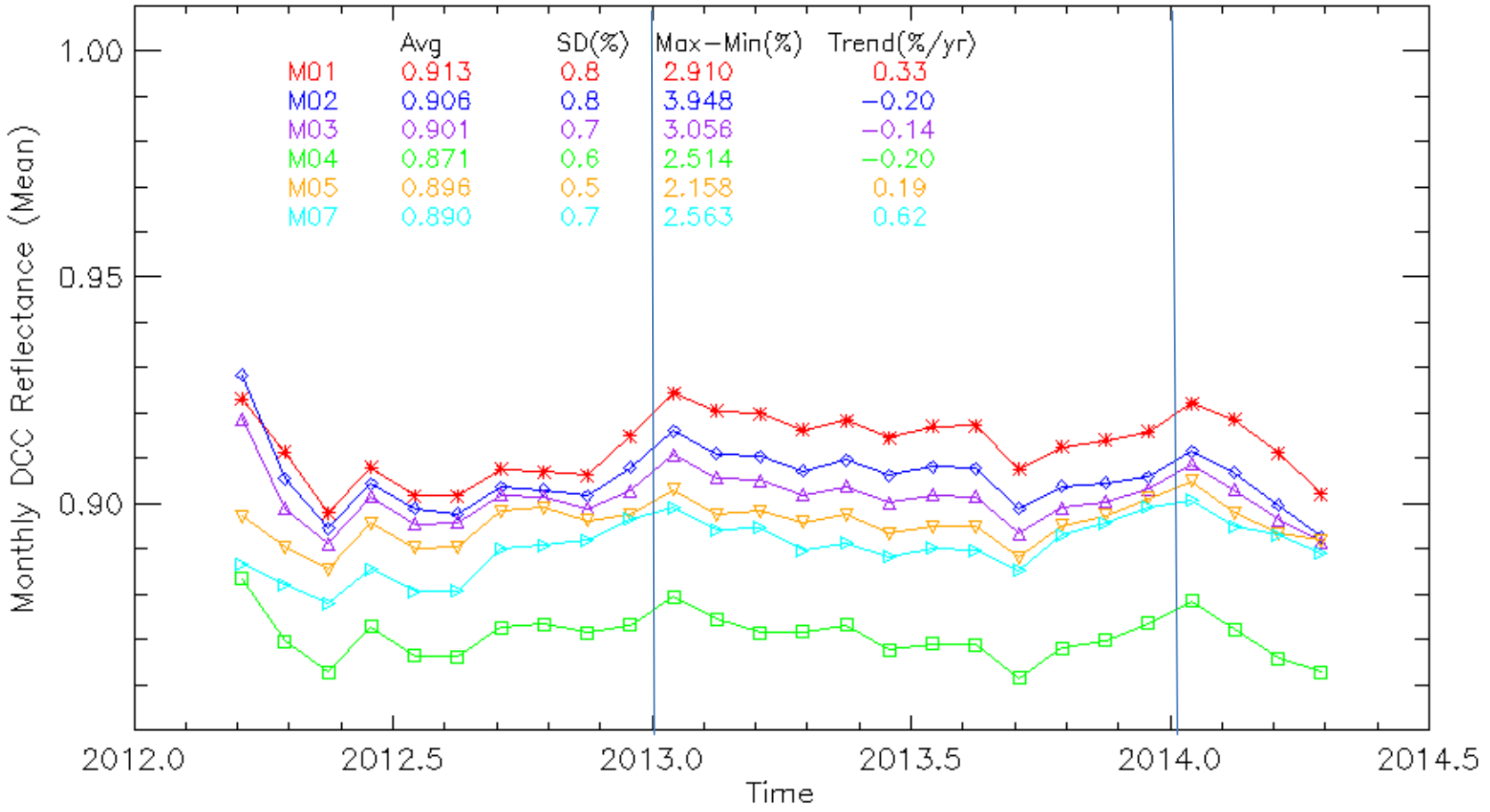

Major calibration changes can also be observed in the mean time series
But, annual cycle more obvious than the mode time series

JPSS J1 VIIRS Polarization Sensitivity Analysis and Impact

May 14, 2014

Jeff McIntire, Hassan Oudrari, and Xiaoxiong Xiong
VCST / NASA GSFC

Outline

JPSS J1 VIIRS Polarization Sensitivity

- Sensor requirements
- Testing overview
- Analysis methodology
- Results
- Impact on science
- Future work

Sensor Requirements

Polarization Sensitivity Requirements

V_PRD-12624 The VIIRS Sensor linear polarization sensitivity of the VIS and NIR bands shall be less than or equal to the values indicated in table for scan angles less than 45 degrees of Nadir.

Band	Sensitivity [%]
I2, M1, M7	3
I1, M2, M3, M4, M5, M6	2.5

V_PRD-12667 The VIIRS Sensor linear polarization sensitivity shall be measured within a characterization uncertainty of 0.5% (one sigma) for scan angles less than 55.84 degrees off Nadir.

Test Setup

JPSS J1 VIIRS Polarization Sensitivity

- Sensor level test – FP-11 (component level testing also performed)
  - Source – SIS-100-2
  - Two sheet polarizers used – BVO777 and BVONIR
  - Shaping filter used for some bands (Sonoma and Hoya)
  - Various baffling also installed to minimize stray light
- VisNIR bands and DNB tested

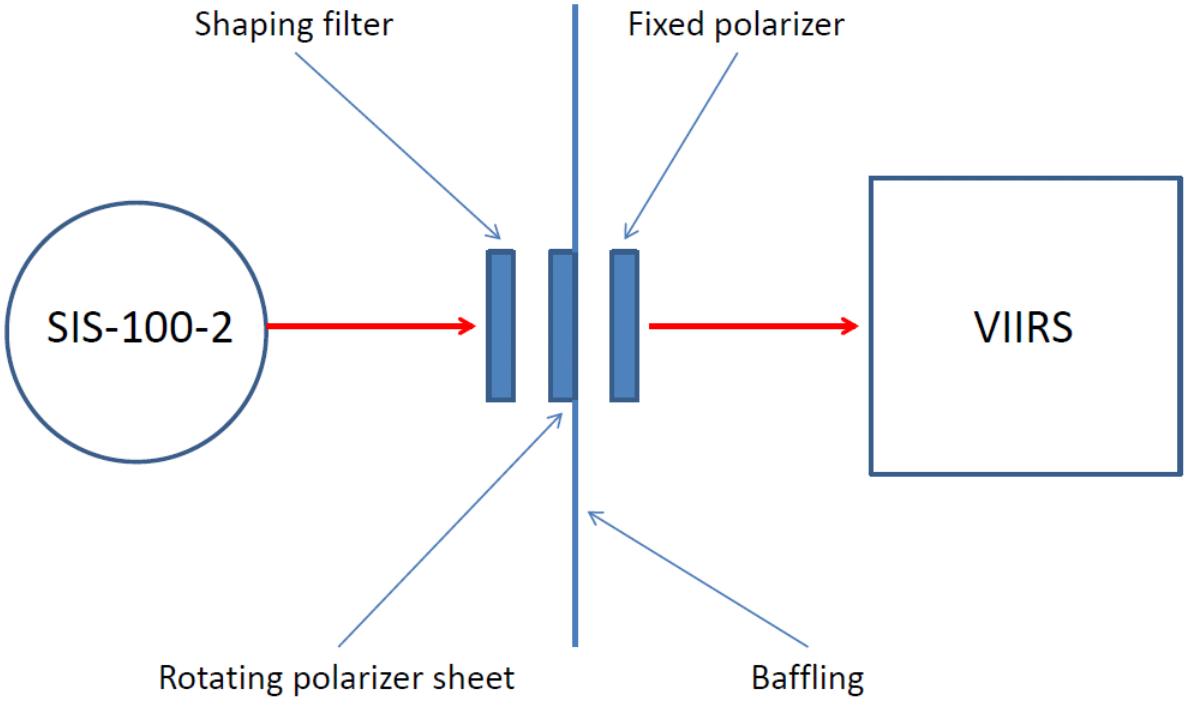

Methodology

1) Check stray light data – both dark and "lollipop" test configurations
   Determine if there is any contamination
2) Determine efficiency of polarizer from cross-polarizer data
   Use zeroth and second order terms in Fourier series
3) Analyze polarization sensitivity data to determine the polarization amplitude and phase
   Use zeroth through fourth order terms in Fourier series

$$dn(\alpha) = \frac{1}{2} c_0 \left[1 + \sum_{n=1}^{4} a_n \cos(2\alpha - \delta_n) \right]$$

where the polarization factor (amplitude) and phase are defined as

$$a_2 = \frac{\sqrt{c_2^2 + d_2^2}}{\frac{1}{2} c_0 \sqrt{a_2^{eff}}} \qquad \delta_n = \tan^{-1}\left(\frac{d_2}{c_2}\right)$$

including polarizer efficiency correction factor (a_2^{eff})

Fourier Analysis

Fourier Analysis – M1 HAM A using the BVONIR polarizer with the Sonoma filter shown (-8 degrees scan angle)

Data is well reproduced by Fourier series

Symbols – measured data; Lines – Fourier series

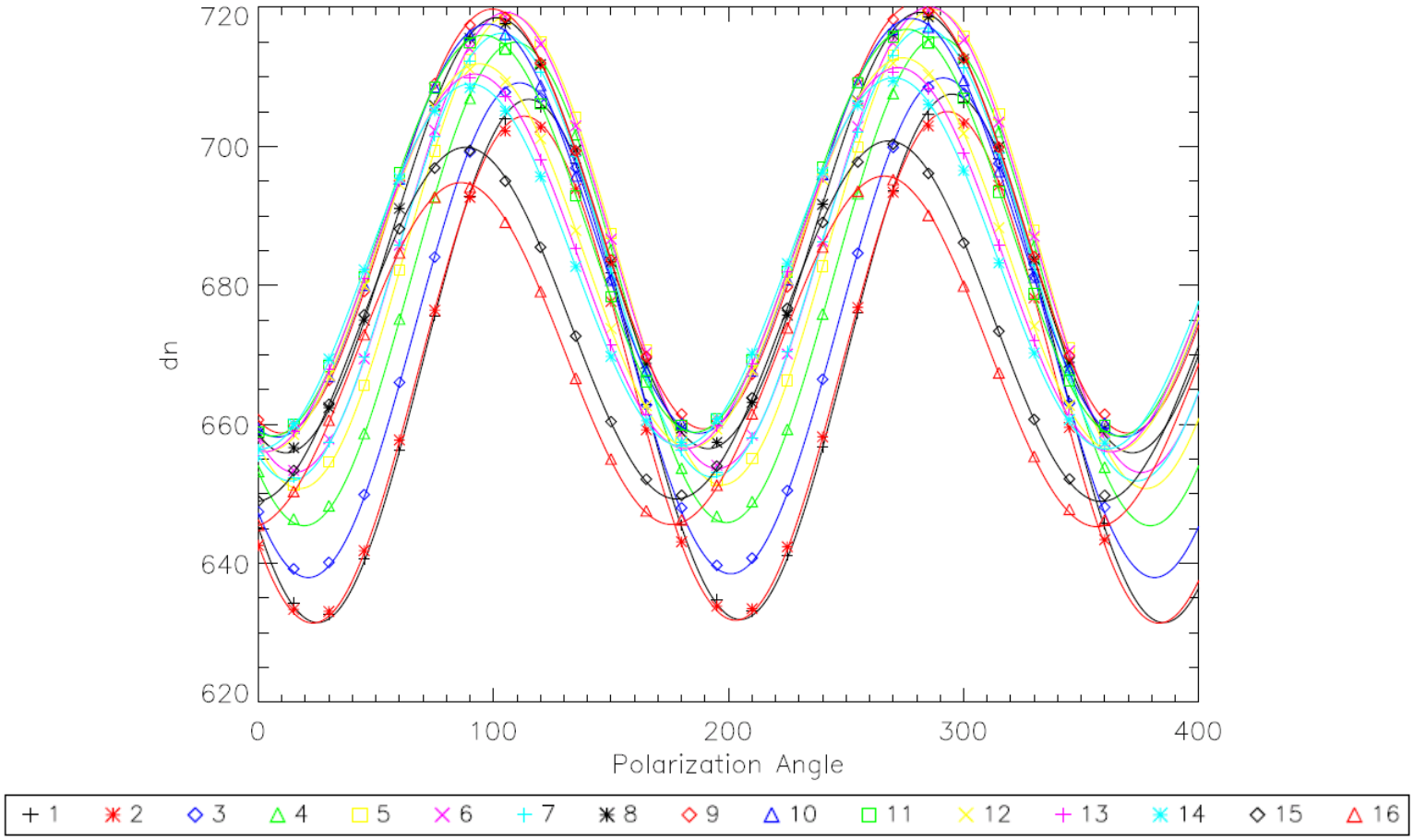

Fourier Analysis

Zeroth through fourth order terms in the Fourier expansion (M1 HAM A, BVONIR polarizer with the Sonoma filter)

- 1st, 3rd, and 4th order terms are generally subdominant (results consistent for all bands)
- Large detector, scan angle, and HAM (not shown) dependence observed

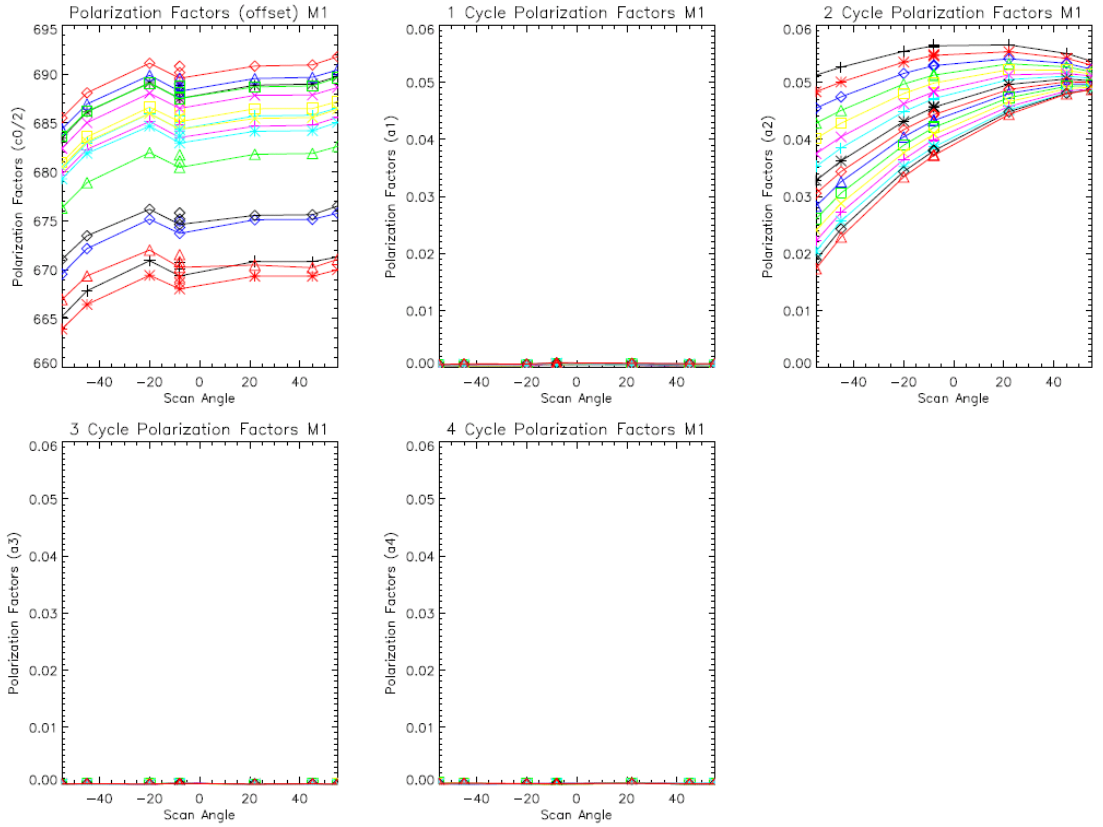

Polarization Factors

Polarization factors (BVONIR)

BVONIR w/ Sonoma: M1-M3; BVONIR w/o Sonoma: I1-I2, M4-M7
HAM side dependence
Large scan angle and detector dependence

HAM A

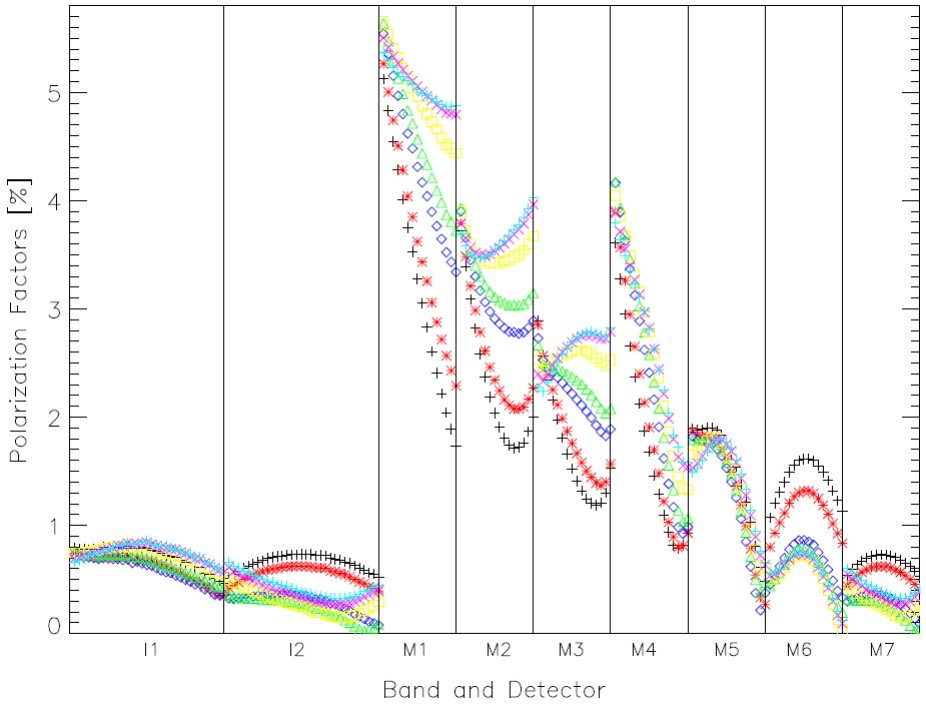

HAM B

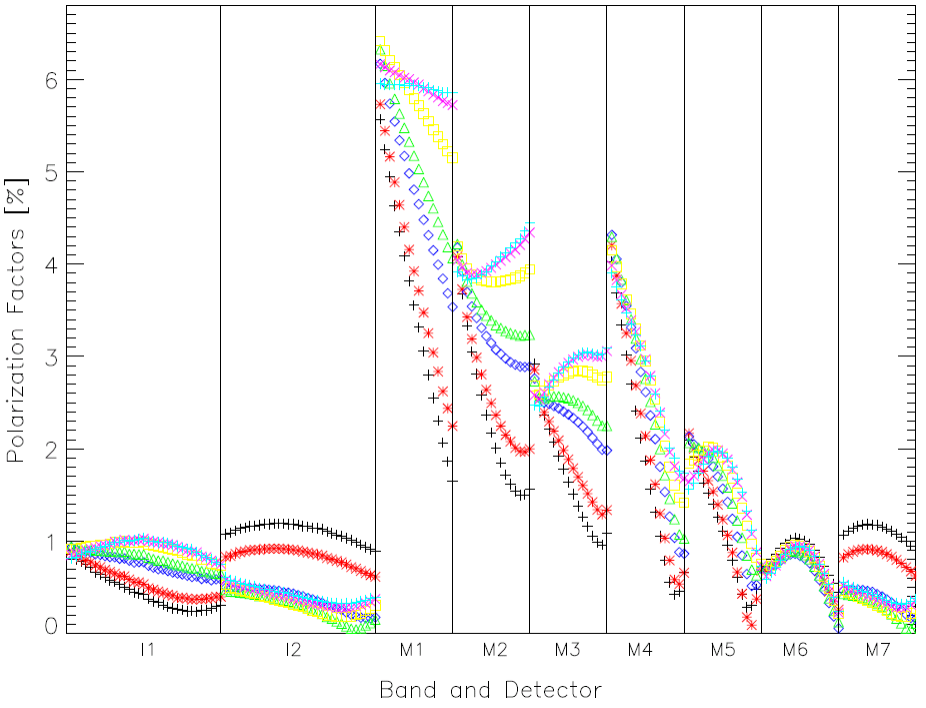

Polarization Phases

Polarization phases (BVONIR)

BVONIR w/ Sonoma: M1-M3; BVONIR w/o Sonoma: I1-I2, M4-M7
HAM side dependence
Large scan angle and detector dependence

HAM A

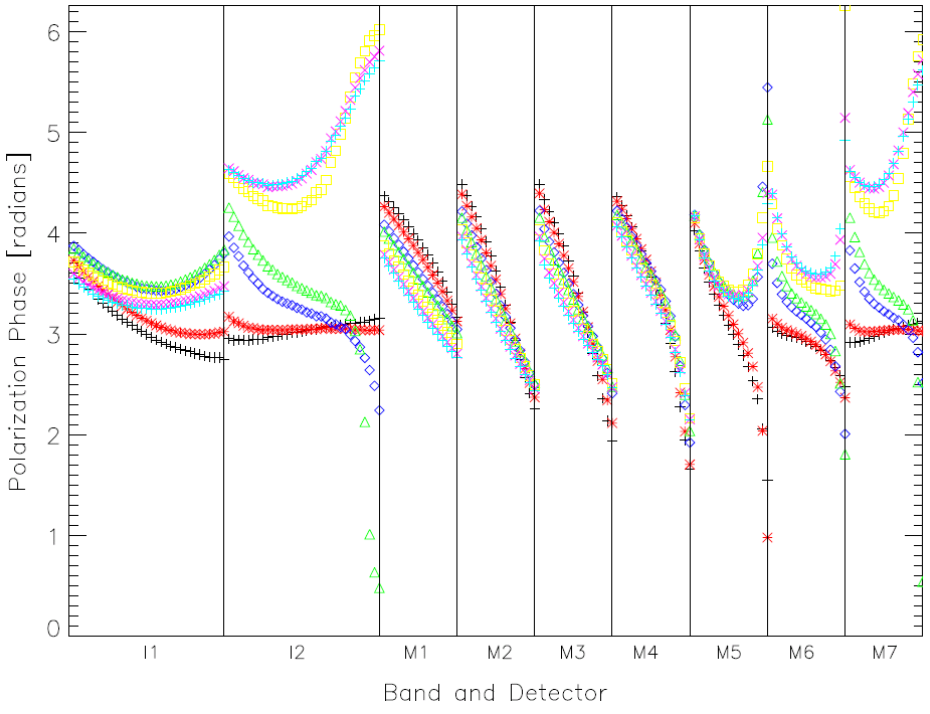

HAM B

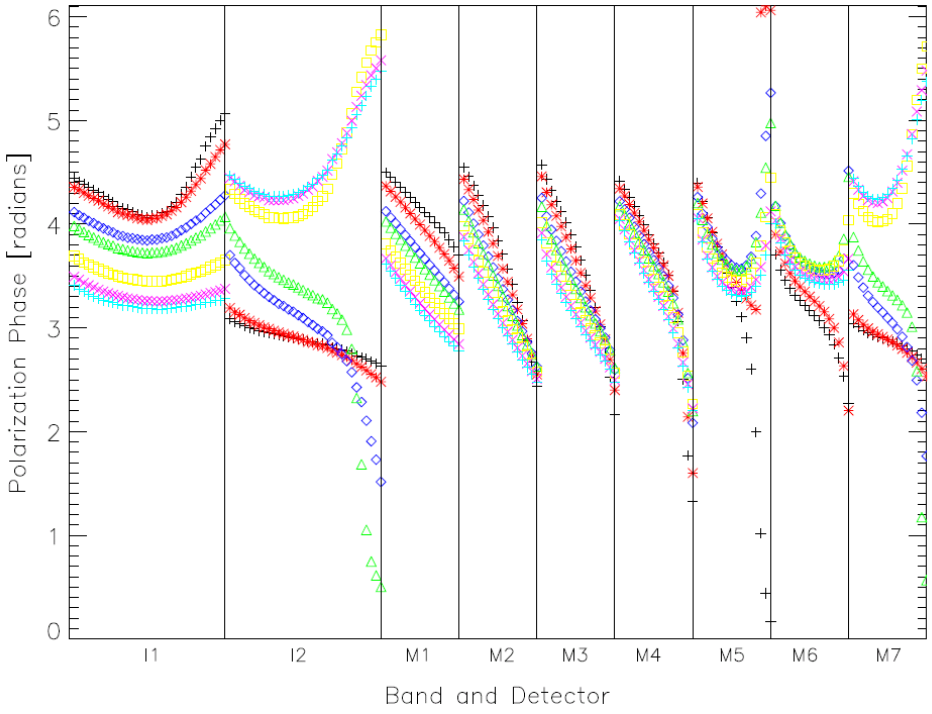

DNB Polarization Factors

DNB LGS polarization factors – BVONIR, HAM A

DNB is broadband (~500 – 900 nm)

Scan angle dependence appears consistent with VisNIR bands

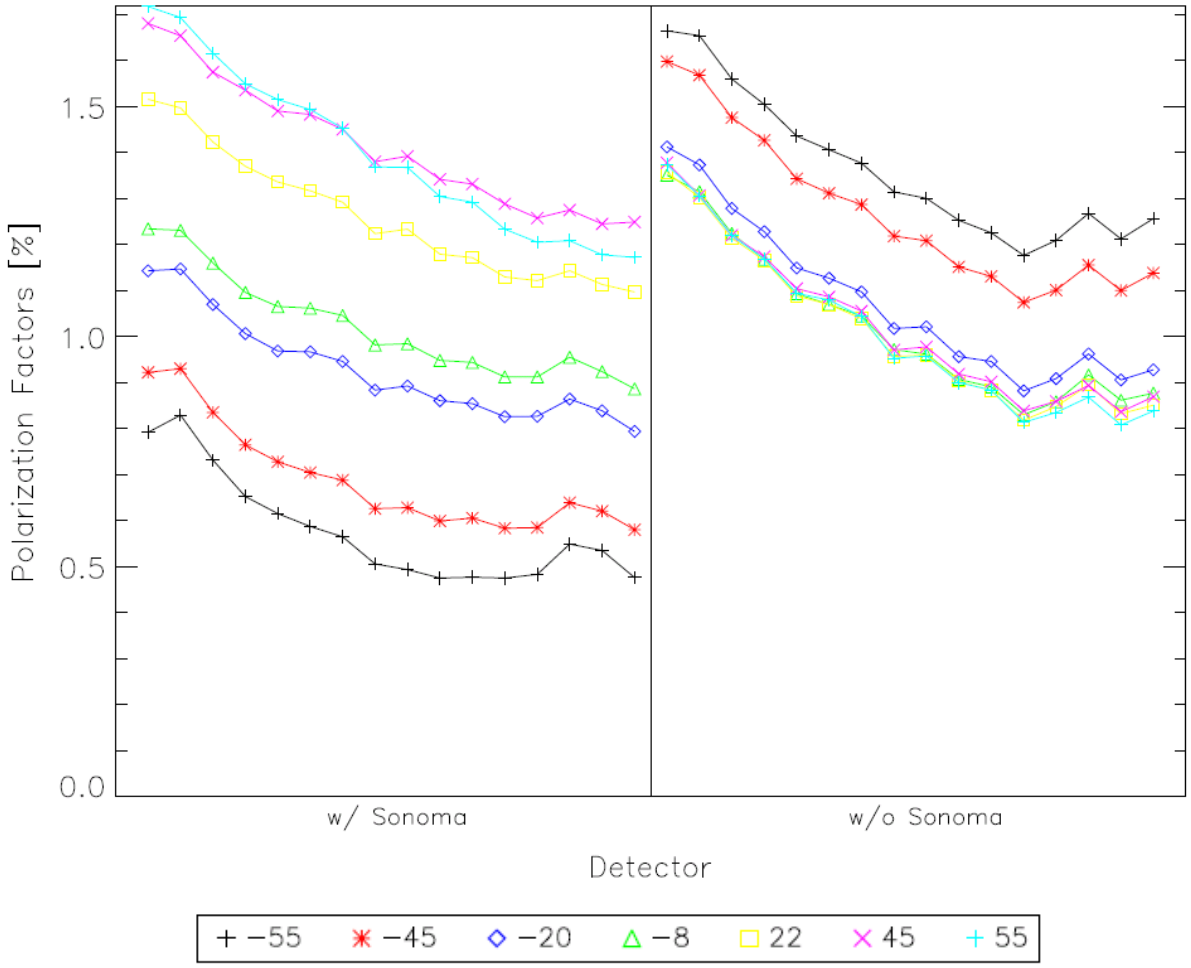

Requirements Verification

Band	Sensor	Scan Angle						
		-55	-45	-22	-8	20	45	55
I1	SNPP	1.50	1.24	0.93	0.85	0.70	0.64	0.62
	JPSS J1	0.81	0.74	0.73	0.76	0.82	0.85	0.85
I2	SNPP	0.29	0.27	0.34	0.37	0.47	0.51	0.51
	JPSS J1	0.73	0.62	0.36	0.37	0.50	0.61	0.66
M1	SNPP	2.99	2.63	1.95	1.79	1.42	1.21	1.40
	JPSS J1	5.13	5.26	5.54	5.65	5.66	5.51	5.37
M2	SNPP	2.11	1.97	1.63	1.53	1.28	1.17	1.29
	JPSS J1	3.72	3.79	3.90	3.94	3.90	3.99	4.04
M3	SNPP	1.20	1.14	0.90	0.82	0.61	0.70	0.80
	JPSS J1	2.89	2.85	2.73	2.68	2.62	2.80	2.84
M4	SNPP	1.05	1.10	1.19	1.16	1.00	0.88	0.84
	JPSS J1	3.61	3.90	4.17	4.18	4.04	3.89	3.80
M5	SNPP	1.19	1.02	0.85	0.84	0.76	0.73	0.69
	JPSS J1	1.90	1.86	1.82	1.79	1.81	1.80	1.80
M6	SNPP	0.99	0.96	0.94	0.94	0.88	0.82	0.76
	JPSS J1	1.62	1.32	0.86	0.79	0.73	0.75	0.76
M7	SNPP	0.17	0.19	0.25	0.28	0.38	0.42	0.41
	JPSS J1	0.73	0.62	0.36	0.32	0.45	0.55	0.60

Requirements verification – maximum polarization factors (HAM A)

I2, M1, M7: less than 3%; I1, M2, M3, M4, M5, M6: less than 2.5%

Applies to scan angles within ±45 degrees of nadir

Requirements Verification

Band	Sensor	Scan Angle						
		-55	-45	-22	-8	20	45	55
I1	SNPP	0.86	0.76	0.62	0.59	0.54	0.58	0.61
	JPSS J1	0.86	0.90	0.94	0.95	1.00	1.03	1.04
I2	SNPP	0.49	0.45	0.47	0.51	0.56	0.56	0.55
	JPSS J1	1.19	0.92	0.50	0.48	0.53	0.58	0.61
M1	SNPP	3.14	2.73	2.01	1.83	1.45	1.23	1.39
	JPSS J1	5.57	5.73	6.17	6.34	6.42	6.17	5.96
M2	SNPP	2.25	2.05	1.65	1.54	1.28	1.17	1.30
	JPSS J1	4.08	4.08	4.18	4.23	4.19	4.36	4.46
M3	SNPP	1.45	1.31	0.96	0.85	0.62	0.71	0.81
	JPSS J1	2.92	2.86	2.76	2.75	2.85	3.08	3.11
M4	SNPP	1.59	1.52	1.37	1.30	1.02	0.86	0.82
	JPSS J1	4.03	4.20	4.32	4.30	4.15	3.99	3.91
M5	SNPP	0.81	0.74	0.70	0.69	0.61	0.59	0.57
	JPSS J1	2.10	2.17	2.13	2.07	2.02	1.99	1.97
M6	SNPP	1.29	1.14	0.96	0.92	0.81	0.75	0.70
	JPSS J1	1.03	0.92	0.86	0.91	0.96	0.95	0.94
M7	SNPP	0.52	0.47	0.43	0.44	0.48	0.47	0.45
	JPSS J1	1.18	0.92	0.48	0.43	0.47	0.52	0.56

Requirements verification – maximum polarization factors (HAM B)

I2, M1, M7: less than 3%; I1, M2, M3, M4, M5, M6: less than 2.5%

Applies to scan angles within ±45 degrees of nadir

Test Configuration Comparison

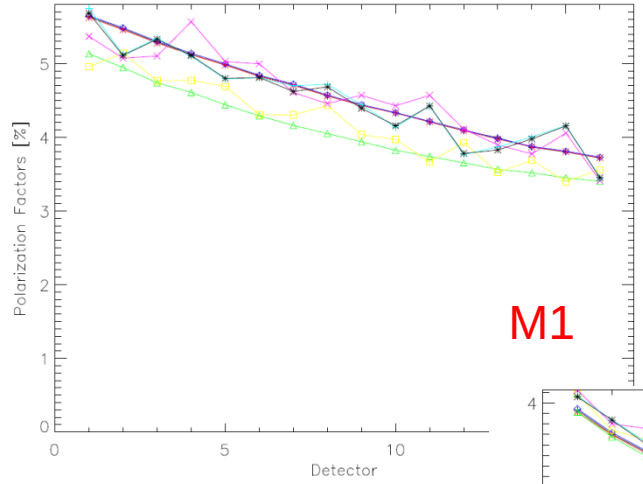

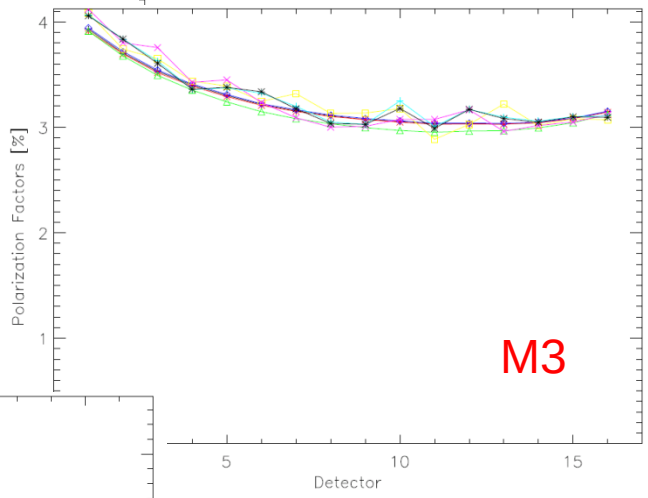

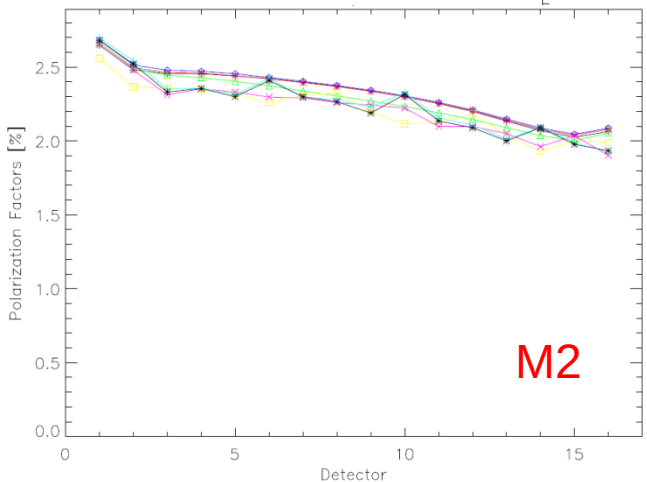

Comparing different test configurations at -8 degrees scan angle

- Polarization factors without the Sonoma filter less well determined for M1 – M3 (much lower source level)
- Polarization factors derived using BVO777 slightly lower than BVONIR (especially for M1)

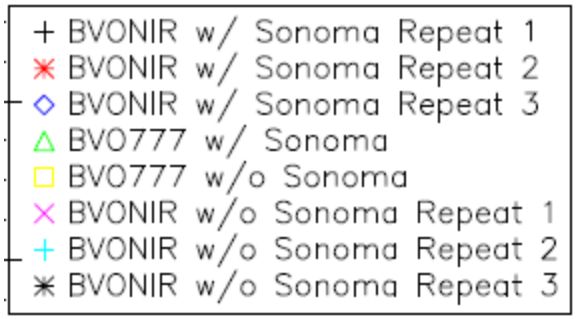

Subassembly / Sensor Comparison

Comparing tests at the subassembly and sensor levels

- Compared subassembly measurements to -8 degrees scan angle sensor measurements (HAM A)
- BVONIR and MOXTEK subassembly measurements were not optimized for M1-M3
- In general, results are consistent

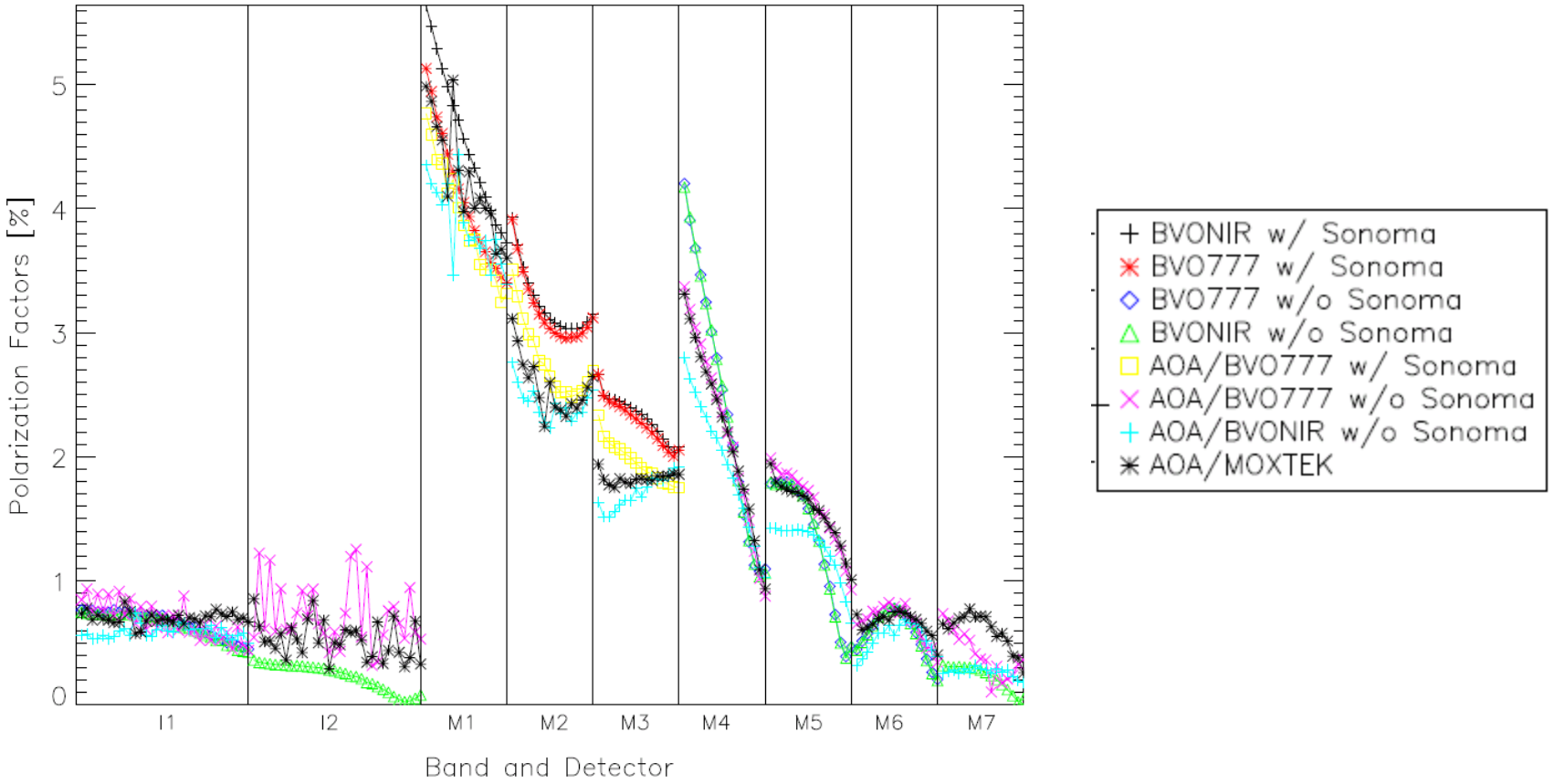

Model / Measurement Comparison

Comparing sensor level test results with model output

- Raytheon FRED model results compared to measurement (BVONIR)
- Results are generally consistent for most bands
  - Some differences observed in M4 and M6

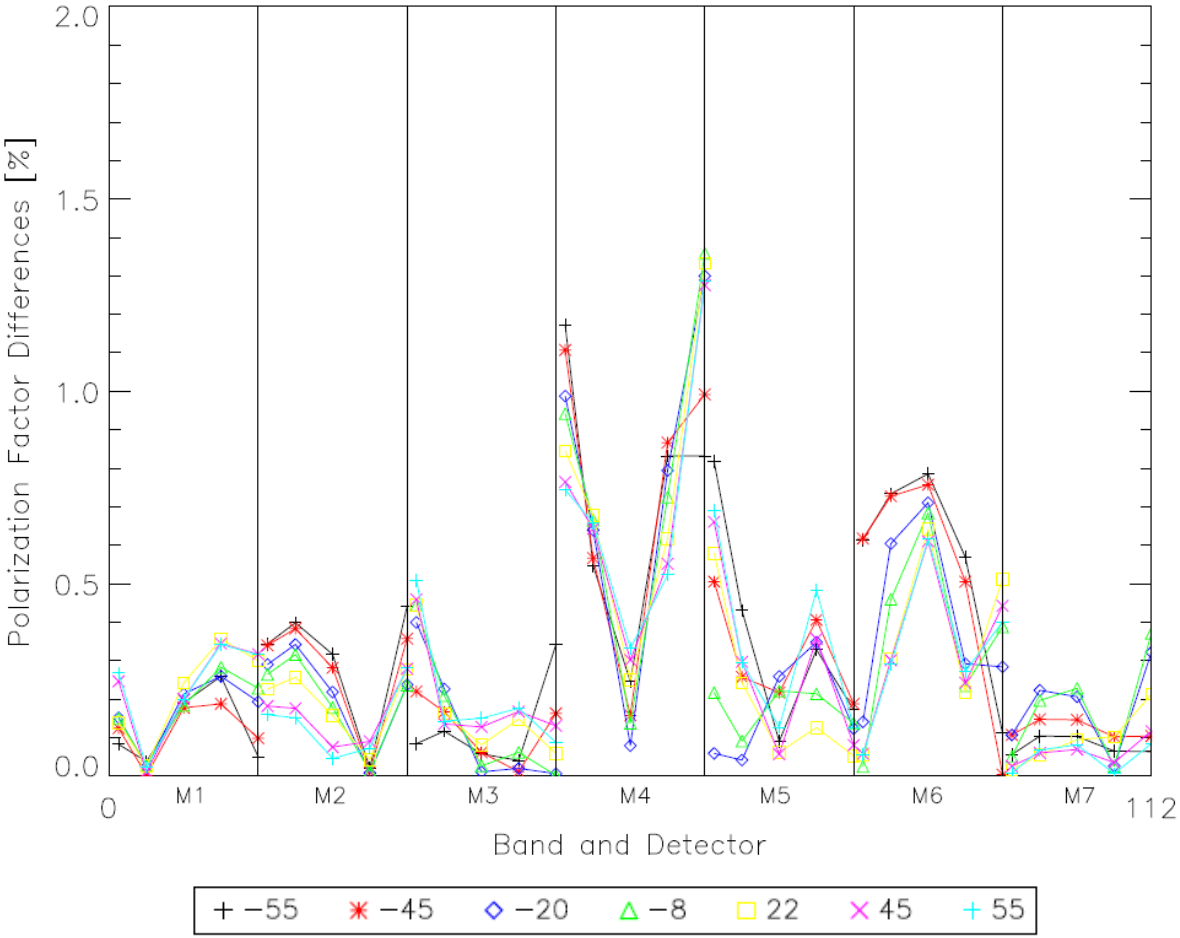

Uncertainty Tree

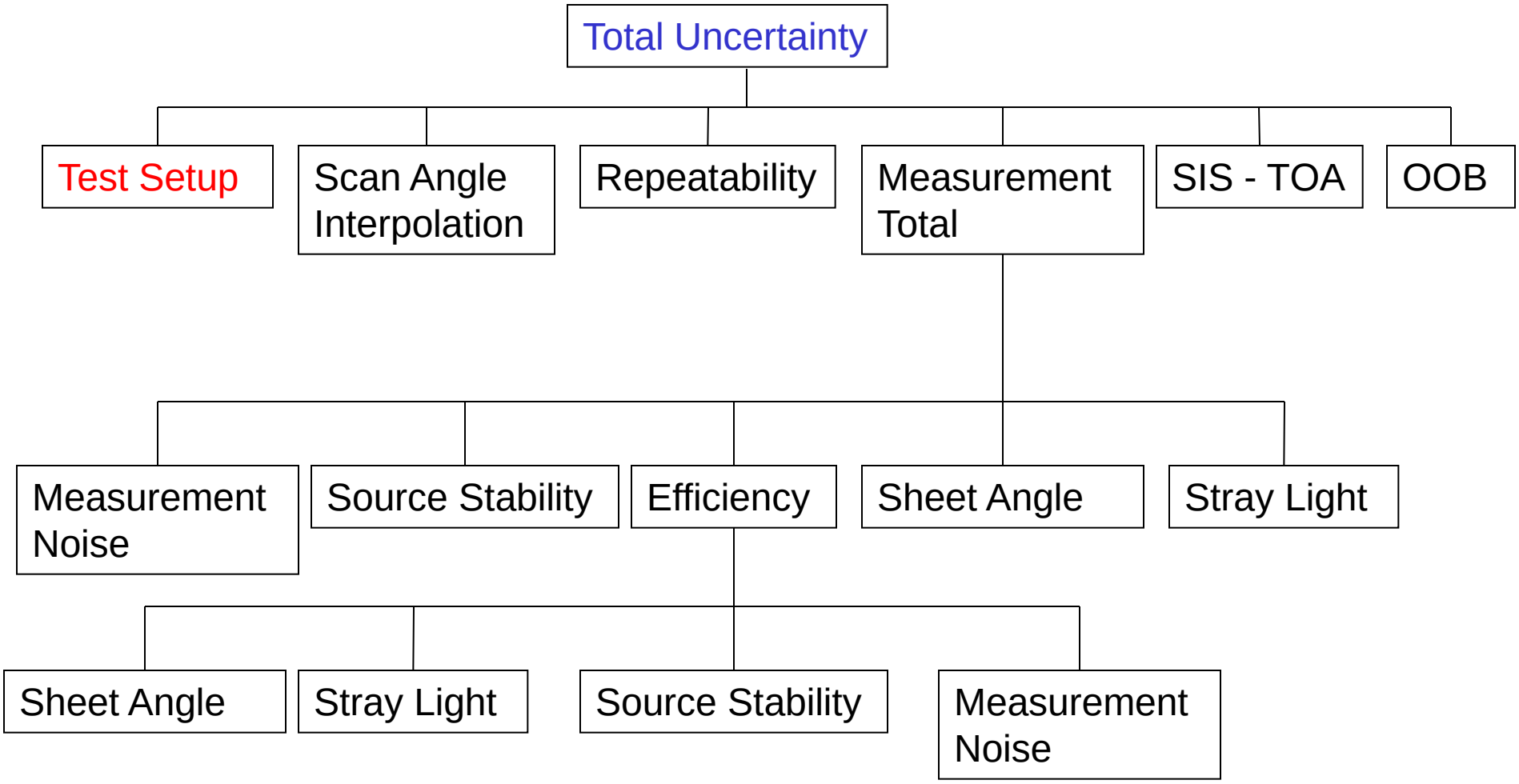

Polarization Factor Uncertainty

Polarization uncertainty – maximum over HAM sides, detectors, and scan angles [in %]

	I1	I2	M1	M2	M3	M4	M5	M6	M7
Measurement noise	0.00	0.00	0.00	0.00	0.00	0.00	0.00	0.00	0.00
Source stability	0.03	0.06	0.00	0.00	0.00	0.04	0.07	0.09	0.06
Stray light	0.02	0.00	0.00	0.00	0.00	0.01	0.00	0.01	0.00
Sheet angle	0.01	0.04	0.06	0.03	0.02	0.02	0.04	0.04	0.04
Efficiency	0.00	0.00	0.02	0.01	0.01	0.00	0.00	0.00	0.00
Measurement total	**0.03**	**0.07**	**0.06**	**0.03**	**0.02**	**0.05**	**0.08**	**0.10**	**0.07**
Repeatability	0.04	0.01	0.03	0.03	0.03	0.06	0.02	0.01	0.01
Scan angle interpolation	0.04	0.07	0.03	0.02	0.04	0.05	0.09	0.05	0.07
SIS – TOA	0.20	0.19	0.34	0.05	0.11	0.05	0.09	0.01	0.03
OOB	0.00	0.00	0.06	0.04	0.08	0.00	0.00	0.00	0.00
Test setup	0.20	0.10	0.14	0.12	0.14	0.10	0.13	0.09	0.10
Total	**0.28**	**0.22**	**0.38**	**0.14**	**0.20**	**0.13**	**0.19**	**0.14**	**0.13**
Specification	**0.50**	**0.50**	**0.50**	**0.50**	**0.50**	**0.50**	**0.50**	**0.50**	**0.50**

J1 Polarization Impact Assessment

A waiver for polarization non-compliances (M1 – M4) is pending

Waiting for NASA / NOAA impact assessments

Major effort is ongoing to understand the impact on J1 VIIRS products and provide corrective approaches

- JPSS science SMEs were selected for Ocean, Land and Aerosol disciplines to provide qualitative and quantitative impact assessments
- Three JPSS telecons were held to discuss a plan to complete impact assessment studies (30-Jan, 2-Feb, and 7-May)
- Three NOAA SDR telecons were held to discuss polarization detector dependence, comparisons to MODIS, and additional testing necessary for on-orbit mitigation (17-Mar, 2-April, and 16-Apr)
- Lessons learned based on MODIS instrument were discussed and analysis was performed
  - Polarization correction approach is available, and is being applied to some MODIS products
  - Results are promising based on MODIS experience

Quantitative Impact Assessment

Effort is ongoing based on SNPP VIIRS scenes to generate quantitative impact assessments

- JPSS Science Leads were assigned for each discipline:
  Ocean (G. Meister), Land (A. Lyapustin), and Aerosol (C. Hsu)
- Contrasted scenes were selected (favorable and worse case)
- Contaminated scenes were generated to assess the impact due to polarization
- Correction approach (if necessary) is available to enhance the quality of the products

Additional J1 sensor testing (proposed post-TVAC)

- Additional sensor level polarization testing for 5 scan angles (4 of which were untested previously)
- Spectral testing for M1 and M4 using T-SIRCUS (two scan angles and thirteen wavelengths)
- Data is expected to enhance the sensor polarization characterization and model predictions in support of the on-orbit corrections to the SDR / EDR products

Assessment Using SNPP VIIRS Scenes

$$L_{TOA-t} = \frac{L_{TOA-m}}{M_{11}} - \frac{M_{12}}{M_{11}} Q - \frac{M_{13}}{M_{11}} U$$

L_{TOA-t} : true TOA radiance (desired quantity)

L_{TOA-m} : measured TOA radiance (VIIRS SDR)

Q, U : linear Stokes vector components, modeled from Rayleigh scattering and glint

M_{11}, M_{12}, M_{13} : fitted instrument characterization parameters (HAM, detector, and scan angle dependent)

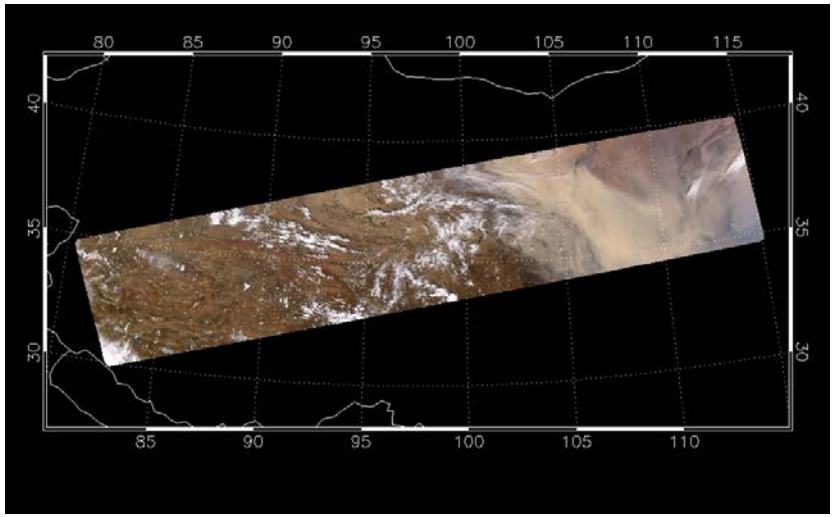

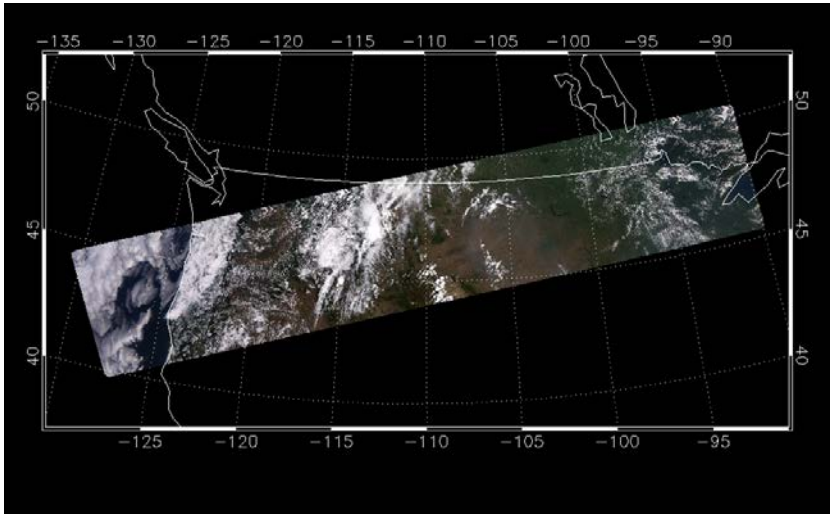

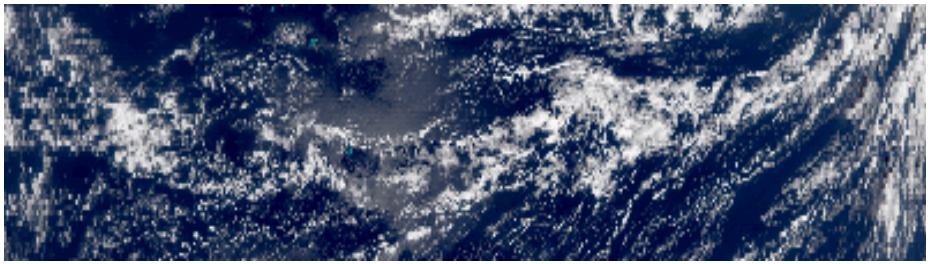

Preliminary Impact Assessment

Preliminary assessments were presented for Ocean, Land and Aerosol products at a meeting on May 7th 2014

- Effect of J1 VIIRS polarization was applied to S-NPP VIIRS granules, using VCST J1 polarization characterization data (polarization factor, phase, and uncertainty)
- Preliminary results provided an estimate of the magnitude of the impact due to J1 polarization, and provided an encouraging path forward for product enhancements
- While Ocean products already have a polarization correction built into the processing algorithm, the final report will determine if there is a need to implement similar corrections in the Land and Aerosol products
- Final reports will include more VIIRS scenes and refined results upon which a waiver will be approved, and recommendations will be generated for the on-orbit VIIRS products cal/val and product quality enhancements

Conclusions

Polarization factors and phases were measured

- M1 – M4 above the sensor requirement for polarization factors
- Significant HAM side, scan angle, and detector dependence observed
- Results are consistent
  - Across testing configuration
  - With subassembly testing
  - With optical model

Uncertainty of polarization factor was also determined

- Maximum uncertainties per band were between 0.13 – 0.38 %
  - Specified maximum uncertainty is 0.5 %
  - Main contributors: test setup, SIS – TOA

Preliminary impact assessments from Science disciplines completed

Backup Slides

Test Overview

FP-11 Polarization Sensitivity (JPSS J1 VIIRS)

Sensor level test

VisNIR bands and DNB tested

Source – SIS100-2

Four configurations tested
- BVO777 polarizer sheet with and without the Sonoma filter (only at -8 degrees scan angle)
- BVONIR polarizer sheet with and without the Sonoma filter

Stray light levels investigated
- Data collected with source off
- Data collected with source on and “lollipop” obscuration in path

Efficiency of each configuration measured
- Second polarizer sheet of same type used to determine efficiency

Polarization sensitivity of VIIRS
- Data collected with each configuration at seven scan angles (only one for BVO777)
- Polarizer rotated from 0 to 360 degrees (in 15 degree increments)
- Measurements repeated at -8 degrees scan angle three times

Test Overview

FP-11 Polarization Sensitivity (JPSS J1 VIIRS)

After nominal testing was completed, special tests were conducted before the test configuration was broken

Configurations tested (all at -8 degrees scan angle)

- Removed cross hairs from aperture stop
  - BVONIR polarizer sheet with and without the Sonoma filter
- Blocked upper and lower half of VIIRS aperture
  - BVONIR polarizer sheet with and without the Sonoma filter
- Replaced blocking filter with the Hoya filter
  - BVONIR polarizer sheet
- Repeated testing during tear down of external baffling
  - BVONIR polarizer sheet with the Sonoma filter only

Compare to nominal testing at -8 degrees scan angle

Test Overview

ETP-078 Polarization Sensitivity (JPSS J1 VIIRS)

Aft Optics Assembly (AOA) subassembly test

VisNIR bands tested

Source – SIS100-2

Four configurations tested
- BVO777 polarizer sheet with and without the Sonoma filter
- BVONIR polarizer sheet without the Sonoma filter
- MOXTEK polarizer without the Sonoma filter

Efficiency of each configuration measured
- Second polarizer sheet of same type used to determine efficiency
- Efficiency not measured with the MOXTEK polarizer

Polarization sensitivity of VIIRS
- Polarizer rotated from 0 to 360 degrees (in 15 degree increments)
- Measurements repeated four times (twice with the MOXTEK polarizer)

Methodology

Model the dn as a Fourier series

$$dn(\alpha) = \frac{1}{2}c_0 + \sum_{n=1}^{4} c_n \cos(n\alpha) + \sum_{n=1}^{4} d_n \sin(n\alpha)$$

where

$$c_n = \frac{1}{\pi}\int_{-\pi}^{\pi} dn(\theta)\cos(n\theta)d\theta \qquad d_n = \frac{1}{\pi}\int_{-\pi}^{\pi} dn(\theta)\sin(n\theta)d\theta$$

This expression can be rewritten as

$$dn(\alpha) = \frac{1}{2}c_0\left[1 + \sum_{n=1}^{4} a_n \cos(2\alpha - \delta_n)\right]$$

where the polarization factor (amplitude) and phase are defined as

$$a_n = \frac{\sqrt{c_n^2 + d_n^2}}{\frac{1}{2}c_0\sqrt{a_2^{eff}}} \qquad \delta_n = \tan^{-1}\left(\frac{d_n}{c_n}\right)$$

The efficiency correction factor (a_2^{eff}) is defined in the same manner as a_n and derived from cross-polarizer data

Methodology

The final Stokes vector (recorded by VIIRS detectors) is related to the initial Stokes vector (entering VIIRS aperture) by the Meuller matrix

$$S_f = MS_i$$

This can be rewritten to isolate the Meuller matrix, or

$$S_f S_i^{-1} = M$$

The final stokes vector was derived from the sensor measurements. Using a model initial Stokes vector, one can determine the Meuller matrix components M_{12} and M_{13}:

$$M_{12} = a_2 \cos \delta_2$$

$$M_{13} = a_2 \sin \delta_2$$

where the polarization amplitude (a_2) and phase (δ_2) were defined on the previous slide

Polar Plots

Polarization factor and phase – polar plots (M1 HAM A)
Specification in red

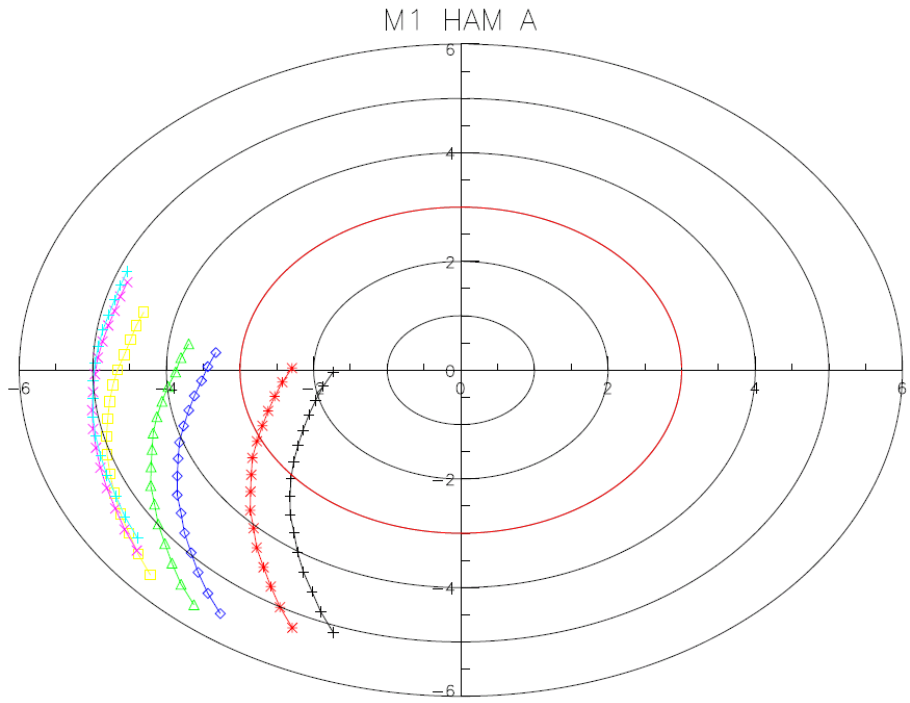

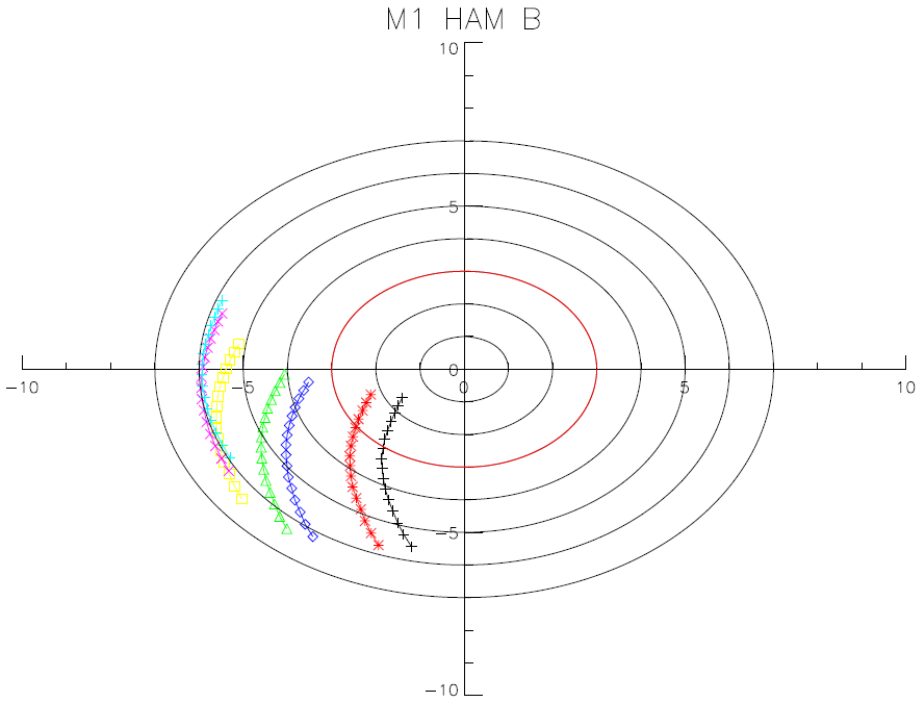

Polar Plots

Polarization factor and phase – polar plots (M2 HAM A)

Specification in red

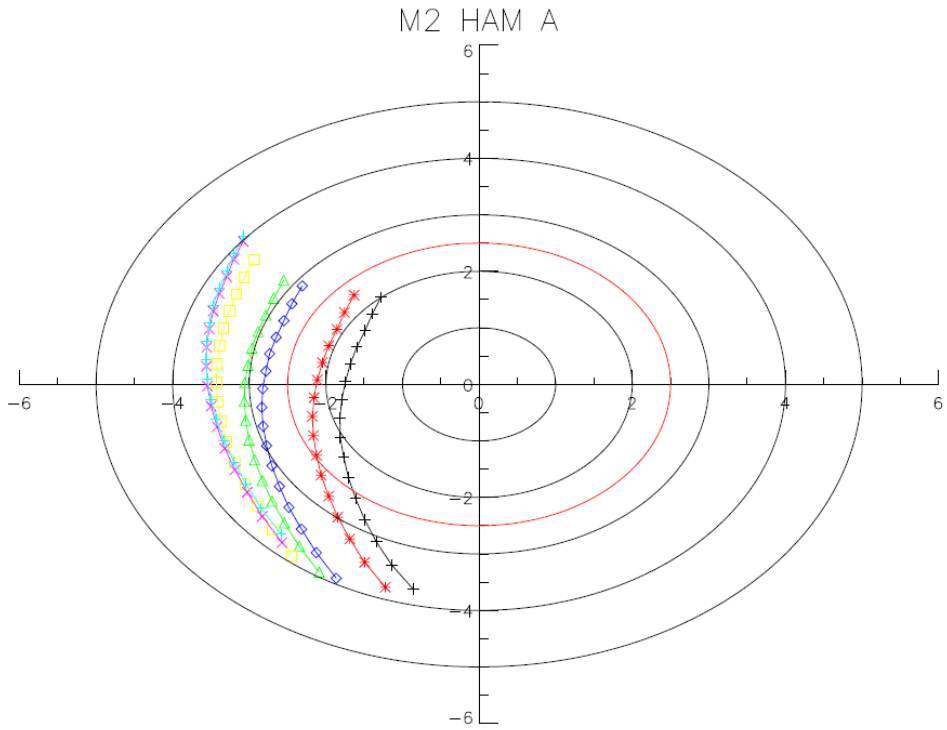

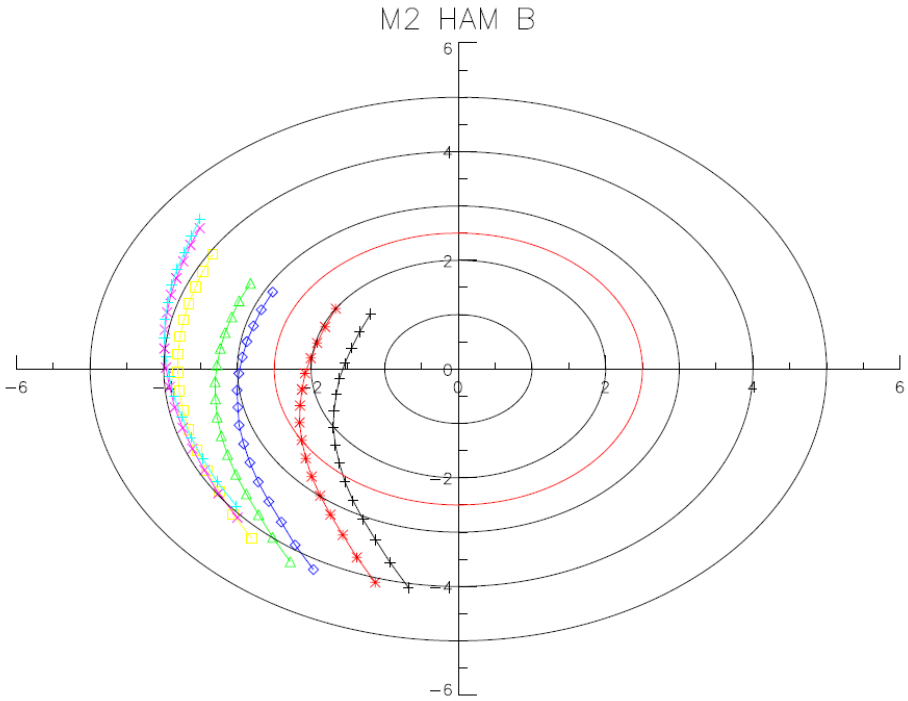

+ −55 ✳ −45 ◇ −20 △ −8 □ 22 × 45 + 55

Polar Plots

Polarization factor and phase – polar plots (M3 HAM A)
Specification in red

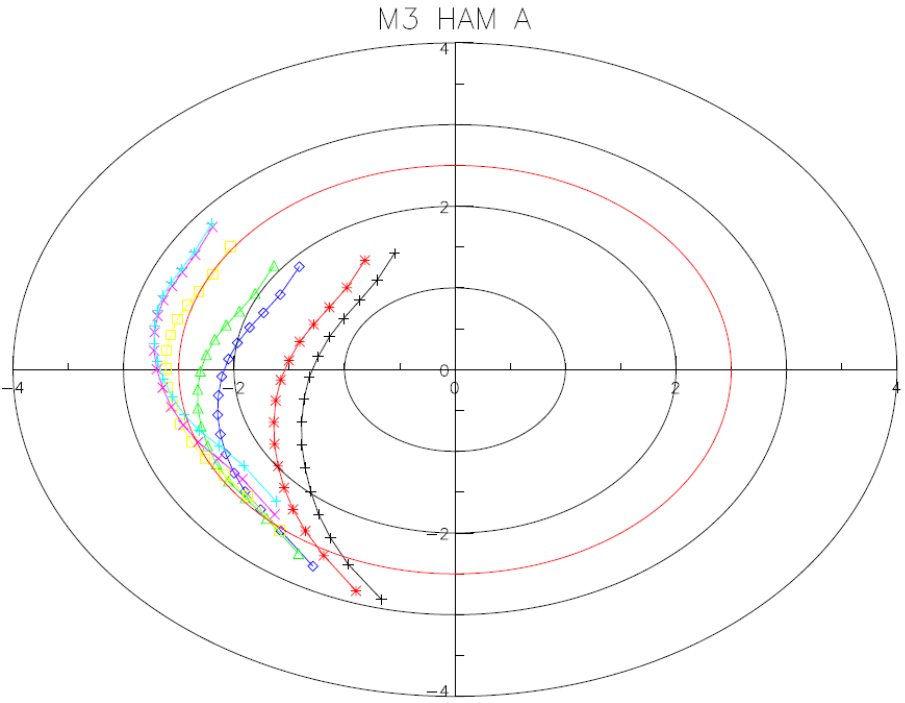

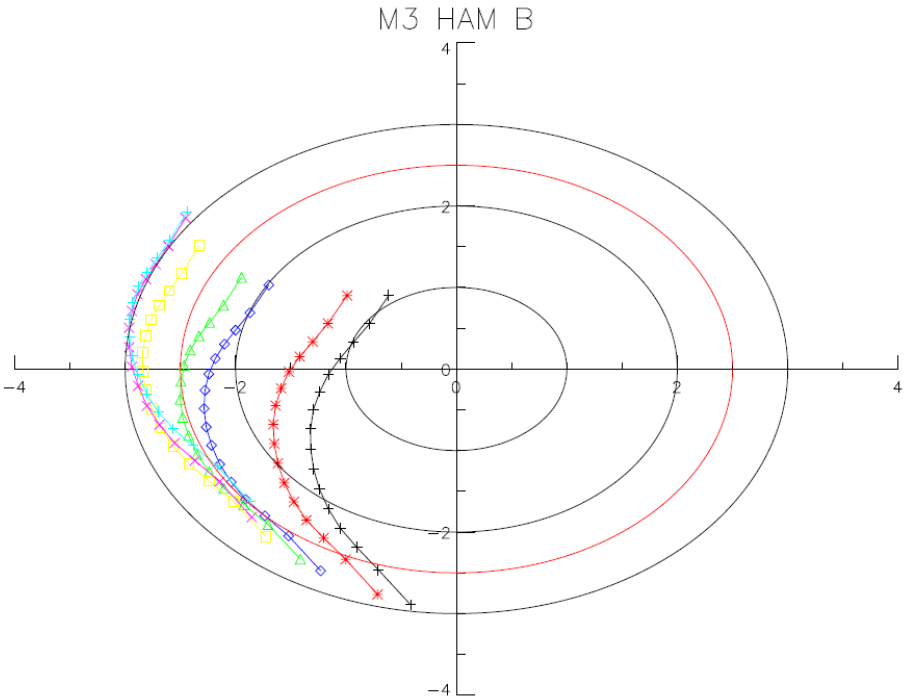

Polar Plots

Polarization factor and phase – polar plots (M4 HAM A)

Specification in red

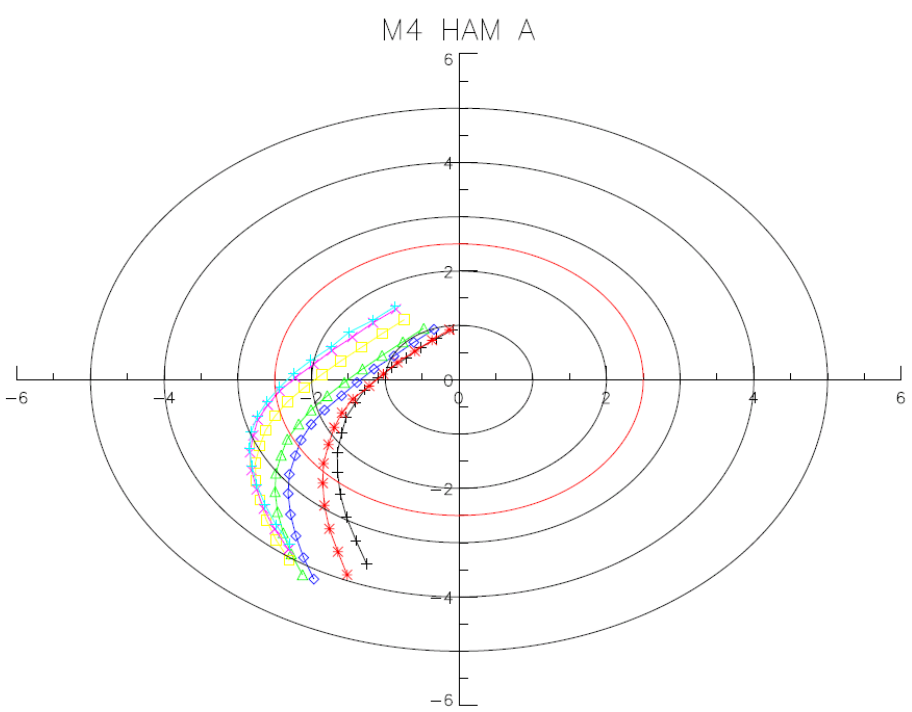

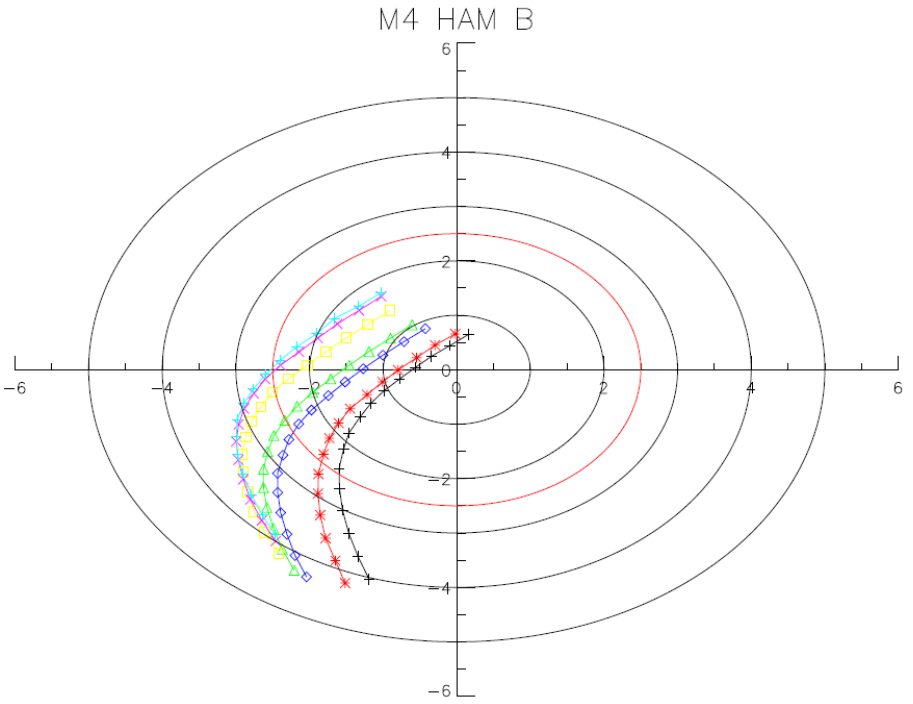

+ −55 ✳ −45 ◇ −20 △ −8 □ 22 × 45 + 55

Polar Plots

Polarization factor and phase – polar plots (M5 HAM A)

Specification in red

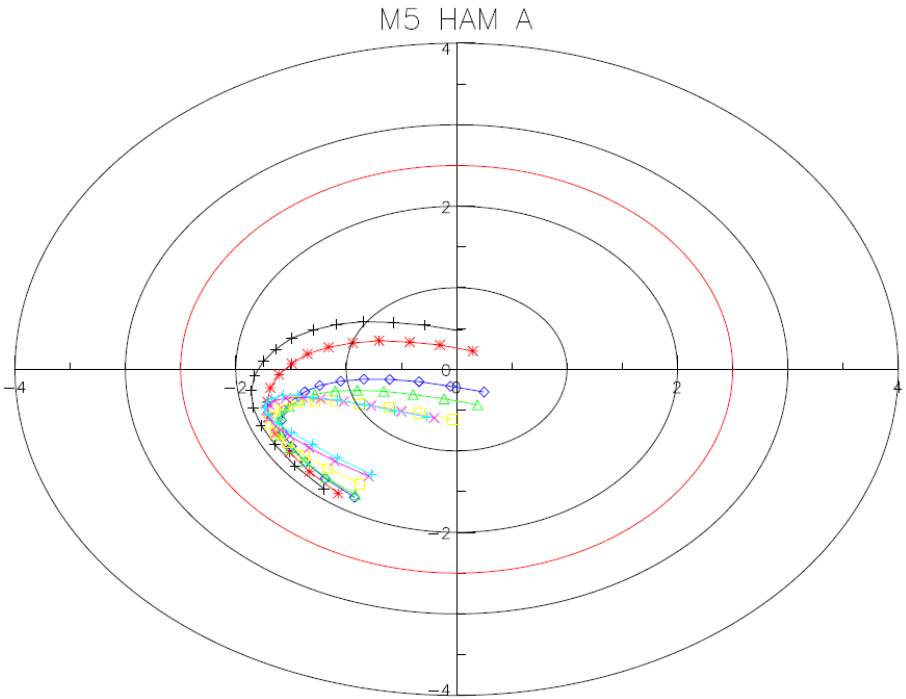

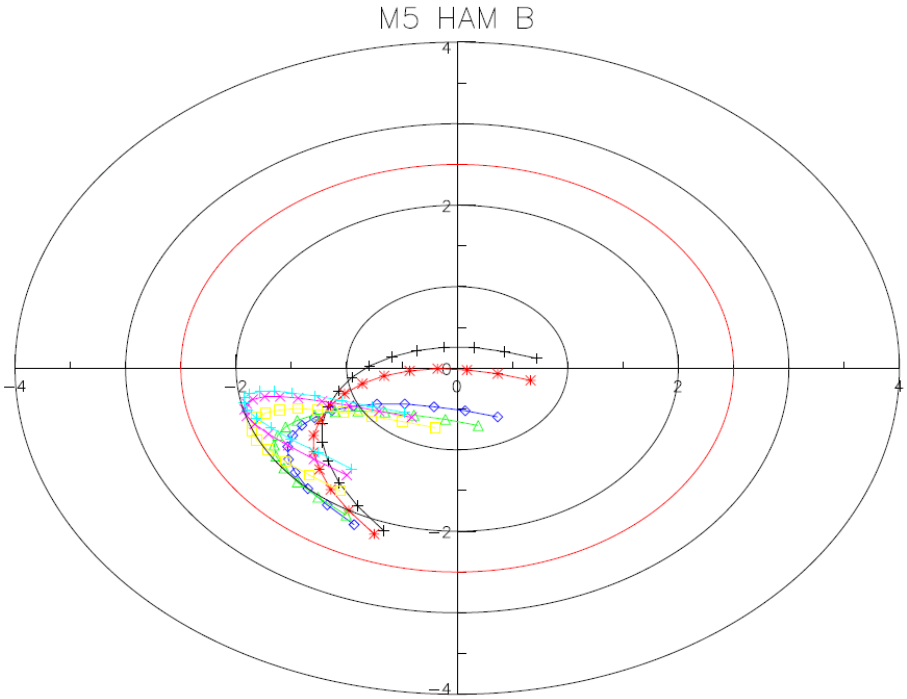

Polar Plots

Polarization factor and phase – polar plots (M6 HAM A)

Specification in red

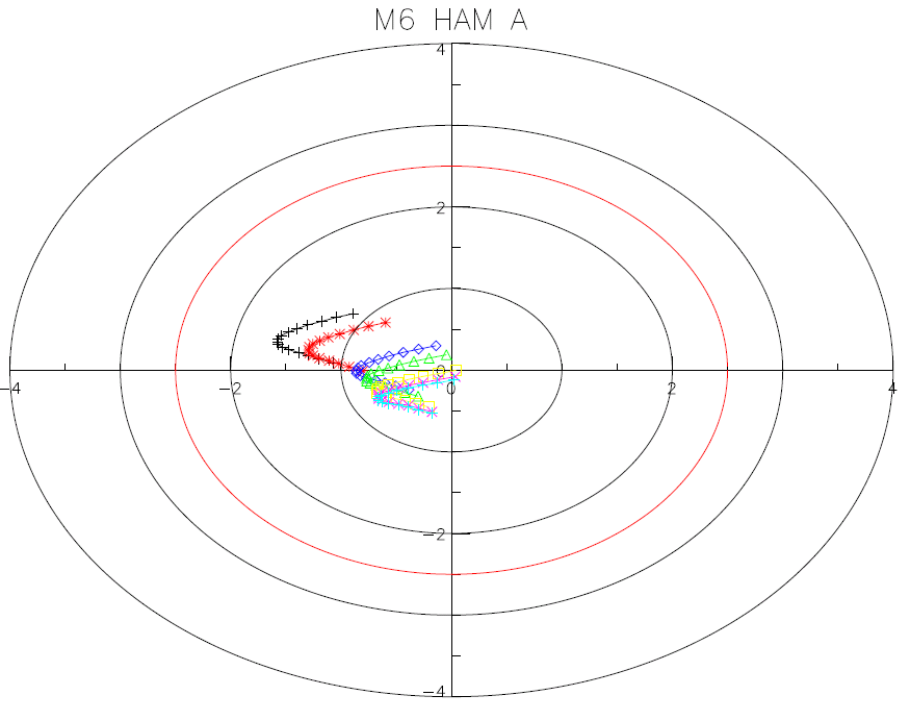

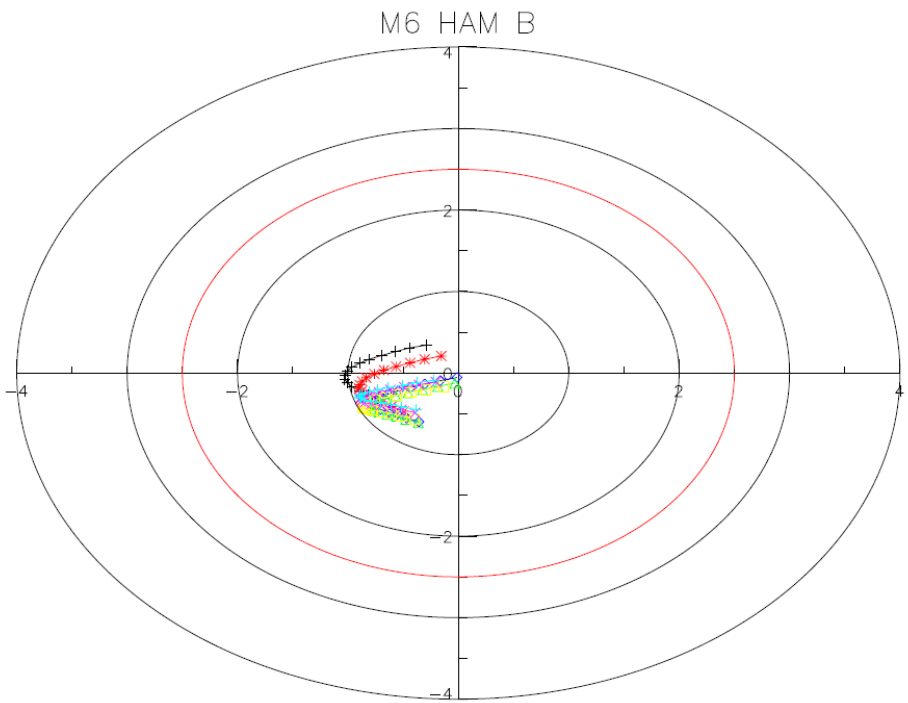

Polar Plots

Polarization factor and phase – polar plots (M7 HAM A)

Specification in red

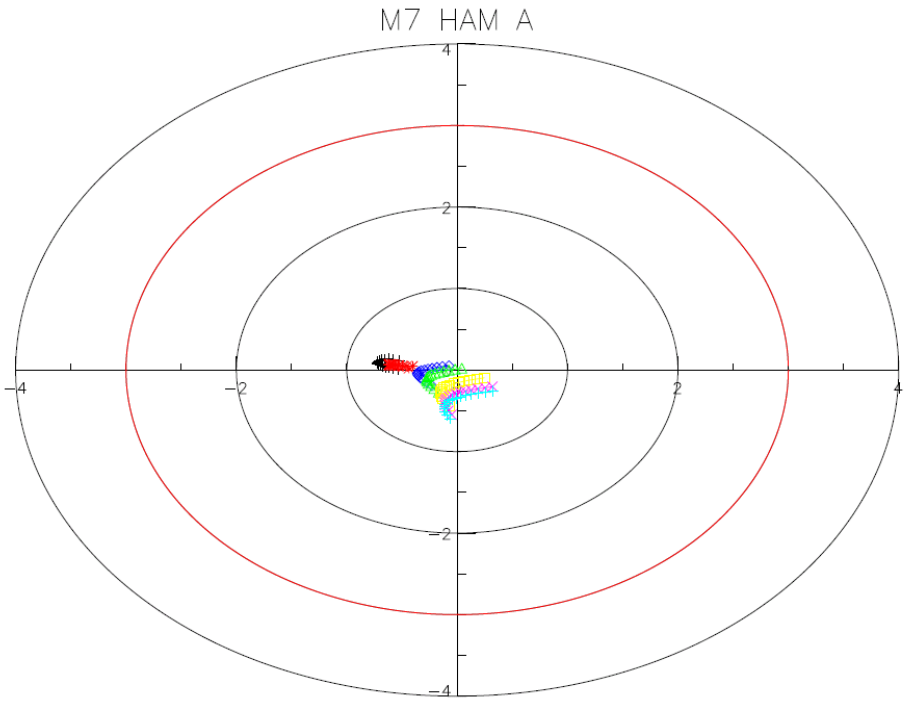

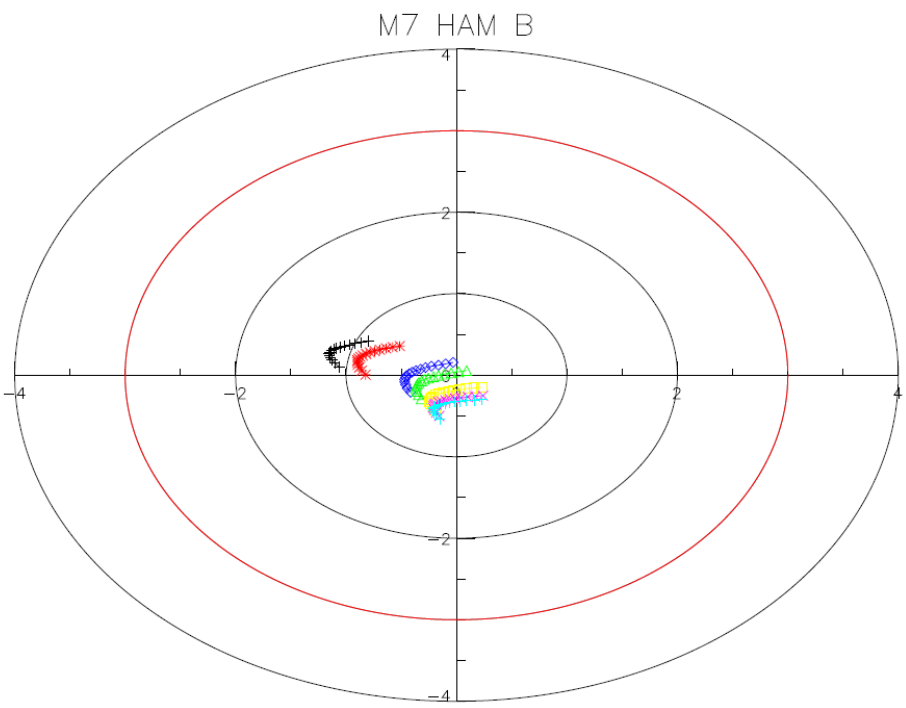

Polar Plots

Polarization factor and phase – polar plots (I1 HAM A)

Specification in red

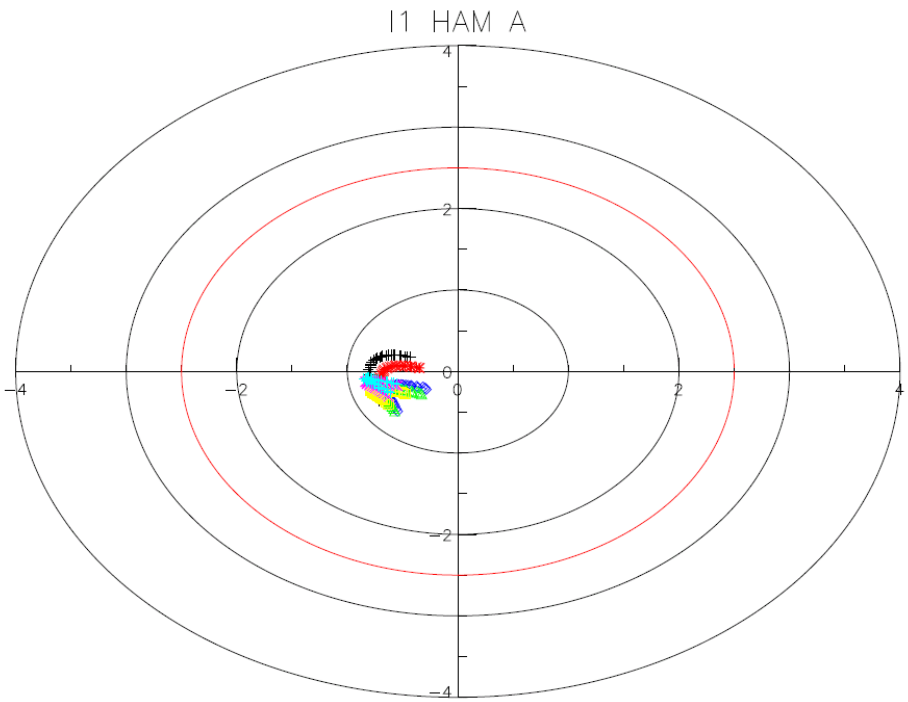

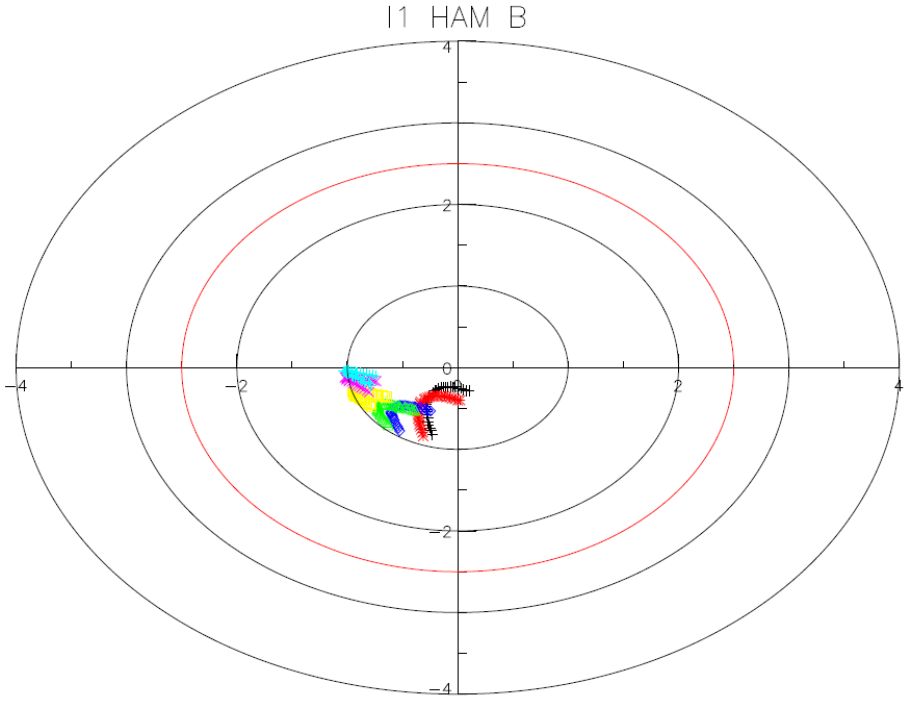

+ −55 ✳ −45 ◇ −20 △ −8 □ 22 × 45 + 55

Polar Plots

Polarization factor and phase – polar plots (I2 HAM A)

Specification in red

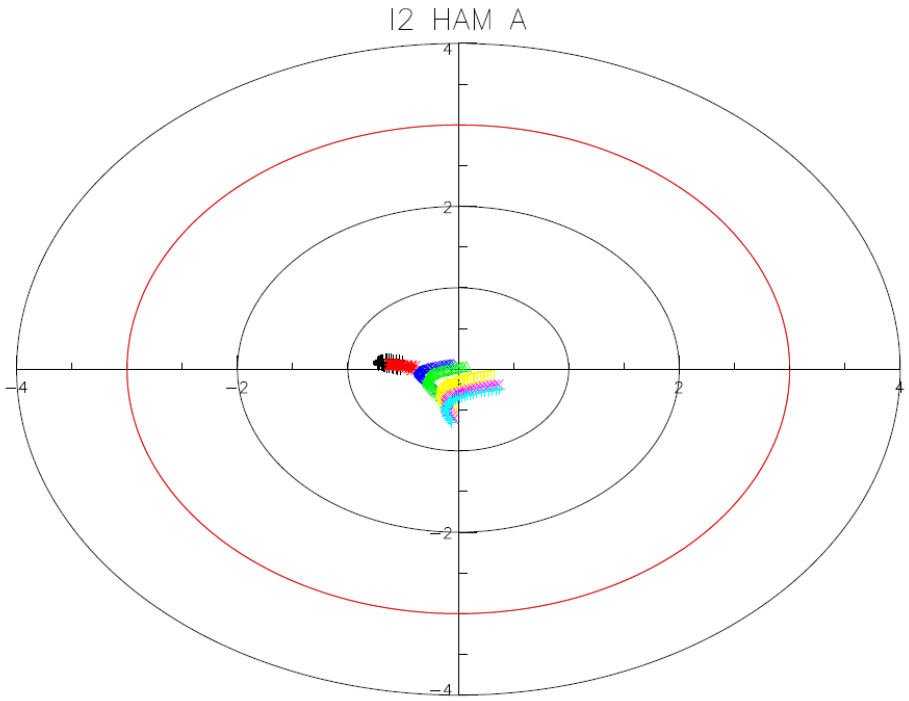

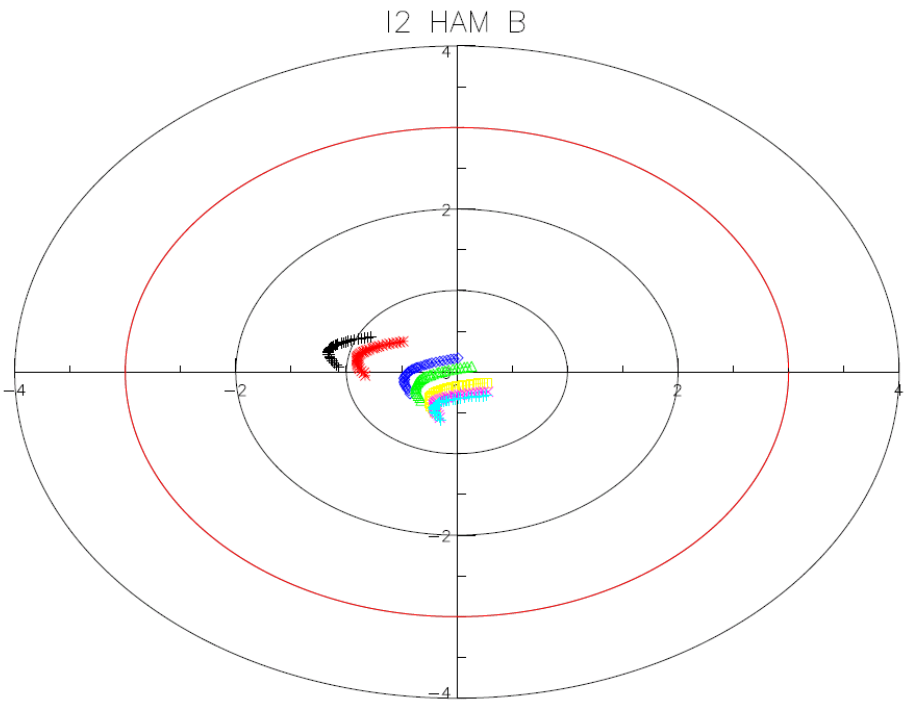

+ −55 ✳ −45 ◇ −20 △ −8 □ 22 × 45 + 55

Polar Plots

Polarization factor and phase – polar plots (DNB LGS HAM A)

Specification in red

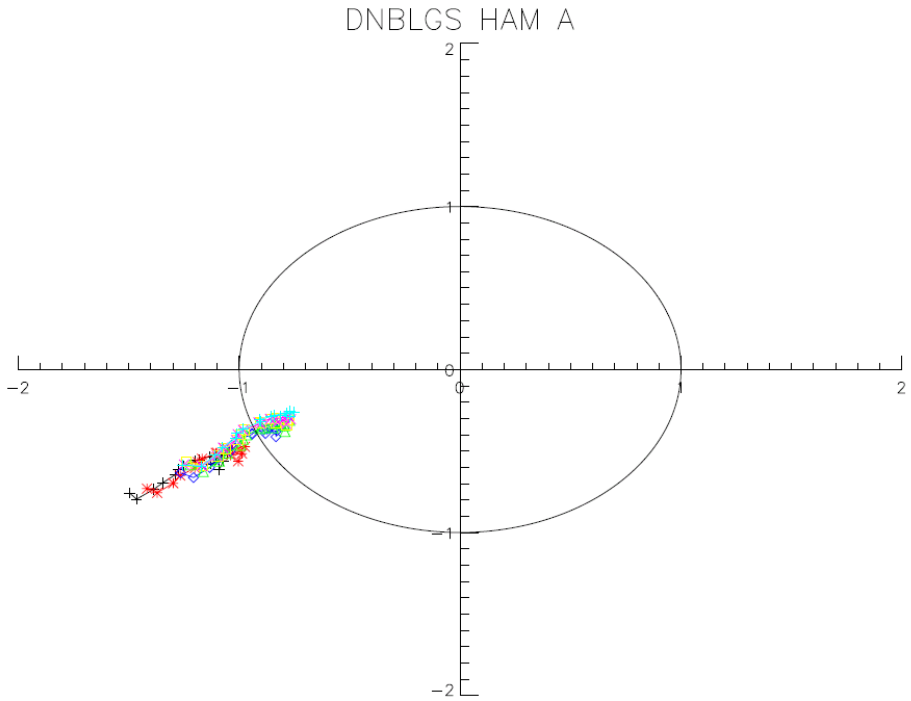

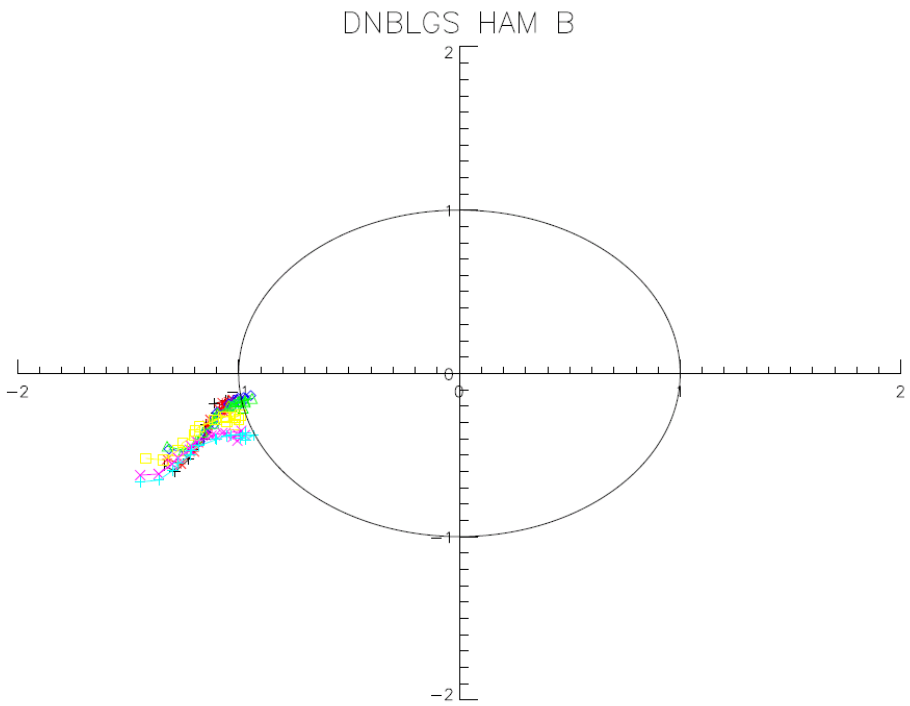

+ −55 ✳ −45 ◇ −20 △ −8 □ 22 × 45 + 55

VIIRS Polarization Sensitivity Assessment

Y. Wang, A. Lyapustin and S. Korkin
NASA GSFC

STAR JPSS Annual Meeting
May 12-16, 2014

Content

1. Basic concepts of polarization correction
2. Polarization effect on TOA reflectance
3. Polarization effects evaluation on AOT and surface reflectance using MAIAC algorithm
4. Summary

Basic Concepts for Polarization Sensitivity and Correction

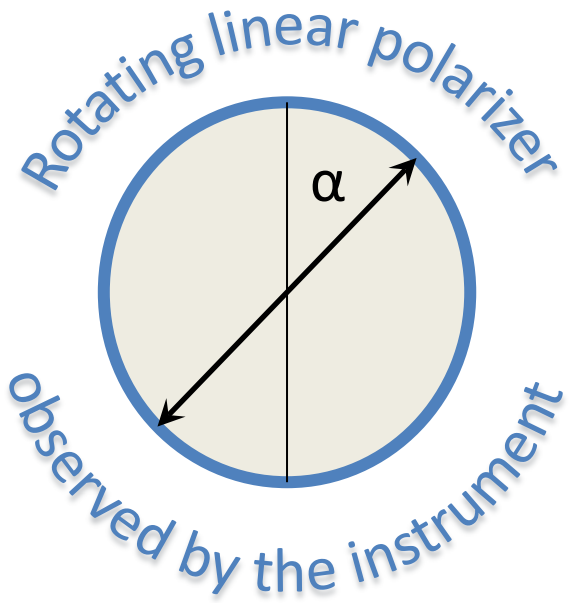

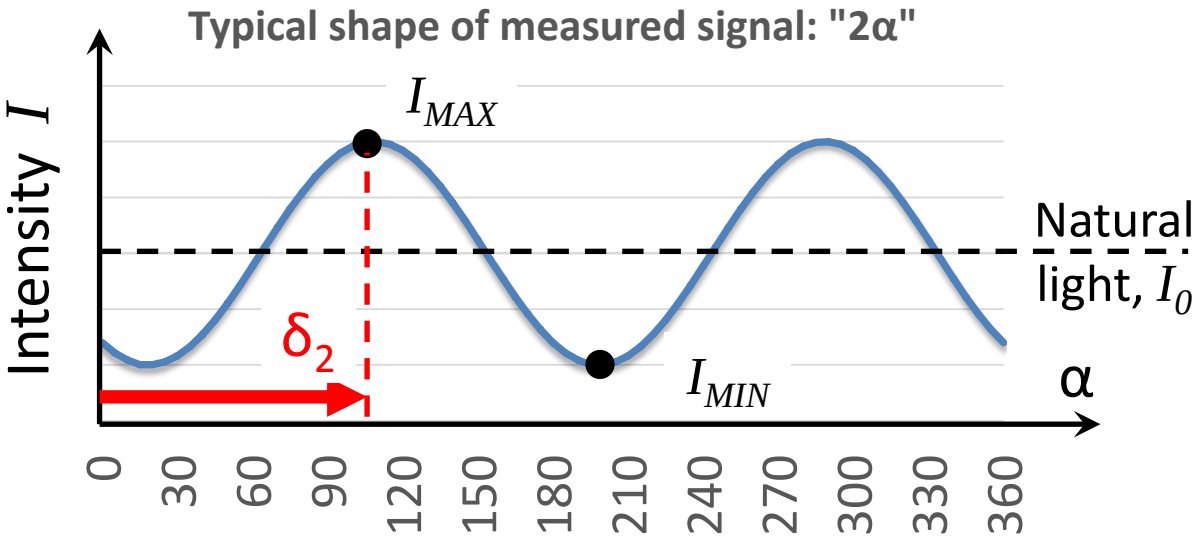

• Plane α=0 determines coordinate system for VIIRS polarization sensitivity studies.

• Polarization correction algorithm uses the VRTE coordinate system: α=90.

$$I_M = I_T \left[1 + m_{12} Q_T / I_T + m_{13} U_T / I_T\right]$$

Polarization phase and polarization factor, a_2,

$$a_2 = \frac{I_{\max} - I_{\min}}{I_{\max} + I_{\min}}$$

determine polarization sensitivity of the system.

The Stokes Vector in the VRTE Coordinate System

$$\begin{bmatrix} I \\ Q \\ U \end{bmatrix} = \begin{bmatrix} 1 & m_{12} & m_{13} \\ \dots & \dots & \dots \\ \dots & \dots & \dots \end{bmatrix} \begin{bmatrix} 1 & 0 & 0 \\ 0 & -1 & 0 \\ 0 & 0 & -1 \end{bmatrix} \frac{1}{2} \begin{bmatrix} I_0 \\ I_0 \cos 2\alpha \\ I_0 \sin 2\alpha \end{bmatrix}$$

VIIRS matrix in the VRTE coordinate system

Rotation of the coordinate system

Linear polarized beam

$$I = 0.5I_0 - m_{12}0.5I_0 \cos 2\alpha - m_{13}0.5I_0 \sin 2\alpha$$

Sign of m12:

$$I(0) = \frac{1}{2}I_0 - m_{12}\frac{1}{2}I_0 < \frac{1}{2}I_0$$

$$m_{12} > 0$$

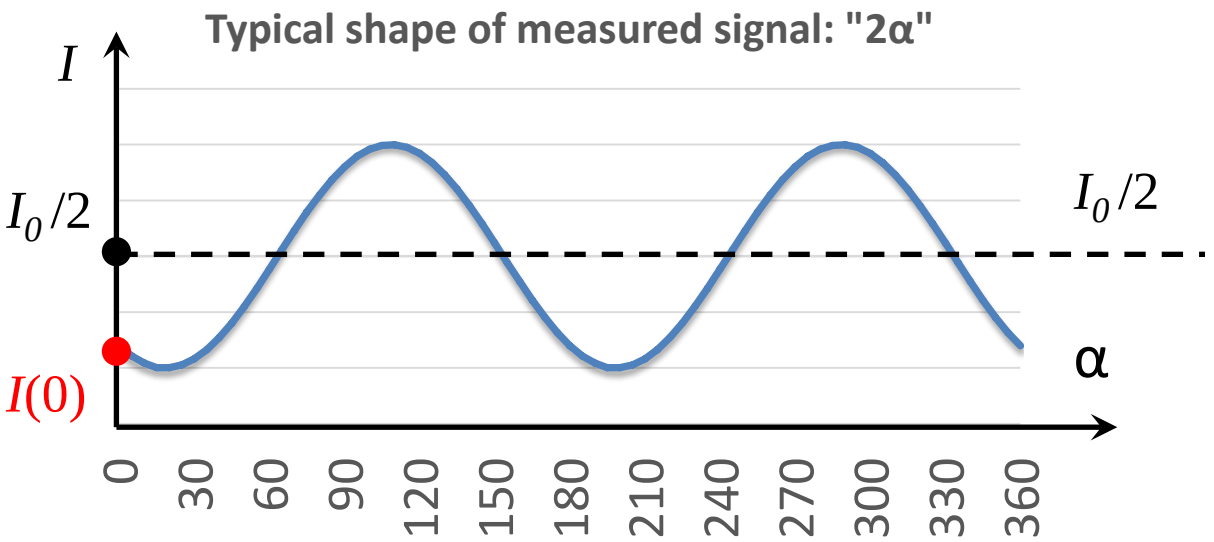

How to Get the Mueller Matrix from Measured Data

VCST_TECH_REPORT_14_012, "Methodology": $dn = \frac{1}{2} c_0 \left[1 + a_2 \cos(2\alpha - \delta_2)\right]$

In our notation **(*)**:

$$I = \frac{1}{2} I_0 - m_{12} \frac{1}{2} I_0 \cos 2\alpha - m_{13} \frac{1}{2} I_0 \sin 2\alpha$$

We define:

$$D = \sqrt{\left[m_{12} \frac{1}{2} I_0\right]^2 + \left[m_{12} \frac{1}{2} I_0\right]^2}; \quad \cos\delta_2 = \frac{-m_{12} \frac{1}{2} I_0}{D}; \quad \sin\delta_2 = \frac{-m_{13} \frac{1}{2} I_0}{D}$$

Rewrite **(*)**: $I = \frac{1}{2} I_0 + D\left[\cos\delta_2 \cos 2\alpha - \sin\delta_2 \sin 2\alpha\right] = \frac{1}{2} I_0 \left[1 + \sqrt{m_{12}^2 + m_{13}^2} \cos(2\alpha - \delta_2)\right]$

Comparing red and blue, we get a system of equations for m12 and m13.

From the system, one immediately gets (note the sign at m12):

$$m_{12} = +\sqrt{\frac{a_2}{1 + \tan^2 \delta_2}}; \qquad m_{13} = m_{12} \tan\delta_2$$

Polarization Effect

(Based on algorithm developed by GSFC ocean color team)

$$L_m = L_t + m_{12}*Q + m_{13}*U$$

L_m: TOA radiance to be measured by J1

L_t: ideal TOA radiance (NPP VIIRS)

Q, U : linear Stokes vector components, modeled from Rayleigh and glint over water

m_{12}, m_{13} : describe instrument polarization sensitivity (depend on band, MS, detector, scan angle)

Angular and Seasonal Sensitivity [M1 (412nm), $(L_t-L_m)/\mu_0$]

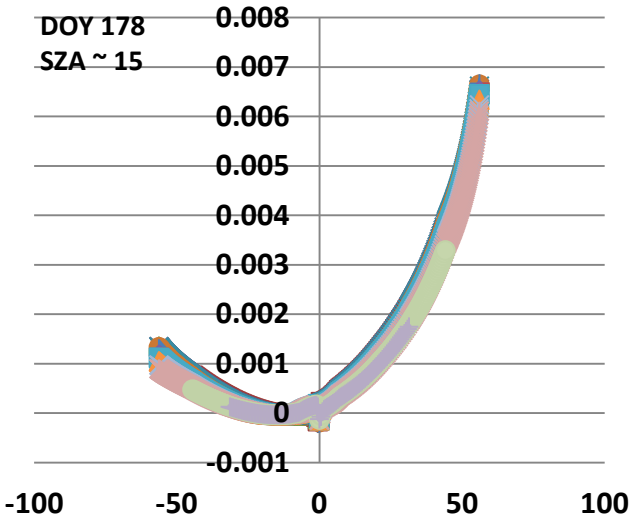

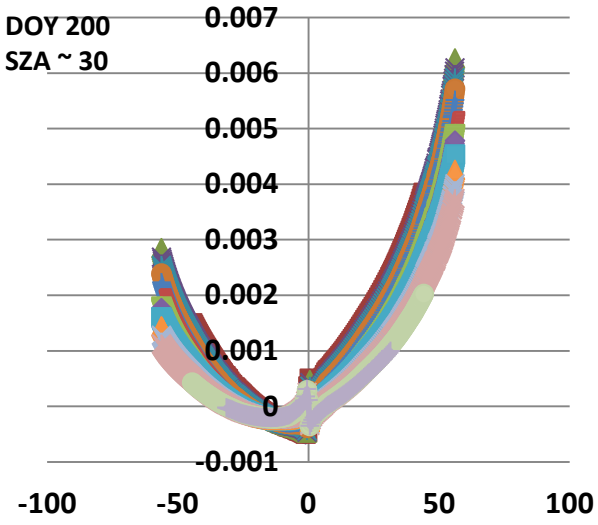

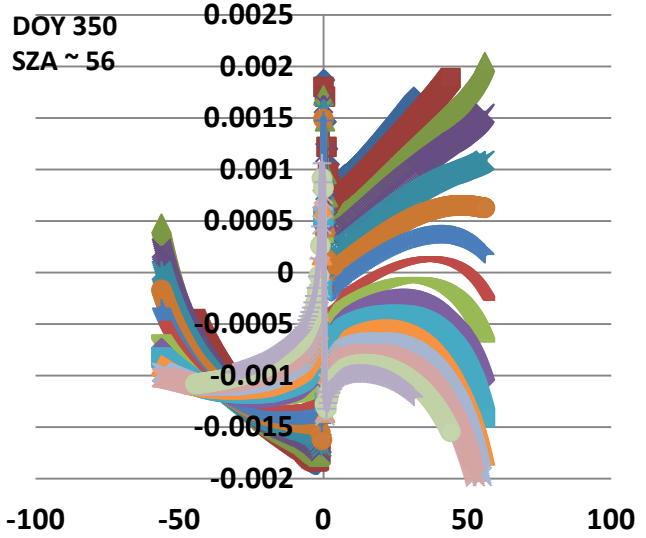

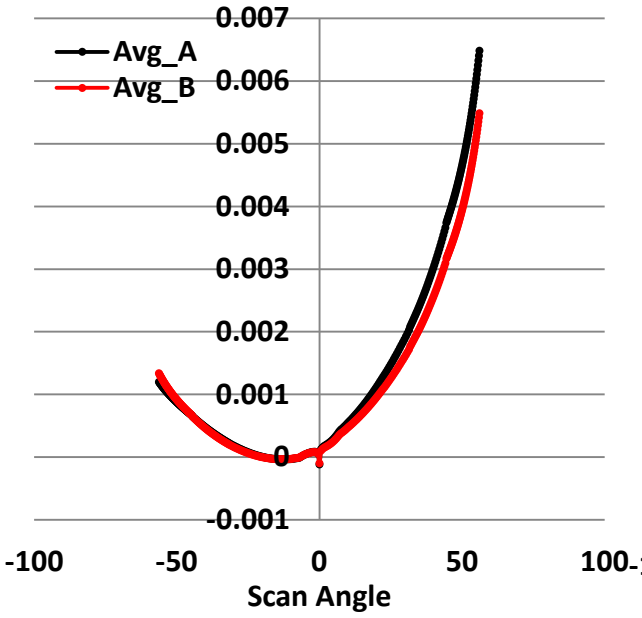

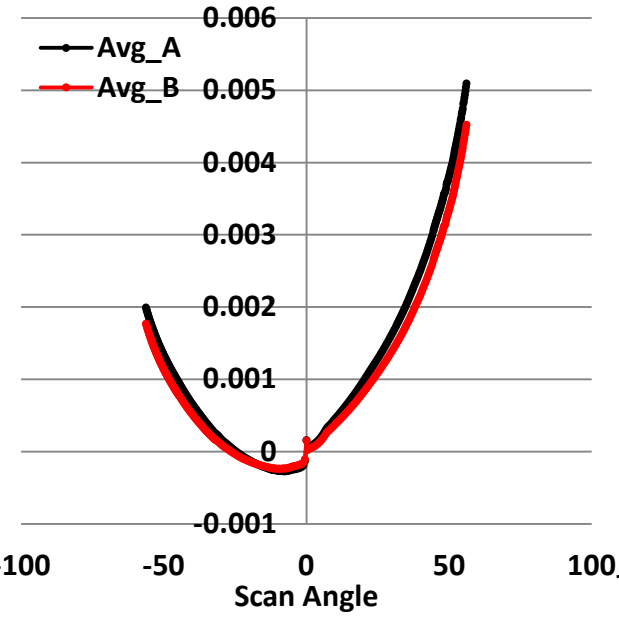

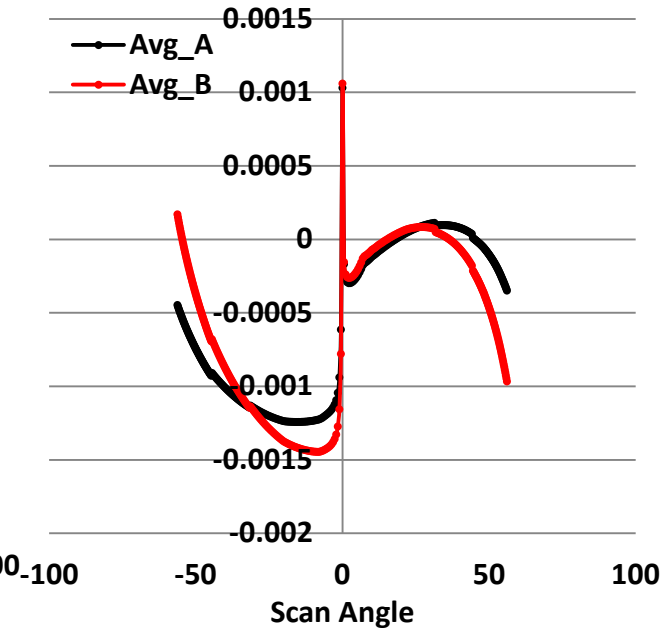

Polarization Differences among Detectors [M1 (412nm), $(L_t-L_m)/\mu_0$]

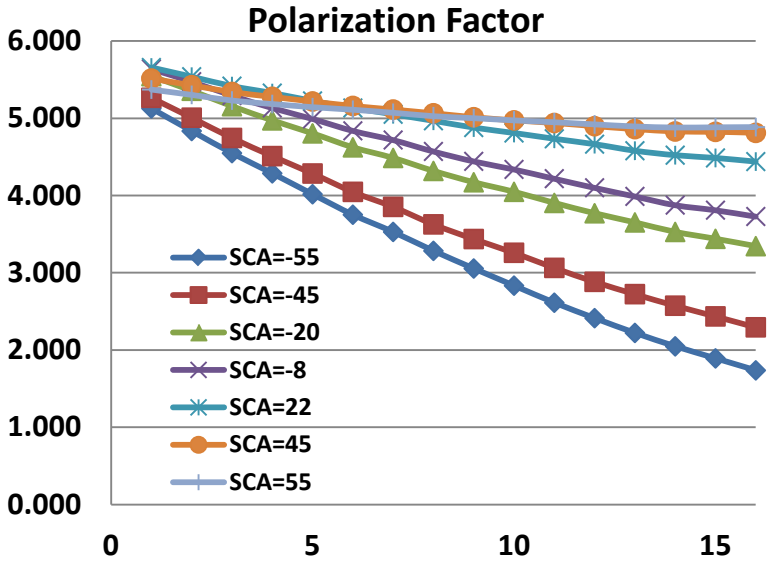

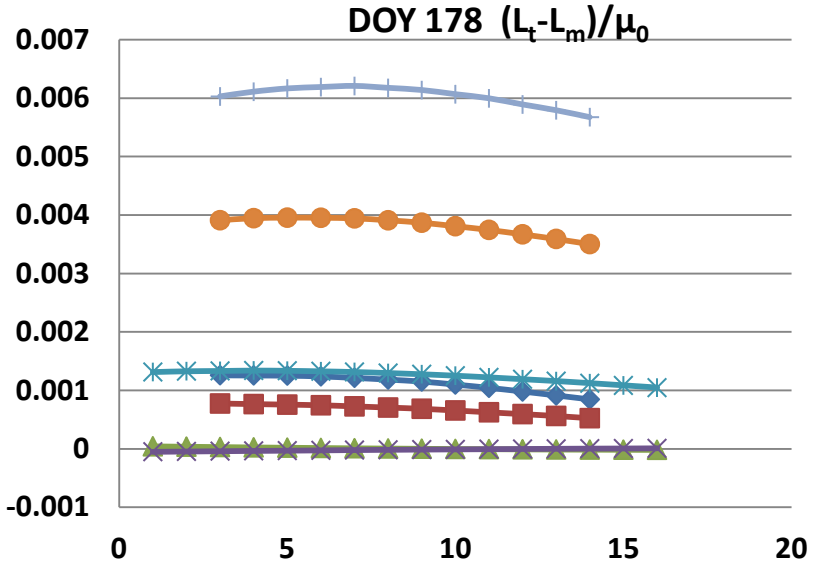

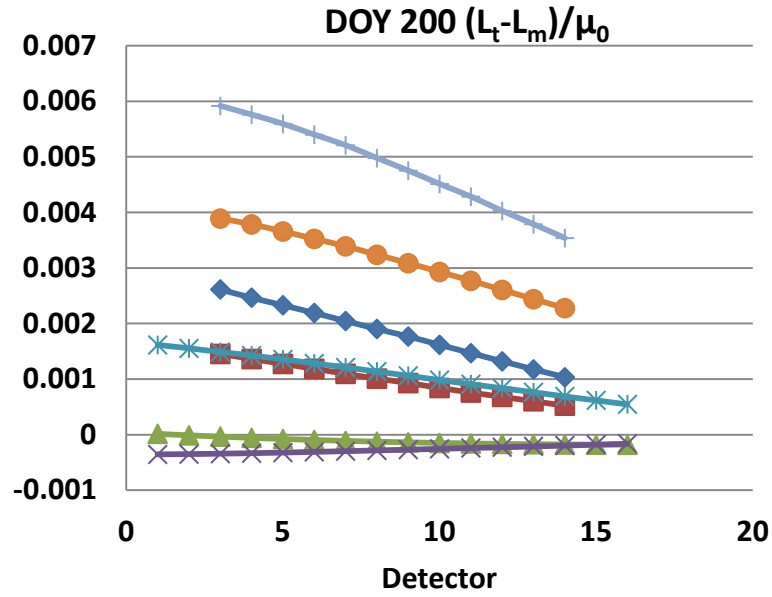

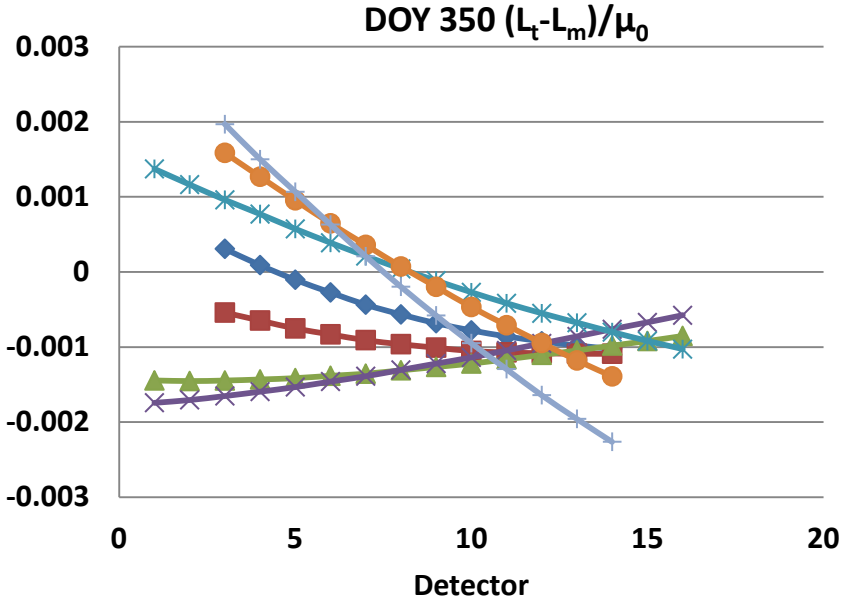

Polarization Spectral Sensitivity $[(L_t-L_m)/\mu_0]$

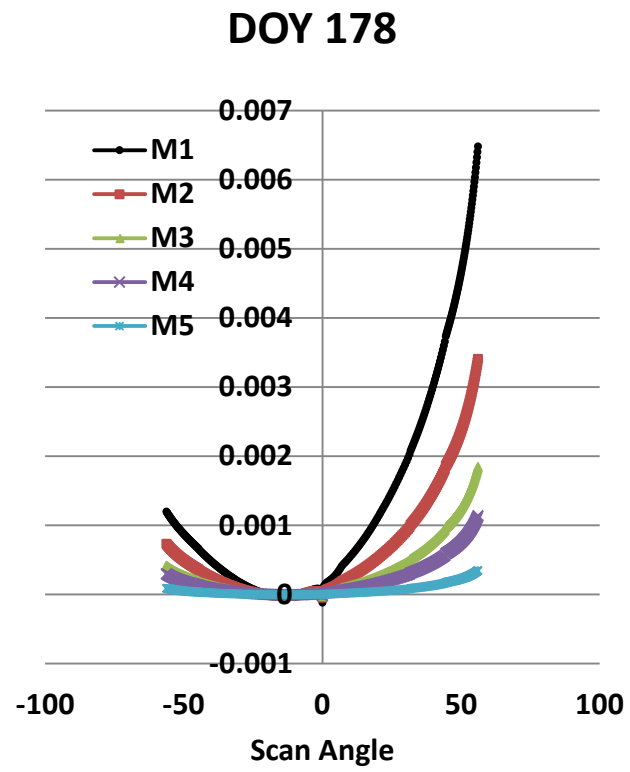

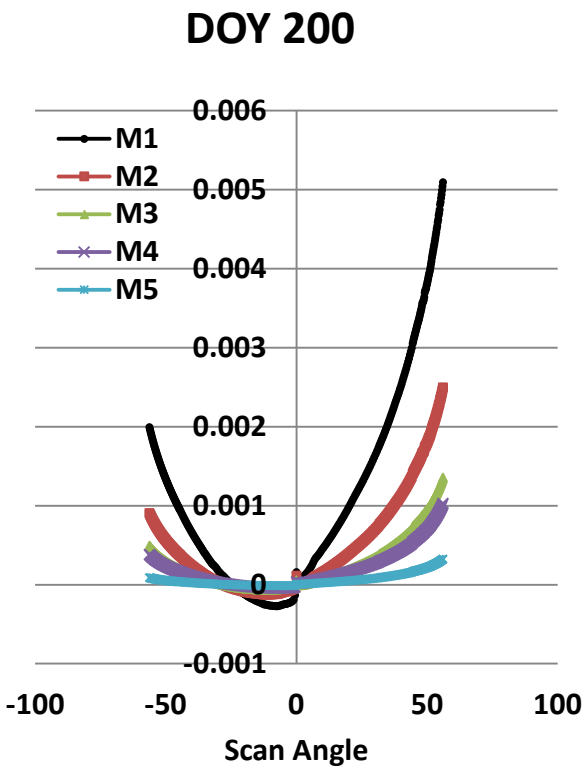

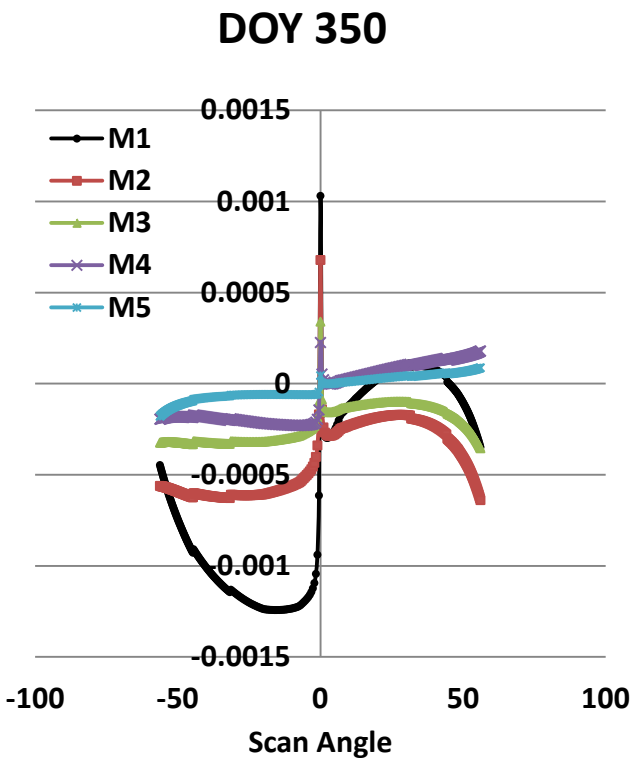

Estimate of Maximum Sensitivity $[(L_t-L_m)/\mu_0]$

	M1	M2	M3	M4	M5
Angular	0.007	0.004	0.002	0.0015	0.0004
Mirror Side difference	0.001	0.0003	0.0002	0.0001	0.00005
variation among Detectors	0.004	0.004	0.002	0.0015	0.00015

MAIAC Land Process

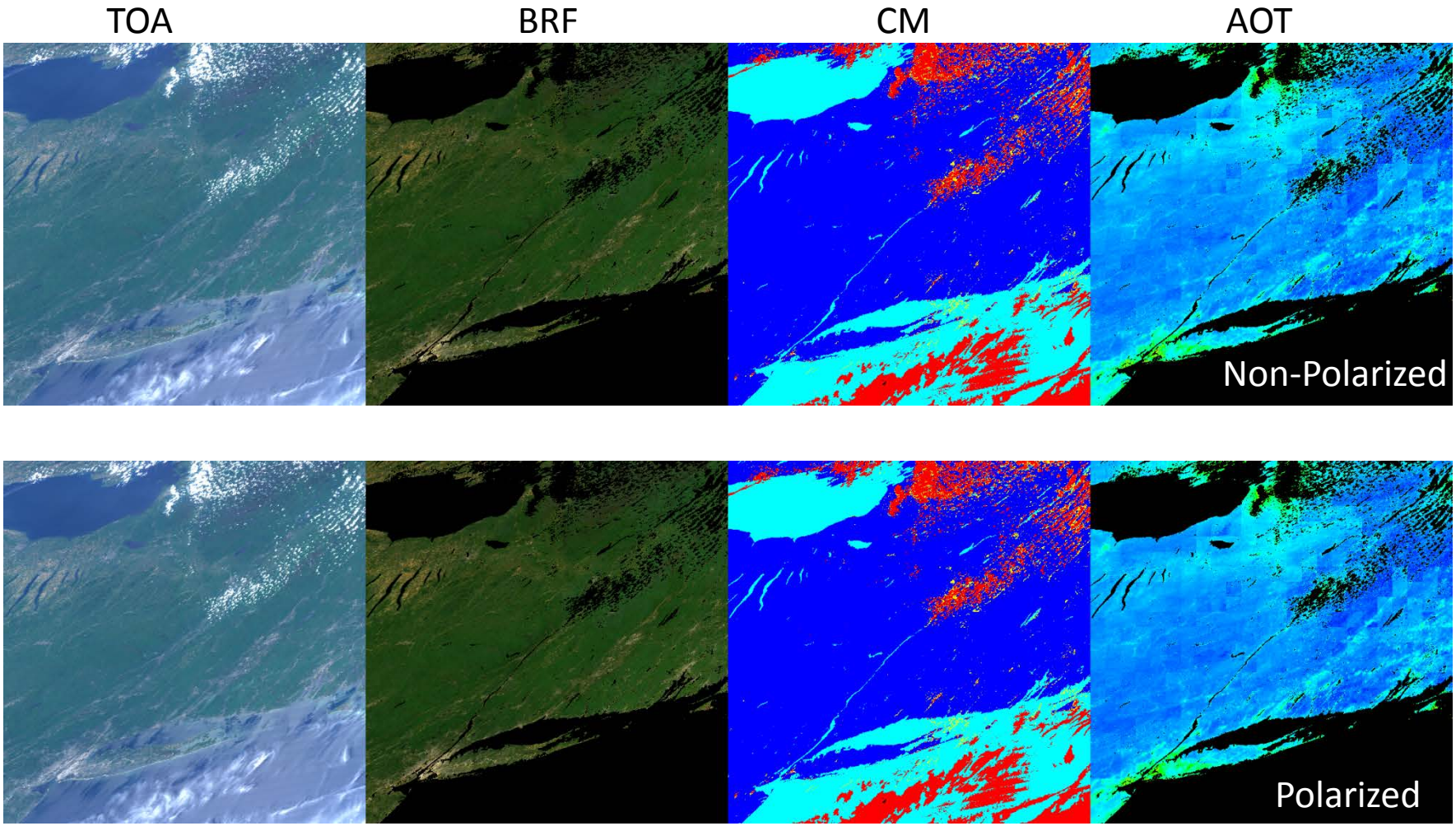

New England Area (450x450KM^2), 2012, day 138

Impacts on AOT Retrieval

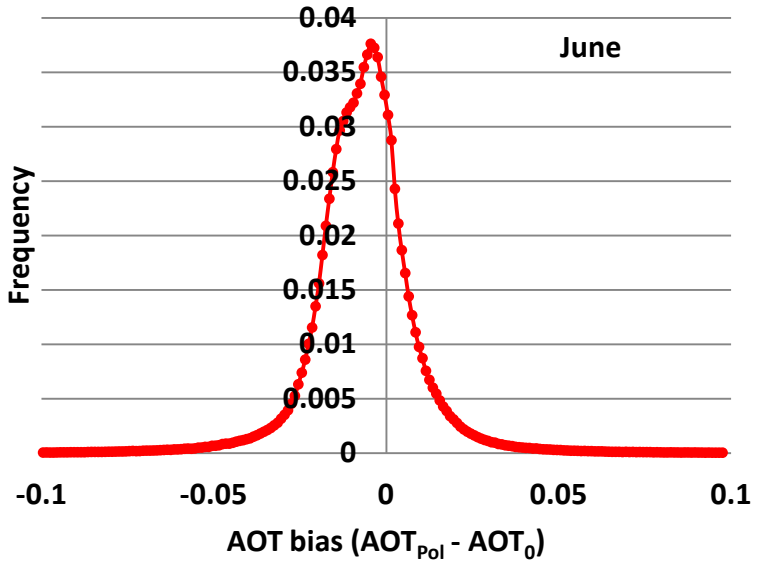

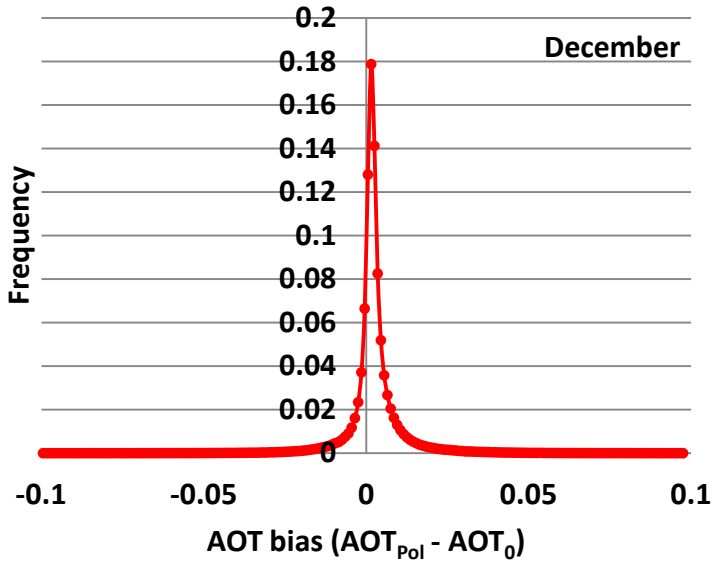

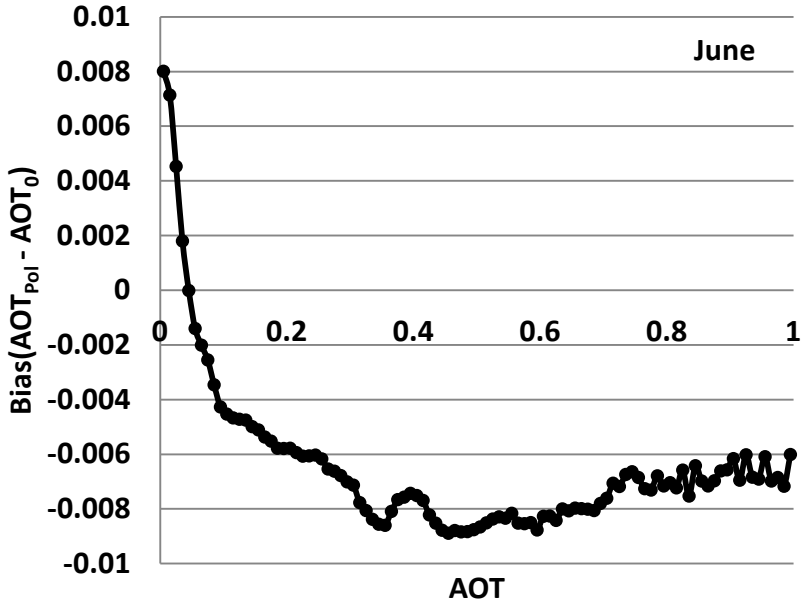

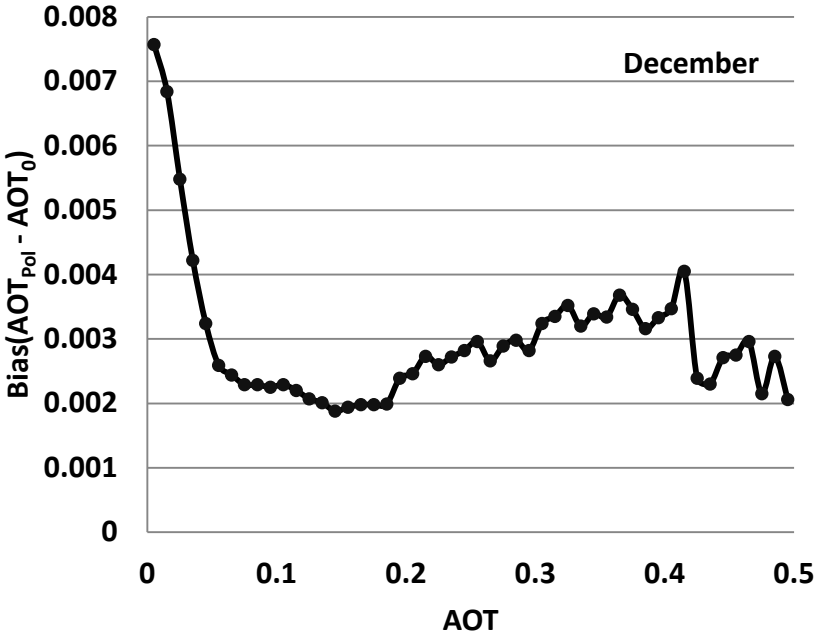

Impacts on Surface Reflectance

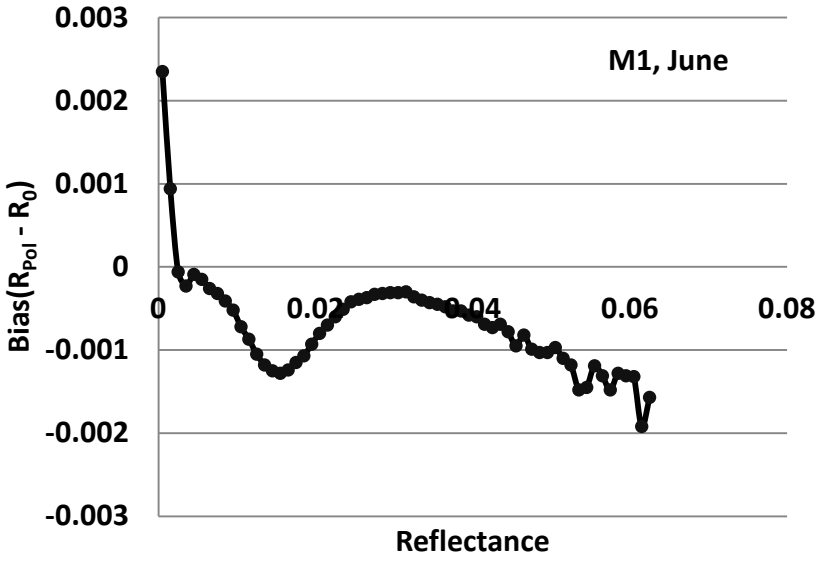

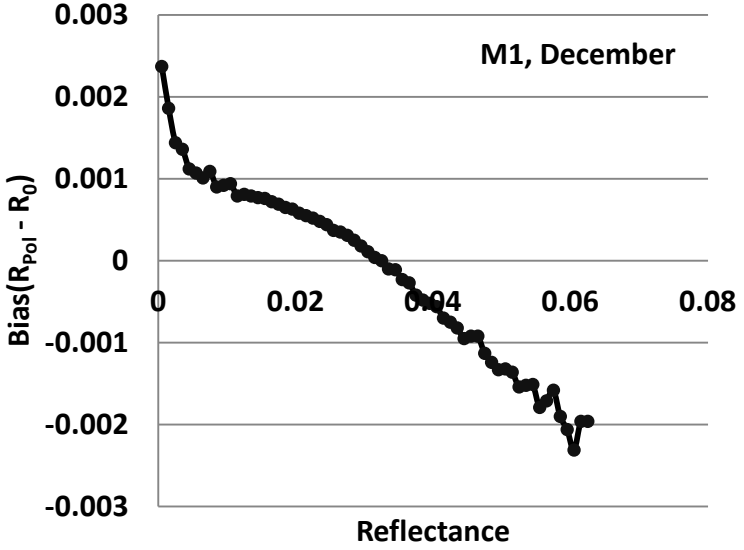

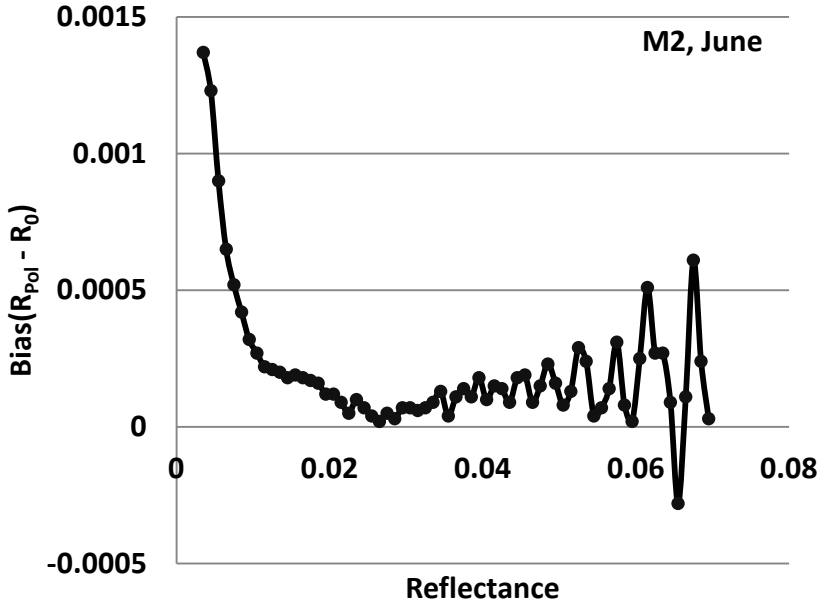

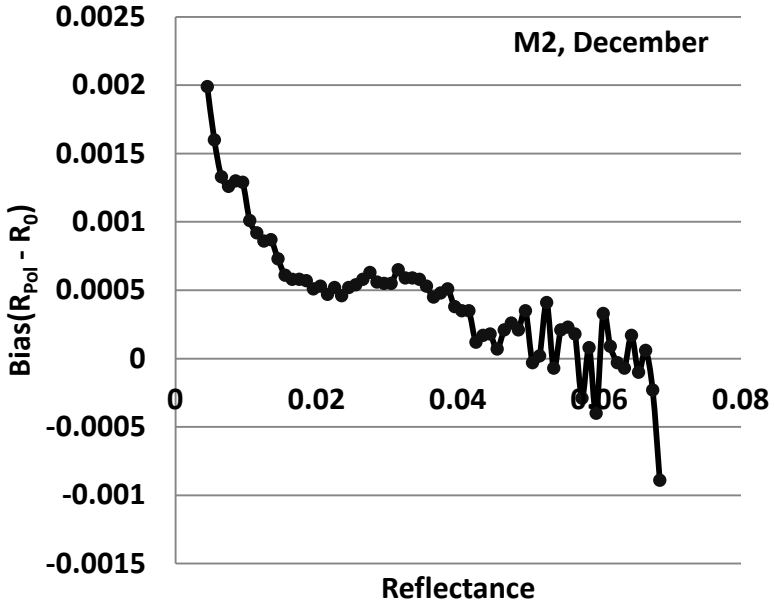

Impacts on Surface Reflectance (cont.)

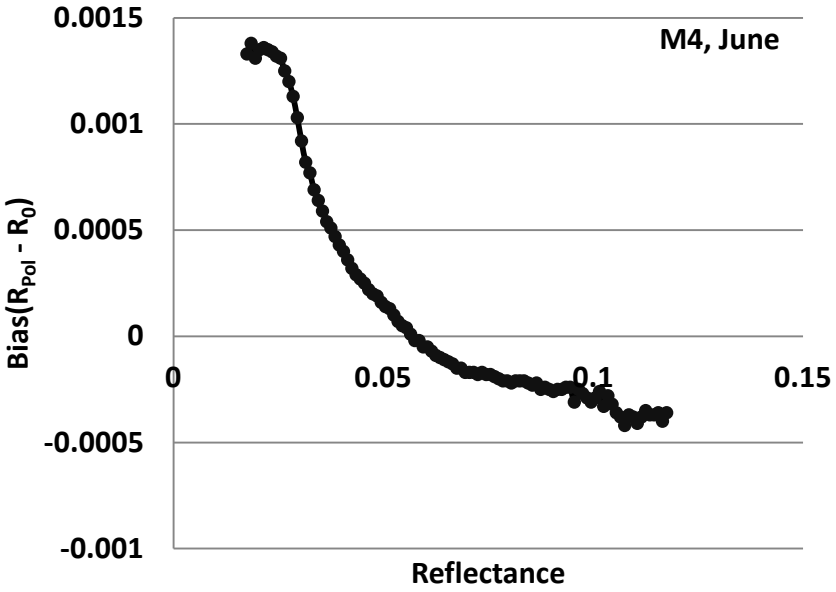

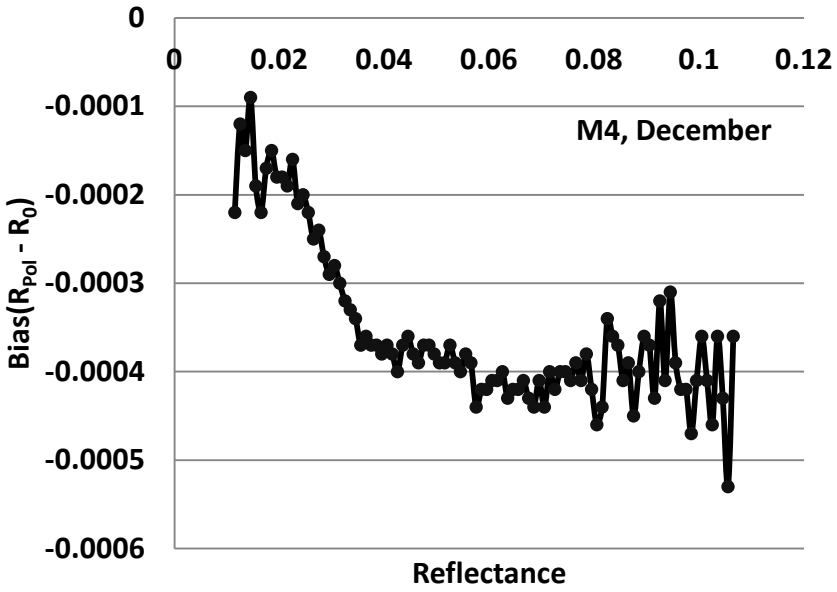

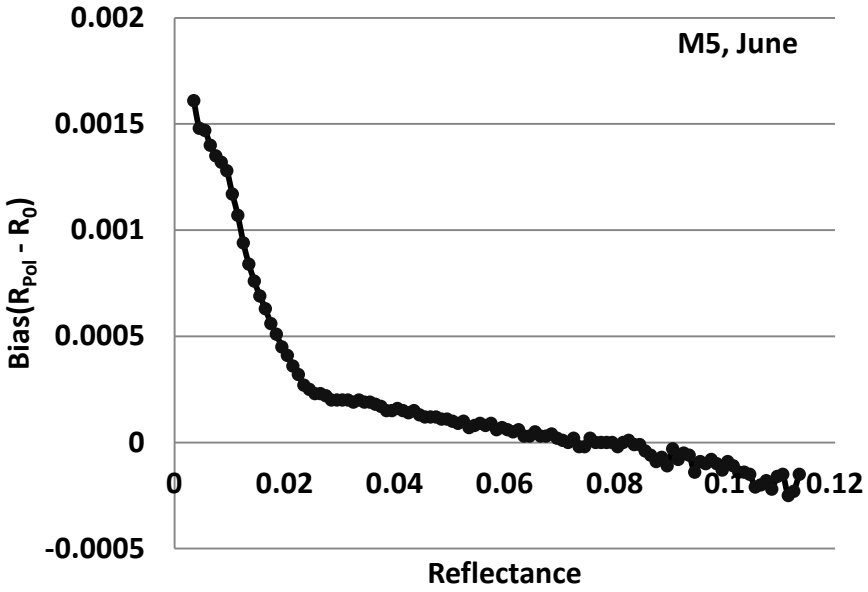

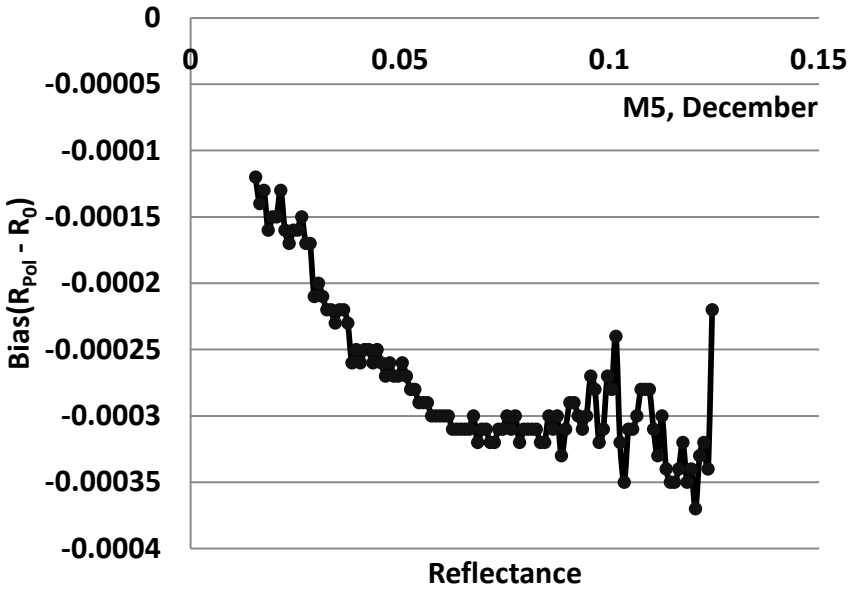

Summary

- Polarization effect strongly depends on Sun-view geometry and sensor polarization features.
- At low sun angle, detector to detector variation increases (more striping).
- The maximum polarization effect at TOA is around 0.007 for M1 band.
- Polarization may create bias up to 0.01 on AOT retrieval and this bias is seasonal dependent.
- Polarization effects on surface reflectance is small except for M1 band, which could reach 0.002.

NOAA'S NATIONAL CLIMATIC DATA CENTER

THE VIIRS CLIMATE RAW DATA RECORD

James C. Biard, Linda Copley, Drew Saunders, Jeff Privette

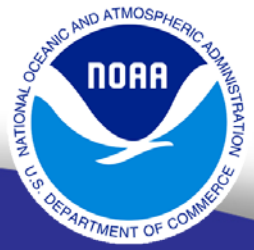

NC STATE UNIVERSITY

The UNIVERSITY of NORTH CAROLINA
A Multi-Campus University

What is a Climate Raw Data Record?

- Climate Raw Data Record (C-RDR) is the name given by the Climate Data Record Program (CDRP) at the National Climatic Data Center (NCDC) to designate a NOAA level 1b dataset that is optimized for use in producing Climate Data Records.
- C-RDRs are designed with reprocessing and long-term preservation in mind.

Why create a C-RDR?

- Climate Data Records (CDRs) are different than real-time mission data products
  - Use different algorithms and processing patterns
  - Require periodic reprocessing of the period of record
  - Generally use the raw sensor data as input
- Suomi National Polar-orbiting Partership (SNPP) Sensor Data Records (SDRs) and Environmental Data Records (EDRs) are processed beyond the point most appropriate for use as CDR inputs.

Why create a C-RDR?

- The Science Raw Data Records (RDRs) for the SNPP instruments are non-optimal for CDR purposes
  - Significant software framework or detailed knowledge of the satellite downlink packet formats is required for use
  - Portions of the raw data are compressed, encoded, and/or not byte-aligned
  - RDR contents are not platform independent (byte order)
- SNPP Science RDRs are not good candidates for long-term preservation efforts

The VIIRS C-RDR

- The NCDC CDRP made a decision to produce C-RDRs for the SNPP mission to provide datasets appropriate for climate science processing and long-term preservation.
- Applications developed using the Application Development Library (ADL)
- Development of the VIIRS C-RDR has been completed, and it has been in operational production since October 19, 2013, with plans to extend the record back to February 2012.

The VIIRS C-RDR

- The VIIRS C-RDR is well-suited for climate science and long-term preservation
  - netCDF-4 data format, Climate and Forecast (CF) Metadata Conventions, and Attribute Convention for Dataset Discovery (ACDD)
  - Raw data is decompressed, decoded, and byte-aligned
  - Each unique quantity stored as a separate variable
  - Each quantity is annotated with provenance and usage metadata
  - Each file annotated with 70 elements of metadata, including ones from the SNPP RDR/SDR set

What does a VIIRS C-RDR contain?

- The VIIRS C-RDR contains
  - 242 engineering variables
  - 38 image variables
    - 4 groups – 375m, 750m Dual-gain, 750m Single-gain, DNB
    - Earth and calibration views stored as multi-band image arrays
  - 19 spacecraft diary variables
    - Includes satellite position, velocity, and attitude vectors
  - 4 quality measure variables
- VIIRS-specific IDPS coefficients and LUTs also stored in grouped variables with metadata

Reading a VIIRS C-RDR variable

- VIIRS C-RDR files readable by many packages
  - IDL, MATLAB, etc
  - Packages that read HDF5 files (e.g. HdfView)
- netCDF-4 and HDF5 libraries available for many programming languages

Reading a VIIRS C-RDR variable


```
import ucar.nc2.*;
import ucar.ma2.*;

...
    // Open the VIIRS C-RDR file.
    //
    NetcdfFile oDataFile = NetcdfFile.open(sInputFilePath, null);

    // Find the calibration view variable for the 750 m dual-gain
    // image group. This variable has dimensions of band, calibration
    // source, line number, and number of samples.
    //
    Variable oVar = oDataFile.findVariable("Image_750m_DualGain/calibview");

    // Get the dimensions of the variable.
    //
    int[] anCounts = oVar.getShape();

    // Create an array of start indices. They all have the value
    // index value of zero.
    //
    int[] anStarts = new int[anCounts.length];

    // Read the values from the variable.
    //
    Array oValues = oVar.read(anStarts, anCounts);
...
```

How to access VIIRS C-RDR files

- VIIRS C-RDR files are available from the NCDC HDSS Access System (HAS)
  - http://has.ncdc.noaa.gov/pls/plhas/HAS.FileAppSelect?datasetname=3658_01
- Currently have coverage from October 19, 2013
- Working to extend coverage to the beginning of VIIRS Science Operations (February 2012)
- Data product home page
  - http://www.ncdc.noaa.gov/data-access/satellite-data/satellite-data-access-datasets/c-rdr-viirs

How to access VIIRS C-RDR files

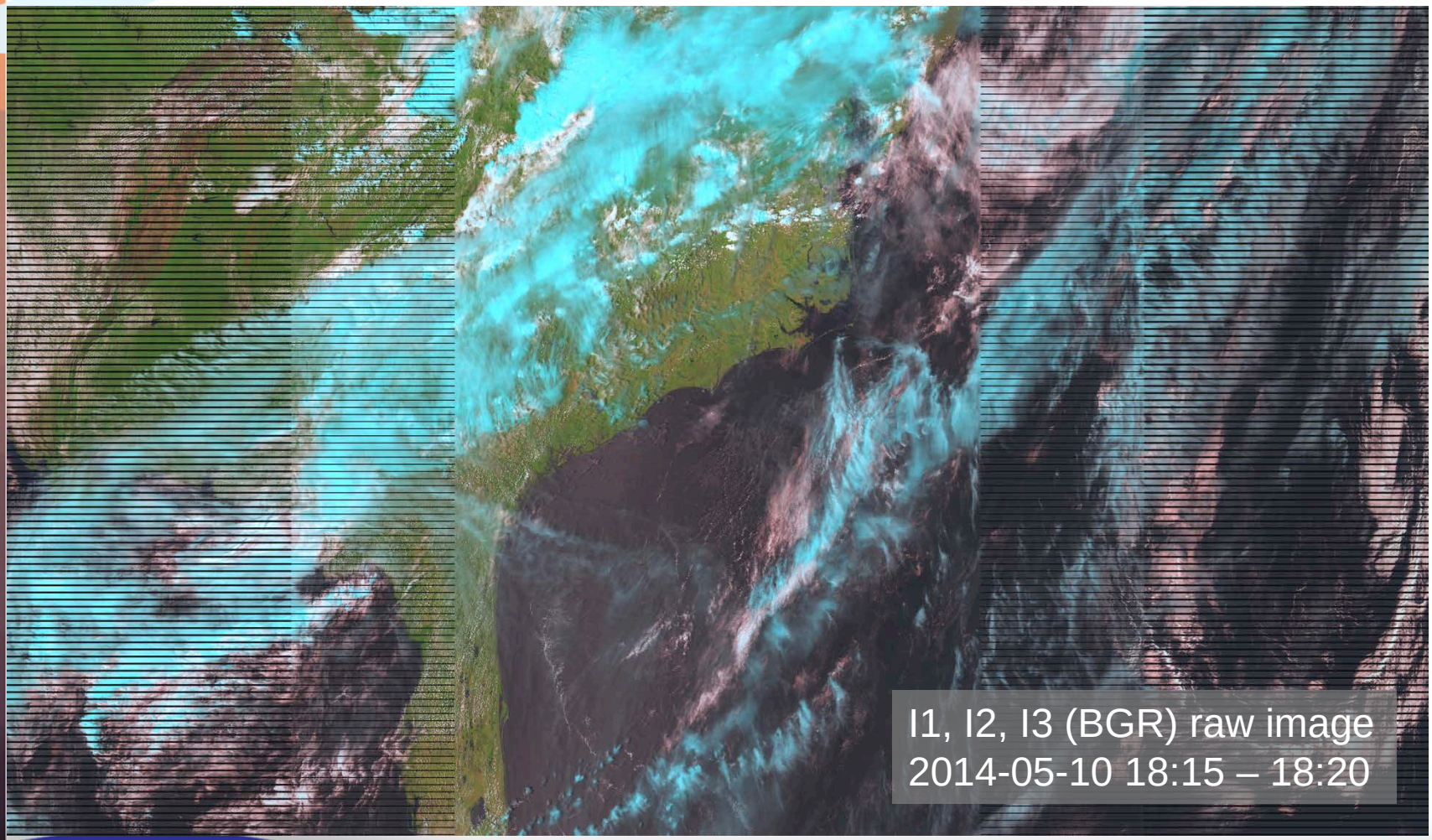

Author information

- Jim Biard
  - Cooperative Institute for Climate and Satellites – North Carolina (CICS-NC)
  - jim.biard@noaa.gov
- Linda Copley
  - CICS-NC
  - Linda.copley@noaa.gov
- Drew Saunders
  - NOAA NCDC
  - drew.saunders@noaa.gov
- Jeff Privette
  - NOAA NCDC
  - Jeff.privette@noaa.gov

THANK YOU

Questions?

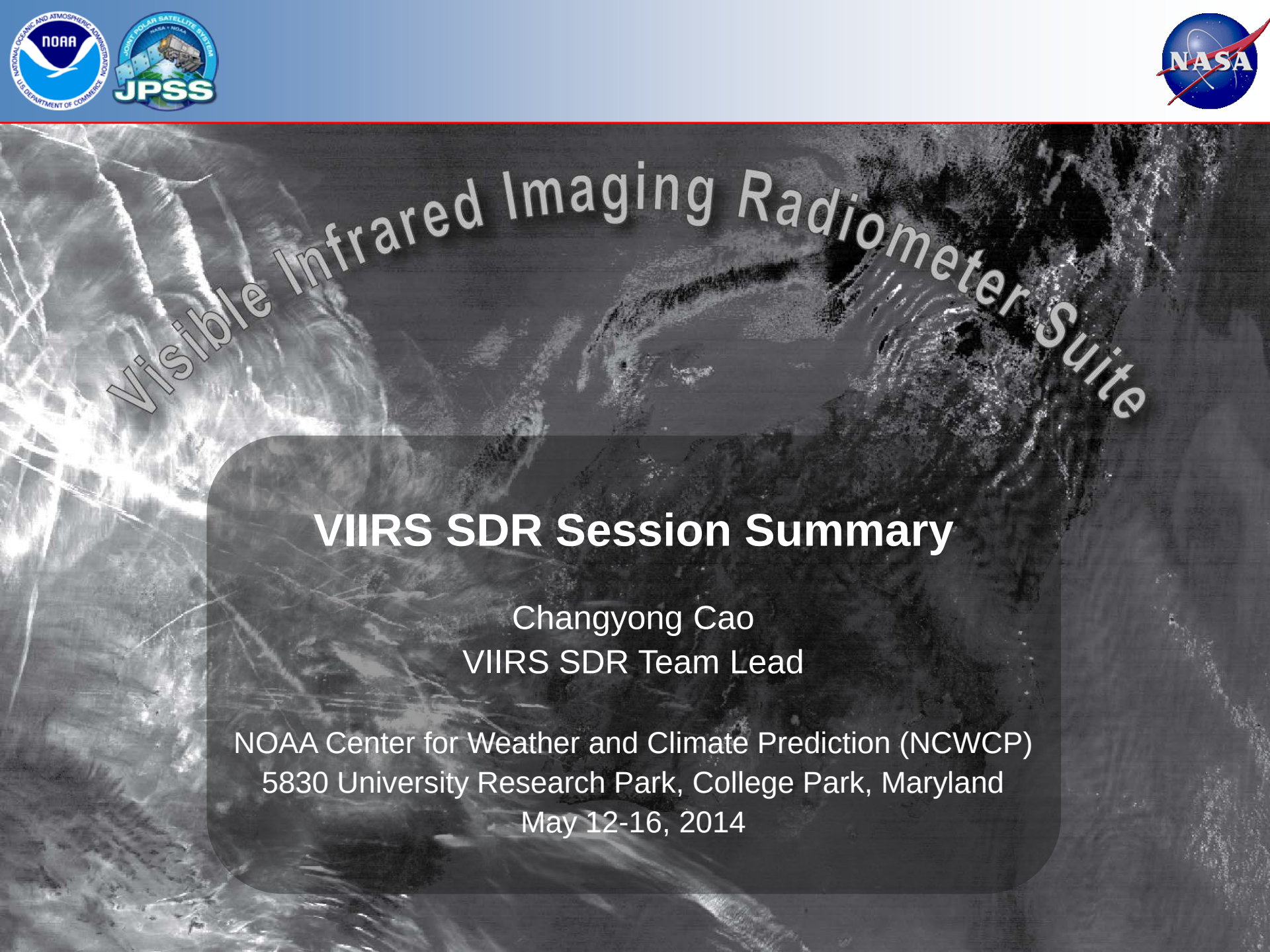

VIIRS SDR Session Summary

Changyong Cao
VIIRS SDR Team Lead

NOAA Center for Weather and Climate Prediction (NCWCP)
5830 University Research Park, College Park, Maryland
May 12-16, 2014

VIIRS SDR Session Summary

- Overall, the VIIRS instrument continues to perform well, meeting performance specifications
- TEB summary:
  - SST striping continues to be an issue that require further investigation. Effects due to detector vs. band average level RSR analyzed. Results show that M13 NEDT at blackboy is 0.04K while noise can be upto 0.15K due to striping, half of which due to band average RSR effects.
    - Action: Further test the striping effect due to RSR averaging in the algorithms.
    -
  - C0 adjustment can reduce the M15 bias but the benefit is marginal given the uncertainties with IASI/AIRS/CrIS consistency at low temperatures (Moeller)
  - "mis-alignments" between scans reported by SST in the bow-tie region. A quick analysis using contrails does confirm the effect (upto 5km displacement found between scans).
    - Action: Further investigation using ground linear featuresneeded because contrails are at much high altitudes.
- DNB summary:
  - Straylight correction works well according to users.
  - Improvements and changes in calibration need to be well documented and made available to the public on-line.
    - Action: Enhance the VIIRS Event Log database to keep track of all changes. Add commentary on anomalies to facilitate reanalysis. Currently the database covers a large number of events but not completely.

Alignment check using contrail (I4-I5)

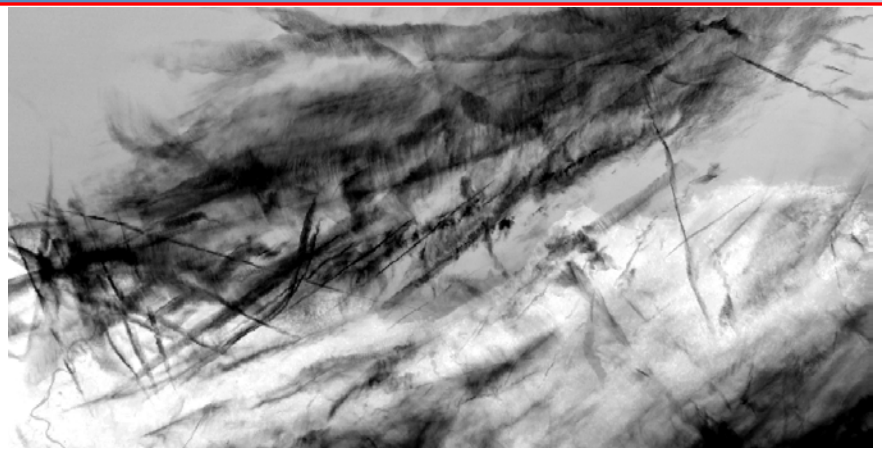

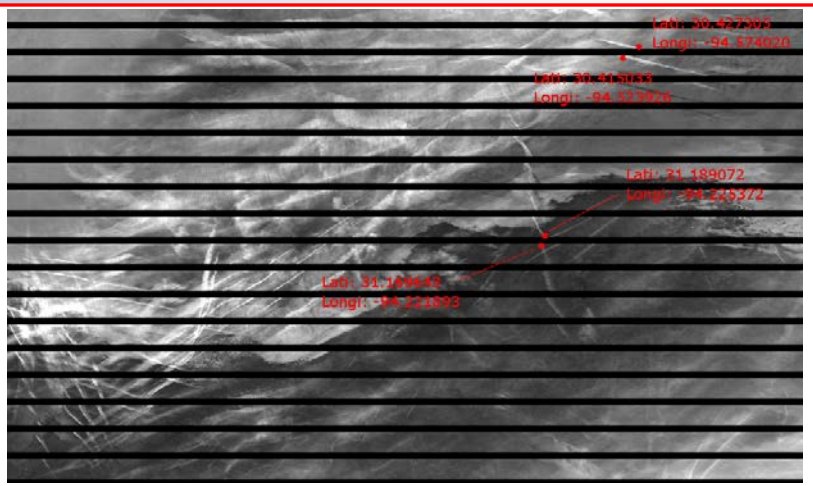

VIIRS SDR Session Summary

- RSB calibration
- H-factor discrepancies between the operational and other versions may cause problems in the F factor trends.
- Recent flattening in the F-factor trend requires further investigation
- Validations at vicarious sites, DCC, and comparisons with MODIS may confirm the discrepancies observed by ocean color groups
- Actions:
  - A) further investigate the root cause for the flattening trend in the F-factors
  - B) Prepare for early transition to RSB autocal to mitigate the recent calibration issues

- J1 Polarization issues
  - Good progress has been made in planning for additional prelaunch characterization, modeling, global observations using GOME, and ground based measurements
  - Uncertainty in the polarization phase is a concern (BG)
- Actions:
  - A) Provide feedback to NASA on the phase uncertainty concerns to see whether it can be improved for J1/J2
  - B) Endorse the current effort to support the polarization studies for J1 VIIRS

Calibration Trend Change

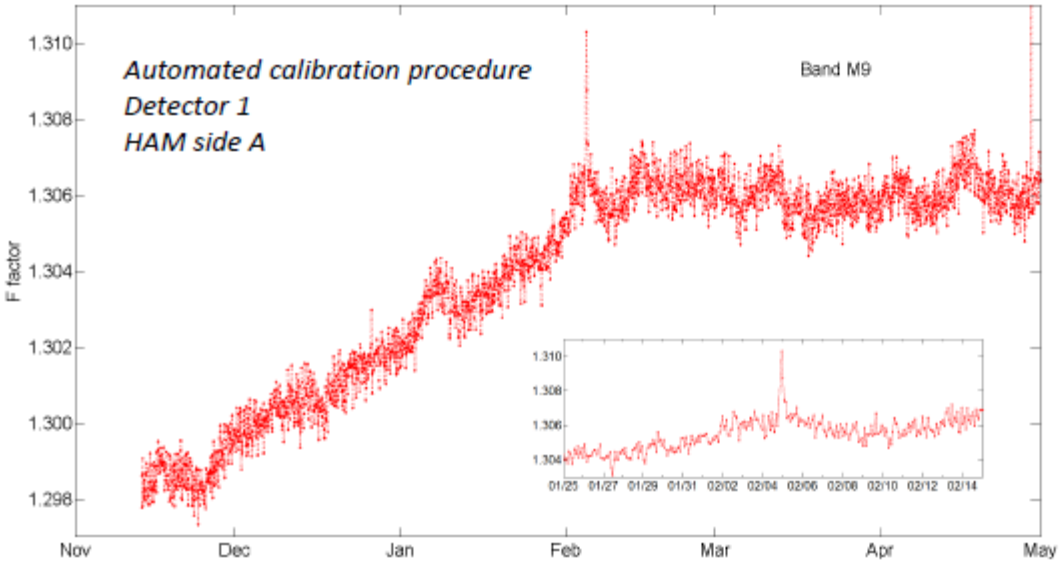

- On February 4, 2014, VIIRS single-board computer lockup anomaly occurred and lasted longer than one orbit
- Following recovery from the anomaly (marked by the spike in the M9 F factors: see the insert graph), the F factor trends have changed

- Despite fluctuations in the calculated F factor values, it is clear that the F factors for the SWIR bands are no longer increasing due to the telescope throughput degradation (note that solar diffuser reflectance is assumed constant for the SWIR bands)
- The telescope degradation may have stopped if during the February 4 anomaly the telescope mirrors temperature increased enough to "bake out" water ice that after the UV photolysis was providing protons for the tungsten oxide color center formation

7

Solar Diffuser Degradation Trend

automated calibration procedure

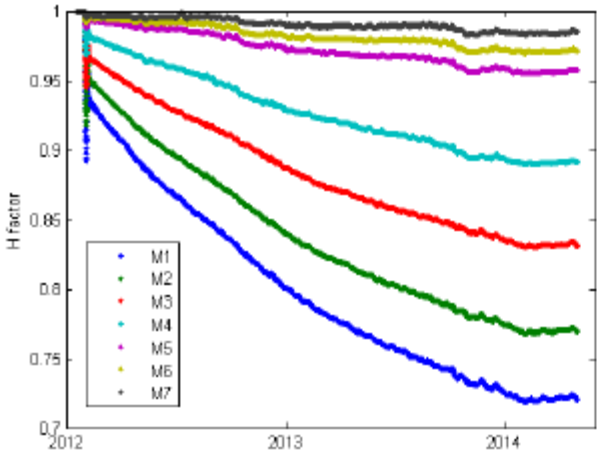

operational SDR production

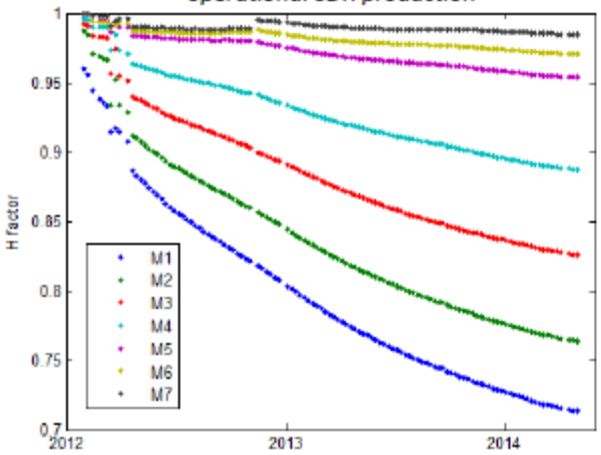

- When the solar diffuser monitoring data are analyzed with the automated calibration procedure, the reflectance degradation trend changes in February 2014: the decrease has diminished
- If during the February 4 anomaly the solar diffuser temperature increased above ~360 K, the hydrocarbons that cause the degradation may have been baked out (in vacuum)

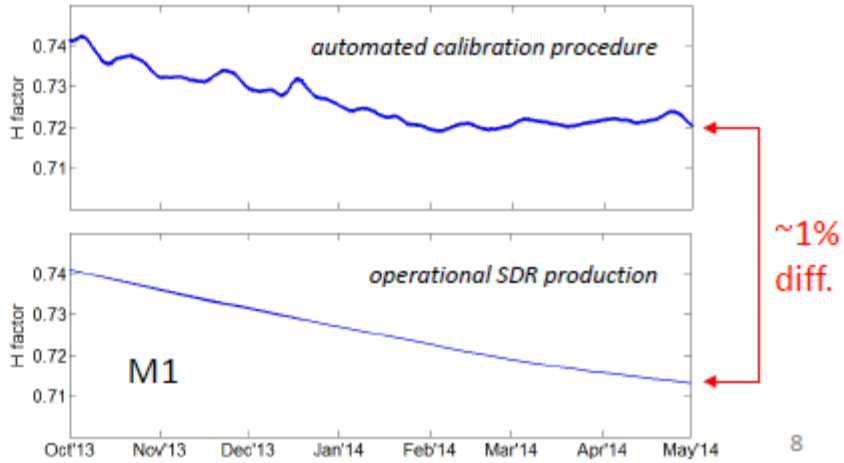

Effects on Radiometric Calibration

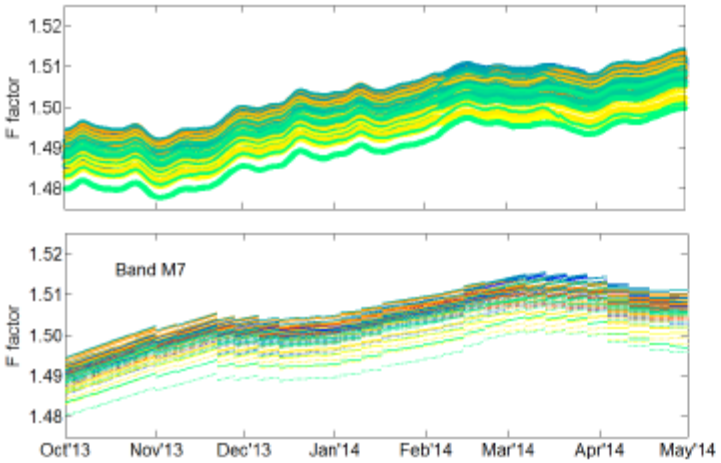

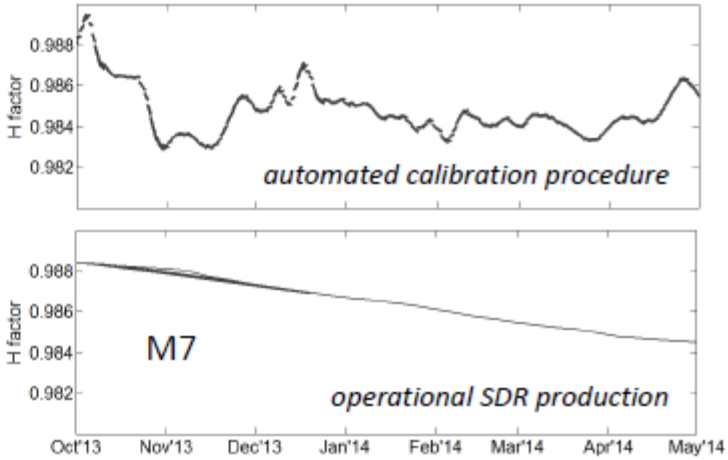

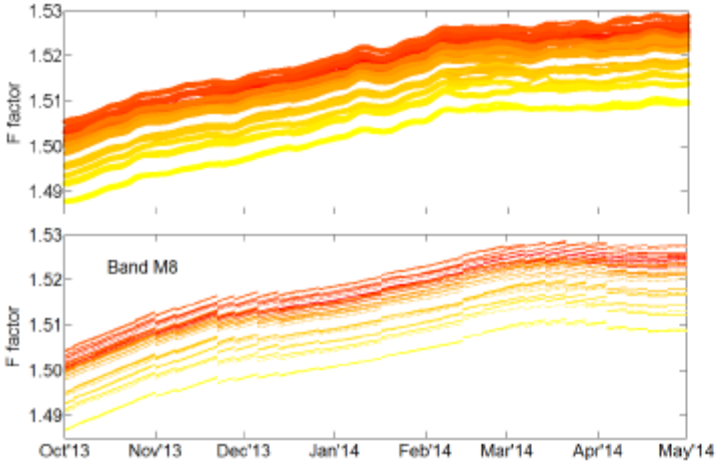

- For the bands not corrected by the H factors (SWIR), the automated procedure calibration responded more timely to the calibration trend changes
- Additionally, for the bands corrected by the H factors, the automated procedure responded better to the changes in the solar diffuser degradation